## *Responsive luminescent lanthanide probes for biological applications*

SERGEY VIKTOROVICH SHUVAEV


# Responsive luminescent lanthanide probes for biological applications

**Sergey Shuvaev**

A thesis submitted for the degree of Doctor of Philosophy

**November 2017**

*Dedicated to my first supervisor and mentor*
*Professor Dr. Natalia Kuzmina for sharing her wisdom and introducing me to a fascinating realm of lanthanide coordination chemistry*

## Declaration

The research described herein was undertaken at the Department of Chemistry, Durham University between September 2014 and October 2017. All of the work is my own; no part of it has previously been submitted for a degree at this, or any other, university.

## Statement of Copyright

# Abstract

Lanthanide-based complexes play a significant role in biological applications, spanning MRI contrast agents to molecular luminescent tags. Regardless of their application, these complexes should conform to general requirements, such as high stability against decomplexation at physiologically relevant conditions and sufficient solubility in water. Other more specific requirements may also apply, demanding a customised design of the ligand for a specific application.

Emissive bio-responsive lanthanide complexes comprise a large and dynamically developing area, which possesses several intrinsic advantages over non-lanthanide analogues. Large Stokes' shifts, long-lived excited states, ratiometric bands in the emission spectrum, strong cirularly-polarised signals are but a few to be named. These beneficial properties can be employed for efficient measurement of pH or determination of bioactive molecules both *in vitro* and *in cellulo*. For instance, europium complexes bearing sulphonamide arms showed reversible pH-response, producing noticeable changes in both the total emission and CPL spectra (Chapter 2). Other europium complexes possessing polarity-sensitive emission intensity were successfully used for detection of human serum albumin and $\alpha_1$-AGP – two the most abundant serum proteins – by following both total emission and CPL spectra, and these results are discussed in Chapter 3.

Selective detection of biologically relevant anions needs specific probe design requirements. Even subtle changes in the structure of the ligand may lead to considerable changes in selectivity and affinity towards selected species. Such a correlation between structure and binding properties was exemplified in a series of europium complexes for the detection of nucleotides and zinc and led to the creation of probes spanning 5 orders of affinity constants. Furthermore, a nucleotide-specific induced CPL signal allowed monitoring the ratio between ADP and ATP – a parameter that characterises metabolic rates in mitochondria. These observations are thoroughly analysed in Chapter 4.

# Table of Contents

## Acknowledgements

First and foremost I would like to thank my supervisor Professor David Parker for giving me this opportunity to spend three years in Durham in an exceptionally amicable atmosphere surrounded by helpful and knowledgeable people. During these three years I gained a unique experience working hand in hand with people from different scientific and cultural backgrounds. Looking back now I am absolutely confident that these three years in North East of England changed me dramatically and laid the basis for my future personal and scientific development.

I also want to express my deepest gratitude to Kanthi for providing her help and support on multiple occasions, from solving my synthetic issues to dealing with domestic problems.

I would like to thank Robek for his encouragement and help with multiple photophysical and cellular experiments.

Special thanks go to Alice, for making me laugh and having both scientific and non-scienitific conversations. I will definitely miss your easily recognisable footsteps in the corridor! ☺

I want to thank Kevin for keeping me company watching football in the New Inn in the evenings, having breakfasts in Palatine and being a good friend.

I want to thank Martina, Alex and Brian, who despite our very short overlap managed to make my introduction into the lab and the country very smooth and easy. Also I want to thank Matthieu, Nicola, Katie, Emily, Andrew, Edward, Amandine, Cidalia, Laura and other previous and current residents of CG-27 for offering their help and support. Last but definitely not the least I want to thank all analytical services of the Department of Chemistry for quickly and professionally resolving all my requests.

These three years would be much harder for me without support of my Mum, Dad, Roman, Sasha, my uncles Alexander and Boris, my cousin Ilya and of course my two best friends – Dmitry (already Dr.) and Alexander (soon to be).

# Abbreviations

| | |
|---|---|
| AMP | adenosine 5’-monophosphate |
| ADP | adenosine 5’-diphosphate |
| ATP | adenosine 5’-triphosphate |
| Boc | *tert*-butoxycarbonyl |
| BSA | bovine serum albumin |
| Cbz | carboxybenzyl |
| CCD | charge-coupled device |
| COSY | correlation spectroscopy |
| CPL | circularly polarised luminescence |
| CPS | counts per second |
| CT | charge transfer |
| Cyclen | 1,4,7,10-tetraazacyclododecane |
| d | doublet |
| dd | doublet of doublets |
| DCM | dichloromethane |
| DFT | density functional theoory |
| DO3A | 1,4,7,10- tetraazacyclododecane-1,4,7-triacetic acid |
| dppf | 1,1'-*Bis*(diphenylphosphino)ferrocene |
| ESI | electrospray ionisation |
| EtOAc | ethyl acetate |
| EtOH | ethanol |
| FCS | foetal calf serum |
| FRET | Förster resonance energy transfer |
| GFP | green fluorescent protein |
| GSA | goat serum albumin |

| | |
|---|---|
| HEPES | (4-(2-hydroxyethyl)-1-piperazineethanesulfonic acid) |
| HMBC | heteronuclear multiple bond correlation |
| HPLC | high performance liquid chromatography |
| HRMS | high-resolution mass spectrometry |
| HSA | human serum albumin |
| HSQC | heteronuclear single quantum correlation |
| IR | infrared |
| ISC | inter-system crossing |
| ICT | internal charge transfer |
| LC | liquid chromatography |
| LMCT | ligand-to-metal charge-transfer |
| Ln | lanthanide |
| MeOH | methanol |
| MES | 2-(N-morpholino)ethanesulfonic acid |
| MRI | magnetic resonance imaging |
| MW | molecular weight |
| MS | mass spectrometry |
| NMR | nuclear magnetic resonance |
| NOESY | nuclear Overhauser effect spectroscopy |
| PBS | phosphate buffered saline |
| PET | photoinduced electron transfer |
| PMT | photomultiplier tube |
| q | quartet |
| *q* | hydration number |
| ROESY | rotating-frame Overhauser effect spectroscopy |
| rt | room temperature |

| | |
|---|---|
| s | singlet |
| SAP | square antiprism |
| t | triplet |
| THF | tetrahydrofuran |
| TFA | trifluoroacetic acid |
| TLC | thin-layer chromatography |
| TPPO | triphenylphosphine oxide |
| TSAP | twisted square antiprism |
| UV | ultra-violet |

# Scientific abbreviations

| | |
|---|---|
| Å | angstrom |
| λ | wavelength |
| μ | micro |
| ϕ | quantum yield |
| ε | molar extinction coefficient |
| τ | lifetime of the excited state |
| $\tau_R$ | rotational correlation time |
| δ | chemical shift |
| A | absorbance |
| $B^k_q$ | crystal field parameters |
| $C^k_q$ | spherical tensor operators |
| $g_{em}$ | dissymmetry factor |
| S | singlet state |
| T | triplet state |

# Chapter one

# Introduction

# I.1. Theoretical background of the Eu(III) luminescence

## *I.1.1. Historical milestones*

The very first luminescence spectrum of $Eu^{3+}$ was recorded[1] in 1885 by Sir William Crookes (Fig.I.1), sixteen years before the element europium was isolated[2] by Eugène-Anatole Demarçay (Fig. I.1), analysing yttria and samarium-containing ores. The transition band, which is now known as a hypersensitive $^5D_0 \rightarrow {}^7F_2$ transition was described by him as having 'great brilliancy of a fine orange-red colour, as sharp as a gasline'. This band could not be ascribed to either samarium or yttrium, which had been already isolated and whose emission spectra had been analysed, and therefore this band corresponded to another unknown element, present as an impurity in samaria. This fact encouraged Demarçay to proceed further with multiple extractions of samaria until the penultimate lanthanide element was obtained; the last stable rare earth element, lutetium, was isolated in 1907.

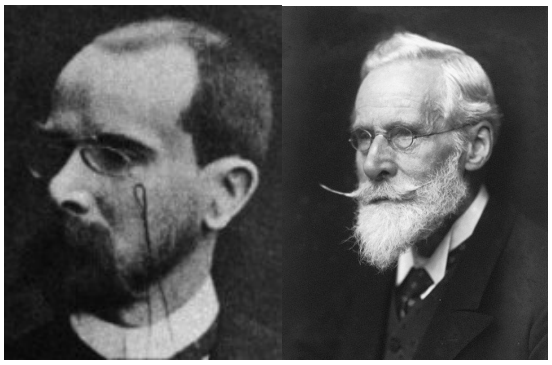

**Fig. I.1** Portraits of Eugène-Anatole Demarçay (*left*) and Sir William Crookes (*right*).

The luminescence properties of Eu(III) compounds were scarcely studied until the late 1930s, when Van Vleck made a first attempt[3] to investigate the influence of chemical structure on the emission spectrum. Van Vleck deduced that the luminescence observed was due to f-f intraconfigurational transitions of the Eu(III) ion, mainly of magnetic-dipole nature, and suggested that the excitation is vibronically induced. Within the next decade a considerable breakthrough was achieved on both chemical and physical fronts. In 1942, Weissman published his thorough study[4] of several europium complexes with different organic ligands, possessing much brighter luminescence than inorganic phosphors. Trying to explain

this difference, a so-called ‘antenna effect’ was suggested, i.e. an indirect excitation of Eu(III) via the organic ligand bound to it – a conception solely based on Van Vleck’s assumption of the intraconfigurational nature of observed emission lines in the spectrum, for which direct excitation is Laporte forbidden.

The development of new emission detectors resulted in a series of works[5] produced by a group of spectroscopists from the Zeeman Laboratories (University of Amsterdam), which published the first high-resolution spectra of lanthanide ions in aqueous solution. As a result, they managed to calculate oscillator strengths of several transitions. Moreover, it was shown that transitions of magnetic-dipole origin were substantially less probable than induced electric dipole ones and were only possible for those transitions that cannot borrow intensity by an induced electric dipole mechanism. They also concluded that static and vibrational perturbations are comparable in terms of the probability to induce an electric dipole transition.

The last step towards the creation of a consistent theory of electron transitions in lanthanides was made simultaneously by Judd[6] and Ofelt[7] in 1962. They derived an expression to calculate the oscillator strength of the transition at given positions of coordinated atoms around the lanthanide ion, along with polarizabilities of these ligated atoms. The main assumption underlying the proposed theory is an admixture of $4f^{n-1}5d$ states of opposite parity to $4f^n$, induced by odd-parity terms of crystal-field components.

Judd-Ofelt theory is unable to provide *ab initio* predictions of spectroscopic data based on crystal structure data. Fundamental computational obstacles (e.g. the precision of calculation of radial integrals and crystal field parameters) need to be overcome to make this theory more widely used. Judd-Ofelt parameters can be used for approximate spectroscopic analysis as phenomenological parameters, especially in the case of the complexes of europium, for which a mathematical description substantially simplifies.

## *I.1.2. Electronic structure of lanthanides*

Extensive attempts to determine energy structure of lanthanides in various crystal matrices were carried out in 1950s and 1960s by Dieke and co-workers[8], which were finally summarised in his book published in 1968[9]. The so-called 'Dieke diagram' has since been extended to a theoretically calculated energy diagram – the 'extended Dieke diagram'[10], which is shown in Fig. I.2.

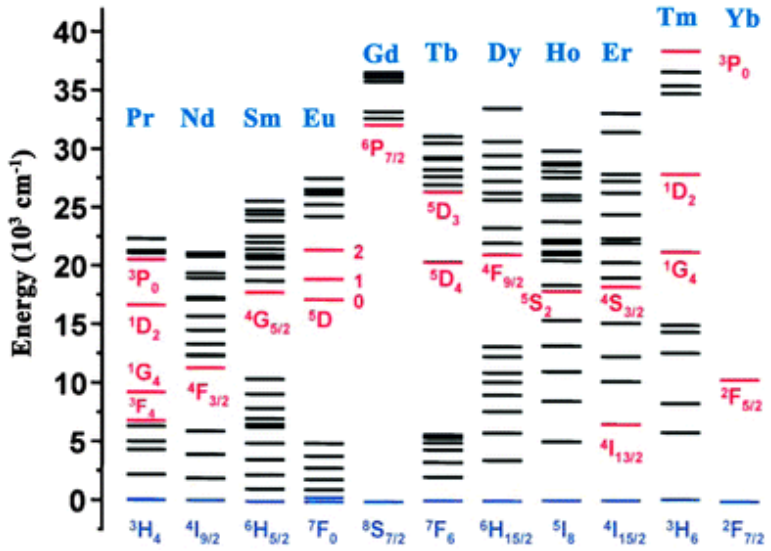


**Fig. I.2** Energy level diagram for $Ln^{3+}$ ions (referred to as 'Dieke diagram') with the energy levels up to 40,000 $cm^{-1}$ accessible within a typical optical experiment[11]. The most common resonance levels are marked red.

Due to the fact that the conventional electronic configuration $[Xe]4f^n$ corresponds to the single electron model, it neglects electron repulsion and the impact of spin-orbital coupling. These factors should be considered differently for lighter and heavier elements, as the value of spin-orbital coupling is proportional to the atomic number. Two schemes have been put forward: the so-called Russell-Saunders coupling for lighter elements and 'jj-coupling' for heavier ones. In the case of lanthanides, the spin-orbit coupling constant is comparable to the electrostatic interaction energy between electrons. This implies that the 'intermediate coupling' scheme (in this case the electronic configuration is considered as the linear combination of L-S configurations) instead of pure L-S (Russell-Saunders) coupling or 'jj-coupling', is valid for light and heavy elements respectively. Nevertheless, the assignment is undertaken in accordance with the L-S scheme[12]. This assumption sometimes causes controversies in the interpretation of emission and absorption spectra, because

*J*, frankly speaking, is no longer a good quantum number. For example, a splitting of the $^5D_0 \rightarrow {}^7F_0$ transition in complexes with only one type of coordination environment is usually considered as breaking the L-S scheme. However, it should be always kept in mind that energy levels in Dieke diagram are not pure, and certain level of admixing of adjacent energy levels is expected ('*J*-mixing').

The number of possible microstates ($N_{states}$) for a lanthanide ion with a configuration of [Xe]$4f^N$ is given by $N_{states} = \frac{14!}{N!(14-N)!}$, and in the case of $Eu^{3+}$ ([Xe]$4f^6$) 3003 microstates exist. It is often forgotten that for a lanthanide (III) ion with $3 \leq N \leq 11$, an additional seniority quantum number ($\tau$) should be used, since several $^{2S+1}L_J$ terms with the same S, L and J numbers, but with different energies may exist[13]. For example in the case of $Eu^{3+}$, three $^5D_0$ states are present with energies of 17200 $cm^{-1}$, ca. 42000 $cm^{-1}$ and ca. 75000 $cm^{-1}$, which can be designated as $^5D(3)_0$, $^5D(2)_0$ and $^5D(1)_0$, respectively[14]. Both $^5D(3)_0$ and $^5D(1)_0$ are believed to contribute to the $^7F_0$ state: $93.4\%\ ^7F_0 + 3.5\%\ ^5D(1)_0 + 2.8\%\ ^5D(3)_0 + 0.12\%\ ^3P(6)_0$.[14]

### *I.1.3. Lanthanide complexes for bio-imaging applications*

Two major advantageous optical features of lanthanide complexes are that bands in emission are narrow, with energies only slightly affected by the nature of the ligand, and there is a large separation (a "pseudo-Stokes' shift") between the absorbing (ligand-antenna) and emitting (lanthanide ion) photon energies. These favourable properties create a myriad of opportunities to devise responsive systems by judicious ligand design. Europium(III) complexes have particular advantages over other lanthanide complexes in biologically relevant applications: the higher transparency of biological tissue towards the red region of the visible spectrum; their high inherent brightness and low sensitivity to quenching by oxygen; the presence of three excited states ($^5D_2$, $^5D_1$ and $^5D_0$) spanning the range 17500-21000 $cm^{-1}$ that are lower in energy than the triplet levels of many different types of ligands; the presence of an environmentally insensitive magnetic-dipole transition $^5D_0$ to $^7F_1$ in the luminescence spectrum, that can be used as an internal reference to the hypersensitive transition bands around 620 ($^5D_0 \rightarrow {}^7F_2$) and 700 nm ($^5D_0 \rightarrow {}^7F_4$); the high emission anisotropy factors, $g_{em}$, in circularly polarised luminescence (CPL) spectra.

A simplified photophysical schematic pathway, involving energy transfer from an absorbing antenna with appropriate singlet (S) and triplet (T) energies in the sequence, S→T→$Eu^{3+}$, has been shown to be valid for the majority of complexes studied. There are a few cases in which the pathway involves competitive direct energy transfer from the singlet excited state to the lanthanide ion, but these are generally considered to be rare[15],[16]. The photophysical phenomena observed in certain special cases requires further consideration. For example, a significant dependence of emission and excitation spectra on solvent polarity can be observed sometimes, and a very low efficiency of $Eu^{3+}$ sensitisation has been reported in certain systems, notwithstanding an optimal value of the energy gap between triplet level and a resonance energy level of $Eu^{3+}$. The presence of donor and acceptor groups within the same molecule, separated by a conjugated system, gives rise to charge-transfer states. The term can be used in a broad definition to embrace all energy states that involve at least partial separation of charge in an excited state. Accordingly, the energy of these transitions can be highly dependent on the polarity of the solvent, and therefore the observation of solvatochromism provides evidence in support of the assignment of these bands as charge-transfer (CT) transitions.

The question of the participation of these bands in the sensitisation pathway of $Eu^{3+}$ emission has been often raised. It has been suggested that the intervention of an intra-ligand charge-transfer (ILCT) state can efficiently compete with a pathway involving the ligand triplet, for sensitisation of $Eu^{3+}$ luminescence, provided that it has a suitable energy to match the resonance levels of $Eu^{3+}$. Evidence in favour of the predominant singlet character of these bands is given by observation of direct excitation into the ILCT band, with a decay rate of the order of nanoseconds and the absence of triplet oxygen quenching of metal emission.

Besides ligand-centred ILCT states, ligand-to-metal charge-transfer (LMCT) states, involving intermediate reduction of $Eu^{3+}$ to $Eu^{2+}$ can be observed in the absorption/excitation spectra of europium(III) complexes. The reduction potential for $Eu^{3+}/Eu^{2+}$ is the lowest in the lanthanide(III) series, for example −0.35 V for the aqua ion, and approximately −1.1 V for Eu(III) complexes with many strongly coordinating octadentate ligands that stabilise Eu(III) with respect to Eu(II)[17],[18]. The energy of these broad LMCT bands, with widths in the range 5,000–15,000

$cm^{-1}$, varies considerably depending on the electron-donating ability of the ligand[19]. The states have mainly singlet character. If an LMCT state is located close to the resonant excited state levels of $Eu^{3+}$, it serves as an efficient quenching pathway, permitting non-radiative depopulation of an excited state of $Eu^{3+}$. Since the energy of the LMCT state is proportional to the reduction potential of the triply charged lanthanide ion, isostructural complexes with lanthanide ions other than $Eu^{3+}$ should shift this band hypsochromically in their absorption spectra, by a fixed value that is independent of the nature of the ligand.

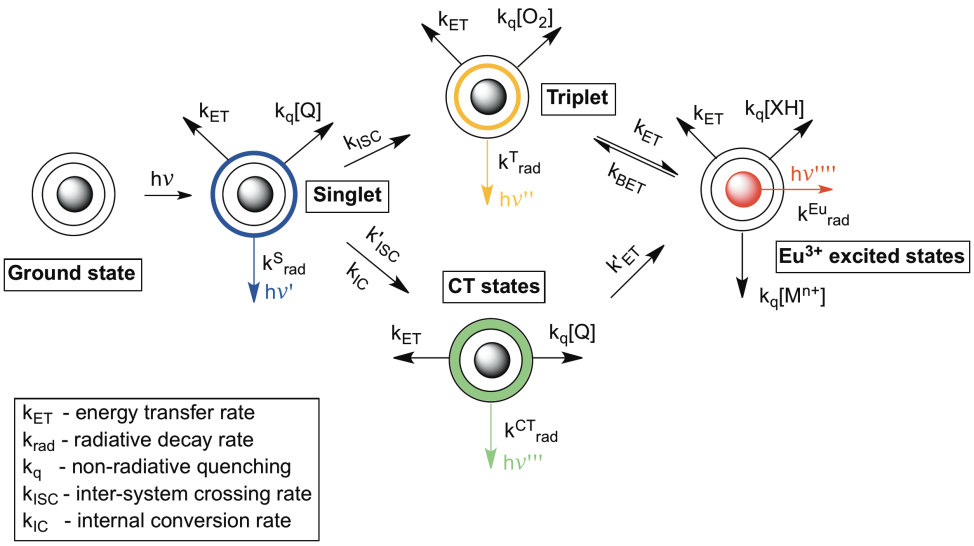


**Fig. I.3** Schematic representation of the major energy transfer processes occurring in responsive europium(III) complexes, including interactions with quenching species (Q), dioxygen, proximate vibrational oscillators (X-H; X = C, N, O) and transition metal ions ($M^{n+}$).

A variety of excited state pathways characterises the sensitisation of $Eu^{3+}$ emission (Fig. I.3). External perturbation of these energy-transfer processes allows different types of luminescent responsive probes to be devised. These probes can be divided into three major groups: those involving a change in the overall intensity of $Eu^{3+}$-centred emission; those involving changes of the spectral profile without major change of total emission intensity; those that involve changes in both the overall intensity and the emission spectral signature. The first group can be subdivided into three sections, depending on the multiplicity of the excited state involved or a charge-transfer character.

*Perturbation of the singlet excited state.* In this case, efficient energy transfer may occur between the singlet state of the antenna and the singlet state of another

molecule (or moiety within the same molecule), either by a long-range (Förster mechanism) or by a close contact interaction (e.g., π–π stacking). Alternatively, the coupling to a charge transfer state (ILCT or LMCT) can lead to deactivation of the antenna $S_1$ state. In the limit, this process may involve complete electron transfer, and is often simply termed as photoinduced electron transfer.

*Perturbation of the triplet excited state*. Deactivation of the triplet level can occur either by back energy transfer from resonant levels of $Eu^{3+}$, if the energy gap is less than 1800 $cm^{-1}$, or by ligand phosphorescence or non-radiative vibrational quenching, if the energy gap is too large and the rate of energy transfer is relatively slow. Such back-energy transfer processes are much more common in analogous terbium complexes, owing to the higher lying $^5D_4$ excited state. Alternatively, coupling with a charge-transfer state (ILCT or MLCT) can also quench a triplet state. An efficient deactivation by energy transfer to triplet oxygen in solution is occasionally observed, leading to formation of singlet oxygen.

*Perturbation of the excited states of $Eu^{3+}$*. Non-radiative deactivation of the excited state of the europium ion can occur by energy transfer to electronic energy levels of transition metal ions (e.g. Cu(II), Mn(II) or Co(II)) or by a FRET-mechanism to different acceptor molecules/ions. These probes can be ratiometric in nature and may be addressed using excitation spectroscopy, if the induced response to an external stimulus is accompanied by an absorption spectral shift.

The second group involve changes in the coordination environment of the $Eu^{3+}$ ion. They are usually ratiometric probes and typically involve observation of the 'hypersensitive' electric-dipole transitions whose intensities can be referenced to the emission intensity of the magnetic-dipole transition, $^5D_0 \rightarrow {}^7F_1$ that is usually insensitive to change in the primary coordination sphere. Typically, perturbation of the coordination environment is accompanied by variation in the number of quenching oscillators X-H (X = O, N, C). Such a change will alter the overall intensity as well, if the conditions for favourable Franck-Condon overlap are met.

The third group includes probes that combine both sensing mechanisms, i.e. involving perturbation of the coordination environment and energy levels of the chromophore.

## I.2 pH-Sensitive luminescence probes

Many physiologically relevant processes in living organisms are accompanied by changes in the pH of the medium. Inside the living eukaryotic cell, pH values inside the organelle may vary from 4.7 inside the lysosome, which digests all unwanted species by multiple hydrolytic enzymes called hydrolases, up to 8.0 in mitochondria – the 'power plant' of the cell (Fig. I.4). The live monitoring of pH values of specific organelles can provide deeper insight into processes occurring on a cellular level and can be accomplished by utilising organelle-selective luminescent probes.

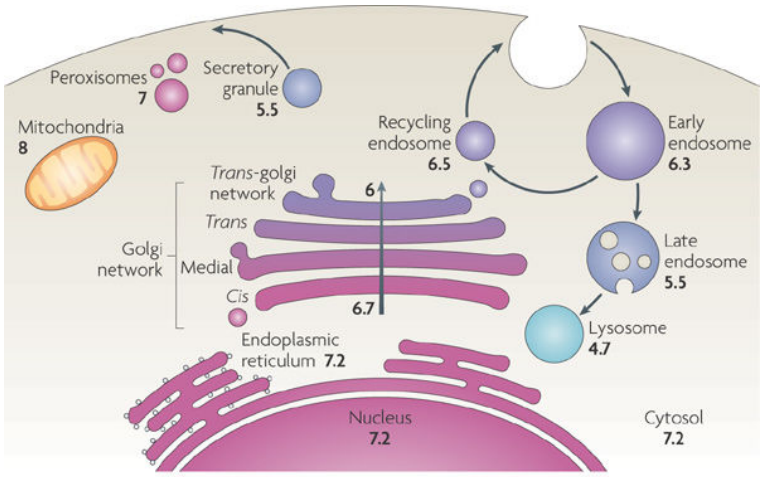


**Fig. I.4** The pH distribution of individual cellular organelles in a prototypical mammalian cell.[20]

Several classifications of pH-sensitive molecular probes are possible, e.g. by chemical structure (e.g. small molecules, metal complexes, fluorescent peptides), type of the response (turn-on/turn-off, ratiometric/non-ratiometric) or signal type detected (e.g. absorption/emission maximum, emission intensity, lifetime of an excited state). In the present work structure-based classification was selected.

### *I.2.1. Commercially available fluorescent pH-probes*

The necessity to monitor pH values on a cellular level has stimulated considerable research activity and led to the appearance of dozens of luminescent pH-responsive probes on the market, spanning the whole range of physiologically relevant pH values (Fig. I.5).[21]

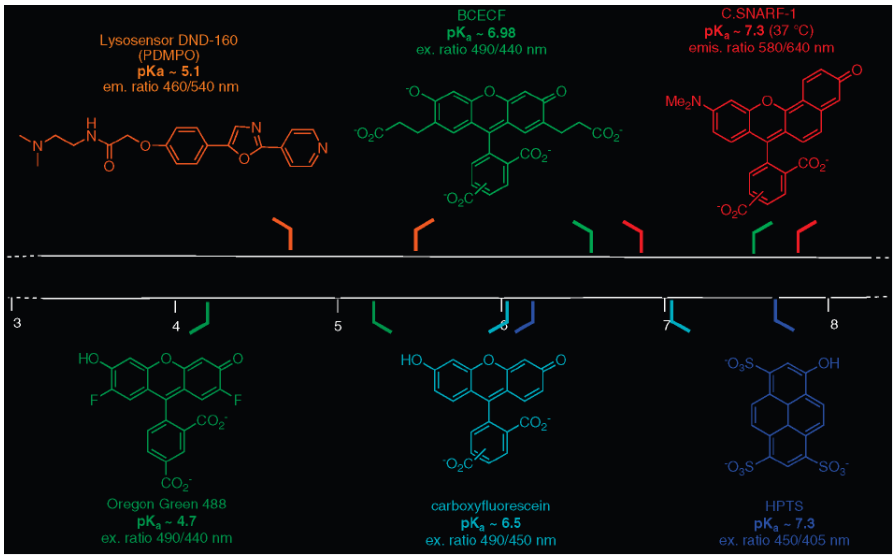


**Fig. I.5** Molecular structures of the most widely used molecular dyes and corresponding pH-sensitive ranges[21]

Oregon Green 488, carboxyfluorescein, BCECF and C.SNARF-2 share the same conjugated core and belong to a large group of fluorescein dyes. Upon reversible protonation, a shift of the emission or excitation band is observed, and by following the ratio between the intensities of protonated and non-protonated forms a pH value can be determined. By extending the conjugation (C.SNARF-2) or by introducing electron-withdrawing groups (Oregon Green 488 and BCECF), the p$K_a$ of the corresponding probes was varied. The common drawback of fluorescein-based probes is their fast leakage from cytosol through cell membrane, potentially giving rise to erroneous readings[21].

The highly water-soluble dye HPTS has a p$K_a$ of 7.3, making it a suitable probe for measuring pH in cytoplasm, by following the shift in its excitation spectrum[22]. However, the lack of cell permeability necessitates direct microinjection, electroporation or scrape loading of this dye into a cell. To monitor changes at the other end of the pH range, a lysosome-specific pyridyl oxasol probe, Lysosensor LD-160, is normally used by monitoring the ratio between the emission bands of protonated and non-protonated forms. High photostability and cell-permeability, along with high quantum yield for both protonated and non-protonated forms makes this probe near-ideal for lysosomal studies[23].

## *I.2.2. Recent advances in small-molecules probes*

Fluorescein and its derivatives are widely used as platforms to create pH-sensitive probes, owing to the change in the emission wavelength following protonation. However, it is impossible to use probes with only a fluorescein-based emission centre, as an additional emission band is required to serve as internal reference, making the responsive probe amenable to ratiometric analysis within a certain pH range. A typical strategy is to graft fluorescein to another emissive pH-insensitive moiety or to an acceptor, such as a BODIPY moiety[24] (Fig. I.6). In the latter case, the energy of the emissive charge transfer state will depend strongly on the pH value. Under neutral and basic conditions, the compound emits in the green (ca. 520 nm) from the fluorescein sub-unit; at acidic pH, charge-transfer state emerges due to the donor-acceptor interaction between fluorescein in its phenolic form and the BODIPY group. Emission in the red then dominates (ca. 600 nm).

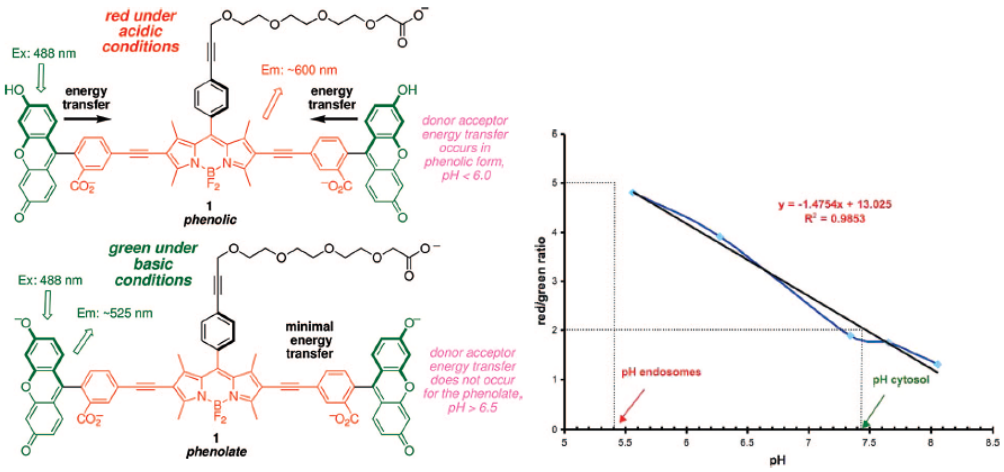


**Fig. I.6** Variation of pH leads to change of the maximum in the emission spectrum (*left*); *ex vivo* calibration curves with values observed in endosomes at 37 °C and cytosol at 4 °C (*right*).[24]

*In vitro* studies show that by varying the temperature, the probe-protein-peptide adduct with bovine serum albumin and 'Pep-1' non-covalently bound peptide predominantly is located in either the endosomes (at 37 °C) or in the cytosol (4 °C). However, this selectivity is driven by peptide Pep-1, rather than by the behaviour of the probe itself, as it was previously demonstrated that protein-dye conjugates containing Pep-1 specifically localize in endosomes.

Another well-known dye, rhodamine, is also used as a building block in pH-responsive systems, being sensitive to pH over a broad pH range. One of the most recent examples is a dual-excitation ratiometric probe based on coumarin-rhodamine FRET dyads[25] (Fig. I.7), where Förster energy transfer between the coumarin and rhodamine moieties is strongly pH-dependent. The main requirement for dual-excitation ratiometric probes is a large separation between maxima of excitation spectra of each component comprising the probe. Such a separation is observed in this pair (350 nm and 560 nm for the coumarin and rhodamine units, respectively). Upon increasing pH, population of the coumarin phenolate increases, giving rise to a new excitation band at 400 nm. The band is ascribed to an ICT transition (intramolecular charge transfer); emission intensity corresponding to the phenolic form correspondingly decreases. At the same time, the intensity of the rhodamine-based excitation band remains relatively constant over the whole pH range, and hence can be used as an internal reference in ratiometric analysis.

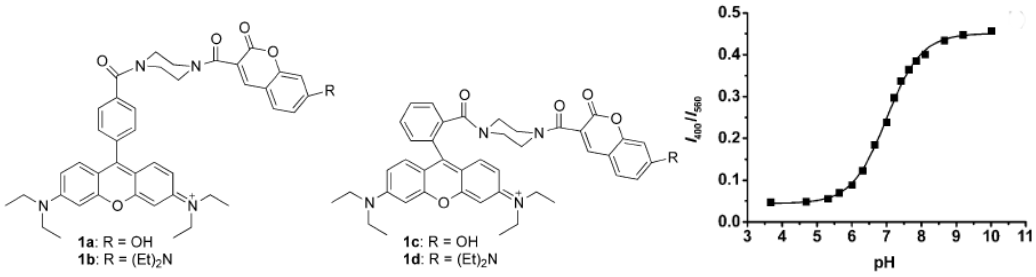


**Fig. I.7** Coumarin-rhodamine FRET dyads (*left*); calibration curve for **1a** (*right*).[25]

However, efficient pH-sensitive probes can also be obtained without introduction of energy transfer states and two pH-sensitive dyes can be simply connected with a spacer. In this way, a dual-emissive probe was designed including both fluorescein and rhodamine moieties[26] (Fig. I.8). It operates over a broad range of pH values, since the p$K_a$ values of fluorescein and rhodamine are substantially different (3.1 and 9.2 for rhodamine and fluorescein, respectively). By plotting the ratio between the emission band maxima of each moiety (512 nm and 580 nm), a quasi-linear dependence was observed.

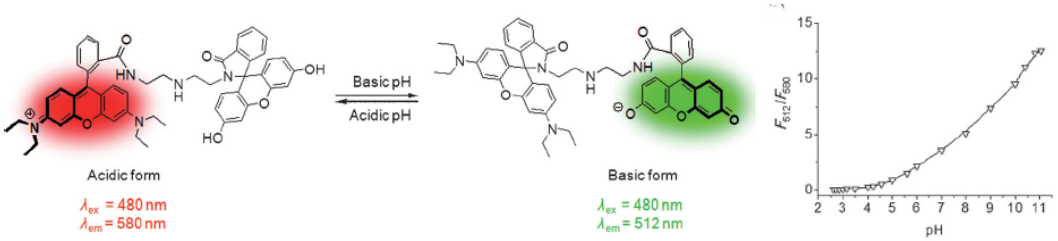


**Fig. I.8** Proposed structural changes upon changing pH (*left*) and pH titration curve (*right*).[26]

The aforementioned examples lack any selectivity towards a specific organelle. Therefore, each cellular study that was performed can be considered only as a 'proof of concept' study, to confirm the absence of toxicity. These examples serve to identify the starting platform in probe design, to which different groups promoting selective recognition can be attached. One of the simplest, but nonetheless most efficient strategies is utilization of weakly basic side chains, making the whole probe acidotropic, thereby promoting its accumulation within acidic organelles, such as lysosomes and endosomes. The p$K_a$ of this type of weak base, typically a secondary amine, should correspond to the expected pH value inside the organelle. For example, this principle is employed in commercially available **Lysotracker Green™** (Fig. I.9). This molecule comprises of an amine containing side chain, which quenches the luminescence of an adjacent emitting core by intramolecular photo-induced electron transfer (PET) upon deprotonation at alkaline pH.

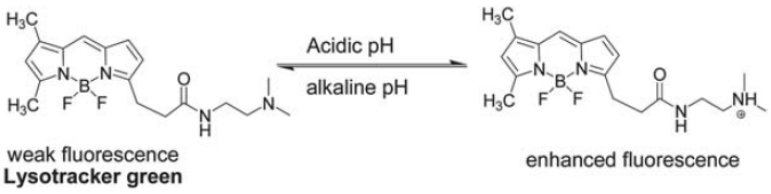


**Fig. I.9** Protonation of **Lysotracker Green™** leads to enhanced fluorescence.[27]

Another interesting example of a lysosomal probe **R6G-EDA** – a rhodamine containing a lactam group[27] (Fig. I.10), which is non-luminescent at neutral and basic pH due to formation of the rigid lactam ring, making it stable against photo-induced degradation. On lowering the pH, ring opening can occur resulting in the formation of highly luminescent product. Apart from the aforementioned example, a side chain does not serve as a 'quencher' and is only used to promote the probe inside the lysosome. In fact, the proposed pH probe has a substantial drawback – the lack of an internal reference; it therefore cannot be considered as a useful probe.

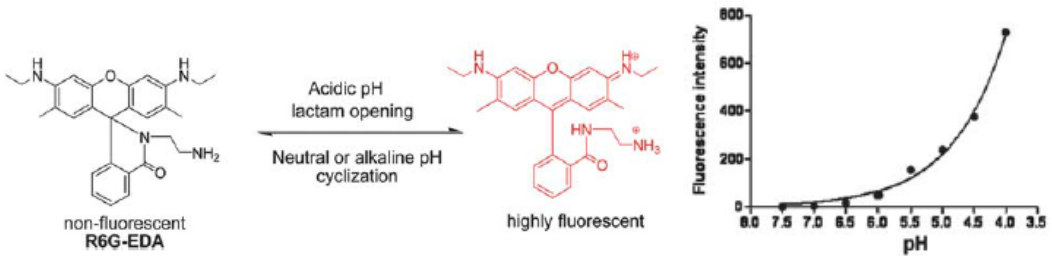


**Fig. I.10** Structural rearrangement of **R6G-EDA** upon varying pH (*left*) and the pH titration curve (*right*).[27]

In theory, by knowing the exact concentration of the probe used for *in vitro* measurements, an estimate of the pH value can be obtained. However, *in cellulo* studies require an internal reference as the concentration of the probe can vary substantially and does not correspond to that of prepared solutions.

The same intrinsic flaw can be found in another example of a rhodamine-based lysosomal probe (**RML**), with a highly pH-sensitive spirocyclic structure[28] (Fig. I.11). An aminoethylmorpholine group (p$K_a$ *ca*. 7.4) was introduced to replace the aminoethyl group in order to promote lysosome targeting, in accordance with previous empirical reports. In the present case, the pH response is not solely rhodamine-based and is partially mediated by the side-chain via formation of an intramolecular hydrogen bond with the amide moiety of a rhodamine unit. Formation of this hydrogen bond enhances the pH-sensitivity, as shown by comparison with the probe, where a dehydro-2H-pyran group replaces the aminoethylmorpholine moiety. The pyran probe exhibited significantly less intense luminescence upon lowering the pH.

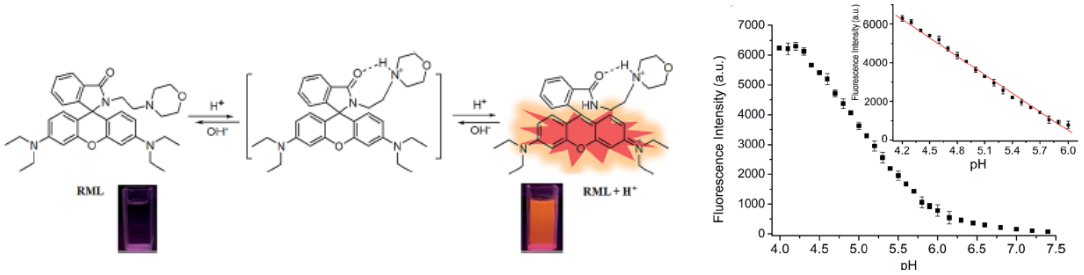


**Fig. I.11** Structural rearrangement in **RML** on varying pH (*left*) and pH titration curve (*right*).[28]

A guiding theme in cellular studies is the adoption of experimental conditions that minimise the energy needed to study the system. Thus there is a strong desire to use probes that can be excited at longer wavelengths. Moreover, detection of emission in

the near-IR region has the advantage that cellular autofluorescence can be excluded. One of the few examples in the literature is the class of cyanine-based probes, since cyanine derivatives typically emit in the near-IR region.

In a recent paper, Ma employed a commercially available heptamethine dye (IR780) to synthesize a new pH-sensitive lysosome-targeted probe **Lyso-pH**[29] (Fig. I.12) by attaching a morpholine moiety to act as the lysome-targeting group. Heptamethine is a decomposition product of cyanines, and has substantially higher photostability compared to the initial compound. It also emits in the near-IR region, and hence has advantages for practical applications. Upon changing the pH, a red shift of the emission band was observed, giving a quasi-linear dependence over the region 4<pH<6. Furthermore, variable temperature fluorescence imaging was performed in order to mimic the processes that occur during heat shock, a side effect of many diseases, and evaluate its impact on lysosomes. It was revealed that a temperature increase causes an irreversible rise of pH in lysosomes, presumably caused by partial neutralisation between the cytosol and lysosome.

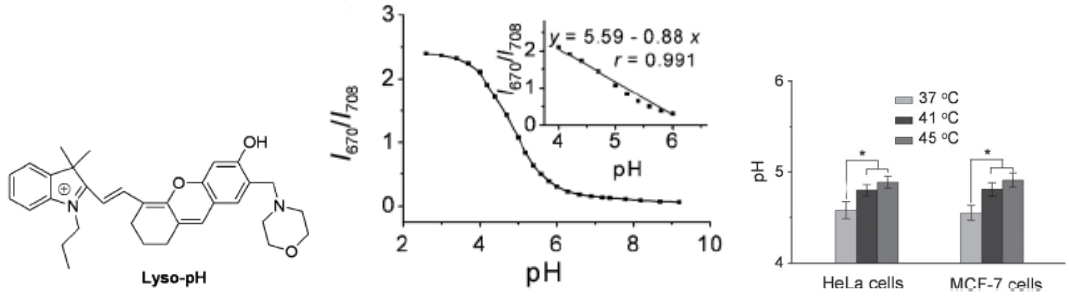


**Fig. I.12** Structure of cyanine-based pH-sensitive probe **Lyso-pH** (*left*), a titration curve (middle) and temperature dependence of pH in lysosomes (*right*).[29]

Various attempts to use cyanines as pH-ratiometric probes have been reported, particularly with systems employing protonated monoamine groups to promote a pH-dependent response of the system. Unfortunately, in spite of their wide operational pH range, these probes undergo irreversible tranformations. However, introduction of a diamine moiety that is able to form a bifurcated hydrogen bond, improved the stability and reversibility of the pH dependent behaviour of the system[30] (Fig. I.13), resulting in the creation of an effective pH-ratiometric probe. The p$K_a$ of the system can be tuned by choosing a diamine moiety with an appropriate p$K_a$ value.

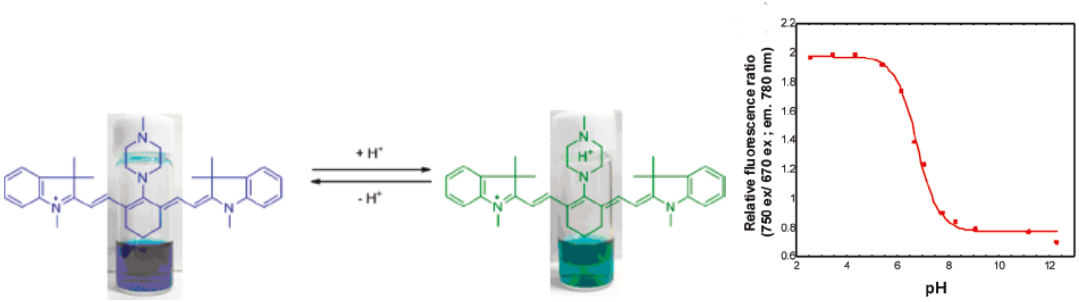


**Fig. I.13** Structural rearrangement upon pH change (*left*) and pH-titration curve (*right*).[30]

A specific aspect of the chemical structure of cyanines gave rise to another pH-dependent response – aggregation induced emission (AIE). Cyanine dyes normally consist of large aromatic $\pi$-conjugated cores with sparsely distributed electrically charged head groups. Therefore, $\pi$-interactions and hydrophobic effects promote aggregation of cyanines in aqueous media. Typically, AIE-active molecules are twisted and strained. The fluorescence is effectively quenched due to the low-frequency motions. Upon aggregation, those motions are physically restricted, and therefore the excited state can be radiatively depopulated. Pursuing an opportunity to combine both effects – aggregation and AIE – in a single molecule, Tsang reported a new hybrid pH-responsive probe **TPE-Cy**[31] (Fig. I.14). The mechanism underpinning the pH-dependent response is the protonation of a sulfonate group at low pH (p$K_a$ = 6.42), combined with nucleophilic attack by $OH^-$ at the double bond, with a subsequent disruption of conjugation. In each case, the hydrophobicity of the whole system decreases due to neutralization of the sulfonate group in an acidic medium and the presence of an overall negative charge in more basic media.

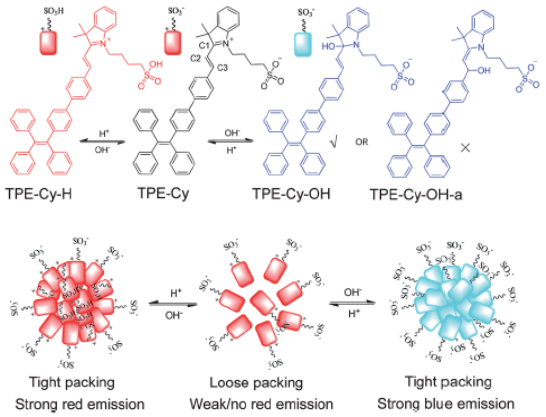


**Fig. I.14** Structural rearrangements (*top*) and change in aggregation (*bottom*), accompanying pH variation in **TPE-Cy** probes.[31]

Another prominent class of pH-responsive probes is based on naphthalimide derivatives. The ease of structural modification, along with the bright fluorescence of these compounds has attracted much interest. It is difficult to suggest any plausible classification for the numerous derivatives of naphthalimide. Therefore only a few examples are discussed.

One of the most recent examples is a lysosome-targeted probe with a *N*,*N*-dimethylaminoethyl group appended in order to promote the specific penetration of lysosomes and to provide a pH-sensitive PET quenching of the naphthalimide core[32] (Fig. I.15). Despite the high Stokes' shift, high fluorescence quantum yield and almost linear pH response in the range 4<pH<7, allowing detection in both lysosomes and cytoplasm, the proposed system lacks any internal reference. This limits the use of this probe in obtaining reliable pH values.

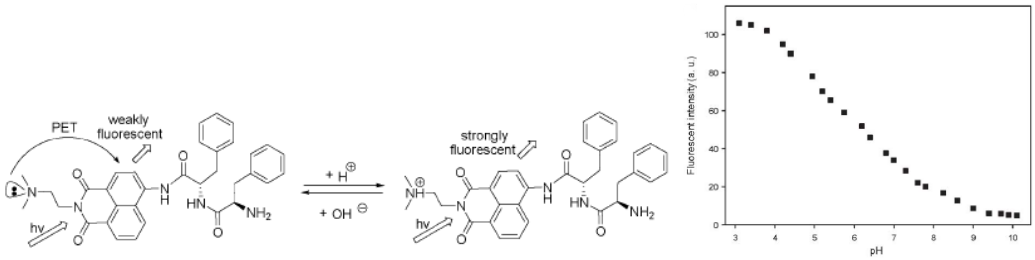


**Fig. I.15** Structural rearrangement upon changing pH (*left*) and pH-titration curve (*right*).[32]

There are many examples of ICT-based ratiometric fluorophores, bearing a naphthalimide core. They are typically coupled with other conjugated groups, for instance, with a triazole moiety at the 9-position (Fig. I.16)[33], without significantly affecting the photophysical properties of the naphthalimide core. The pH response is attributed to reversible deprotonation of the N-H group in the heterocycle-fused naphthalimide structure, while a long-chain substituent attached to nitrogen of naphthalimide makes it cell membrane permeable. It is worth noting that a sample with a $(CH_2)_{15}CH_3$ substituent was localised both on the cell surface and inside the cell. This behaviour enables measurement of the pH values in intra- and extracellular regions, which could be useful in analysing tumour cell pH, as they may exhibit lower extracellular pH values compared to healthy cells.

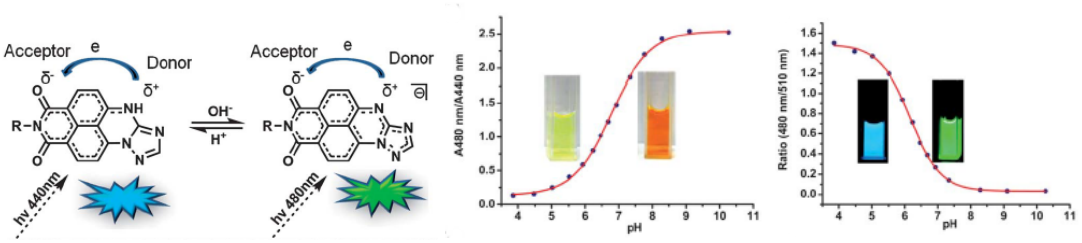


**Fig. I.16** Structural rearrangement on changing pH (*left*), pH-titration curve based on absorption (*centre*) and luminescence (*right*) spectra, corresponding to R = $CH_2CH_2OH$.[33]

Naphthalene derivatives have also been examined as active units in pH-responsive luminescent probes due to similar advantageous properties; high photostability, high quantum yields of fluorescence and diverse opportunities for structural modification. One of the prominent examples, is a probe termed **NP1**, which is a 2-methoxy-6-(5-oxazolyl)naphthalene with an attached pyridine group[34] (Fig. I.17). It has been used to investigate living cells by two-photon microscopy (TPM). This technique has certain advantages in comparison with conventional one-photon microscopy (OPM), such as increased penetration depth, localised excitation and enhanced observation time. Protonation of the pyridine group in a slightly acidic medium (p$K_a \approx 5.0$) enhanced ICT between two parts of the molecule, effectively quenching the naphthalene-centred fluorescence. The pyridine moiety enhanced the acidotropic character of the whole molecule and was believed to lead to an increased accumulation of the probe within lysosomes and the cytoplasm. The authors emphasised that the emission maximum strongly depends on the polarity of the medium, and speculated about its possible utilisation to estimate the polarity of intercellular fluids. Such behaviour is typical for ICT-based probes, making the generation of a pH calibration curve difficult due to concomitant medium polarity dependence, limiting the wider implementation of this probe.

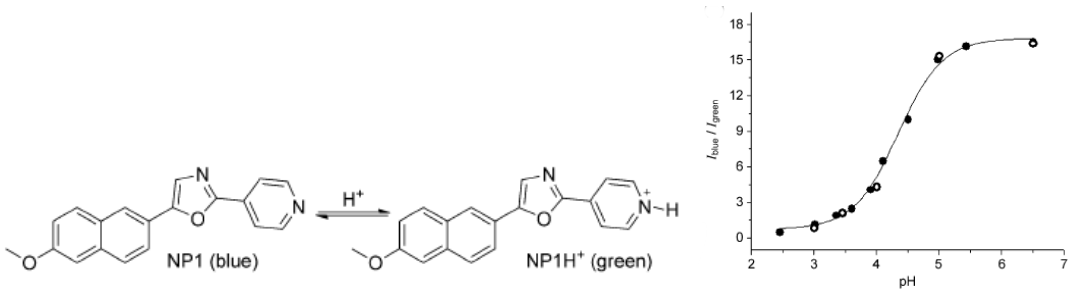


**Fig. I.17** Structural rearrangement upon changing pH (*left*) and pH-titration curve (*right)* in probe **NP1**.[34]

Notwithstanding the useful information gained with the **NP1** probe with regard to the pH values of esophagus tissues obtained from patients with esophagitis, the low quantum yield (less than 0.1) and fairly narrow operational pH range restricts the scope of possible applications. Therefore, in attempting to address these problems, this research group substituted the pyridine moiety with a benzimidazole group[35] (Fig. I.18). The operational pH range only shifted slightly, but improved luminescence efficiency was found. The introduction of the protonated dimethylaminoethyl side chain (**BH1L**) can be tentatively linked to its lysosomal uptake, enabling real time monitoring of fluctuations as small as 0.1 pH units.

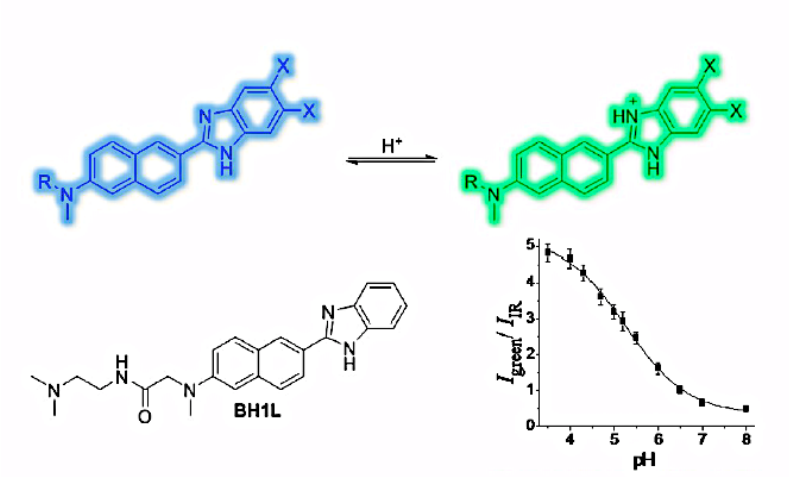


**Fig. 18** Structural rearrangement upon changing pH ; chemical structure of a lysosome-targeted **BH1L** dye (*left)* and *in cellulo* pH-titration curve (*right*).[35]

As the last example of the latest developments in the area of pH-sensing based on small molecules, an unusual example of a pH-responsive fluorescent false neurotransmitter (FFN) will be discussed. Monoamine neurotransmitters are accumulated in synaptic vesicles by vesicular monoamine transporter 2 (VMAT2), which translocates the monoamines (e.g., dopamine) from the cytosol to the lumen of synaptic vesicles. A pH gradient is the driving force, promoting the transport of neurotransmitters into vesicles. Since there are not any examples of pH-dependent probes specifically targeting synaptic vesicles. FFN (**FFN511**), a commercially available vesicle stain, used to stain vesicles, was used as a starting point to create a pH-responsive probe[36] (Fig. I.19). The structure was modified to resemble that of 7-hydroxycoumarin (umbelliferone) to give the probe **Mini101**, which demonstrates pH-dependent luminescent properties, while an additional alkyl chain was attached to investigate the influence of lipophilicity on penetration of synaptic vesicles. The

probe specifically targeted synaptic vesicles without penetration of other acidic organelles, demonstrating the exceptional recognition of the coumarin core structure by synaptic vesicles.

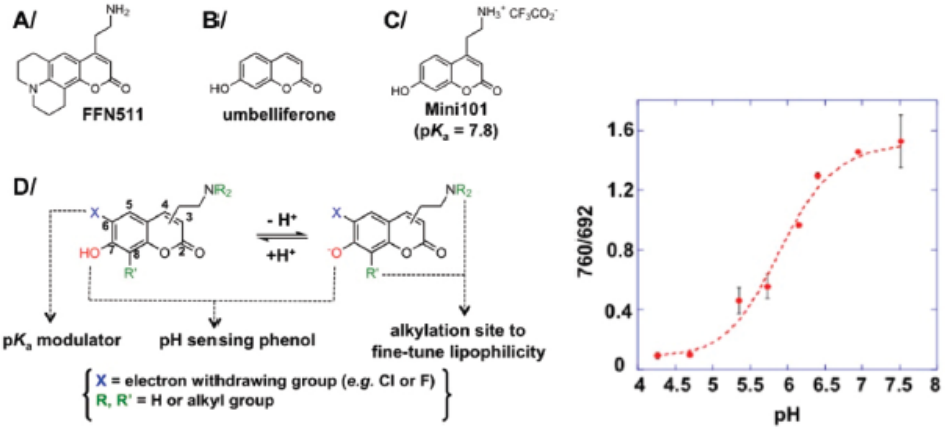


**Fig. I.19** Structures of commercially available **FFN511**, pH-responsive umbelliferone, **Mini101** and the final synaptic vesicle targeting pH-responsive probe (*left*); *in cellulo* pH-titration curve (*right*).[36]

## *I.2.3 pH-sensitive luminescent europium-based probes*

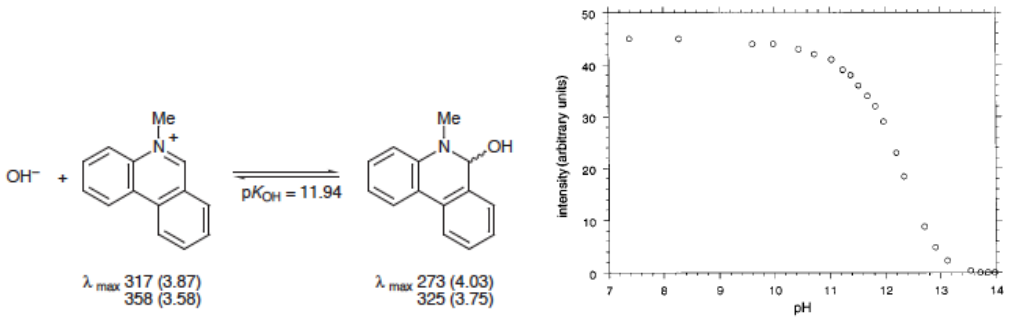


**Fig. I.20** Structural rearrangement upon changing pH (*left*) and pH-dependent change of luminescent intensity of MD transition (*right*).[37]

One of the early examples of a lanthanide-based pH-sensitive probe was given by Parker and was based on the reversible linkage of a hydroxide anion, leading to the formation of a pseudo-base[37] (Fig. I.20). Such transformation resulted in efficient quenching of Eu(III) luminescence upon increasing pH, thought to be due to the considerable hypsochromic shift of the triplet level, resulting in inefficient energy transfer between the ligand and $Eu^{3+}$.

Another class of lanthanide-based pH-sensitive luminescent probes is based on the

principle of quenching of the luminescence of the lanthanide ion by reversible replacement of a coordinated anionic group in the coordination sphere with one or more water molecules[38] (Fig. I.21).

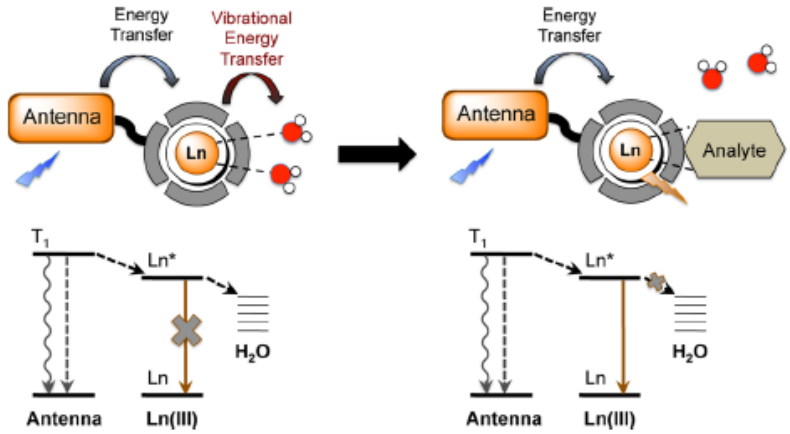


**Fig. I.21** Replacement of water molecules in the coordination sphere of the lanthanide with an intermolecular anionic analyte gives rise to enhanced luminescence intensity.[38]

The most widely used ligand platforms are 1,4,7-triazacyclononane and 1,4,7,10-tetraazacyclododecane (cyclen), which have being thoroughly studied by Parker. These platforms provide several opportunities for chemical modification along with low toxicity, whilst the macrocyclic structure enhances the kinetic stability of the complex with respect to metal dissociation. For example, using a cyclen platform a lysosome-targeting pH-responsive probe was synthesised, that exhibited a dual ratiometric luminescence and CPL response[39] (Fig. I.22). The substituted sulphonamide nitrogen reversibly binds to the $Eu^{3+}$ centre creating the pH-dependent response. The CPL response was related to complex rigidification in the N-bound form at higher pH, resulting in a larger emission dissymmetry factor. The integral azaxanthone chromophore serves both as an efficient antenna to harvest incident light in near UV-region, and as an efficient recognition moiety, promoting cell uptake by macropinocytosis, followed by accumulation of the complex in the lysosomes.

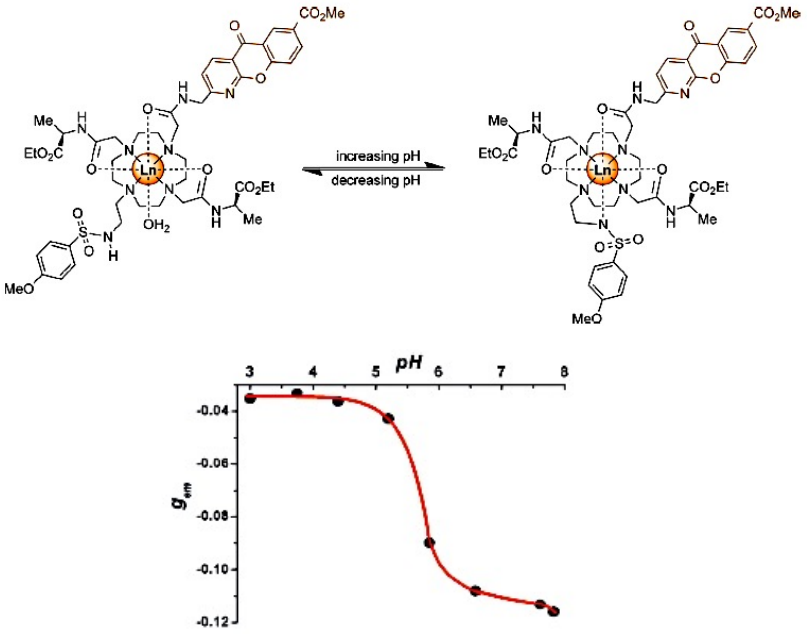


**Fig. I.22** Structural rearrangement upon changing pH (*top*) and pH-dependent variation of dissymmetry factor $g_{em}$ (*bottom*).[39]

Another example is based on 1,4,7-triazacyclononane[40], where a substituted sulphonamide is again the key motif governing the pH response, whilst two pyridylalkynylaryl-based chromophores provide efficient energy harvesting in the near-UV region, along with rigid coordination around $Eu^{3+}$. This probe localised selectively to the endoplasmic reticulum. In this case, both the relative intensity of the hypersensitive transition and the lifetime of the $^5D_0$ excited state were monitored as a function of pH (Fig. I.23). The influence of several bioactive species that can compete with sulphonamide ligation was also studied, revealing that only the hydrogencarbonate ion can bind to the $Eu^{3+}$ causing changes in emission spectral form. The reasons behind selective accumulation of the complex in the endoplasmic reticulum remained uncertain, since analogous complexes with three pyridylalkynylaryl-based chromophores had previously shown selective accumulation in mitochondria[41].

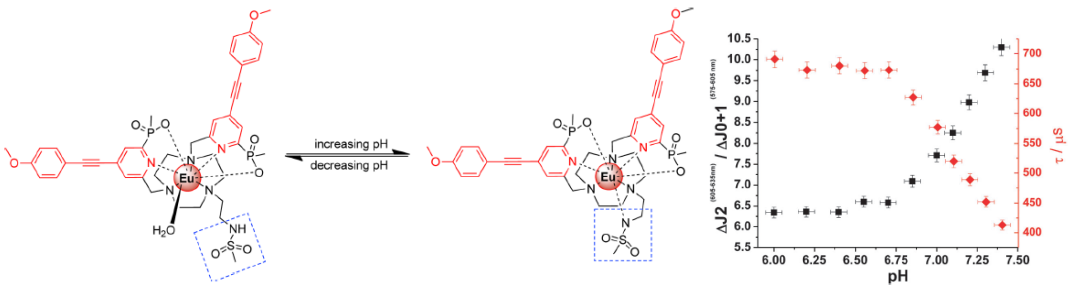


**Fig. I.23** Structural rearrangement upon changing pH (*left*) and pH-dependent variation of relative intensity of the hypersensitive transition (black squares) and lifetime of the $^5D_0$ excited state (red squares) (*right*).[40]

An alternative strategy was employed in recent work by Faulkner, where pH-sensitivity was triggered by reversible changes in the conjugation of the chromophore[42] (Fig. I.24). Upon increasing pH, deprotonation of the $CH_2CO$ group occurs, giving rise to a putative low-lying LMCT state, effectively quenching the $^5D_0$ excited state. In the analogous ytterbium complexes lacking this quenching pathway, such behaviour was not observed. It was also demonstrated that subtle variations in the chemical structure of the chromophore led to considerable changes in the p$K_a$ value of the resulting complex. For this example the p$K_a$ value lies outside the key range and the simple on/off switching mechanism does not allow internal calibration, limiting the scope for any practical application.

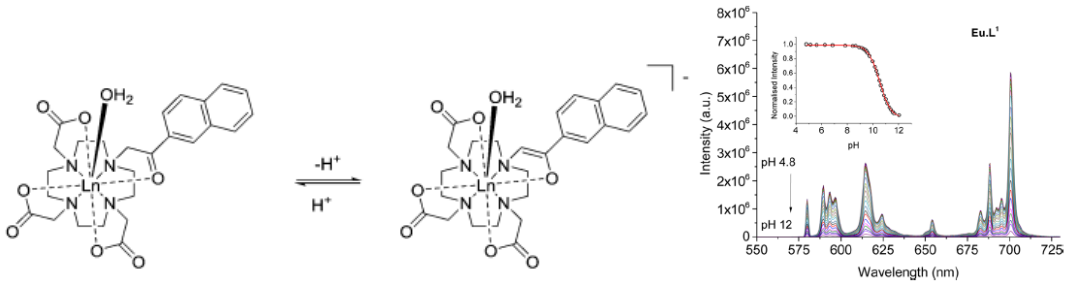


**Fig. I.24** Structural rearrangement upon changing pH (*left*) and the pH-dependent change in luminescence intensity, plotted also in the inset (*right*).[42]

A bimetallic probe with two DO3A fragments with 4-nitrophenol as both a bridging and pH-sensitive moiety has also been reported[43]. Depending on pH of the medium reversible binding of the hydroxyl group of nitrophenolic moiety with one or two of the DO3A fragments occurs, modulating the change in the emission and absorption spectra (Fig. I.25). At low pH values the nitrophenolic moiety is protonated and is not coordinated by either of the metal centres, leading to low emission intensity as a result of quenching $Eu^{3+}$ ions by outer-sphere water molecules. At elevated pH

levels, deprotonation of nitrophenolic occurs leading to its binding first to one DO3A fragment, and then to both of them, giving rise to a significant increase of the total emission intensity as a result of removing outer-sphere water molecules from coordination spheres of $Eu^{3+}$ ions. Thus, two distinct pH-dependent transitions between three states occur in this system, even though the second transition is somewhat less pronounced.

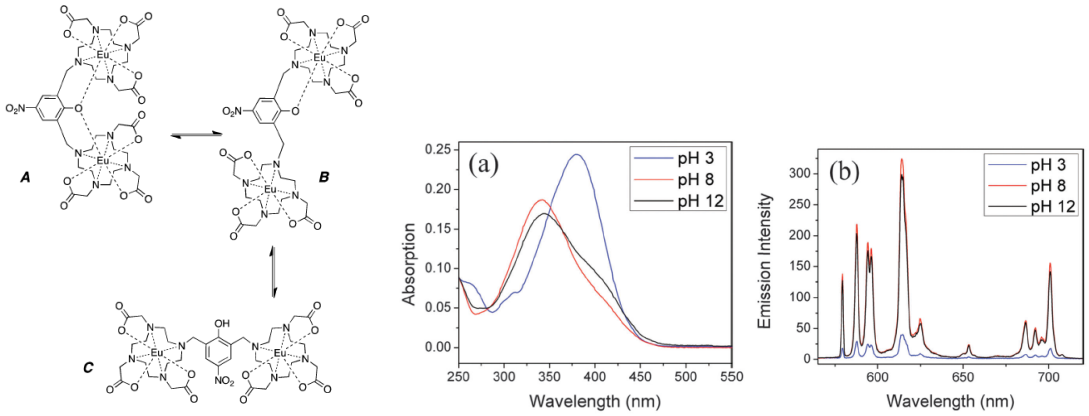


**Fig. I.25** Putative mechanism of reversible binding of nitrophenolic moiety as a function of pH (left) and concomitant changes in the absorption (middle) and emission (right) spectra.[43]

In a related system developed by Allen, the 2-hydroxypropyl group was used in a pH-sensitive moiety bridging two DO3A fragments, which was also reversibly protonated/deprotonated as a function of pH (Fig. I.26)[44]. However, in the present case a bridging hydroxyl group was much closer to both europium centres and therefore renders a more significant perturbation on both metals following pH variation. This resulted in a considerable change of crystal field splittings in the emission spectrum, as well as in the lifetime of an excited state.

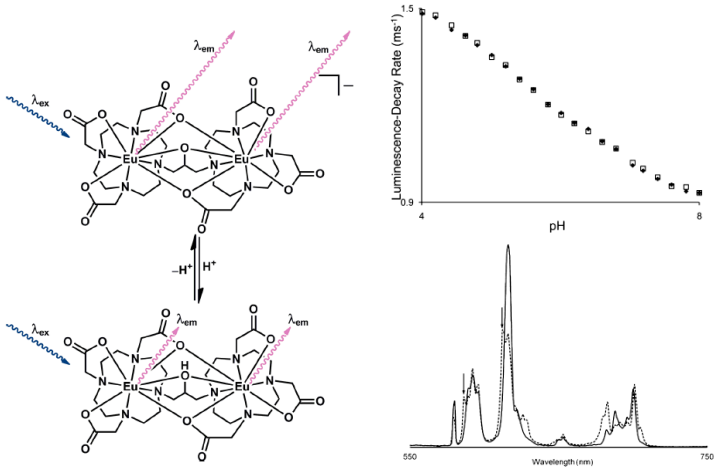


**Fig. I.26** Proposed mechanism of reversible ratiometric pH sensitivity (*left*) and corresponding changes of the lifetime (*top right*) and the total emission intensity (*bottom right*).[44]

A pH-dependent reversible tautomerism can be also employed for modulating a change in the photophysical properties of europium centre, as shown by Lowe in example of a DO3A derivative with a phosphinamide arm (Fig. I.27)[45]. Once protonated, a phosphinamide arm was displaced by coordinated water molecule, increasing the *q* value from 1 to 2 and leading to the decrease of the emission intensity.

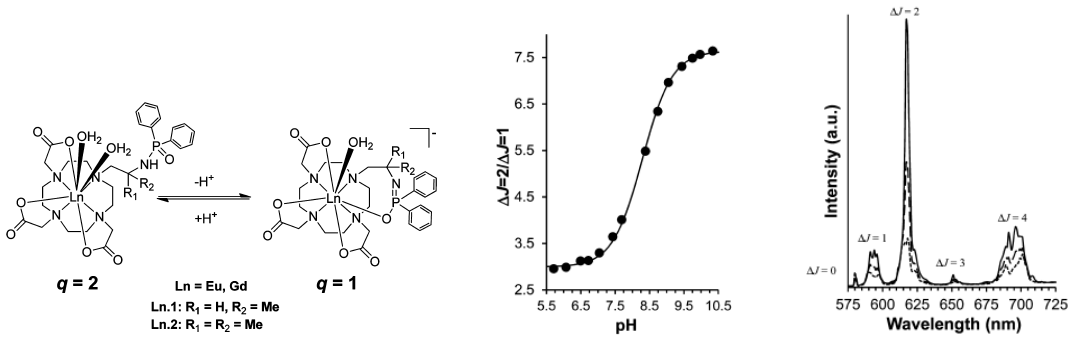


**Fig. I.27** Proposed mechanism of reversible ratiometric pH sensitivity (*left*), pH-titration curve of Eu.1 (middle) and corresponding changes of the total emission intensity (*right*).[45]

## I.3 Sensing of plasma proteins

Human serum is a complex mixture of different proteins, electrolytes, antibodies, antigens, hormones along with compounds of exogenous origin (e.g., drugs and viruses) that can be used for monitoring the health status of a patient. An approximate composition of human plasma is given in Fig. I.28, where all human plasma proteins are subdivided into three groups: classical plasma proteins, tissue leakage proteins and cytokines, spanning a concentration range of at least 10 orders of magnitude. The deviation from a standard concentration of certain proteins may indicate the malfunctioning of certain body systems. In particular, those proteins, which are designated as acute phase proteins, show a large enhancement or decrease of their concentration in response to inflammation processes occurring in the body (e.g. $\alpha_1$-AGP, $\alpha_1$-AAT, etc.).

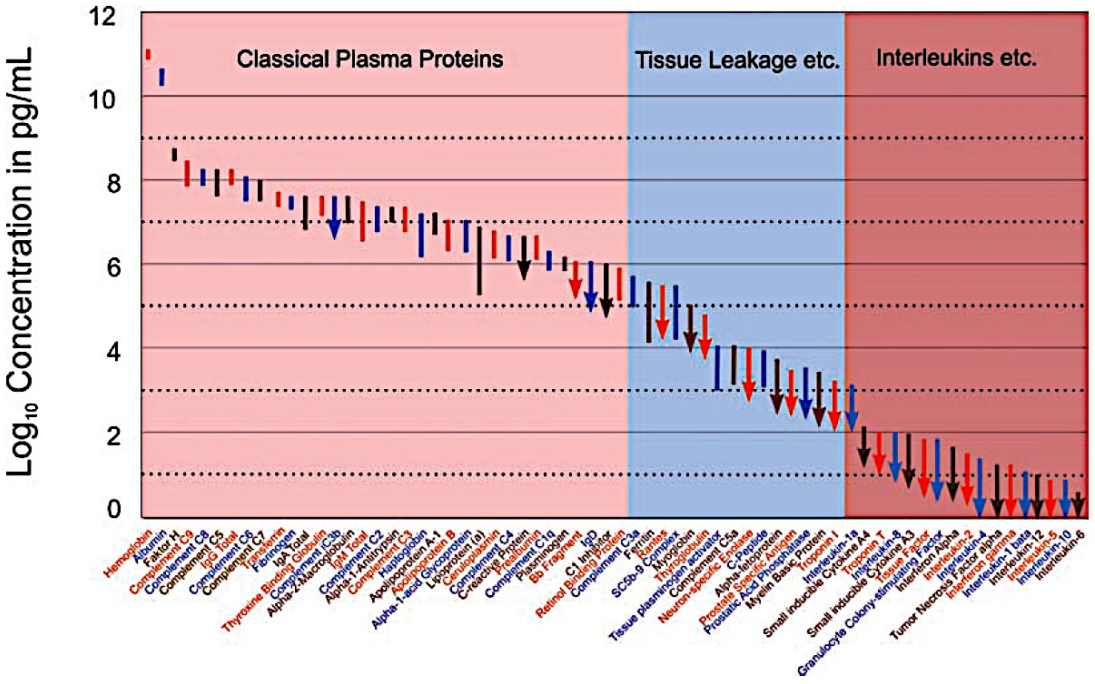


**Fig. I.28** Concentration ranges of major proteins in human plasma. An arrowhead indicates that only the upper limit is indicated.[46]

The nomenclature of serum proteins (α, β, γ, etc.) derives from the order of fractions during electrophoresis of a serum sample (Fig. I.29).

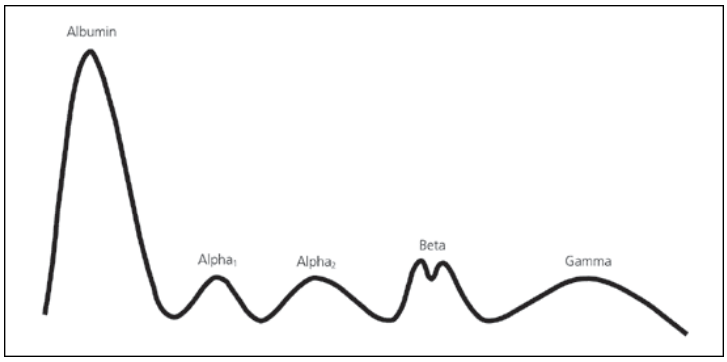


**Fig. I.29** Typical pattern for serum electrophoresis in a healthy human.[47]

### *I.3.1 Binding human serum albumin*

The most abundant protein (55% of total amount of serum proteins) in human serum – serum albumin – plays a significant role as a carrier, delivering fatty acids, hormones and drugs, maintaining the oncotic pressure and pH of the blood. Even though its physiological role is not completely understood, several studies suggest that it can be used as a biomarker to predict the survival rate of patients with terminal conditions[48],[49]. Since serum albumin is biosynthesised in the liver and excreted through the kidneys, its concentration may be indicative of chronic liver (under-expression) or kidney (over-expression) failure.

Multiple studies on binding essential drugs were carried out over the past decades, which revealed two primary binding sites in HSA, which are according to Sudlow's nomenclature, are called site I and site II and sometimes are referred to as warfarin and ibuprofen binding sites, respectively, named after two drugs that bind to these two pockets (Fig. I.30). In general, it has been demonstrated that bulky heterocyclic anionic drugs preferentially bind to FA-1 (FA-1 to FA-7 are seven fatty acid binding pockets), whilst extended aromatic carboxylates are more likely to bind to FA-2[50]. However, secondary binding sites are sometimes observed for those drugs, which had been previously considered to bind selectively at just one site. For example, although the thyroid hormone thyroxine preferentially binds to site I, it also binds to site II and FA5 as secondary sites with different binding constants. The binding constant values given for the drugs in the literature are usually averaged values over all binding sites. They are usually determined by an equilibrium dialysis of the HSA/drug complex from any excess of added drug or by competitive binding studies with a drug with a known binding constant by following changes in the absorption and emission spectrum. The primary binding site of a drug can be determined from

the crystal structure of HSA co-crystallised with this drug, or by competitive bindings studies with drugs having a well-established primary binding pocket.

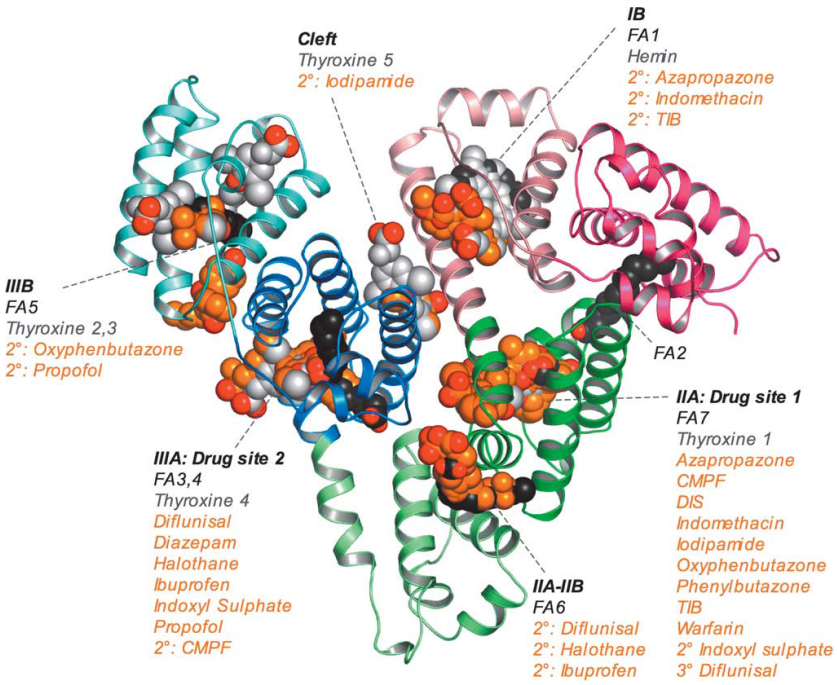


**Fig. I.30** Primary drug-binding sites in human serum albumin and corresponding site-selective drugs. Drug-site selectivity is provided from crystallographic data.[51]

The advent of new bright and selective probes for HSA might help to follow the subtle changes in its concentration and can also help to establish the binding pattern of novel drugs. From a practical point of view, only the probes showing a turn-on response upon binding to HSA possess a real interest and therefore only those probes will be considered henceforth. Also, it seems that in many cases no discrimination between human and bovine serum albumins is made and the latter is usually used as a more affordable alternative, although it was shown that the response in both cases can be dramatically different.

One of the basic principles behind the enhancement of the emission intensity once the probe is bound to the protein is the change of the local medium surrounding the probe going from water molecules to amino acid residues of the protein with little or no access of water molecules, giving rise to changes of physical parameters, such as dielectric constants, viscosity, spacious confinement, lack of OH-oscillators as potential quenchers of the emission, etc.

Solvent dependent aggregation is a well-known phenomenon, which is highly dependent on the nature of the solvent used, but usually it is considered detrimental for practical applications, as formation of excimers and exciplexes may serve as efficient quenching pathways. However, a few examples of exactly the opposite behaviour have been reported, for instance the sodium 1,2-*bis*[4-(3-sulfonatopropoxyl)phenyl]-1,2-diphenylethene (**BSPOTPE**), which showed a turn-on of the total emission intensity on going from aqueous solution to acetonitrile due to formation of emissive aggregates, which restrict molecular rotation in the molecule causing very low emission efficiency. The same principle was employed for sensing HSA, since binding of **BSPOTPE** to the protein causes the restriction of molecular motion inside the binding pocket, giving rise to an enhancement of the emission intensity (Fig. I.31)[52].

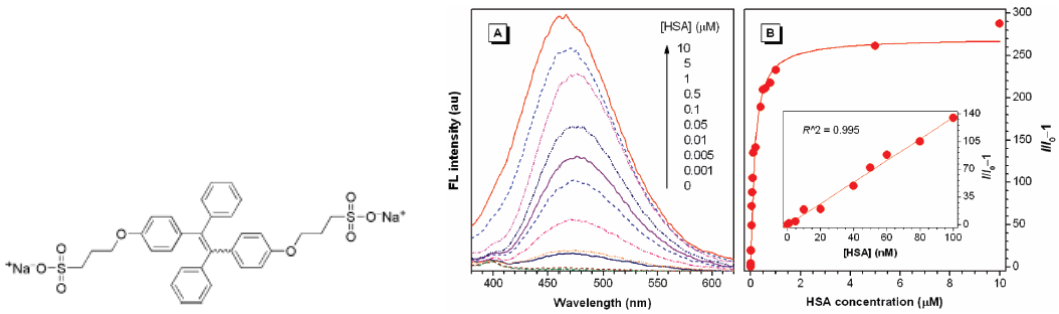


**Fig. I.31** Molecular structure of **BSPOTPE** (*left*) and the emission intensity response as a function of added HSA (*right*).[52]

On the other hand, a more classical approach was demonstrated with 3,30-di(3-sulfopropyl)-4,5,40,50-dibenzo-9-methylthiacarbocyanine triethylammonium salt (**MTS**), where an initial aggregate in aqueous solution dissociates upon binding to the protein, giving rise to the appearance of new absorption and emission bands corresponding to the monomer, with a concomitant decrease of the bands corresponding to the aggregate (Fig. I.32)[53]. Since in each case (a monomer and an aggregate) the absorption band is in the visible part of the spectrum, an easy evaluation of colour can be undertaken.

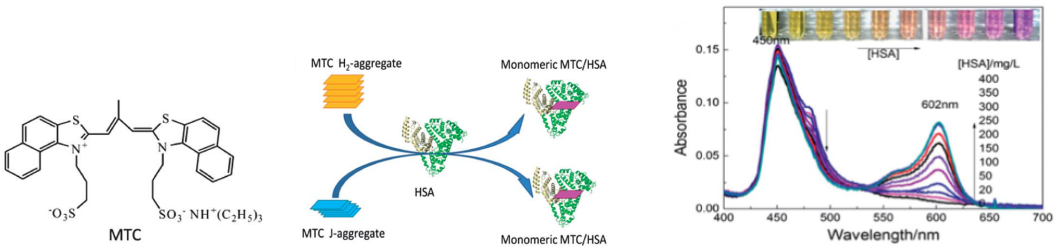


**Fig. I.32** Molecular structure of **MTC** (*left*), sensing mechanism upon binding to HSA (*middle*) and change in the emission spectrum upon addition of HSA for $H_2$-aggregates (*right*).[53]

The high hydrophobicity of HSA was also invoked to account for the high selectivity of 2,4-dihydroxyl-3-iodo salicylaldehyde azine (**DISA**) towards HSA, where a ten-fold increase of the emission intensity was observed upon binding to HSA (Fig. I.33)[54]. It was shown that an increase in emission intensity follows the hydrophobicity trend for selected proteins, being large for HSA and lowest for ovalbumin.

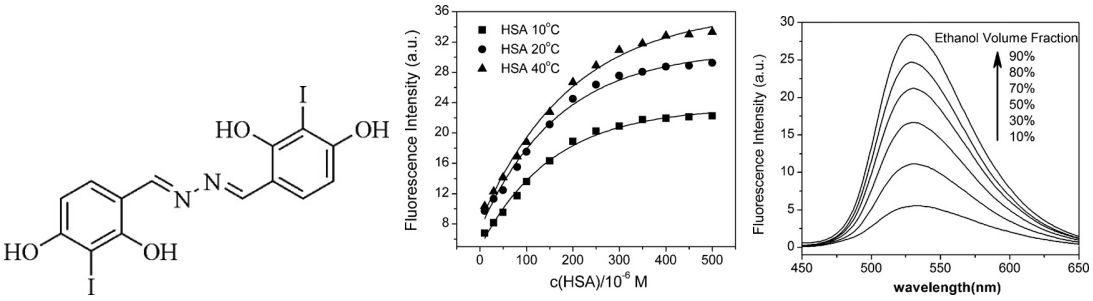


**Fig. I.33** Molecular structure of **DISA** (*left*), enhancement of the emission intensity upon addition of HSA (middle) and change of the emission intensity following the change in polarity (right).[54]

Even though very limited attention has been dedicated to the probes that can detect human serum albumin selectively over serum albumins of other species, a study on the binding of rosamine **G13** with different serum albumins has been carried out (Fig. I.34). The HSA showed the most significant rise (36-fold) in the emission intensity over rabbit serum albumin (15-fold), bovine, sheep, porcine (all less than 5-7-fold)[55]. The response behind the proposed probe is based on a restricted rotation of the 9-phenyl ring in the protein, leading to an increased quantum yield of the emission. The observed variation in quenching efficiency reflects subtle changes in the structure of the binding pockets, despite at least 75% homologenity in their structures.

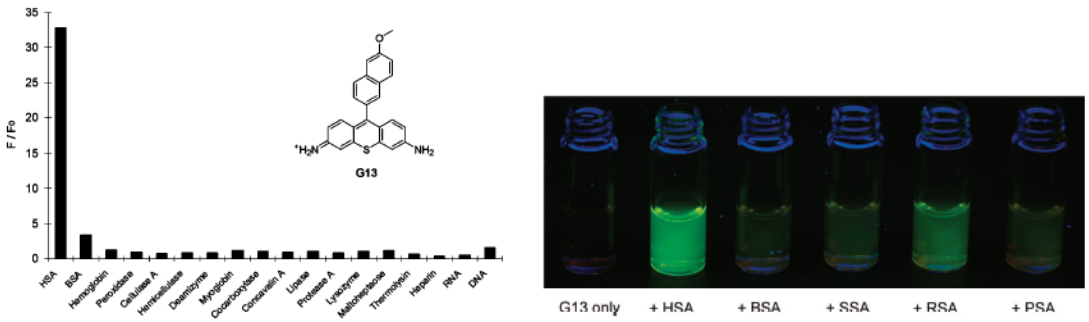


**Fig. I.34** Molecular structure of **G13** and its selectivity towards selected proteins (*left*) and photographs of solutions containing **G13** and different serum albumins (*right*).[55]

Another example of a different response towards HSA over other species' serum albumin is the 'push-pull' system **DH1**, where the aromatic amine served as an electron donor and malononitrile as an electron acceptor, giving rise to a strong ICT state that is very sensitive to the local environment. Bearing in mind that the hydrophobicity of HSA and BSA binding pockets is different, the intensity increase upon binding to HSA (70-fold) and BSA (9-fold) is very different. The ICT state which quenches the fluorescence is highly dependent on the medium polarity, and consequently on the hydrophobicity of the binding pocket (Fig. I.35)[56].

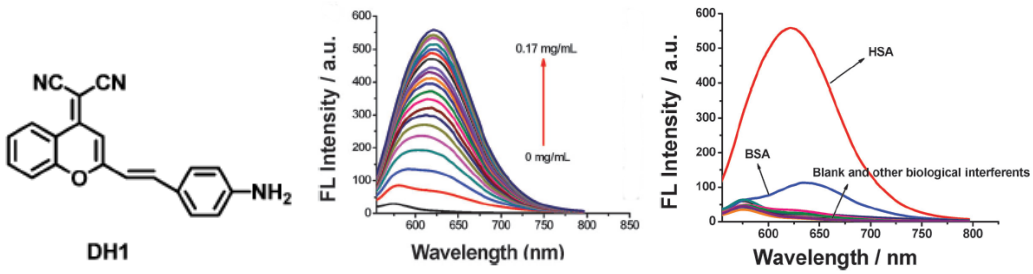


**Fig. I.35** Molecular structure of **DH1** (*left*), enhancement of luminescence intensity of **DH1** as a function of HSA added (*middle*) and selectivity of **DH1** over other selected proteins, in particular BSA (*right*).[56]

Evidence in favour of these hypotheses was provided by polarity-dependent studies of the emission intensity in water/1,4-dioxane mixtures, showing a steady increase in the emission intensity upon reducing solution polarity. In a related study, another 'push-pull' probe **PQX** was thoroughly investigated to probe the polarity of the binding site of BSA (Fig. I.36)[56]. To calibrate the polarity probe, a series of organic solvents with different polarities (expressed in terms of Reichardt's coefficients $E^N_T$) was used to plot the dependence between the emission maximum and $E^N_T$. Upon

binding to BSA, the fluorescence maximum of **PQX** was blue-shifted from 608 nm for the unbound probe to 530 nm, approximately corresponding to the band maximum of **PQX** in acetone.

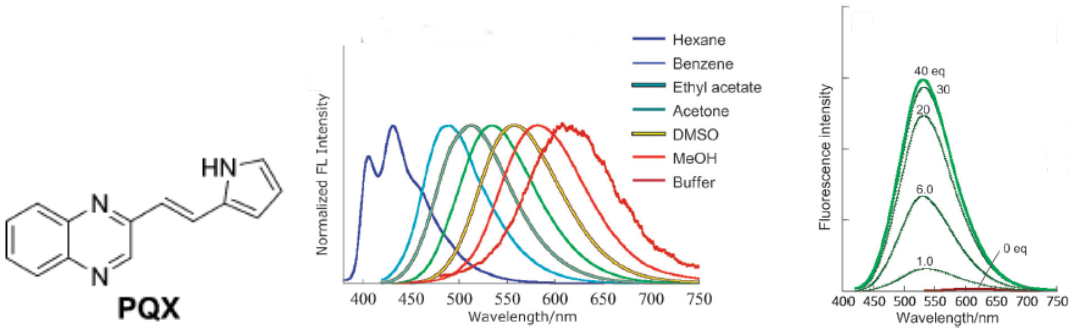


**Fig. I.36** Molecular structure of **PQX** (*left*), emission spectra of **PQX** in different solvents (*middle*) and change of the emission spectrum upon addition of BSA (*right*).[56]

As an example of the rational design of these 'push-pull' systems, the nature of the substituent was varied to alter the magnitude of the dipole moment and hence the energy of the ICT state. It was demonstrated (Fig. I.37) that on going from dimethyl- to diethyl- and diphenylamine the polarity-sensitivity reduced, as well as selectivity towards HSA. The significant decrease from diethyl- to diphenylamine could be partially explained by an increased steric demand and lower solubility[56]. In the case of diphenylamine, no selectivity was observed towards HSA over other abundant proteins.

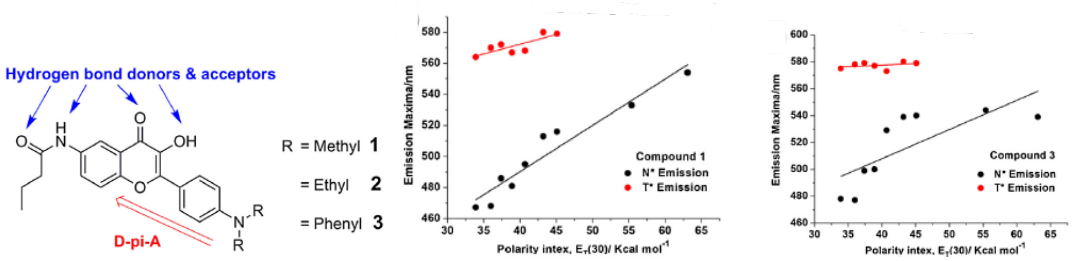


**Fig. I.37** Molecular structure of a studied series of probes with a dipole moment depicted (*left*), change of the emission intensity of probe **1** (*middle*) and probe **3** (*right*) as a function of polarity of the solvent used.[56]

The development of two-photon probes has been gaining momentum over the last decade and therefore it is not surprising that a two-photon probe **Ant-PIm** for HSA sensing was reported[57]. A 'push-pull' system with anthracene as an electron acceptor and two substituted alkynylaniline moieties as electron donors provided both a relatively high TPA cross-sections for the unbound ($\sigma_{2\text{Ant-PIm}}$ = 813GM at 820

nm) and bound dye ($\sigma_{2Ant\text{-}PIm-HSA}$ = 469 GM and $\sigma_{2Ant\text{-}PIm-BSA}$ = 443 GM at 820 nm), along with high polarity dependence of the emission intensity. The latter effect was manifested in the rise of the emission intensity with a concomitant hypsochromic shift of the emission band upon binding HSA (Fig. I.38).

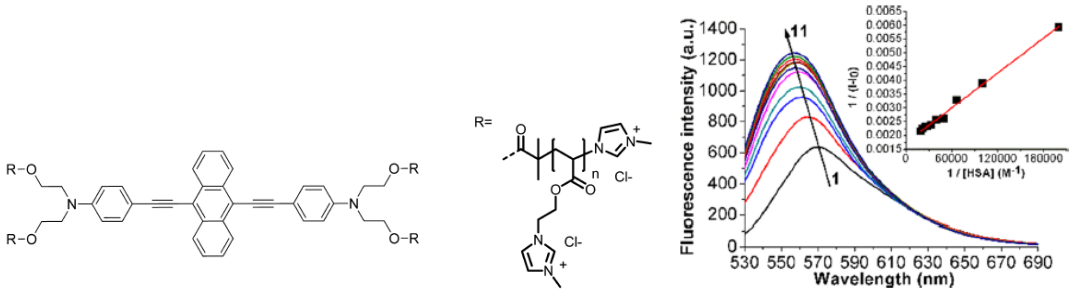


**Fig. I.38** Molecular structure of **Ant-PIm** and change of the fluorescence intensity upon addition of HSA.[57]

A combination of the two aforementioned sensing principles – polarity-sensitive ICT state and TICT state – was devised in a single probe **AL-1**, which showed both high selectivity towards HSA over BSA due to the presence of an ICT state and a 'turn-on' response upon binding of the protein, as a result of unrestricted torsional motion in aqueous media (Fig. I.39)[58]. In a very similar study, an additional functionality – pH-sensitive emission response – was introduced to the polar probe benzo[e]indolium, whilst the electron-donating moiety and the length of the spacer was altered (Fig. I.39)[59]. Similarly to the previous example, both the TICT and ICT states are responsible for quenching of the total emission intensity in aqueous solution.

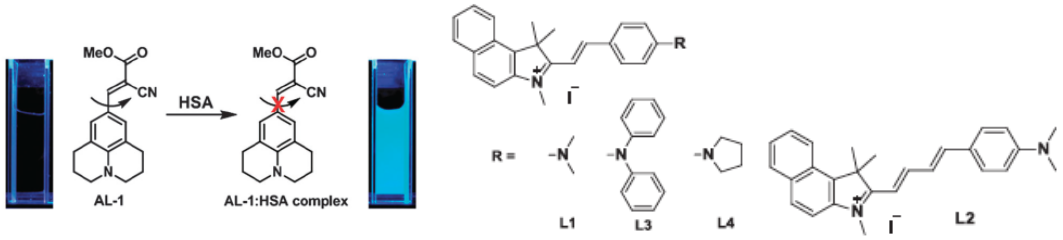


**Fig. I.39** Restricted rotation of **AL-1** bound to HSA leads to an increase of the emission intensity (left)[58] and benzo[e]indolium derivatives **L1-L4** (*right*).[59]

Apart from reversible probes, which have been considered so far and which can be easily displaced by addition of a more strongly binding drug, irreversibly binding probes have also been created. It was shown that HSA hydrolyses drugs possessing

ester groups and this finding was employed in the irreversible tagging of HSA by a series of probes (Fig. I.40)[60]. In the absence of HSA the emission from these probes was quenched by PET, but was recovered once the probe bound to HSA.

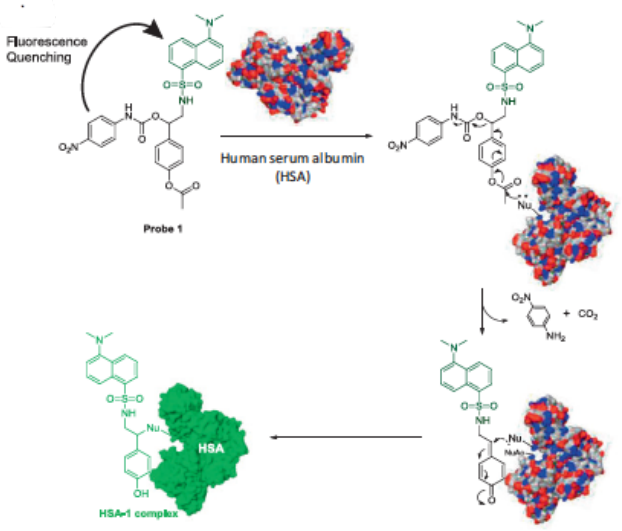


**Fig. I.40** Mechanism of irreversible binding of luminescent tags as a result of pseudo-esterase activity of HSA.[60]

The analysis of HSA content is often performed in complex mixtures, as blood plasma and urine, which gives significant residual emission bands in the total emission spectrum, hampering the read-out of data. One possible solution to overcome this obstacle is the use of time-gating instrumentation using probes emitting on a millisecond timescale. Transition metal and lanthanide complexes are among those probes, which are worthy of mention, even though just a few examples of these systems have been reported so far. The cyclometalated iridium(III) complex with a 'push-pull' ligand, showed a 5-fold increase in the emission intensity along with a 25-nm hypsochromic shift (Fig. I.41)[61]. The response towards BSA was only 4 times lower, what can be again ascribed to the differences in hydrophobicity of drug-binding pockets between HSA and BSA. Competitive binding studies suggest Sudlow's site I as the binding site. Binding to both of the Sudlow's sites has been observed for an iridium(III) complex with two different N,S-chelating ligands[62].

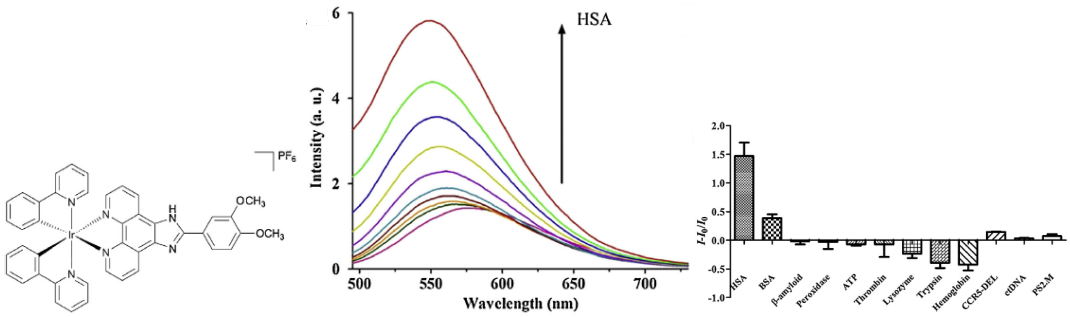


**Fig. I.41** Molecular structure of cyclometalated iridium complex (*left*), change of the phosphorescence intensity upon binding to HSA (*middle*) and selectivity over other selected proteins (*right*).[61]

The only reported example of a lanthanide complex as an HSA probe was a terbium complex with a polydentate ligand bearing two 2-methyl-5-nitroimidazole moieties, known for their binding to HSA (Fig. I.42)[63]. The complex had one water molecule bound in the absence of the protein and this water molecule is likely retained upon binding to the protein, although no q values were provided for the complex with HSA bound. The apparent mechanism behind an enhancement of the total emission intensity upon HSA binding is reduction of $-NO_2$ groups in 1,3-diazole moieties, which were probably responsible for quenching of the emission in the absence of the protein. On the other hand, as the complex was excited at $\lambda = 265$ nm, it was probably primarily sensitised through conjugated amino-acids on a side chain of HSA, which was the major cause of the observed increase of the total emission intensity.

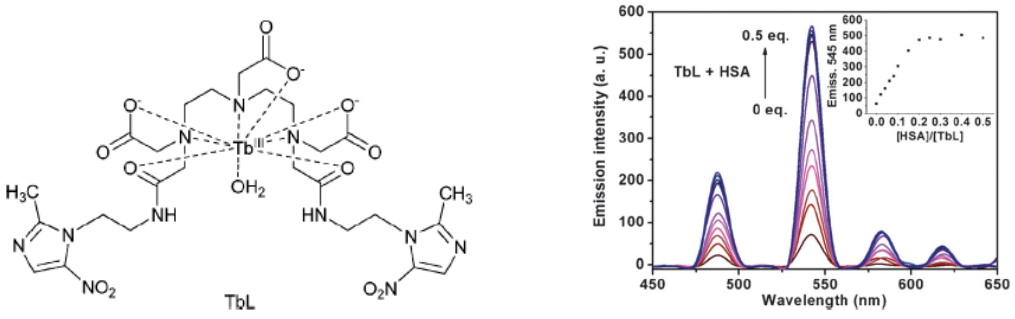


**Fig. I.42** Molecular structure of terbium complex and change of its emission intensity upon binding to HSA.[63]

### *I.3.2 Binding human acidic glycoprotein ($\alpha_1$-AGP)*

Acidic glycoprotein is the second most abundant protein in the blood plasma and belongs to the group of acute phase proteins, meaning that their concentration is highly susceptible to the occurrence of inflammation processes in the body. In comparison with HSA, there are fewer reports of the sensing of $\alpha_1$-AGP *in vitro* and in biological samples, primarily due to the 30 times lower concentration of $\alpha_1$-AGP compared to HSA. Since $\alpha_1$-AGP also plays a significant role in drug delivery, multiple studies have been dedicated to unraveling binding motifs of common drugs. It was revealed that only one primary binding site is present in $\alpha_1$-AGP. However, the analysis is considerably hampered by the presence of different human $\alpha_1$-AGP polymorphs (F1 and/or S and A) with different amino acid sequences, which are usually not separated before performing binding studies. F1 and S polymorphs, which make up 70% of commercially available $\alpha_1$-AGP, differ in only one amino acid only at position 20 (Gln/Arg substitution). Therefore, they are often considered together as the F1*S polymorph (ORM 1)[64].

At the same time, polymorph A (ORM 2) has 22 amino acids replaced and in several cases showed different drug-binding properties. Apart from the co-existence of three polymorphs with variable ratio between them, the glycosylation pattern of $\alpha_1$-AGP varies as well. However, it was shown that these changes do not have a pronounced effect on drug-binding properties and therefore are usually ignored.

The only example of the selective binding of luminescent tag to human $\alpha_1$-AGP is the Eu(III) achiral DO2A-derived complex **[EuL$^{x1}$]** bearing two azaxanthone chromophores, which showed both the increase of the total emission intensity, as well as the appearance of the strong induced CPL signal (Fig. I.43)[65]. It was hypothesized that upon protein binding, the nitrogen of one of the chromophores is replaced by the oxygen of Glu-64 in the coordination sphere of Eu(III). In addition one of the chromophores dissociates and is bound to the $\alpha_1$-AGP drug-binding site. Indeed, CD studies revealed the presence of two different azaxanthone chromophores in the protein adduct. Even though the overall emission intensity changed in the presence other plasma proteins, the induced CPL signal was

considerably less intense and its spectral form was easily distinguishable from the one caused by $\alpha_1$-AGP. Furthermore, competitive drug-binding studies were carried out by following the change of the dissymmetry factor $g_{em}$[66].

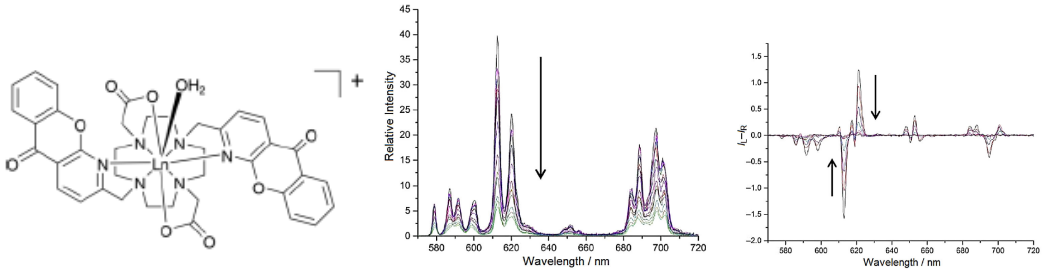


**Fig. I.43** Molecular structure of europium complex **[EuL$^{x1}$]** (*left*), decrease of the total emission intensity (*middle*) and CPL signal (*right*) upon addition of racemic bupivacaine to a complex **[EuL$^{x1}$]*a$_1$-AGP**.[65],[66]

## *I.3.3 Other plasma proteins*

Other plasma proteins can potentially be used as targets for molecular probes. $\alpha_1$-Antitrypsin – an endogenous and exogenous protease inhibitor – is also an acute phase protein, whose concentration in blood changes in response to inflammatory processes. Unlike $\alpha_1$-AGP, very few attempts of drug-binding studies have been reported[65] and therefore very limited data is available on its drug-binding site behaviour.

A series of publications was dedicated to the binding of lanthanide ions to apo-transferrins (Tf) – an iron-binding glycoprotein, which controls the level of free iron in plasma by reversible binding of two Fe(III) ions – one binding site per lobe (Fig. I.44). The lanthanide ions occupy the same coordination sites as Fe(III) with the only difference that two additional water molecules are bound to the lanthanide, increasing the coordination number from 6 – typical for Fe(III) – to 8[67]. The total emission and CPL spectral studies of EuTf and TbTf complexes revealed the equivalence of both binding sites in a transferrin, by comparing spectral signature after addition of one equivalent of $Tb^{3+}$ to monoferric N- and T-terminal transferrins (Fig. I.44)[68]. Despite the fact that the binding constant for lanthanides (p$K_b$ = 13) was much lower than for iron (p$K_b$ = 20), addition of $Tb^{3+}$ to a human body-fluid sample facilitated detection and subsequent separation of TbTf complex using HPLC, without interference from residual signals[69].

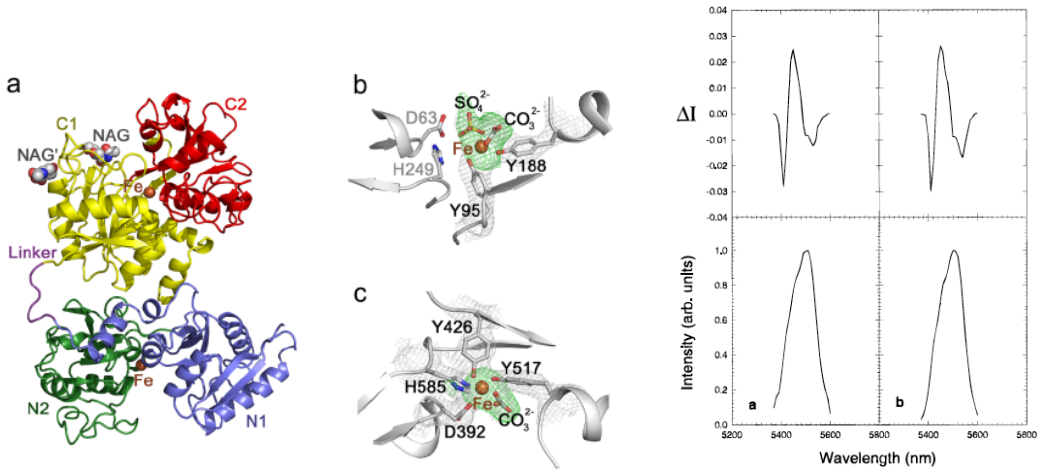


**Fig. I.44** Two coordination sites for binding Fe(III) in human serum transferrin (*left*).[70] CPL (*top right*) and total emission spectra (*bottom right*) of $Tb^{3+}$ bound to monoferric N-terminal (a) and C-terminal (b) transferrins.[68]

## I.4 Sensing of biologically relevant anions with europium(III) complexes

The design of anion-selective probes is governed by the physicochemical properties of the analyte. Key properties to consider include the nature of anion binding to the metal centre, the potential to engage in stabilising hydrogen bonding or π–π-stacking with the probe, the anion charge density and p$K_a$. Such considerations have been taken into account in the series of ratiometric Eu(III) probes that have been devised for citrate, lactate, urate and bicarbonate, used successfully in complex media and applied in biological studies both *in vitro* and *in cellulo*[71],[72],[73].

Europium complexes with high selectivity towards specific anions are still relatively scarce. Here, the discussion is restricted to two limiting cases–examining fluoride and nucleotide sensors. In the first case, the small fluoride ion can replace a water molecule in the coordination sphere of $Eu^{3+}$ at sub-millimolar concentrations, if additional stabilisation through formation of hydrogen bonds with $F^-$ is provided. In the second case, the bulky nucleotide molecules possess both a nitrogenous base capable of π–π-interactions with a probe and a phosphate group, which can coordinate to $Eu^{3+}$.

In the majority of cases discussed in this section the binding molecule/ion replaces a coordinated water molecule(s), so that the photophysical response accompanying the binding event is an increase of total luminescence intensity, upon removal of the O−H quenching oscillators. In parallel, alterations to the $Eu^{3+}$ spectral profile occur, caused by changes in the nature and polarisability of the coordinated donors that define the ligand field.

The fluoride ion plays an essential role in many physiological processes, such as bone and enamel mineralisation. However, if fluoride is present in excessive amounts, it can lead to disturbances of bone homeostasis (skeletal fluorosis) and enamel development (dental fluorosis)[74]. Therefore, its concentration in drinking water and biological tissues needs to be monitored. The fluoride anion is comparable in size with $OH^-$ (1.29 Å for $F^-$ and 1.32 Å for $OH^-$), and their competitive binding can present a challenge. However, within the physiologically relevant pH range, the concentration of $OH^-$ in aqueous solutions is very low and does not usually hamper

$F^-$ binding. As a hard Lewis base, fluoride has a relatively high affinity towards hard Lewis acids, such as lanthanide ions. Therefore, the use of lanthanide complexes as fluoride probes is sensible. However, the usually observed binding constants of fluoride ions for lanthanide complexes in water are relatively low ($\log K_a$=1.5–3), due to the high free energy of hydration of the fluoride ion ($-\Delta G°_{hydr}$=465 kJ mol$^{-1}$). Efficient binding has been observed only with cationic complexes, where a water molecule in the ninth coordination site of europium can be replaced by the fluoride ion, stabilised by additional interactions. For instance, the coordinated $F^-$ can be additionally stabilised by $F^-\cdots$CH interactions, as in the europium complex reported by Butler[75]. The europium complex **EuL$^{1\text{-}2}$** based on a cyclen ring and bearing two quinoline chromophores in trans-positions has a coordinated water molecule that can be replaced by $F^-$, giving rise to a 9-fold increase of luminescence intensity (Fig. I.45). In parallel, a large change of the emission profile was observed within the relevant range (20–210 μm), typical for water fluorination. Although no anion binding was observed in the case of $Cl^-$, $Br^-$, $I^-$, $NO_3^-$, $HSO_4^-$, $HPO_4^{2-}$, and $CH_3CO^{2-}$, competitive binding of $HCO_3^-$ was revealed, resulting in similar photophysical changes. The high selectivity towards $F^-$ and high stability of the formed complex ($\log K_a$ = 4.1) was attributed to an additional stabilisation through formation of relatively strong C−H$\cdots$F$^-\cdots$H−C interactions between coordinated $F^-$ and the quinoline moieties.

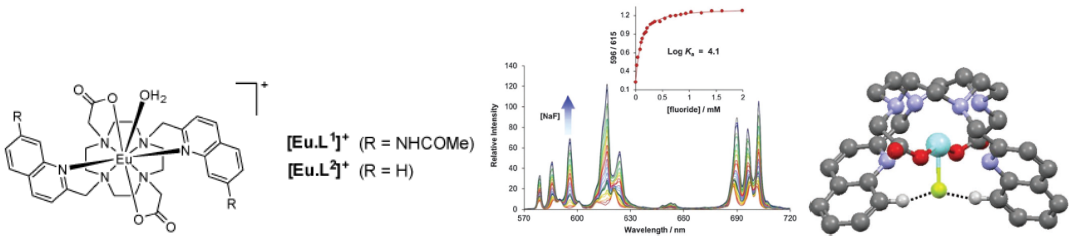


**Fig. I.45** Molecular structure of complexes **EuL$^{1\text{-}2}$** (*left*), change of the total emission intensity upon addition of $F^-$ (*middle*) and DFT-optimised structure of **EuL$^2$** with a bound fluoride anion (*right*).[75]

Another example, involving stabilisation of fluoride binding by hydrogen bond formation, was reported by Tripier[74]. In this case, a fluoride anion bridges two cationic cyclen-based europium complexes bearing two picolyl and two acetamide pendant arms featuring a linear Eu−F$^-$−Eu bonding array. Upon addition of fluoride, two water molecules are displaced from each site by one fluoride ion, giving rise to the "sandwich"-like structure, **[EuL$^{x2}$]**, which is stabilised by π–π stacking

interactions between opposite pyridyl rings (Fig. I.46). The fluoride ion gains additional stabilisation inside this double-decker structure by formation of C−H···F$^-$···H−C hydrogen bonds with pyridyl moieties. When pyridyl moieties were substituted with two other acetamide arms, the formation of "sandwich"-like structure was not observed and substantially lower affinity towards F$^-$ was discovered, emphasising the importance of the pyridyl units in enhancing fluoride binding.

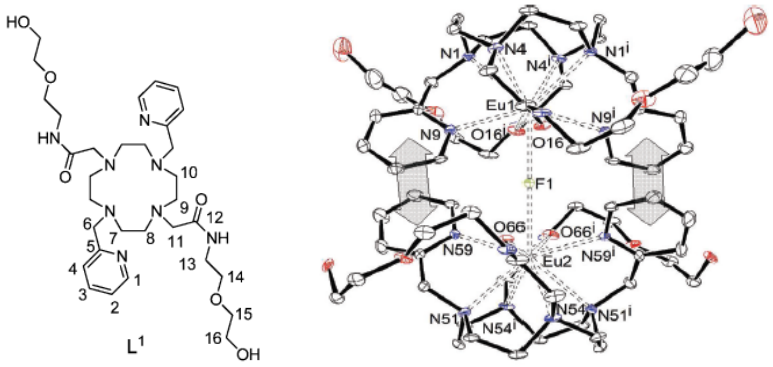


**Fig. I.46** Molecular structure of the ligand (*left*) and the crystal structure of a dimer **[EuFL$^{x2}$]$_2$**, with a fluoride anion embedded in between (*right*).[76]

In a subsequent study[77] Tripier modified the complex by replacing the acetamide arms with carboxylate moieties to reduce the overall complex charge, alleviating repulsion during formation of the putative dimer. Substituted pyridyl units were replaced with indazole moieties, in order to provide additional stabilisation by hydrogen bonding between F$^-$ and NH groups of indazole. An increased molar extinction coefficient also resulted. The dimeric complex, **[EuL$^{x3}$(H$_2$O)]**, showed very high sensitivity (24 nm) and selectivity towards fluoride anions over Cl$^-$, Br$^-$, $HCO_3^-$, $CH_3CO_2^-$, and $HPO_4^{2-}$, resulting in the 22-fold increase of the overall emission intensity, accompanied by a pronounced change of the spectral profile (Fig. I.47). Analysis of the crystal structure reveals that the high association constant (log$K_a$ = 13.0) can be explained by stabilisation of the dimer by four hydrogen bonds formed between the nitrogen atoms of the indazole moiety of one complex and the oxygen atoms of the carboxylate arms of another, as well as by formation of a Eu−F$^-$−Eu bond.

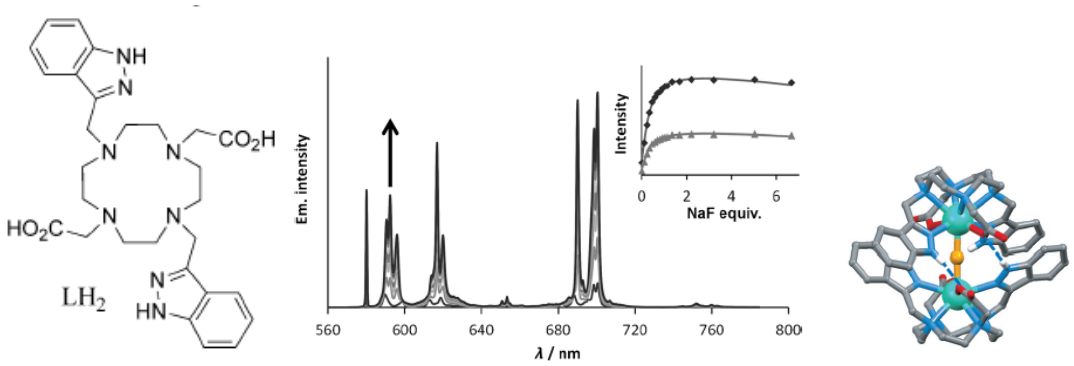


**Fig. I.47** Molecular structure of the ligand (*left*), enhancement of the total emission intensity as a function of added $F^-$ (*middle*) and the crystal structure of a dimer $\mathbf{[EuFL^{x3}]_2}$ with a fluoride anion embedded in between (*right*).[77]

A symmetric europium complex $\mathbf{EuL^{Py}}$ based on the cyclen core with four pyridyl substituents has been analysed by Faulkner (Fig. I.48)[78], revealing a high affinity towards $F^-$ ($\log K_a = 5.0$). Since no competitive binding studies have been carried out, the selectivity of the proposed complex towards fluoride ions remains unclear, although additional stabilisation of $F^-$ might be expected by formation of hydrogen bonds with the nitrogen atoms of the pyridyl groups.

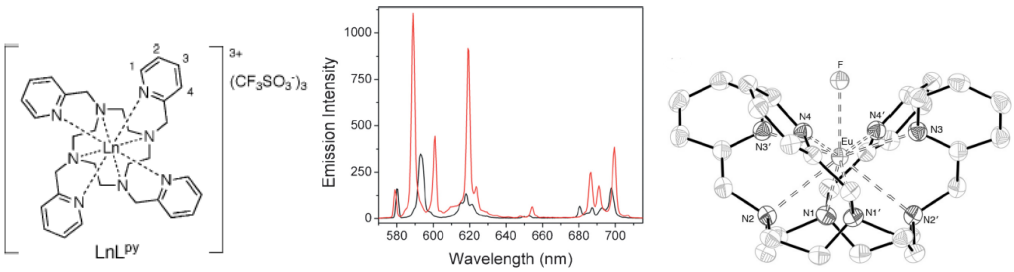


**Fig. I.48** Molecular structure of the ligand (*left*), the total emission intensity before (black line) and after (red line) addition of $F^-$ (*middle*) and the crystal structure of a $\mathbf{EuL^{Py}}$ (*right*).[78]

Adenine nucleotides - adenosine monophosphate (AMP), adenosine diphosphate (ADP) and adenosine triphosphate (ATP) - play an essential role in bioenergetics, participating in energy-transfer processes required for normal functioning of the cell. In order to create luminescent europium probes that can bind one adenosine derivative selectively, steric control should be imposed by ingenious design of the ligands, so that the binding interaction involves both the adenosine and phosphate parts of the molecule. In general the affinity order, determined by the charge of the phosphate moiety, is usually found to be ATP>ADP>AMP, and a different order of selectivity between these species remains a challenge. With this in mind, Albrecht[79] has studied a coordinatively unsaturated double-stranded helical dinuclear europium

complex **[EuL$^{x4}$]** that causes a significant 64-fold increase of luminescence intensity upon binding AMP molecules with selectivity over ATP and ADP, as well as other biologically relevant ions (Fig. I.49). Two strands of *bis*(tridentate) diamide ligands encapsulate two $Eu^{3+}$ ions, whose coordination spheres are saturated with water molecules and nitrate ions. Upon addition of AMP, bound water molecules and nitrate ions are replaced by one AMP molecule, coordinated by a nitrogen atom of the adenosine group to one $Eu^{3+}$ ion and by two oxygen atoms of a phosphate group to another $Eu^{3+}$, leading to an increase in the emission intensity of the complex. Computational studies suggested that an extension of the phosphate chain in ADP and ATP leads to a repulsive interaction; no significant binding was observed in these cases. Competitive binding data established the high stability of the **[EuL$^{x4}$]*AMP** aggregate, consistent with formation of a triple-stranded structure.

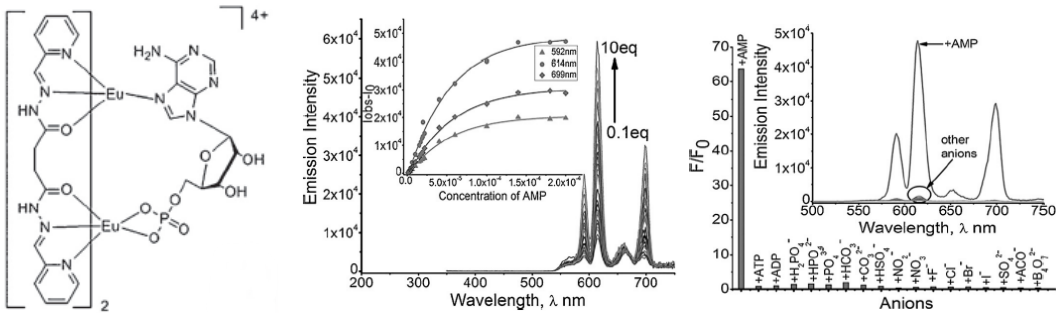


**Fig. I.49** Putative binding mode of AMP (*left*), enhancement of the total emission intensity as a function of added AMP (*middle*) and the selectivity of **[EuL$^{x4}$]** towards selected biologically relevant anions (*right*).[79]

By tuning the degree of saturation of the coordination sphere of $Eu^{3+}$, the selectivity towards different nucleotides can be varied. For instance, Schäfferling reported a family of europium complexes **[Eu$^{n-D}$]** (n = 5, 6, 7) with an alkynylpyridine sensitiser that differ in the number of acetate arms, giving 5-, 6-, and 7-dentate ligands (Fig. I.50)[80]. These complexes showed quite different affinities towards AMP, ADP, ATP, and cyclic AMP. The europium complex with a heptadentate complex showed no affinity towards either nucleotide, whilst the complex with the hexadentate ligand exhibited poor selectivity. The complex with the pentadentate ligand apparently showed relatively good selectivity towards ATP over ADP, and a low affinity towards AMP, following the order of decreasing charge. The similar affinity of the latter complex towards ATP and polyphosphates - the by-product of hydrolysis of ATP into AMP - suggests that only the phosphate part of ATP

participates in binding to the complex. The system was claimed to be reversible in its binding to ATP. However, pentadentate europium complexes are usually rather unstable with respect to metal decomplexation and this process may occur in solution over time, or as the concentration of the coordinating anion increases.

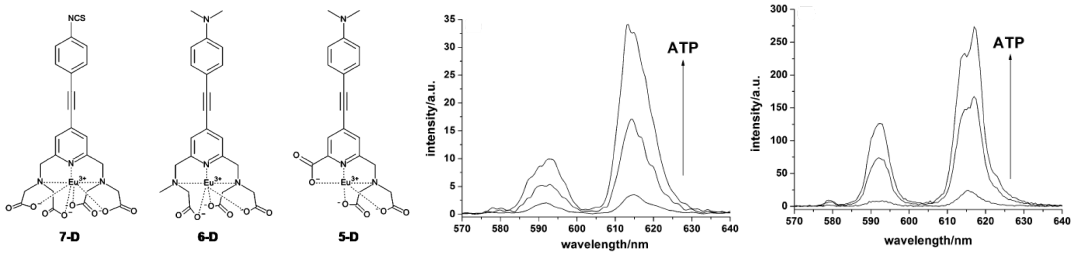


**Fig. I.50** Molecular structures of the complexes **[Eu$^{n\text{-}D}$]** (*left*), enhancement of the total emission intensity of **[Eu$^{6\text{-}D}$]** (*middle*) and **[Eu$^{7\text{-}D}$]** (*right*) as a function of added ATP.[80]

The ability of a nitrogenous base to participate in π–π stacking interactions can be used to discriminate between different nucleotides, for example, pyrimidines and purines, as shown by Pierre (Fig. I.51)[81]. A phenanthridine moiety attached to an amide arm of the cyclen-based europium complex, **[Eu-DOTA-Phen]**, and terbium complex, **[Tb-DOTAm-Phen]**, can participate in favourable π–π stacking interactions with nitrogenous base of nucleotides. **[Tb-DOTAm-Phen]**, due to more favourable electrostatic interactions, is selective towards tri- over mono- and diphosphate nucleotides, whilst neutral **[Eu-DOTA-Phen]** does not possess that selectivity. π–π stacking quenches the excited state of the phenanthridine antenna, due to photoinduced electron transfer (PET), leading to a decrease of the total emission of $Eu^{3+}$ and $Tb^{3+}$. Both, the magnitude of the π–π stacking interactions, the efficacy of PET, and hence the sensitivity of the probe depends on the match between the LUMO level of the phenanthridine moiety and the HOMO of the nucleotide. The more conjugated purines have a higher lying HOMO level than related pyrimidines, and hence much lower sensitivity towards the latter was observed.

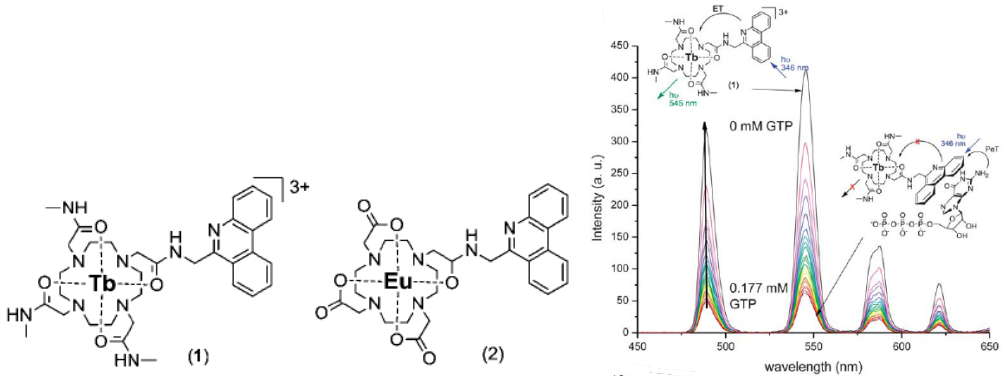


**Fig. I.51** Molecular structures of **[Tb-DOTAm-Phen]** (1) and **[Eu-DOTA-Phen]** (2) (*left*) and enhancement of total emission of **[Tb-DOTAm-Phen]** along with the proposed binding mechanism of GTP (*right*).[81]

## I.5. Circularly-polarised luminescence

The first observation of the difference spectrum of left and right circularly polarised luminescence (CPL) was reported in 1948 for sodium uranyl acetate by a Soviet physicist Boris Samoilov[82]. In the following years, a comprehensive theoretical background of CPL spectroscopy was developed with numerous CPL spectra of chiral compounds being reported. The major parameter, which defines how strongly the luminescence spectrum is polarised is a dissymmetry factor, $g_{em}$, which is defined as a ratio between the difference of left ($I_L$) and right ($I_R$) circularly polarised emission intensities and half of the total emission intensity:

$$g_{em} = \frac{2(I_L - I_R)}{I_L + I_R}.$$

For the majority of organic compounds and transition metal complexes this values lies within the range $10^{-3}$-$10^{-2}$, making recording of CPL spectra for these compounds time-consuming and resulting in poor spectral resolution, especially for weakly emissive compounds. On the contrary, lanthanide complexes (notably terbium and europium) possess much higher dissymmetry factors (0.1-1.4)[83], which allow shorter acquisition times and improved spectral resolution. Besides the information on the chirality of local environment, which makes CPL spectroscopy complementary to circular dichroism (CD) spectroscopy, it also enables resolving those transitions which might otherwise be unresolved in the total emission spectrum (Fig. I.52)[84].

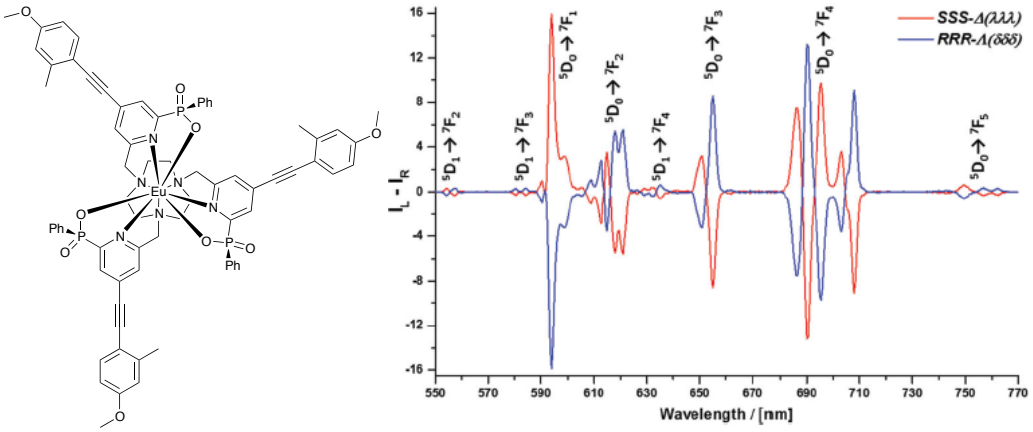


**Fig. I.52** Molecular structure of the europium complex and corresponding CPL spectra of both enantiomers (*SSS-Δ(λλλ)* and *RRR-Λ(δδδ)*). Transitions from $^5D_1$ level are clearly visible.[84]

The primary focus of research on chiral lanthanide complexes in recent years has been directed on using macrocyclic ligands, which provide a well-defined and relatively rigid coordination environment. Different synthetic strategies have been employed to increase the degree of rigidity, and hence increase $g_{em}$ values and stability of the complexes against racemisation. Apart from attaching chiral arms to a macrocycle, the separation of racemic mixtures of *Δ* and *Λ* enantiomers has been more recently performed using RP-HPLC with chiral columns (Fig. I.53). Furthermore, in racemic mixtures one of enantiomers may be preferentially quenched or sensitised upon binding anions or the proteins, thereby giving rise to a CPL signal from a racemic mixture with added chiral analyte. Thus, $g_{em}$ values can be used to monitor the concentration of added analyte to an aqueous solution containing a racemic mixture of lanthanide complex.

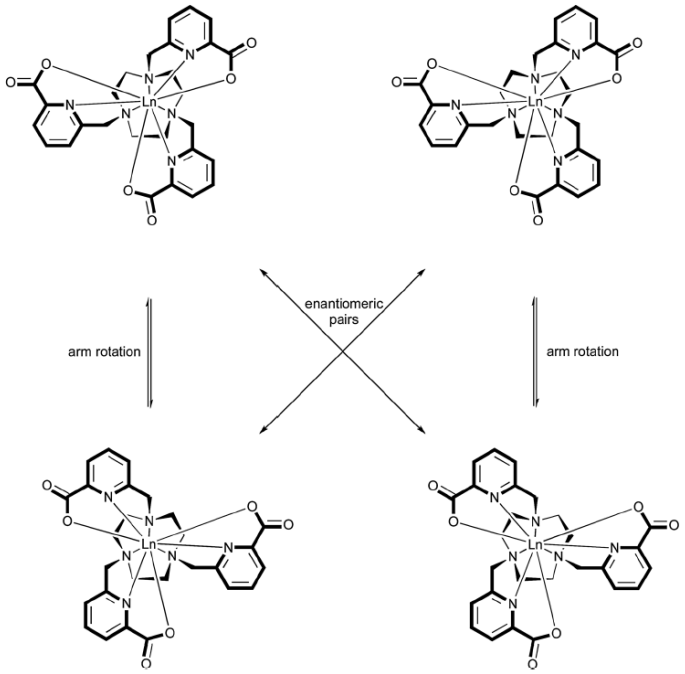


**Fig. I.53** Four different enantiomers of europium complex and possible route of their interconversion through arm rotation and ring inversion.[85]

## I.5 Aims and scope of the work

The aim of the present research project is to design, synthesise, characterise and if necessary optimise europium lanthanide macrocyclic complexes as responsive reversible and ratiometric probes for pH- and analyte-sensing. The design of the probes should rest on the existing knowledge of structure-property relationships in lanthanide macrocyclic complexes, whilst significant improvement in selectivity towards selected analytes is sought. This research projects aims to create the following probes:

i) **pH-responsive probes** applicable for lysosome-selective monitoring of pH *in cellulo* using an aklynylpyridine chromophore. The use of this chromophore in europium complexes resulted in bright, non-toxic and photostable complexes, successfully used as cellular stains.[41] By varying the nature of substituents the change of p$K_a$ values, as well as cellular uptake may be modulated.

ii) **Protein-selective probes**, which are based on strong solvatochormic properties of alkynylpyridine and biaryl chromophores. This can give rise

to a change of the total emission intensity upon binding to hydrophobic binding pockets of the proteins. The use of the mixture of europium and terbium complexes should render ratiometric response, as these complexes are expected to have significantly different sensitivities to the solvent polarity.

iii) **Metal- and anion-selective probes**, which should employ a metal-specific moiety, and modulate spectral change upon rearrangements in the coordination environment. An attempt to introduce and vary the number of hydrogen bond donors can possibly vary the affinity of europium complexes towards biologically relevant anions, i.e. phosphate, nucleotides, citrate, etc. Furthermore, binding of chiral anions should induce a CPL signal, which can be also followed as a function of anion concentration.

The following four chapters described the synthesis, characterisation and thorough photophysical responses of aforementioned classes of molecular lanthanide-based probes. *Chapter 2* describes a new class of pH-sensitive molecular probes and their brief cellular studies. Novel HSA and $\alpha_1$-AGP probes, which switch on upon binding to a protein are discussed in *Chapter 3*. Probes which showed selectivity and high affinity towards $Zn^{2+}$ and nucleotides are reported in *Chapter 4*.

# I.6 References


[1] W. Crookes, *Proc. R. Soc. A Math. Phys. Eng. Sci.* **1905**, *76*, 411–414.

[2] E.-A. Demarçay, *Comptes rendus* **1901**, *132*, 1484–1486.

[3] J. H. Van Vleck, *J. Phys. Chem.* **1937**, *41*, 67–80.

[4] S. I. Weissman, *J. Chem. Phys.* **1942**, *10*, 214–217.

[5] P. Franzen, J. P. . Woudenberg, C. . Gorter, *Physica* **1943**, *10*, 365–368.

[6] B. R. Judd, *Phys. Rev.* **1962**, *127*, 750–761.

[7] G. S. Ofelt, *J. Chem. Phys.* **1962**, *37*, 511–520.

[8] G. H. Dieke, H. M. Crosswhite, B. Dunn, *J. Opt. Soc. Am.* **1961**, *51*, 820-827.

[9] G. H. Dieke, *Spectra and Energy Levels of Rare Earth Ions in Crystals*, John Wiley & Sons Inc, New York, **1969**.

[10] R. T. Wegh, A. Meijerink, R. J. Lamminmäki, Jorma Hölsä, *J. Lumin.* **2000**, *87*, 1002–1004.

[11] Y. Liu, D. Tu, H. Zhu, X. Chen, *Chem. Soc. Rev.* **2013**, *42*, 6924-6958.

[12] R. D. Peacock, *Struct. Bond.* **1975**, *22*, 83–122.

[13] M. P. Hehlen, M. G. Brik, K. W. Krämer, *J. Lumin.* **2013**, *136*, 221–239.

[14] P. A. Tanner, *Chem. Soc. Rev.* **2013**, *42*, 5090–5101.

[15] A. Beeby, S. Faulkner, D. Parker, J. A. G. Williams, *J. Chem. Soc. Perkin Trans. 2* **2001**, 1268–1273.

[16] J. Andres, A. S. Chauvin, *Eur. J. Inorg. Chem.* **2010**, 2700–2713.

[17] L. A. Ekanger, D. R. Mills, M. M. Ali, L. A. Polin, Y. Shen, E. M. Haacke, M. J. Allen, *Inorg. Chem.* **2016**, *55*, 9981–9988.

[18] M. Gál, F. Kielar, R. Sokolová, Š. Ramešová, V. Kolivoška, *Eur. J. Inorg. Chem.* **2013**, 3217–3223.

[19] G. K. Liu, M. P. Jensen, P. M. Almond, *J. Phys. Chem. A* **2006**, *110*, 2081–2088.

[20] J. R. Casey, S. Grinstein, J. Orlowski, *Nat. Rev. Mol. Cell Biol.* **2010**, *11*, 50–61.

[21] J. Han, K. Burgess, *Chem. Rev.* **2010**, *110*, 2709–2728.

[22] C. C. Overly, K. D. Lee, E. Berthiaume, P. J. Hollenbeck, *Proc. Natl. Acad. Sci.* **1995**, *92*, 3156–3160.

[23] Z. Diwu, C. S. Chen, C. Zhang, D. H. Klaubert, R. P. Haugland, *Chem. Biol.* **1999**, *6*, 411–418.

[24] J. Han, A. Loudet, R. Barhoumi, R. C. Burghardt, K. Burgess, *J. Am. Chem. Soc.* **2009**, *131*, 1642–1643.

[25] L. Yuan, W. Lin, Z. Cao, J. Wang, B. Chen, *Chem. - Eur. J.* **2012**, *18*, 1247–1255.

[26] M. H. Lee, J. H. Han, J. H. Lee, N. Park, R. Kumar, C. Kang, J. S. Kim, *Angew. Chem. - Int. Ed.* **2013**, *52*, 6206–6209.

[27] Z. Li, S. Wu, J. Han, S. Han, *Analyst* **2011**, *136*, 3698–3706.

[28] S.-L. Shen, X.-P. Chen, X.-F. Zhang, J.-Y. Miao, B.-X. Zhao, *J. Mater. Chem. B* **2015**, *3*, 919–925.

[29] Q. Wan, S. Chen, W. Shi, L. Li, H. Ma, *Angew. Chem. - Int. Ed.* **2014**, *53*, 10916-10920

[30] T. Myochin, K. Kiyose, K. Hanaoka, H. Kojima, T. Terai, T. Nagano, *J. Am. Chem. Soc.* **2011**, *133*, 3401–3409.

[31] S. Chen, J. Liu, Y. Liu, H. Su, Y. Hong, C. K. W. Jim, R. T. K. Kwok, N. Zhao, W. Qin, J. W. Y. Lam, et al., *Chem. Sci.* **2012**, *3*, 1804.

[32] L. Chen, J. Li, Z. Liu, Z. Ma, W. Zhang, L. Du, W. Xu, H. Fang, M. Li, *RSC Adv.* **2013**, *3*, 13412.

[33] J. Zhou, C. Fang, T. Chang, X. Liu, D. Shangguan, *J. Mater. Chem. B* **2013**, *1*, 661.

[34] H. J. Park, C. S. Lim, E. S. Kim, J. H. Han, T. H. Lee, H. J. Chun, B. R. Cho, *Angew. Chem. - Int. Ed.* **2012**, *51*, 2673–2676.

[35] H. J. Kim, C. H. Heo, H. M. Kim, *J. Am. Chem. Soc.* **2013**, *135*, 17969–17977.

[36] M. Lee, N. G. Gubernator, D. Sulzer, D. Sames, *J. Am. Chem. Soc.* **2010**, *132*, 8828–8830.

[37] D. Parker, P. K. Senanayake, J. A. Gareth Williams, *J. Chem. Soc. Perkin Trans. 2* **1998**, 2129–2140.

[38] M. C. Heffern, L. M. Matosziuk, T. J. Meade, *Chem. Rev.* **2014**, *114*, 4496–4539.

[39] D. G. Smith, B. K. McMahon, R. Pal, D. Parker, *Chem. Comm.* **2012**, *48*, 8520-8522.

[40] B. K. McMahon, R. Pal, D. Parker, *Chem. Comm.* **2013**, *49*, 5363–5365.

[41] J. W. Walton, A. Bourdolle, S. J. Butler, M. Soulie, M. Delbianco, B. K. McMahon, R. Pal, H. Puschmann, J. M. Zwier, L. Lamarque, et al., *Chem. Comm.* **2013**, *49*, 1600–1602.

[42] J. D. Routledge, M. W. Jones, S. Faulkner, M. Tropiano, *Inorg. Chem.* **2015**, *54*, 3337-3345.

[43] O. a Blackburn, M. Tropiano, L. S. Natrajan, A. M. Kenwright, S. Faulkner, *Chem. Comm.*. **2016**, *52*, 6111–6114.

[44] J. D. Moore, R. L. Lord, G. A. Cisneros, M. J. Allen, *J. Am. Chem. Soc.* **2012**, *134*, 17372–17375.

[45] M. Giardiello, M. Botta, M. P. Lowe, *Inorg. Chem.* **2013**, *52*, 14264–14269.

[46] F. J. Schaller, S. Gerber, C. Trachsel, *Human Blood Plasma Proteins Structure and Function*, Wiley, **2008**.

[47] T. J. Horita, B. Kasravi, *Am. Fam. Physician* **2005**, *71*, 105–112.

[48] S. Han, Y. Huang, Z. Li, H. Hou, A. Wu, *BMC Cancer* **2015**, 1–9.

[49] C. G. Lis, J. F. Grutsch, P. G. Vashi, C. A. Lammersfeld, *J. Parenter. Enteral Nutririon* **2003**, *27*, 10–15.

[50] M. Fasano, S. Curry, E. Terreno, M. Galliano, G. Fanali, P. Narciso, S. Notari, P. Ascenzi, *Life* **2005**, *57*, 787–796.

[51] J. Ghuman, P. A. Zunszain, I. Petitpas, A. A. Bhattacharya, M. Otagiri, S. Curry, *J. Mol. Biol.* **2005**, *353*, 38–52.

[52] Y. Hong, C. Feng, Y. Yu, J. Liu, J. Wing, Y. Lam, K. Q. Luo, B. Z. Tang, *Anal.Chem.* **2010**, *82*, 7035–7043.

[53] H. Sun, J. Xiang, X. Zhang, H. Chen, Q. Yang, Q. Li, A. Guan, Q. Shang, Y. Tang, G. Xu, *Analyst* **2014**, *139*, 581–584.

[54] X. tong Chen, Y. Xiang, A. jun Tong, *Talanta* **2010**, *80*, 1952–1958.

[55] Y. H. Ahn, J. S. Lee, Y. T. Chang, *J. Comb. Chem.* **2008**, *10*, 376–380.

[56] J. Fan, W. Sun, Z. Wang, X. Peng, Y. Li, J. Cao, *Chem. Comm.* **2014**, *50*, 9573–9576.

[57] M. Deiana, B. Mettra, L. M. Mazur, C. Andraud, M. Samoc, C. Monnereau, K. Matczyszyn, *ACS Omega* **2017**, *2*, 5715–5725.

[58] Y.-Y. Wu, W.-T. Yu, T.-C. Hou, T.-K. Liu, C.-L. Huang, I.-C. Chen, K.-T. Tan, *Chem. Comm.* **2014**, *50*, 11507–11510.

[59] W. Yang, C. Liu, S. Lu, S. Cheng, J. Du, Q. Gao, P. Shen, H. Luo, Y. Liu, C. Yang, *J. Lumin.* **2017**, *192*, 478–485.

[60] S. J. Kim, H. W. Rhee, H. J. Park, H. Y. Kim, H. S. Kim, J. I. Hong, *Bioorganic Med. Chem. Lett.* **2013**, *23*, 2093–2097.

[61] L. Lu, H. Z. He, H. J. Zhong, L. J. Liu, D. S. H. Chan, C. H. Leung, D. L. Ma, *Sensors Actuators, B Chem.* **2014**, *201*, 177–184.

[62] J. Ruiz, C. Vicente, C. De Haro, D. Bautista, *Inorg. Chem.* **2013**, *52*, 974–982.

[63] X. Wang, X. Wang, Y. Wang, Z. Guo, *Chem. Comm.* **2011**, *47*, 8127–8129.

[64] I. Fitos, Á. Simon, F. Zsila, G. Mády, Á. Bencsura, Z. Varga, L. Orfi, G. Kéri, J. Visy, *Int. J. Biol. Macromol.* **2012**, *50*, 788–795.

[65] R. Carr, L. Di Bari, S. Lo Piano, D. Parker, R. D. Peacock, J. M. Sanderson, *Dalton Trans.* **2012**, *41*, 13154-13158.

[66] L. Jennings, R. S. Waters, R. Pal, D. Parker, *ChemMedChem* **2017**, *12*, 271–277.

[67] G. F. White, K. L. Litvinenko, S. R. Meech, D. L. Andrews, A. J. Thomson, *Photochem. Photobiol. Sci.* **2004**, *3*, 47–55.

[68] S. Abdollahi, W. R. Harris, J. P. Riehl, *J. Phys. Chem.* **1996**, *100*, 1950–1956.

[69] D. Sorio, E. F. De Palo, A. Bertaso, F. Bortolotti, F. Tagliaro, *Anal. Bioanal. Chem.* **2017**, *409*, 1369–1378.

[70] N. Yang, H. Zhang, M. Wang, Q. Hao, H. Sun, *Sci. Rep.* **2012**, *2*, 999.

[71] R. Poole, F. Kielar, S. L. Richardson, P. Stenson, D. Parker, *Chem. Comm.* **2006**, 4084–4086.

[72] R. Pal, D. Parker, L. C. Costello, *Org. Biomol. Chem.* **2009**, *7*, 1525–8.

[73] D. G. Smith, R. Pal, D. Parker, *Chem. - Eur. J.* **2012**, *18*, 11604–11613.

[74] E. T. Everett, *J. Dent. Res.* **2011**, *90*, 552–560.

[75] S. J. Butler, *Chem. Comm.* **2015**, *51*, 10879–10882.

[76] L. M. P. Lima, A. Lecointre, J. F. Morfin, A. De Blas, D. Visvikis, L. J. Charbonnière, C. Platas-Iglesias, R. Tripier, *Inorg. Chem.* **2011**, *50*, 12508–12521.

[77] T. Liu, A. Nonat, M. Beyler, M. Regueiro-Figueroa, K. Nchiminono, O. Jeannin, F. Camerel, F. Debaene, S. Cianférani-Sanglier, R. Tripier, et al., *Angew. Chem. - Int. Ed.* **2014**, *53*, 7259–7263.

[78] O. a. Blackburn, A. M. Kenwright, A. R. Jupp, J. M. Goicoechea, P. D. Beer, S. Faulkner, *Chem. - Eur. J.* **2016**, *22*, 8929–8936.

[79] J. Sahoo, R. Arunachalam, P. S. Subramanian, E. Suresh, A. Valkonen, K. Rissanen, M. Albrecht, *Angew. Chem. - Int. Ed.* **2016**, *55*, 9625–9629.

[80] M. Schäferling, T. Aäritalo, T. Soukka, *Chem. - Eur. J.* **2014**, *20*, 5298–5308.

[81] E. Weitz, J. Y. Chang, A. H. Rosenfield, E. Morrow, V. C. Pierre, *Chem. Sci.* **2013**, *4*, 4052-4060.

[82] B. N. Samoilov, *J Exp Theor Phys* **1948**, *18*, 1030–1040.

[83] F. Zinna, L. Di Bari, *Chirality* **2015**, *27*, 1–13.

[84] A. T. Frawley, R. Pal, D. Parker, *Chem. Comm.* **2016**, *52*, 13349–13352.

[85] R. Carr, N. H. Evans, D. Parker, *Chem. Soc. Rev.* **2012**, *41*, 7673-7686.

# Chapter two

# Europium complexes as pH-sensitive probes

# II.1 Lanthanide-based pH-sensitive probes with a sulphonamide arm

Biologically relevant processes within cells usually occur within a tightly defined pH range – typically between 6 and 8. Exceptionally lower pH values are observed in lysosomes and endosomes, whose pH value can be as low as 4.0-4.5, in order to provide efficient operational conditions for hydrolytic enzymes, to digest unwanted biomolecules. For a certain class of usually hereditary diseases grouped under the name 'lysosomal storage diseases' (LSD), the pH value of lysosomes is elevated. This hampers efficient functioning of hydrolytic enzymes, leading to accumulation of toxic compounds inside the cell and eventually causing apoptosis of the cell. To gain a better insight into the processes accompanying malfunctioning of the cell in people with LSD, a molecular probe with high sensitivity within the desired pH range is required to track pH changes in response to external stimuli, over a specific period of time.

Several pH-sensitive lysosomal luminescent bio-imaging probes are currently commercially available, for example LysoSensor$^{TM}$ (Fig. II.1), although they possess considerable drawbacks, which limit their wider use. Firstly, these probes are usually very prone to photo-bleaching, and therefore long-term experiments with these probes are actually excluded. Secondly, the singlet excited states of purely organic probes have nanosecond lifetimes, and hence no time-gating is available for these probes to subtract residual emission from other organic fluorophores present in the cell, or any scattered light from the light source.

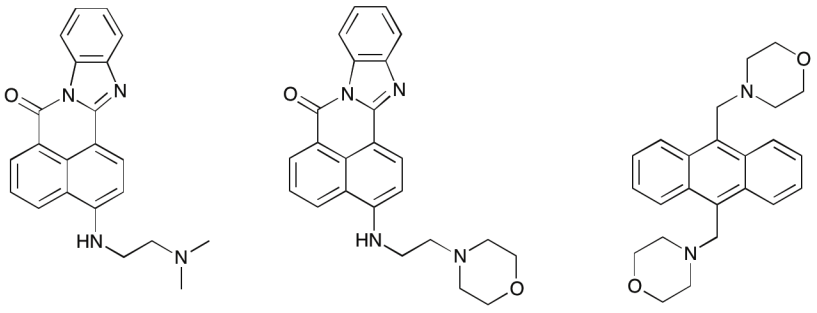


**Fig. II.1** Molecular stuctures of LysoSensor$^{TM}$ Green DND-153 (*left*), LysoSensor$^{TM}$ Green DND-189 (*centre*) and LysoSensor$^{TM}$ Blue DND-167 (*right*)

These flaws can be overcome in molecular probes based on lanthanide complexes, as it was shown that if designed properly these compounds are non-toxic. Emission lifetimes for $Eu^{3+}$ and $Tb^{3+}$ probes are in a millisecond range and therefore permit efficient time-gating. Furthermore, the electronic structure of europium(III) gives rise to the presence of several electronic transitions, which differ in their sensitivity towards perturbation of the metal coordination sphere. This intrinsic feature of the europium ion allows monitoring the relative emission intensities as a function of an induced structural rearrangement in the coordination sphere, for example, in response to a change in the pH of the medium, and hence provides a ratiometric response.

Examples of ratiometric pH-sensitive lanthanide complexes were pioneered by Parker[1],[2], where a sulphonamide arm was used to modulate changes in the emission spectrum, following reversible binding of the nitrogen atom to the lanthanide ion. By varying the nature of the substituent in the sulphonamide arm, the p$K_a$ of the complex was adjusted (Fig. II.2). It was emphasised that the primary flaws of these systems are the presence of two water molecules, which replace the sulphonamide nitrogen once it is protonated at lower pH values, leading to quenching of the total emission intensity. Furthermore, the diaqua complex was shown to bind oxyanions, which can significantly shift the observed p$K_a$ of the complex in biological media. Substitution of carboxylate arms with glutarate arms inhibited intermolecular anion binding in the q = 2 complex and showed its potential for further modifications in order to get a complex excitable at higher wavelengths with affordable laser diodes.

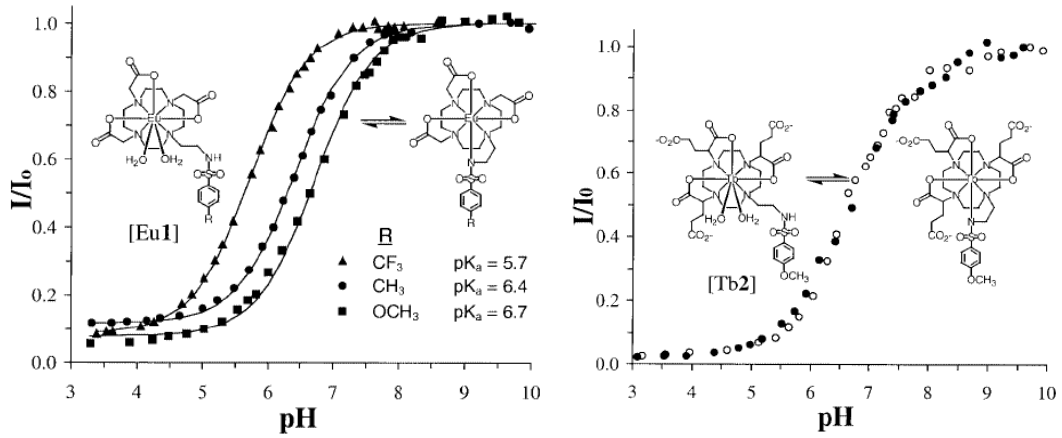


**Fig. II.2** Calibration pH curves for cyclen-based europium complex with a sulphonamide arm with three carboxylate (*left*) and glutarate (*right*) arms (295 K, I = 0.1 M NaCl).[1]

Subsequently, an azathiaxanthone chromophore was introduced to provide efficient sensitisation of the complex at 365 nm and even 405 nm (Fig. II.3)[3]. However, substitution of one of the glutarate arms with a chromophore restored competitive binding of oxyanions (most importantly bicarbonate anions), which impeded ligation of the sulphonamide nitrogen and shifted the p$K_a$ of the complex towards higher values outside the lysosomal range. The complex was tested *in cellulo* and showed localisation in the nucleolus and ribosomes.

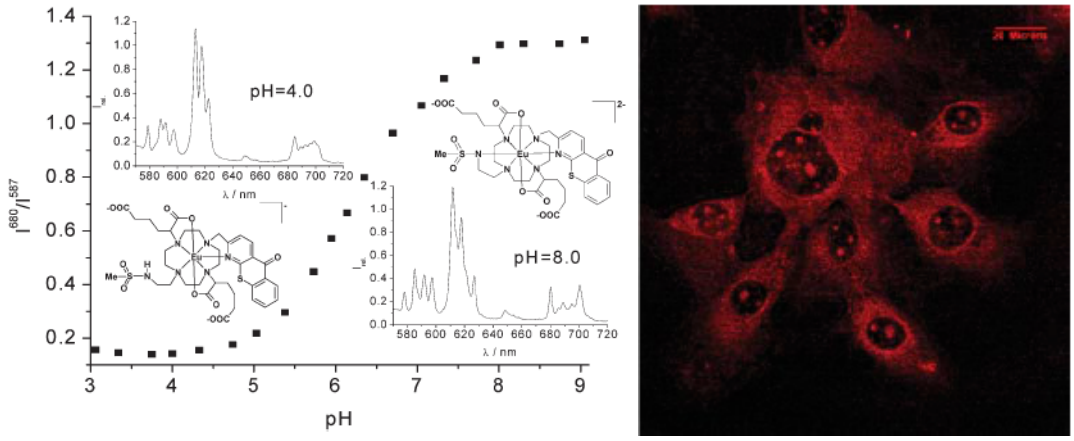


**Fig. II.3** Calibration pH curve for the europium complex bearing an azathiaxanthone chromophore (*left*) and confocal fluorescent microscopy image of NIH-3T3 cells loaded with the complex (*right*).[3]

In subsequent work, an azaxanthone chromophore was introduced through an amide bond and glutarate arms were substituted with chiral amides (Fig. II.4)[4]. It was shown that azaxanthone chromophores are trapped by the cells via micropinocytosis mechanism, with an initial mitochondrial localisation, followed by trafficking of the probe to the lysosome[5].

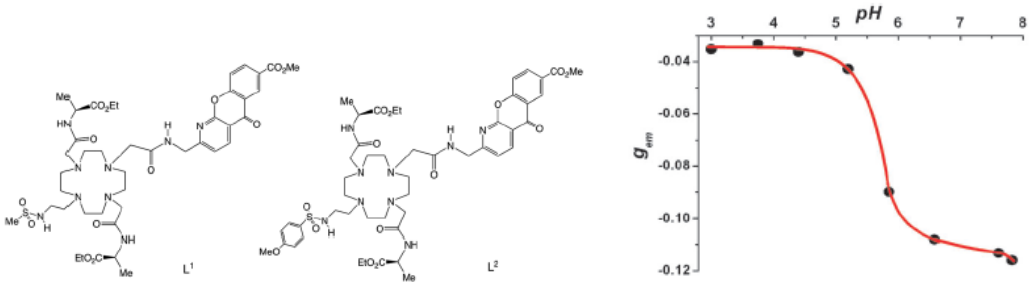


**Fig. II.4** Molecular structure of the complexes (*left*) and variation of the emission dissymmetry factor ($g_{em}$) of **[EuL²]** as a function of pH (*right*).[4]

An unusual rise of the total emission intensity was observed upon lowering the pH, indicating the removal of PET quenching of the chromophore by an electron-rich *p*-

MeOPh substituent in the sulphonamide arm following its protonation. The use of chiral arms in the structure modulated a chiral response as a function of pH. Significantly lowered values of the emission dissymmetry factor, $g_{em}$, were observed upon protonation of the sulphonamide nitrogen, consistent with a less rigid structure of the complex when the sulfonamide nitrogen is replaced with two water molecules. As the azaxanthone chromophore was suitable for sensitisation of both europium and terbium ions and they possessed different degrees of emission intensity variation with pH, their mixture could be successfully used to monitor lysosomal pH *in cellulo* (Fig. II.5).

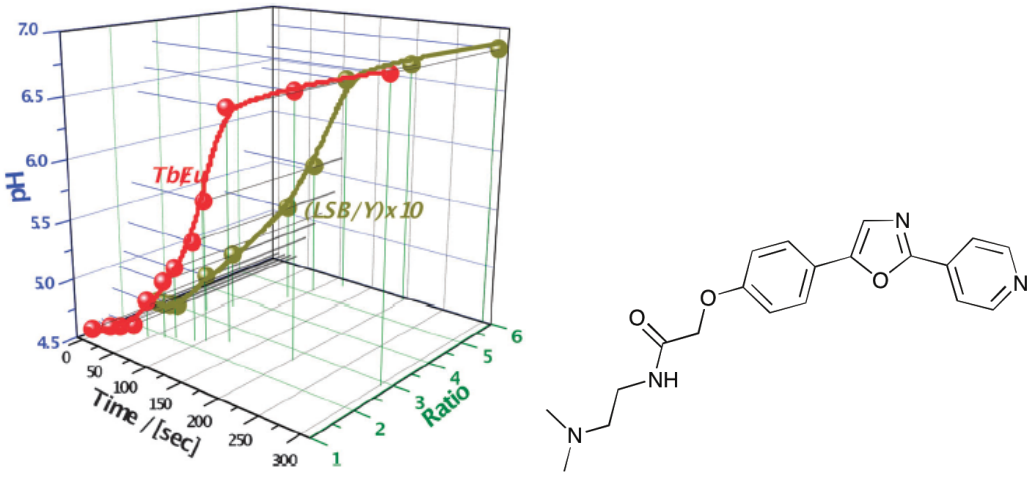


**Fig. II.5** Variation of lysosomal pH as a function of time (*left*), following treatment with nigericin in NIH-3T3 cells, monitoring the relative emission intensity of Tb/Eu component along with blue/yellow fluorescent intensity of the commercial stain LysoSensor™ DND160 (*right*).[4]

Despite this progress with azaxanthone-based probes, the advent of EuroTracker® dyes with improved photostability and brightness made their use as lysosome-selective luminescent probes highly attractive. Changes in the structure of the rod-like chromophore provided opportunities to vary the excitation wavelength as well as the nature of ligating atoms[6]. The first attempt to use a sulfonamide arm in combination with alkynyl-pyridine chromophore with a methylphosphinate group based on a 9-$N_3$ platform resulted in an unexpectedly high p$K_a$ for the complex (p$K_a$ = 7.1 *in cellulo*), apparently as a result of a specific interaction of the rod-like chromophore with albumin. A similar value was observed using a 'simulated extracellular' ionic background containing added HSA (Fig. II.6)[7]. However, even in the absence of oxyanions and added protein, the observed p$K_a$ was higher than was previously observed for related systems with the same sulphonamide arm (p$K_a$ = 6.5). This enhanced value was attributed to the enhanced steric demand associated

with reversible binding of a sulphonamide arm, which resulted in easier protonation of the sulphonamide nitrogen. Furthermore, the complex showed an unusual localisation to the endoplasmic reticulum (ER), which could possibly be a result of the higher p$K_a$ of the complex.

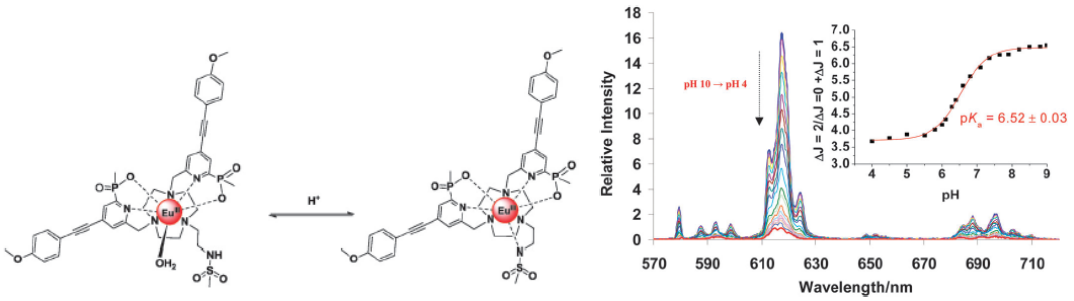


**Fig. II.6** Reversible protonation of the sulphonamide arm in the complex (*left*) and variation of the relative emission intensity as a function of pH (*right*) (295K, I = 0.1 M).[7]

With this background in mind, it was decided to analyse the possibility of using a less sterically demanding 12-$N_4$ platform bearing an alkynyl-pyridine chromophore, alleviating the steric constraints imposed on reversible sulphonamide ligation, and hence leading to a lower p$K_a$ of the complex.

## II.2 pH-Responsive, Lysosome-Selective Probes

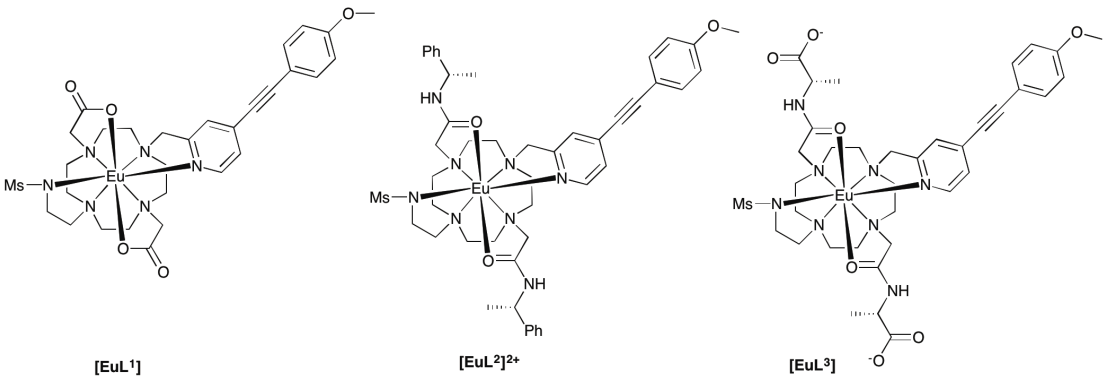


**Fig. II.7** Molecular of the pH probes **[EuL$^{1,3}$]** and **[EuL$^2$]Cl$_2$** studied

In order to evaluate the effect of different factors, such as overall charge and the nature of the ligating groups a series of three europium complexes was synthesised and studied both *in vitro* and *in cellulo* (Fig. II.7). A neutral complex **[EuL$^1$]** with two carboxylate arms, a positively charged variant, **[EuL$^2$]$^{2+}$**, with two chiral amide arms and a neutral complex **[EuL$^3$]** with chiral amide arms bearing terminal charged

carboxylate groups were synthesised by successive alkylation reactions of a di-substituted cyclen intermediate (Scheme II.1).

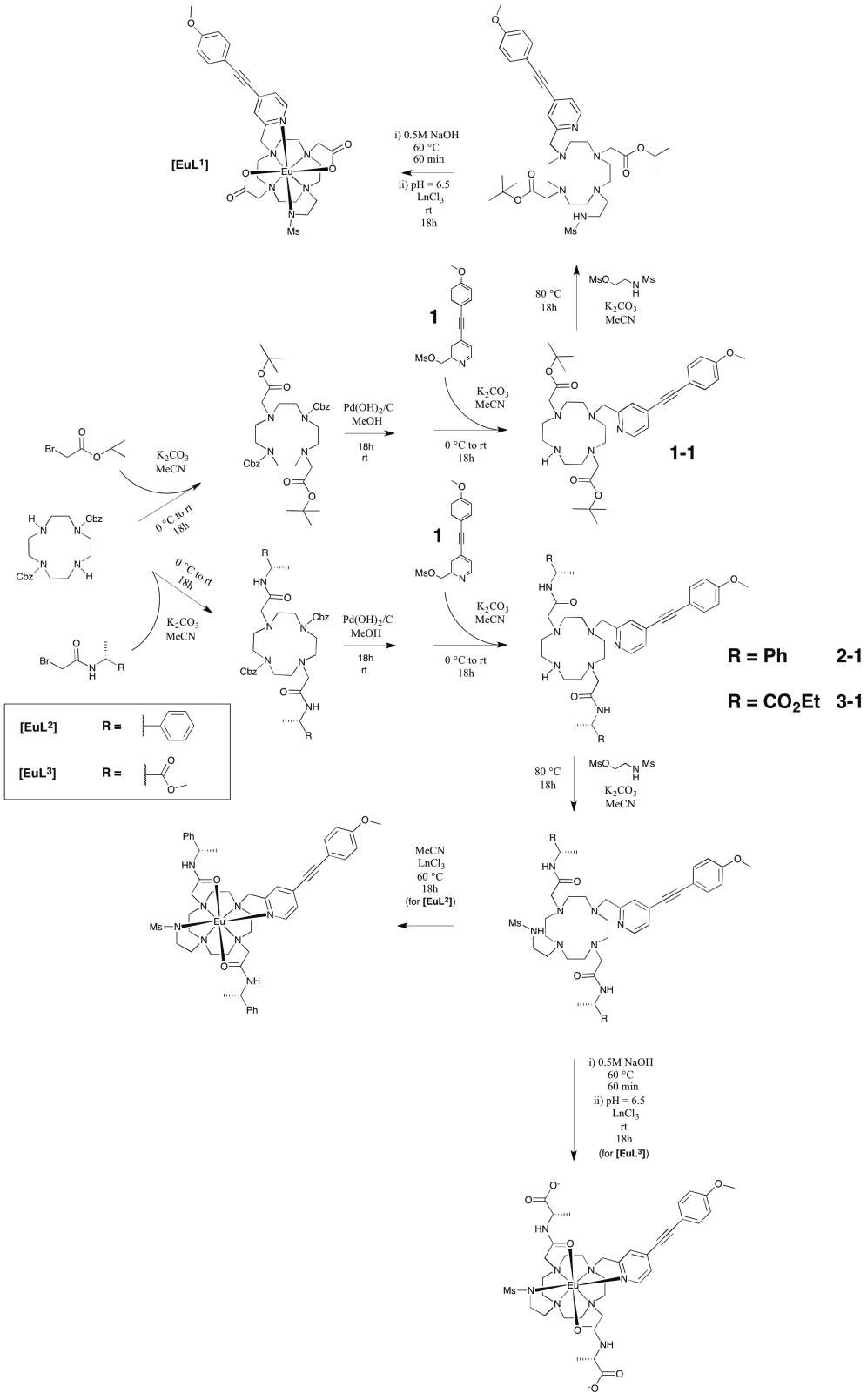


**Scheme II.1** Synthetic pathway for **[EuL$^{1\text{-}3}$]**.

An unsubstituted alkynyl-pyridine chromophore was synthesised in accordance with an adopted procedure from reference [8], and its freshly prepared mesylate was reacted with a di-substituted cyclen. The major tri-substituted product was reacted with a mesylate to introduce the sulphonamide arm, giving the desired ligand. For complexes **[EuL$^1$]** and **[EuL$^3$]**, the ligand was hydrolysed in 0.5 M NaOH, followed by neutralisation and complexation with $EuCl_3$, whilst in the case of **[EuL$^2$]** the ligand was dissolved in acetonitrile and then reacted with $EuCl_3$. Complexes **[EuL$^1$]** and **[EuL$^3$]** were purified using RP-HPLC, whilst **[EuL$^2$]** was purified by washing any excess of the sulphonamide arm with DCM and precipitating any excess metal by increasing the pH to 10 with aqueous ammonia.

**Table II.1** Photophysical properties of **[EuL$^{1\text{-}3}$]** in aqueous solution

| | | **pH = 2.8** | | | **pH = 7.8** | | |
|---|---|---|---|---|---|---|---|
| | $\varepsilon_{325nm}$/M$^{-1}$cm$^{-1}$ | $\tau$ ($H_2O$)/ms | $\tau$ ($D_2O$)/ms | $q$ | $\tau$ ($H_2O$)/ms | $\tau$ ($D_2O$)/ms | $q$ |
| **[EuL$^1$]** | 35 400 | 0.31 | 1.32 | 2.7 | 0.73 | 1.06 | 0.2 |
| **[EuL$^2$]$^{2+}$** | 35 400 | 0.41 | 0.79 | 1.1 | 0.54 | 0.68 | 0.2 |
| **[EuL$^3$]** | 35 400 | 0.48 | 0.98 | 1.0 | 0.48 | 0.58 | 0.1 |

Complex **[EuL$^1$]** showed reversible binding of the sulphonamide arm, which was monitored by examining both the lifetime of the excited state and the relative intensities of the $^5D_0 \rightarrow {}^7F_2$ and $^5D_0 \rightarrow {}^7F_1$ transitions in aqueous solution (I = 0.1 M) (Fig. II.8). By following changes in the lifetime of the $^5D_0$ excited state, a p$K_a$ = 4.1 was deduced with a lifetime decreasing from $\tau$ = 0.72 ms at pH = 6.0 to $\tau$ = 0.31 ms at pH = 2.5. The change in the relative intensities of the electric-dipole hypersensitive $^5D_0 \rightarrow {}^7F_2$ transition against the magnetic-dipole transition $^5D_0 \rightarrow {}^7F_1$ revealed a decrease upon lowering the pH, and gave a p$K_a$ = 3.8 (Fig. II.9).

The $^5D_0 \rightarrow {}^7F_1$ transition manifold also experienced considerable changes as a function of pH, exhibiting change of the sign of the ligand field parameter $B_0^2$. Unfortunately, no evidence from $^1$H NMR spectra could be provided to demonstrate corresponding changes in chemical shifts, as exchange broadened $^1$H NMR signals were observed at lower pH values – the result of fast magnetisation exchange when two water molecules replaced the sulphonamide nitrogen. Also, the total emission intensity experienced a significant reduction, primarily as a result of efficient vibrational quenching by the bound water molecules.

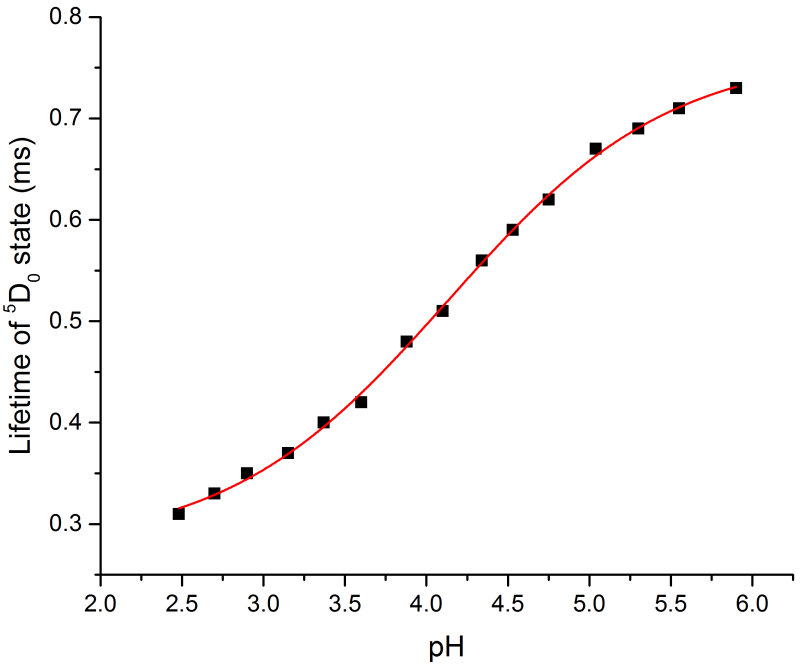


**Fig. II.8** Variation of the lifetime of the excited $^5D_0$ state of **[EuL$^1$]** as a function of pH (p$K_a$ = 4.1, T = 22 °C, 0.1 M NaCl, $\lambda_{ex}$ = 325 nm).

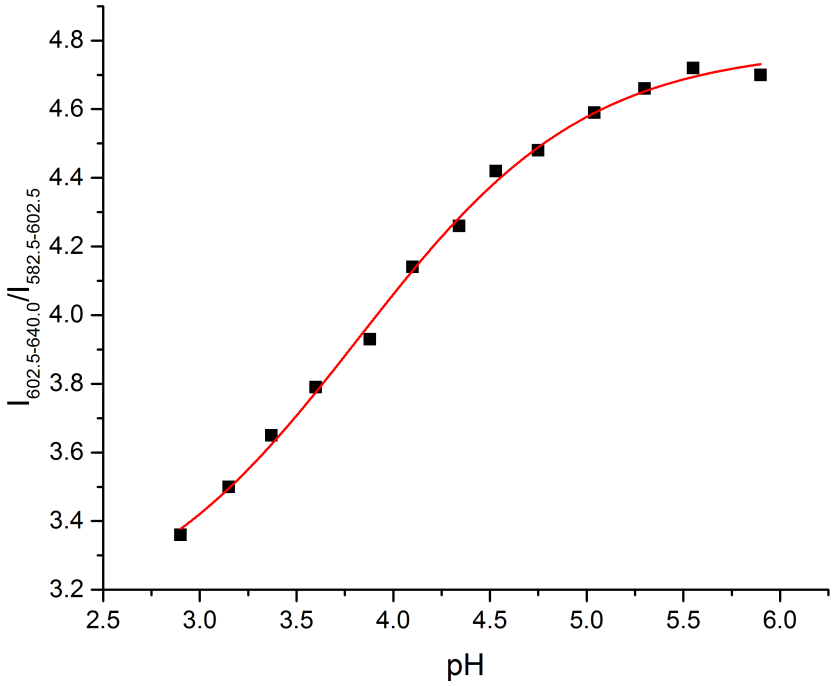


**Fig. II.9** Variation of ratio between $^5D_0 \rightarrow {}^7F_2$ (602.5-640.0 nm) and $^5D_0 \rightarrow {}^7F_1$ (582.5-602.5 nm) transitions of **[EuL$^1$]** as a function of pH (p$K_a$ = 3.8, T = 22 °C, 0.1 M NaCl, $\lambda_{ex}$ = 325 nm).

As has been already discussed, addition of oxyanions and proteins can significantly perturb the reversible binding of the sulphonamide arm in lanthanide complexes, shifting the observed p$K_a$ towards higher values. To evaluate this change in the

present case, a calibration curve was obtained in a cell lysate that mimics an extracellular medium (Fig. II.10). Both the lifetime of the excited state and the relative intensities of emission bands were followed, revealing an increased p$K_a$ value (p$K_a$ = 7.1), consistent with specific binding to a protein and/or oxyanions. It is worth mentioning that a reciprocal trend in the lifetime was observed upon lowering the pH of cell lysate, rising from $\tau$ = 0.37 ms at pH = 9.0 to $\tau$ = 0.72 ms at pH = 4.0.

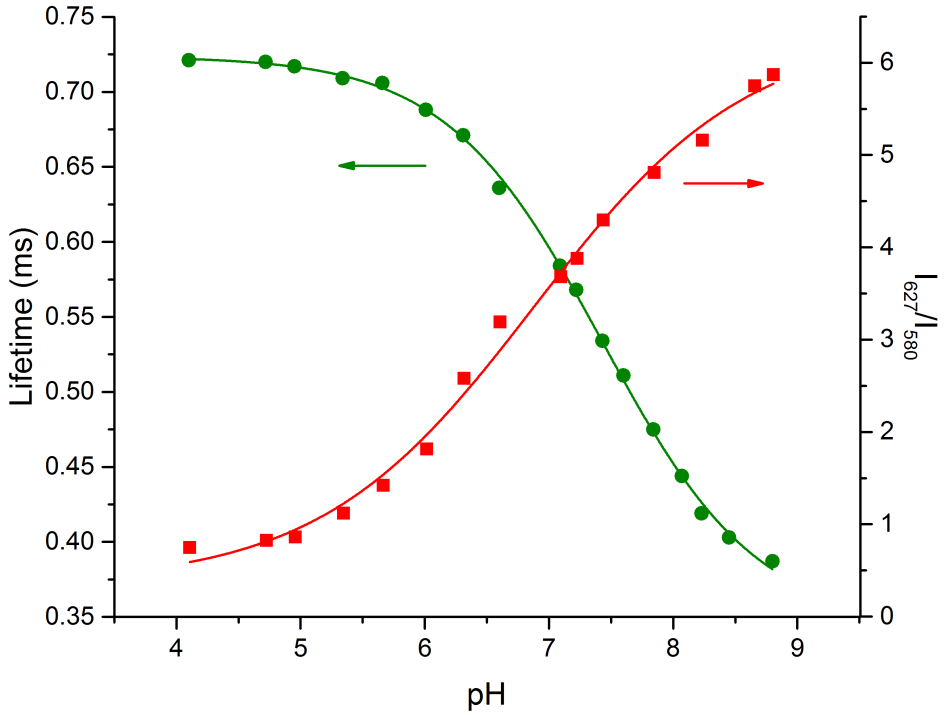


**Fig. II.10** Variation of the emission intensity and the lifetime of **[EuL$^1$]** in cell lysate (p$K_a$ = 7.1, T = 22 °C, $\lambda_{ex}$ = 325 nm).

At the same time, the total emission spectrum experienced quite different transformations, with a significant increase of the total emission intensity upon lowering the pH of the medium. Although an identical spectral signature was observed in both 0.1 M NaCl solution and cell lysate, when the sulphonamide nitrogen was bound to $Eu^{3+}$, at lower pH values their patterns were different, i.e. when the sulphonamide nitrogen is unbound (Fig. II.11). In spite of the similar change in the $B^2_0$ sign following the decrease of the pH, the relative intensities of $^5D_0 \rightarrow {}^7F_2$ vs $^5D_0 \rightarrow {}^7F_1$ were different. Whereas in the case of 0.1 M NaCl solution the relative intensity of the magnetic-dipole $^5D_0 \rightarrow {}^7F_1$ transition decreased, in the cell lysate it remained virtually the same. This behaviour is indicative of specific binding to oxyanions or amino-acids of the serum albumin side chain of the europium(III) ion.

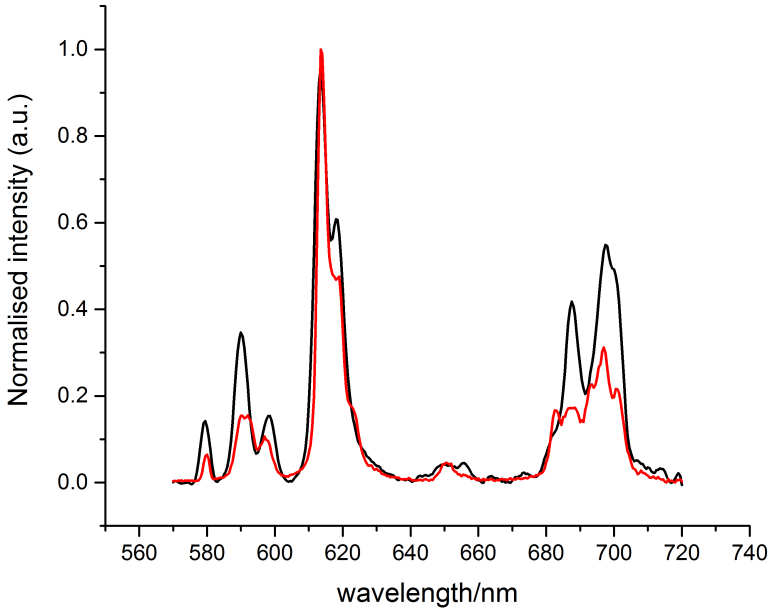


**Fig. II.11** Emission spectra of **[EuL$^1$]** in the 0.1 M NaCl solution at pH 2.5 (*black*) and in the cell lysate at pH 4.0 (*red*) (T = 22 °C, 0.1 M NaCl, $\lambda_{ex}$ = 325 nm).

In a similar experiment, the impact of added HSA was separately evaluated for a related complex **[EuL$^5$]** (Fig. II.12), which possesses a similar p$K_a$ value (p$K_a$ = 7.3). Such behaviour shows a decisive role of the protein binding in shifting the protonation constant of the sulphonamide arm. The binding of the complex **[EuL$^1$]** to HSA was accompanied by a very slight decrease of the total emission intensity (PLQY decreased from 6.6% to 6.0%) and led to an induced CPL spectrum ($g_{em}$ = 0.02 (589 nm)) (Fig. II.13).

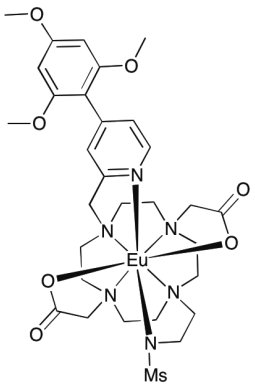


**Fig. II.12** Molecular structure of **[EuL$^5$]**

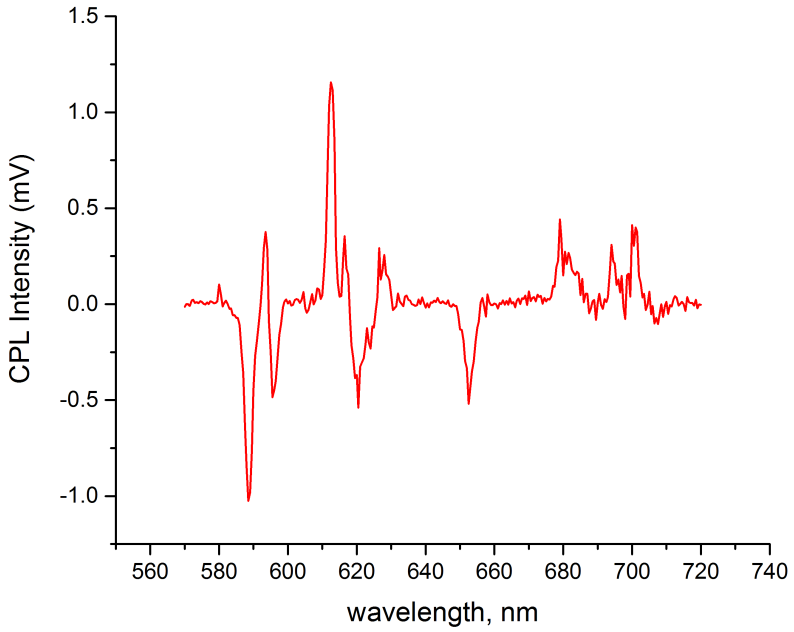


**Fig. II.13** Circularly polarised emission spectrum of **[EuL$^1$]** (10 μM) in the presence of human SA (0.4 mM) (T = 22 °C, $\lambda_{ex}$ = 325 nm).

## II.3 Cellular studies of [EuL$^1$]

The complex **[EuL$^1$]** was examined as a luminescent cellular stain in mouse skin fibroblast cells (NIH-3T3), using both live cell epifluorescence and confocal microscopy. In the incubation medium, 10% foetal calf-serum (FCS) is normally added to promote cell growth.

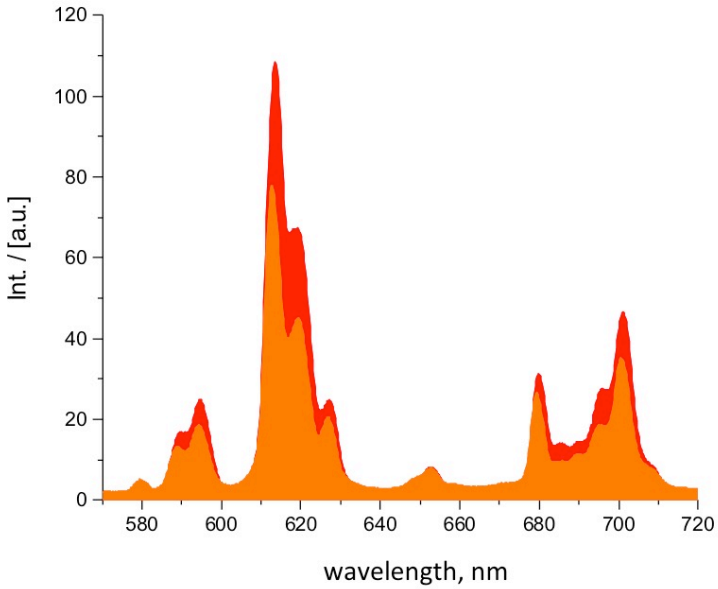


**Fig. II.14** Emission spectra of **[EuL$^1$]** (10 μM) in the presence of human SA (*red*) and bovine SA (*orange*) in the cell growth medium ($\lambda_{ex}$ = 365 nm).

This medium contains BSA and the expected spectral signature for europium emission was observed. The experiment was repeated with HSA added to FCS and revealed a 50% rise in the emission intensity (Fig. II.14). This 50% increase was also observed by comparing solutions of **[EuL$^1$]** with added HSA and BSA, revealing the same 50% increase of the quantum yield (6.0% with added HSA and 4.3% with added BSA). A lysosomal staining pattern was confirmed by co-staining with LysoTracker$^{TM}$ Green, which revealed a very faint signal after 4 h, with an increasing brightness after 24 h (Fig. II.15).

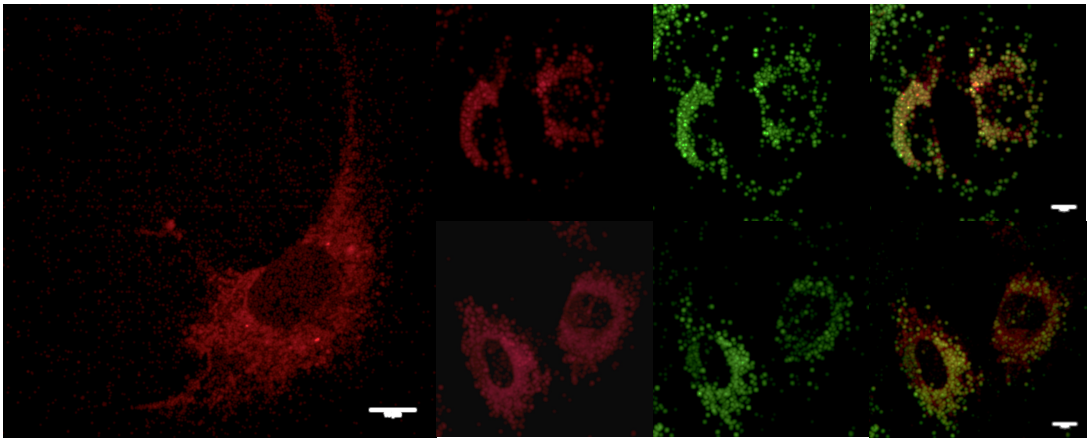

**Fig. II.15** LSCM images (1024x1024 pixel, 100 Hz bidirectional) in NIH-3T3 cells showing: (*left*) predominantly lysosomal staining following a 4 h incubation of 10 μM complex ($\lambda_{ex}$ = 355 nm, $\lambda_{em}$ = 605–720 nm, 8 mW), and and (*right*) following a 24 h incubation, and 5 min incubation of LTG ($\lambda_{ex}$ = 488 nm, $\lambda_{em}$ = 500–530 nm, 2 mW).

The emission spectrum recorded *in cellulo* after 24 h showed a spectral signature corresponding to the complex with a dissociated sulphonamide nitrogen (Fig. II.16), whilst the recorded lifetime of the excited state ($\tau$ = 0.36 ms) corresponded to that observed in an aqueous solution with 0.1 M NaCl as a background electrolyte ($\tau$ = 0.32 ms), rather than to the lifetime recorded in cell lysate ($\tau$ = 0.72 ms). At the same time, the emission spectrum and the lifetime of the excited state recorded in a cell medium ($\tau$ = 0.81 ms) also corresponds to behaviour in 0.1 M NaCl aqueous solution, rather than to that in cell lysate. Furthermore, more detailed inspection of the emission spectrum (Fig. II.16) revealed a spectral signature that neither resembled the one observed in the 0.1M NaCl solution, nor the one observed in the cell lysate. These observations raise the question, whether the *in vitro* measurements in a cell lysate is a good model to calibrate the pH probe for use *in cellulo*, or whether another model should be used instead. Unfortunately, the content of

lysosomes is too complex to be easily simulated *in vitro*, and therefore the only available option is too use such simplified models.

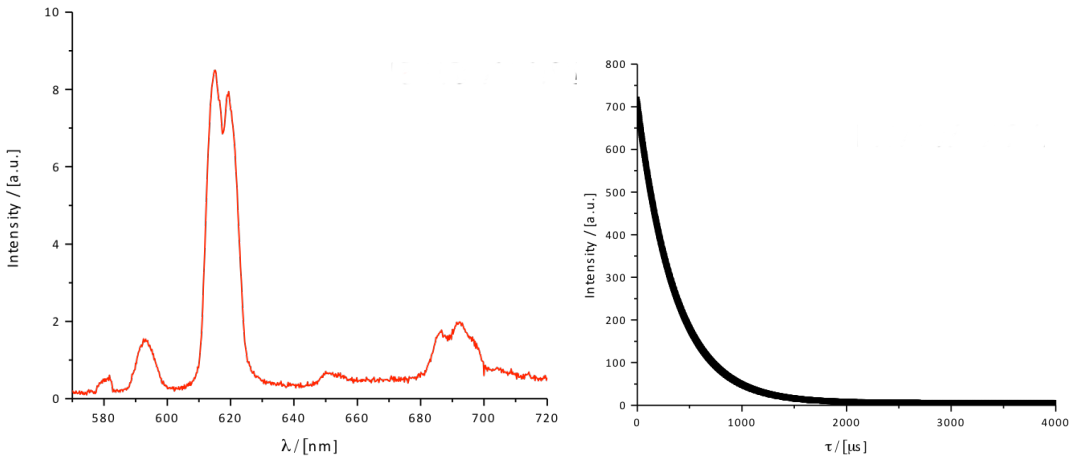


**Fig. II.16** The emission spectrum after a 24 h incubation of **[EuL$^1$]** with NIH-3T3 cells (*left*) and the corresponding decay curve of the emission (*right*) ($\lambda_{ex}$ = 365 nm).

In an attempt to follow the changes in the emission signature and/or lifetime of the excited state, nigericin was added to the cell medium in order to alter the pH inside the lysosome. Even though, the overall emission intensity of **[EuL$^1$]** increased following the addition of nigericin, the spectral pattern and the lifetime did not change following pH variation, suggesting that the p$K_a$ of the complex inside the lysosome was too high.

## II.4 *In vitro* and *in cellulo* studies of [EuL$^2$]$^{2+}$ and [EuL$^3$]

Two other complexes, **[EuL$^2$]$^{2+}$** and **[EuL$^3$]**, bearing two chiral amide arms were designed and synthesised featuring a different partial charge on $Eu^{3+}$ ion. Both complexes showed a strong CPL signal induced by the presence of the chiral substituents in the amide arms. In each case, upon lowering the pH of the medium a gradual decrease of the CPL signal was observed, indicating that a less rigid structure was adopted by the complex, once the sulphonamide nitrogen dissociated. The total emission spectrum also experienced noticeable changes in the relative intensities of the ΔJ=1 and ΔJ=2 bands, as well as in the values of crystal field parameters. However, no change of the lifetime of the excited state was observed in either case ($\tau$ = 0.5 ms for **[EuL$^2$]$^{2+}$** and **[EuL$^3$]**), even though the total emission intensity decreased by half. The spectral signature of the emission spectrum and CPL (Fig. II.17) was identical in both cases, although the dissymmetry ratio $g_{em}$ ($\lambda$ = 589 nm)

was three times higher for **[EuL$^2$]$^{2+}$** ($g_{em}$ = 0.19 for **[EuL$^2$]$^{2+}$** vs $g_{em}$ = 0.06 for **[EuL$^3$]**, both in 0.1 M HEPES buffer at pH = 7.40).

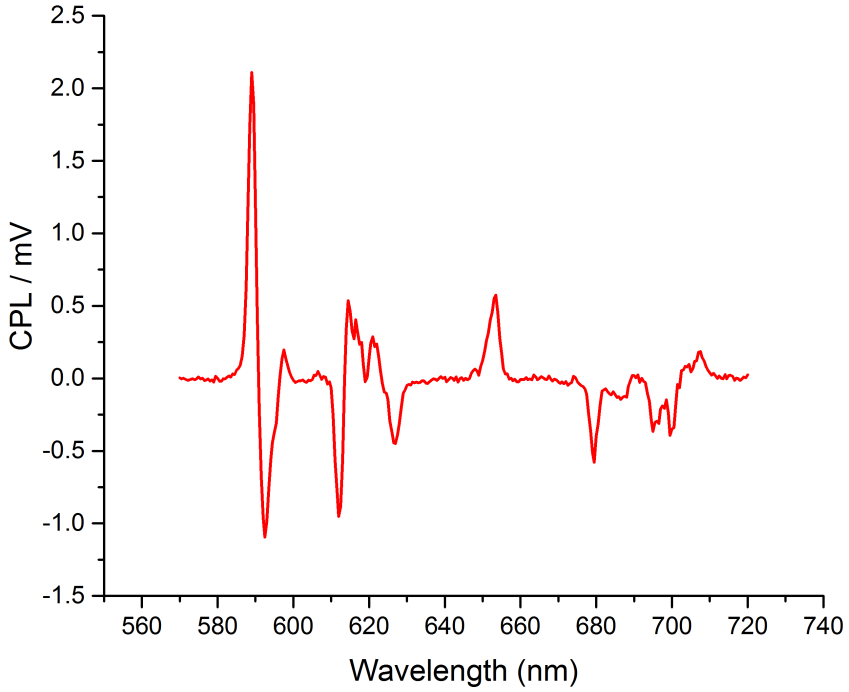


**Fig. II.17** Circularly polarised emission spectrum of **[EuL$^2$]$^{2+}$** (9 μM) (T = 22 °C, $\lambda_{ex}$ = 325 nm, 0.1 M HEPES, pH = 7.40).

The much higher value of $g_{em}$ for **[EuL$^2$]$^{2+}$** may simply reflect the shorter distance between the stereogenic centre and $Eu^{3+}$, as the coordination environment is identical for each complex. Despite a big difference in the dissymmetry factor with the bound sulphonamide arm, upon protonation the CPL signal decreases to nearly zero (Fig. II.18), making **[EuL$^2$]$^{2+}$** the more sensitive CPL probe (higher $\Delta g_{em}/\Delta$pH). The observed p$K_a$ values for both complexes were quite different (p$K_a$ = 3.6 for **[EuL$^2$]$^{2+}$** and p$K_a$ = 4.9 for **[EuL$^3$]** (Fig. II.20)), following the difference in the overall charge of the complex. No changes of the total emission signature or the CPL pattern were observed upon addition of HSA, whilst the total emission intensity and $g_{em}$ value decreased slightly. In contrast to **[EuL$^1$]**, no change of the $B^2_0$ sign was observed upon varying the pH of the medium, whilst the relative intensities of the Stark components in the ΔJ=1 manifold significantly changed. The total emission intensity decreased approximately three times, following the decrease of pH from 7.5 to 2.5.

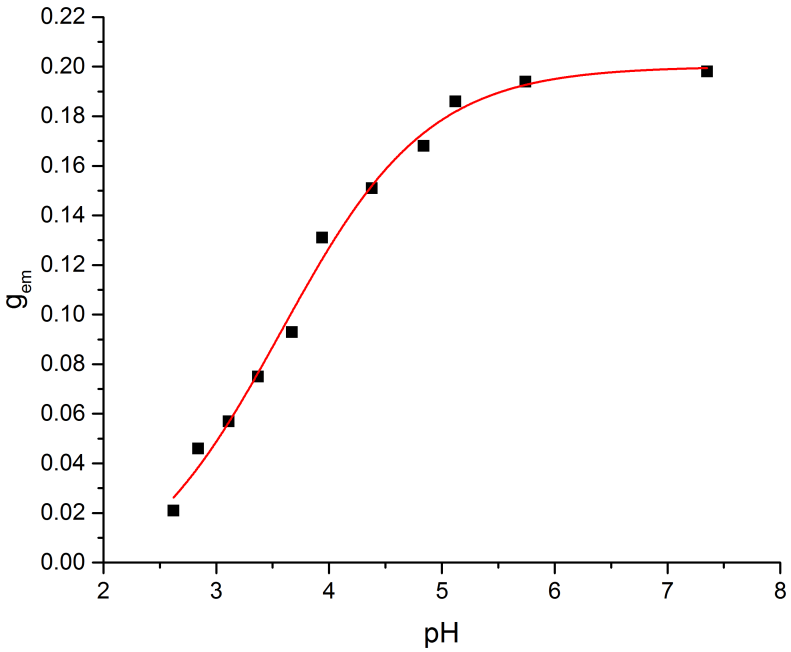


**Fig. II.18** Variation of the dissymmetry factor $g_{em}$ ($\lambda$ = 589 nm) of **[EuL$^2$]$^{2+}$** as a function of pH (p$K_a$ = 3.6, T = 25 °C, 0.1 M NaCl, $\lambda_{ex}$ = 325 nm).

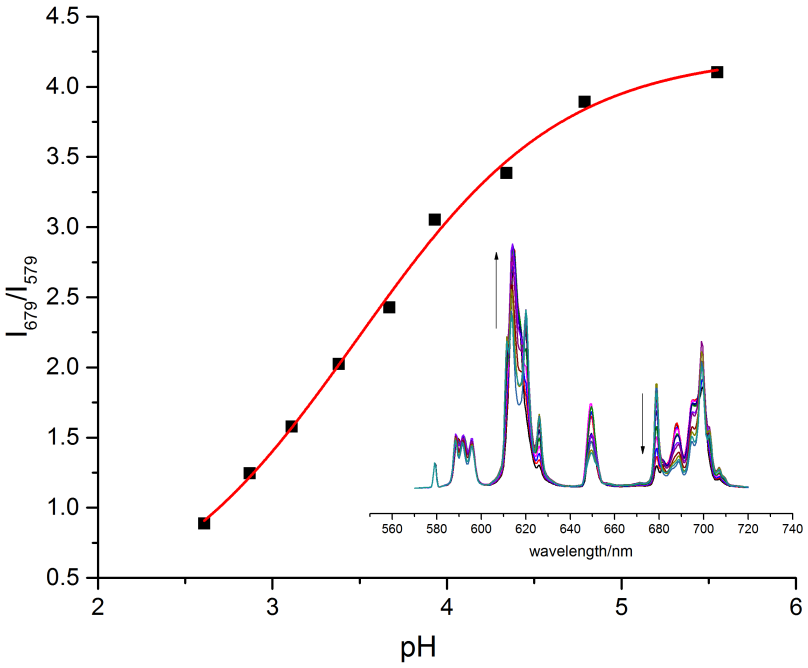


**Fig. II.19** Variation of the intensity of the emission band ($\lambda$ = 679 nm) relative to the intensity of $^5D_0 \rightarrow {}^7F_0$ transition at $\lambda$ = 579 nm of **[EuL$^2$]$^{2+}$** as a function of pH (p$K_a$ = 3.5, T = 25 °C, 0.1 M NaCl, $\lambda_{ex}$ = 325 nm).

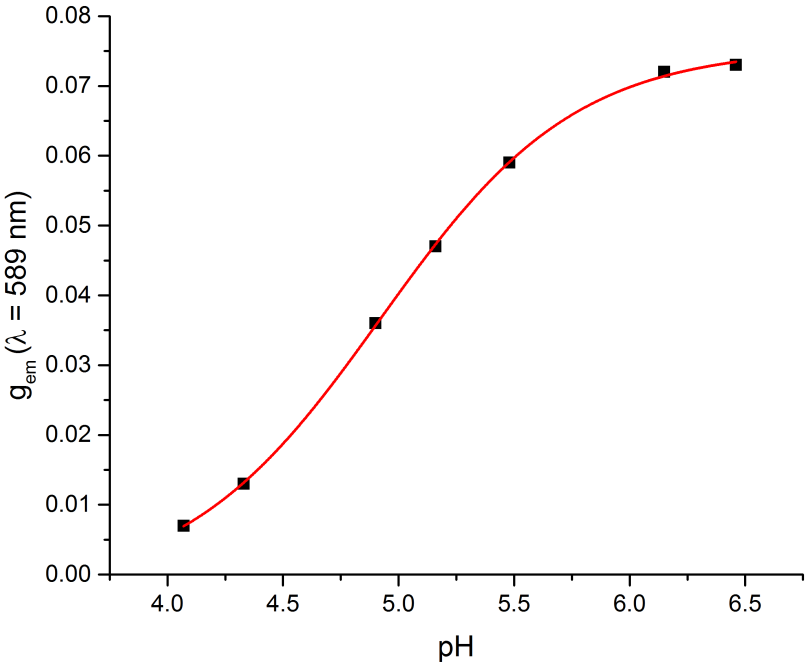


**Fig. II.20** Variation of the dissymmetry factor $g_{em}$ (589 nm) of **[EuL$^3$]** as a function of pH (p$K_a$ = 4.9, T = 25°C, 0.1 M NaCl, $\lambda_{ex}$ = 325 nm).

Both **[EuL$^2$]$^{2+}$** and **[EuL$^3$]** were examined as luminescent cellular stains in living mouse fibroblast cells (NIH-3T3) and human prostate cancer cells (PC-3), at a concentration of 20 μM in the cell growth medium. Unfortunately, already in the cell media the total emission intensity of both probes was significantly quenched, whilst a 24 h incubation revealed a preferential lysosomal localisation pattern (Fig. II.21). Nonetheless, the total emission intensity was too weak to use spectral imaging to acquire the emission spectrum or record the decay time *in cellulo*. No significant difference in localisation pattern and brightness was observed between NIH-3T3 and PC-3, implying a similar uptake mechanism in both cell lines.

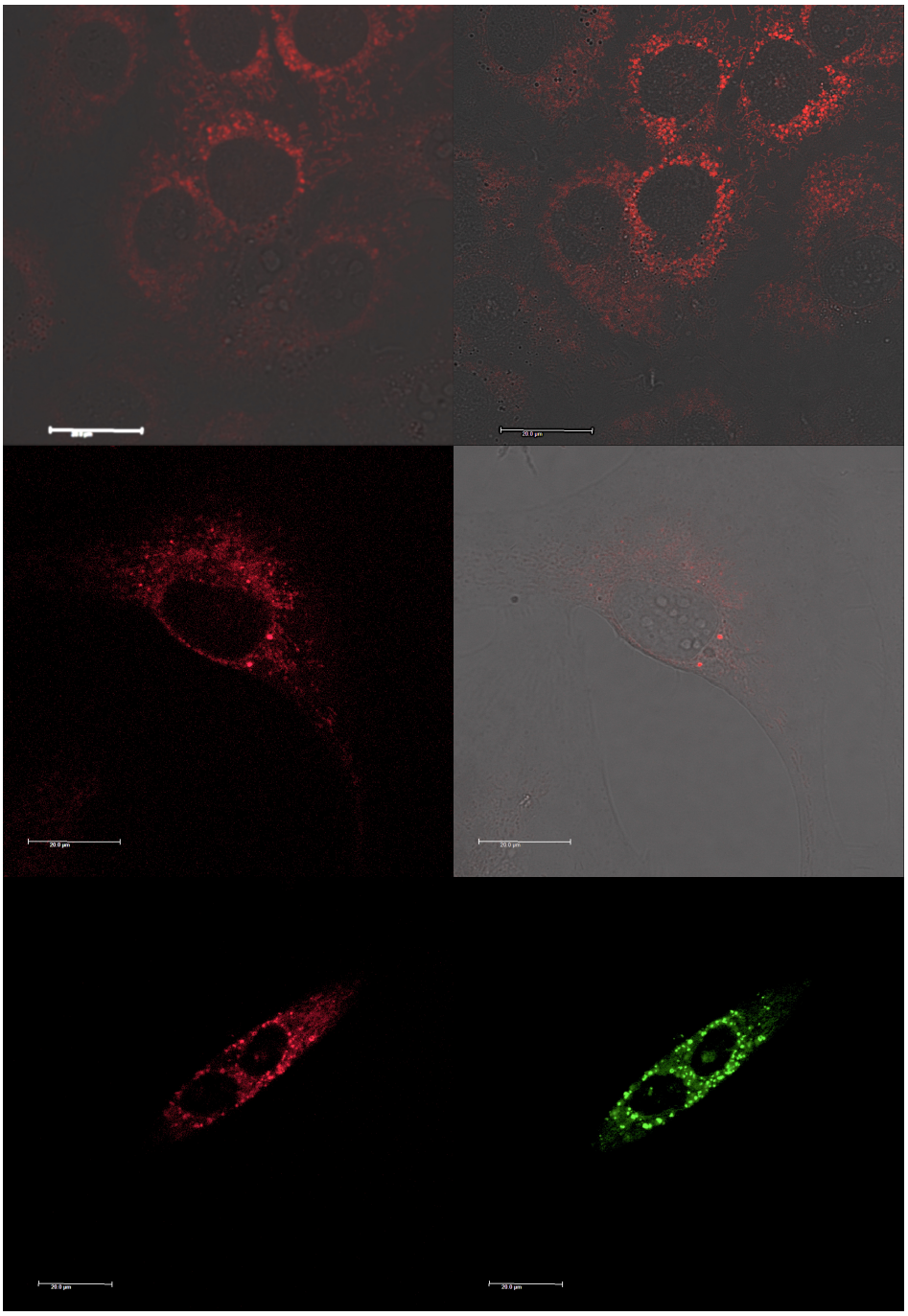

**Fig. II.21** LSCM images (1024x1024 pixel, 100 Hz bidirectional) of **[EuL$^2$]$^{2+}$** in NIH-3T3 cells (*top*), showing a predominantly lysosomal staining following a 2 h (*top left*) and a 24 h (*top right*) incubation of 10 μM complex ($\lambda_{ex}$ = 355 nm, $\lambda_{em}$ = 605–720 nm) and of **[EuL$^3$]** (*middle*) showing a predominantly lysosomal staining following a 24 h incubation of 10 μM complex ($\lambda_{ex}$ = 355 nm, $\lambda_{em}$ = 605–720 nm), and in PC-3 cells (*bottom*) following a 24h incubation of 10 μM complex ($\lambda_{ex}$ = 355 nm, $\lambda_{em}$ = 605–720 nm) and 5 min incubation of LTG ($\lambda_{ex}$ = 488 nm, $\lambda_{em}$ = 500–530 nm), also showing a lysosomal localisation pattern.

## II.5 Conclusions

In the present study, three different lysosome-selective pH-responsive probes were synthesised and their photophysical properties studied. In spite of the fact that all three complexes showed a p$K_a$ within the desired range of lysosomal pH, **[EuL$^1$]** showed an elevated p$K_a$ outside the required pH region, once the complex was bound to a protein, making pH measurements *in cellulo* impossible. Two other chiral probes, **[EuL$^2$]$^{2+}$** and **[EuL$^3$]**, showed drastically quenched emission in the cellular growth medium, consistent with the very faint brightness when localised inside the lysosome. However, all three probes did show a predominantly lysosomal localisation pattern, and therefore by judicious alteration of the ring substituents new probes with higher brightness and responsiveness within the lysosomal pH range should be able to be obtained.

The alkynyl-pyridine chromophore shows a relatively high affinity towards proteins, which is probably one of the reasons for the observed quenching of the europium (III)-centred emission. In order to decrease this affinity or at least to alleviate its quenching impact, a less conjugated chromophore might be used. One of the potential candidates is a biaryl chromophore, successfully used for sensitising both europium(III) and terbium(III) emission[9]. The pyridine bearing a carboxylate arm with trimethoxybenzene ring on the top is expected to have a broad absorbance band with $\lambda_{max}$ = 325 nm[10], and hence should be relatively bright upon excitation with a $\lambda$ = 355 nm laser in a confocal microscope. The proposed complex based on a cyclen core should have two chromophores in *trans* positions, with a sulfonamide arm in between them (Fig. II.22).

The proposed structure should have a q value equal to zero with both a bound and unbound sulphonamide nitrogen atom, making it significantly more stable against competitive anion binding and should inhibit emission quenching via O-H oscillators of bound water molecules at lower pH values. Also, the resulting complex can be used as a mixture of europium(III) and terbium(III) complexes, as their pH-sensitive behavior is usually different, and therefore by following the ratio between their total intensities *in cellulo*, a ratiometric response can be obtained[4].

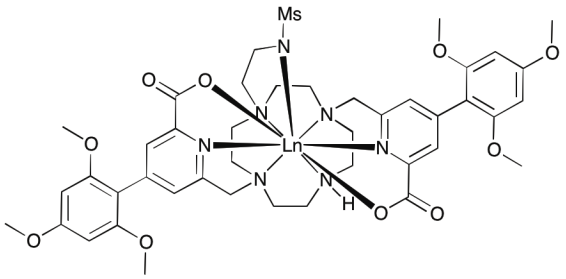


**Fig. II.22** Molecular structure of a proposed lysosomal probe for pH sensing (Ln = Eu, Tb).

Furthermore, the presemce of the biaryl chromophores makes the synthetic pathway significantly easier, as this moiety is stable to both acidic and basic hydrolysis conditions – the usual reactions to cleave protecting groups. The proposed synthetic route involves dialkylation of the *di*-Boc-cyclen with two freshly prepared mesylates of the chromophore, followed by Boc-deprotection using TFA. In the final step, the sulphonamide arm will be introduced by formation of an aziridine *in situ* in acetonitrile (Scheme II.2).

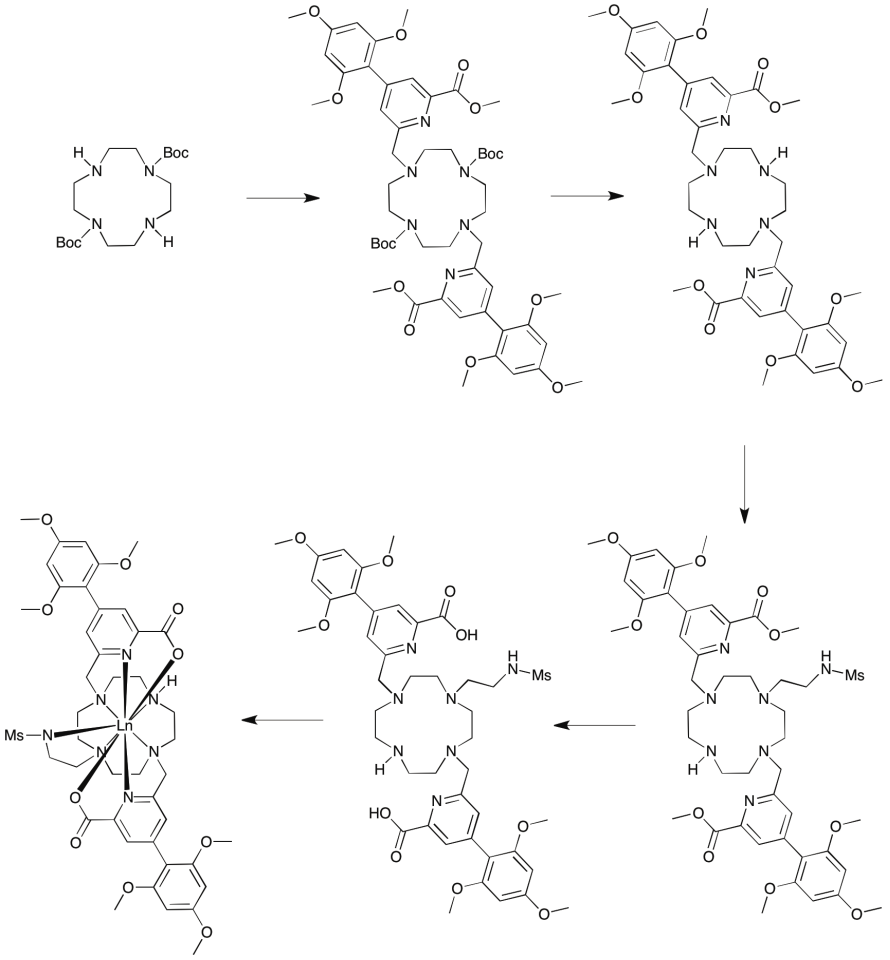


**Scheme II.2** Proposed synthetic pathway for a new pH-sensing complex.

Another possible solution to overcome the problem of competitive anion binding and quenching through bound water molecules is to modulate a spectral change without changing the coordination number of europium(III). It is difficult to predict the effective p$K_a$ of the molecular probe once it has entered a lysosome, as it can be bound to one of multiple proteins present inside. However, as a starting point of this search, a 1,2,3-triazole moiety attached to a pyridine ring can be considered (Fig. II.23). Upon protonation of a triazole moiety, a change in polarizability and partial charge occurs and therefore may be expected to produce a sufficient change in the spectral signature that can be monitored *in cellulo*. This pH-sensing moiety can be attached to either a DO2A platform or to a 9-N3 platform with an alkynyl-pyridine chromophore, giving rise either to a 8- or 9-coordinate systems. The latter system seems more advantageous because it possesses two chromophores with a phosphinite-substituteted pyridine with a 15-nm bathochromically shifted excitation maximum. Furthermore, related 9-N3 compounds typically have shown high brightness *in cellulo*[6].

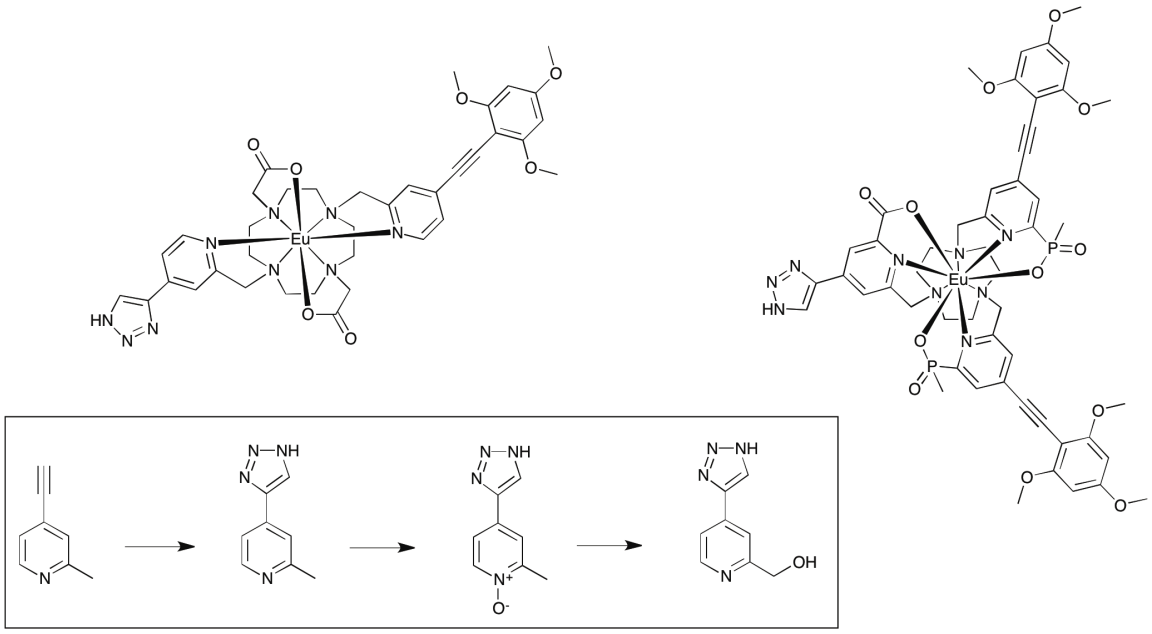


**Fig. II.23** Proposed molecular structures of europium complexes for lysosomal pH-sensing and a synthetic pathway for a pH-sensing arm.

## II.6 References


[1] M. P. Lowe, D. Parker, *Chem. Commun.* **2000**, 707–708.

[2] M. P. Lowe, D. Parker, *Inorg. Chim. Acta* **2001**, *317*, 163–173.

[3] R. Pal, D. Parker, *Chem. Commun.* **2007**, 474–476.

[4] D. G. Smith, B. K. McMahon, R. Pal, D. Parker, *Chem. Commun.* **2012**, *48*, 8520-8522.

[5] E. J. New, A. Congreve, D. Parker, *Chem. Sci.* **2010**, *1*, 111-118.

[6] S. J. Butler, M. Delbianco, L. Lamarque, B. K. McMahon, E. R. Neil, R. Pal, D. Parker, J. W. Walton, J. M. Zwier, *Dalton Trans.* **2015**, *44*, 4791–4803.

[7] B. K. McMahon, R. Pal, D. Parker, *Chem. Commun.* **2013**, *49*, 5363–5365.

[8] H. Li, F. L. Chadbourne, R. Lan, C.-F. Chan, W.-L. Chan, G.-L. Law, C.-S. Lee, S. L. Cobb, K.-L. Wong, *Dalton Trans.* **2013**, *42*, 13495-13501.

[9] T. Nakamura, S. Mizukami, M. Tanaka, K. Kikuchi, *Chem. - Asian J.* **2013**, *8*, 2685–2690.

[10] J. Hovinen, M. Veli-Matti, H. Hakala, J. Peuralahti, *Novel Chelating Agents And Highly Luminescent And Stable Chelates And Their Use*, **2005**, WO 2005/058877 A1.

# Chapter three

# Europium complexes for selective binding to HSA and $\alpha_1$-AGP

# III.1 Solvatochromism and emission

The presence of electron-donating and electron-withdrawing substituents conjugated within the same molecule creates a dipole moment, which upon irradiation with an excitation source creates an excited state, where an instant separation of charges occurs. This excited state can often serve as an efficient non-radiative quenching pathway for other excited states in the molecule, and due to its polar nature its energy is very sensitive to the polarity of the surrounding medium.

The fact that the polarity of solvent molecules can drastically affect the photophysical properties of its solute molecules was established in the early 20$^{th}$ century, when the term 'solvatochromism' was coined by Hantzsch.[1] It was postulated that any hypsochromic shift of the absorption/excitation/emission band upon increasing the solvent polarity is defined as negative solvatochromism, whilst any bathochromic shift is attributed to positive solvatochromism. The primary rationale behind the solvatochromic effect is the difference in energy between the ground and the first excited state caused by solvation changes. If increasing the solvent polarity caused the excited state to be better stabilised than the ground state then a positive solvatochromism results. On the other hand, preferential stabilisation of the ground state over the excited state gives rise to negative solvatochromism.

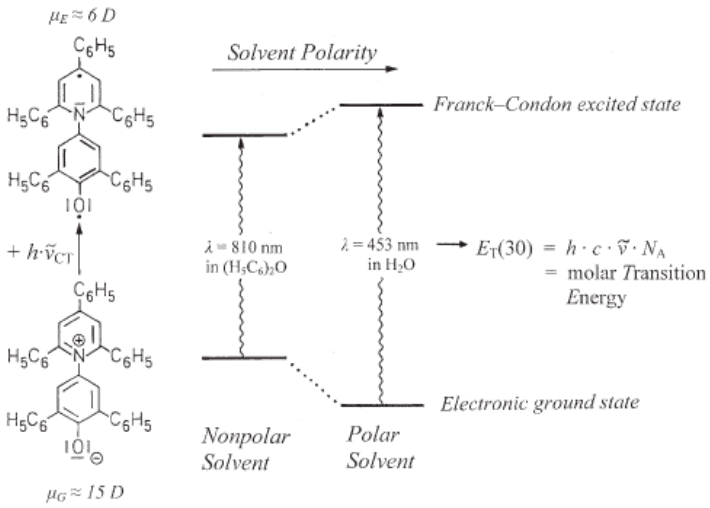


**Fig. III.1** Change of the dipole moment and the energy structure of 2,6-diphenyl-4-(2,4,6-triphenylpyridinium-1-yl)phenolate upon changing polarity of the solvent.[2]

Several attempts to arrange solvents in accordance with their polarities have been made resulting in different polarity scales. However, only the scale suggested by Reichardt has found widespread use and is now considered as a standard scale. A standard betaine dye (2,6-diphenyl-4-(2,4,6-triphenylpyridinium-1-yl)phenolate) was selected as a standard to define the scale (Fig. III.1) and its molar transition energy in different solvents was used as a measure of polarity:

$$E_T(30)/\text{kcal mol}^{-1} = hc\bar{\nu}_{max}N_A = 28591/(\lambda_{max}/\text{nm})$$

However, a normalised scale was later introduced to simplify the analysis of the data; water was chosen as the most polar and TMS as the most non-polar solvents, necessitating the use of a more lipophilic TMS soluble dye:

$$E_T^N = [E_T(\text{solvent}) - E_T(\text{TMS})]/[E_T(\text{water}) - E_T(\text{TMS})] = [E_T(\text{solvent})-30.7]/32.4$$

The data for several hundred different solvents have been tabulated and $E_T^N$ values for a selection of the most commonly used solvents are shown (Fig.III.2).

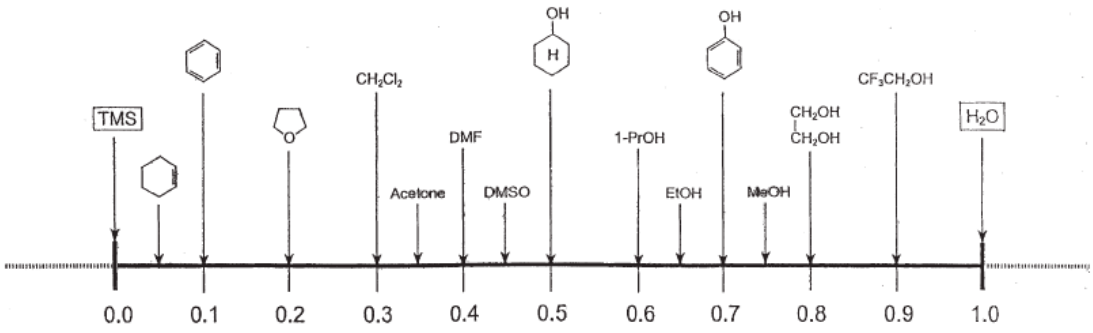


**Fig. III.2** Normalised Reichardt's paramateres $E_T^N$ for the most common solvents.[2]

Polar molecules showing strong solvatochromic effect found wide application for analyses of conformational changes in proteins to which they bind.[3] Once a solvatochromic probe has bound to a protein, the effective polarity of the immediate environment decreases, giving rise to a corresponding change in the photophysical response. If the conformation of the binding pocket in a protein changes as a result of applying an external stimulus, with a concomitant change of the exposure of the bound probe to water molecules, a further change of the solvatochromic response may be detected.

# III.2 [EuL$^4$] as a serum albumin probe

## *III.2.1 Solvatochromic properties of [EuL$^4$]*

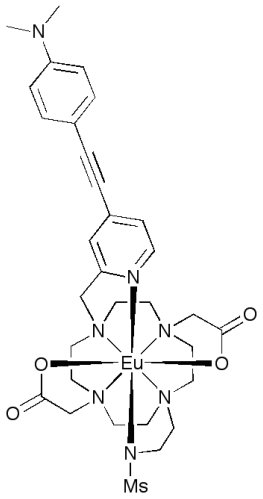


**Fig. III.3** Molecular structure of **[EuL$^4$]**.

In this work, the proposed HSA selective probe, **[EuL$^4$]**, possesses a highly polar chromophore with a dimethylamino electron donating group and the $Eu^{3+}$ ion bound to the pyridine ring serving as the electron withdrawing group, giving rise to an ICT state. The sulfonamide moiety modulates changes in the emission spectrum as a function of pH (Fig. III.3). The probe was synthesised in a similar manner to **[EuL$^1$]**.

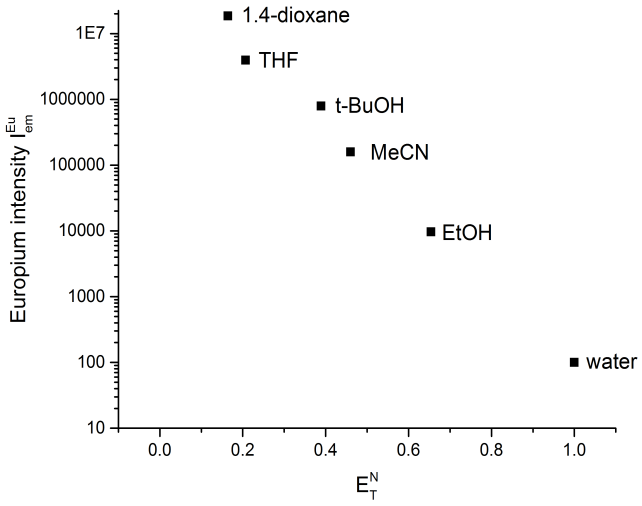


**Fig. III.4** Variation of europium total emission intensity for **[EuL$^4$]** with Reichardt's normalised solvent polarity parameter $E_T^N$ (298 K).

**[EuL$^4$]** showed only very faint emission intensity in aqueous solution at rt, whilst a much brighter $Eu^{3+}$-centred emission was observed in a solid state and in a frozen

aqueous solution. Unsurprisingly, the total emission intensity was strongly dependent on the polarity of the solvent, showing a dramatic increase upon decreasing the polarity of the solvent (Fig. III.4).

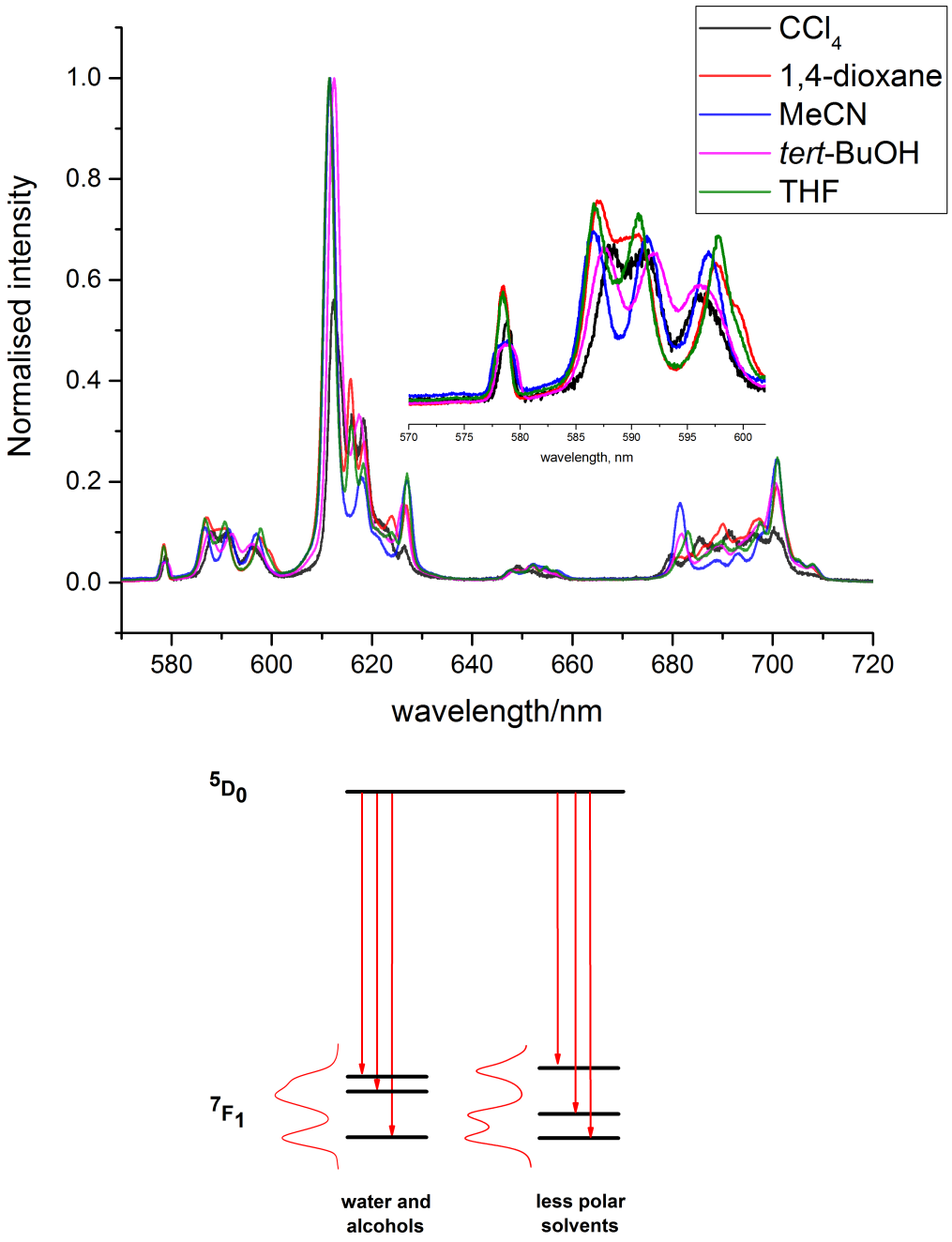


**Fig. III.5** Emission spectra of **[EuL$^4$]** in different organic solvents and water, with a magnified region of $^5D_0 \rightarrow {}^7F_0$ and $^5D_0 \rightarrow {}^7F_1$ and corresponding change in the Stark splittings of the $^7F_1$ manifold (298 K, $\lambda_{ex}$ = 390 nm).

However no significant change in both the absorption and excitation spectra was observed upon varying the solvent polarity ($\lambda_{max}$ ~ 375 nm in all the cases). Therefore, no formal assignment of either a positive or negative solvatochromic

effect is possible. Apart from the change in the total emission intensity, the spectral form experienced considerable changes upon variation of the solvent polarity (Fig. III.5). A careful analysis of $^5D_0 \rightarrow {}^7F_1$ manifold shows a solvent dependency of the crystal field parameters $\boldsymbol{B_0^2}$ and $\boldsymbol{B_2^2}$. Since no change of the coordination environment is expected upon varying solvent, a change in the solvent polarity is likely to be responsible for this significant change. In comparison with aqueous solutions, the sign of $\boldsymbol{B_0^2}$ changes in organic solvents, being close to zero for acetonitrile solution. However, as already shown in the previous chapter, the same change of the emission spectrum is observed upon protonation of a sulfonamide arm and therefore it cannot be excluded that it is displaced in less polar solvents.

The crystal field parameters, which determine the magnitude of $^7F_1$ splitting to a first approximation, depend on the coordinates of the ligating atoms and their effective partial charges. It was previously demonstrated that even subtle structural changes induced by variation of the solvent polarity and/or hydrogen bonding can result in dramatic change of crystal field parameters and hence the luminescence spectral form[4]. In other words, the long-standing assumption that crystal field parameters can be treated as constants regardless of the solvent used is incorrect, and thus emssion spectroscopy has been shown to be a useful means to verify that in each specific case.

Being inspired by the strong solvent-dependent photophysical response of **[EuL$^4$]**, selected abundant serum proteins were tested as potential 'sensitisers' of the emission. No significant change in the overall emission intensity was observed in the case of ImG, fibrinogen and $\alpha_1$-AGP, but a large increase of the emission intensity was observed upon addition of HSA (Fig. III.6). Moreover, a strong induced CPL signal was observed upon binding to HSA with $g_{em}$ = -0.2 ($\lambda$ = 589 nm), which is a very high value for dynamically racemic complexes. Similar behaviour was reported for an $\alpha_1$-AGP sensor based on a europium complex with a DO2A-derived ligand bearing two azaxanthone chromophores[5]. The complex showed a strong CPL signal with $g_{em}$ = - 0.23 ($\lambda$ = 598 nm) upon addition of $\alpha_1$-AGP, which is close to the observed value in this system. However as the dissymmetry factor $g_{em}$ is defined according to the following expression:

$$g_{em} = \frac{2(I_R - I_L)}{I_R + I_L}$$

the overall emission intensity $I_R + I_L$ from all emissive species is taken into account, including those which do not produce any CPL signal. Therefore, the 'real' $g_{em}$ value for the induced CPL signal may be larger, unless an induced CPL signal is solely due to a 'turned on' emission. This is exactly the situation observed for **[EuL$^4$]**, as the very weak emission from **[EuL$^4$]** in the absence of HSA can be ignored.

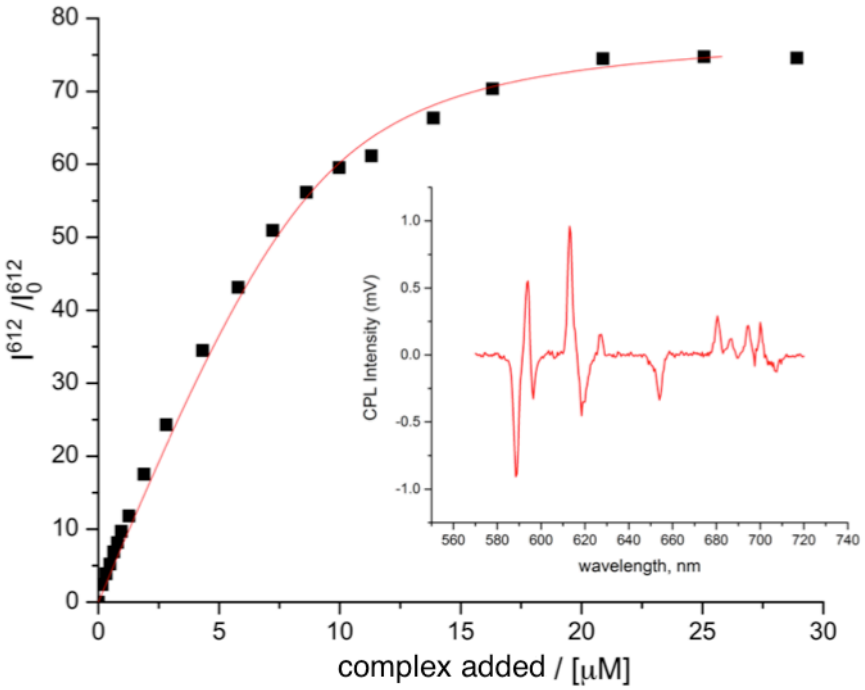


**Fig. III.6** Variation of Eu emission intensity as **[EuL$^4$]** is added to HSA (295 K, 0.1 M NaCl, 11 μM protein; log K = 6.00 (±02); the inset shows the induced CPL spectrum recorded for the protein bound complex ($\lambda_{ex}$ = 390 nm).

Even though the aforementioned europium complex **[EuL$^{x1}$]** with two *trans*-azaxanthone ligands showed a stronger response towards $\alpha_1$-AGP, an induced CPL signal was also observed upon addition of HSA. Since the coordination environment of this complex and **[EuL$^4$]** share some similarities, i.e. two carboxylate arms and the bound pyridine, a similar binding mode in the protein binding site can be expected. A comparison between the induced CPL spectra of each complex (Fig. III.7) suggests that the helicity of the bound complex is the same in each case, consistent with binding to the same pocket. This conclusion is not surpising, bearing in mind the similarity in structure of the complexes, including their relative size and lipophilicity.

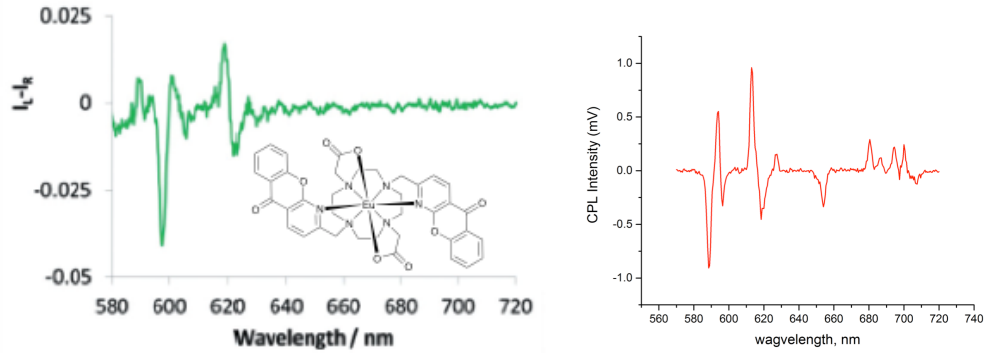


**Fig. III.7** CPL spectra of the europium complex **[EuL$^{x1}$]** reported in ref. [5] (*left*) and **[EuL$^4$]** with added HSA (*right*) (295 K, $H_2O$).

Once **[EuL$^4$]** is bound to HSA, a significant bathochromic shift of the excitation maximum was observed to 396 nm (Fig. III.8). The shift of *ca.* 30 nm, when compared to **[EuL$^4$]** with no added protein, cannot be attributed simply to a change of polarity of the immediate surrounding environment, as even in very non-polar solvents, such as THF or 1,4-dioxane, the excitation maxima were only slightly shifted compared to aqueous solution. This discrepancy may be tentatively explained by the proximity of two complexes within the same binding pocket, in line with the binding curve depicted above. Indeed, the saturation of the binding curve was reached when approximately two equivalents of **[EuL$^4$]** were added.

It has been shown that rod-like, polar conjugated molecules can stack together, ultimately forming either H- or J-aggregates at elevated concentrations[6]. This aggregation process gives rise to either a bathochromic (for J-aggregates) or hypsochromic (for H-aggregates) shift in absorption/excitation spectra. Usually formation of J-aggregates is accompanied by enhancement of total emission intensity, whilst emission from H-aggregates is normally quenched. It might seem surprising, at first glance, that in the case of **[EuL$^1$]** (which can be used as a model compound for **[EuL$^4$]** as no significant difference in the aggregation behaviour should be expected), a bathochromic shift was accompanied by quenching of the total emission, when the complex concentration was increased. However, since the formation of J-aggregates lowers the energy position of both singlet and triplet states, the gap between the latter and the corresponding $^5D_0$ energy level of $Eu^{3+}$ decreases, enhancing the efficiency of back energy transfer and hence lowering the quantum yield for europium emission. With these observations in mind, it can be concluded

that the observed 'turn-on' reflects a competition between these two processes – reduced ICT-mediated quenching by decreasing the polarity of the local environment and decreased overall emission intensity through formation of J-aggregates.

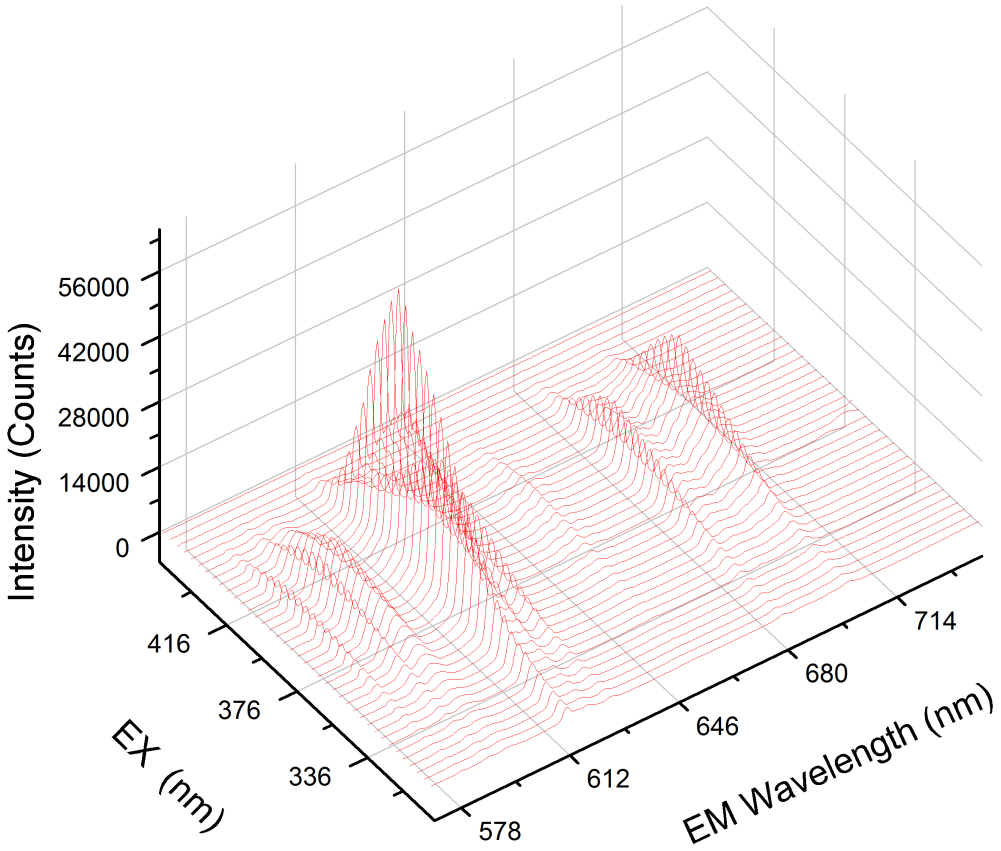


**Fig. III.8** Three-dimensional excitation-emission spectra for **[EuL$^4$]** (10 μM) in the presence of HSA (0.4 mM) (298 K, $H_2O$).

## *III.2.2 Binding of [EuL$^4$] to HSA*

One of the primary biological functions of serum albumin is the transfer of essential exogenous and endogenous drugs. Two primary binding pockets, usually referred to as drug sites (DS) 1 and 2 (or warfarin and ibuprofen sites, respectively), have been identified and many drugs are known to bind selectively to one of those sites. In order to answer the question whether **[EuL$^4$]** selectively binds to either of these two sites, competitive binding studies were undertaken with two DS-1 selective (warfarin and iodipamide) and one DS-2 selective (ibuprofen) drugs.

A preliminary analysis of the literature suggested that a complex with a bulky heterocyclic chromophore is more likely to bind to DS-1[7]. Competitive binding studies with iodipamide showed a significant quenching of **[EuL$^4$]** emission (Fig. III.9), although some residual emission was still observed, even after a 10-fold excess of the drug was added. This behaviour suggests that more than one binding site for **[EuL$^4$]** exists. The calculated affinity constant for **[EuL$^4$]**, based on this competitive method, (log$K$ = 5.29(±03)) agrees reasonably well with the overall binding constant for **[EuL$^4$]** (log$K$ = 6.00(±02)). Competitive binding with warfarin also revealed quenching of the emission intensity, but again some residual emission was still observed, even after addition of a 10-fold excess of the drug.

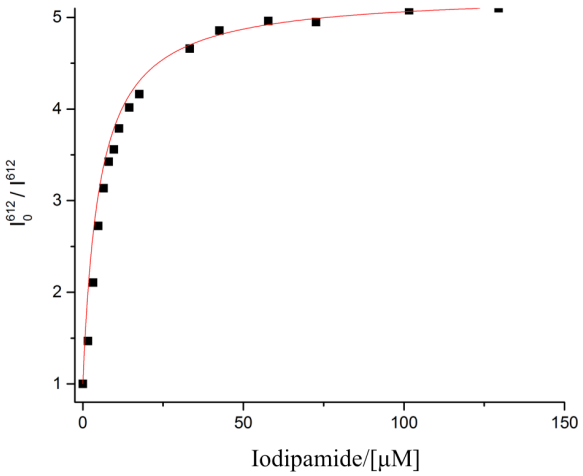


**Fig. III.9** Variation of europium emission intensity in the presence of HSA showing the fit (line) to the data points with added iodipamide (**[EuL$^4$]** 30 μM; [HSA] 9.0 μM), log K = 5.29(03), $\lambda_{ex}$ = 390 nm, 298 K, pH = 7.40).

Competitive binding studies with ibuprofen (Fig. III.10) also revealed quenching of the emission intensity of **[EuL$^4$]**, although the two-step binding curve reached a plateau at *ca.* 50% of the initial intensity. The calculated affinity constant for **[EuL$^4$]** (5.16(±03)) again correlates relatively well with the overall binding constant of 6.00(±02).

Summarising the competitive binding data, several important conclusions can be drawn. Firstly, addition of iodipamide, which possess the highest known affinity for HSA ($K_a$ = 2.3x10$^7$ M), [8] quenched 80% of the total emission intensity, whilst ibuprofen reduced it only by 50%. These findings suggest that **[EuL$^4$]** binds to both DS-1 and DS-2, with an overall site affinity that is of the order of 2x10$^5$ M$^{-1}$.

Secondly, at least one additional binding site exists, which judging from the required steric demand might be localised in the cleft. However, no cleft-selective drugs are known and therefore performing competitive binding studies did not seem feasible. Moreover, it was reported that the cleft is a secondary binding site for ibuprofen[9], and therefore the competitive binding curve obtained may include replacement of **[EuL$^4$]** from both the primary and secondary sites, including the cleft.

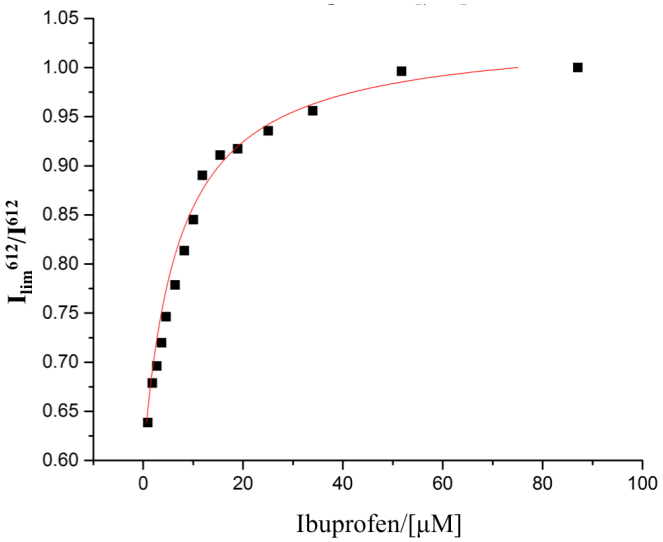


**Fig. III.10** Variation of europium emission intensity in the presence of HSA showing the fit (line) to the data points with added ibuprofen (**[EuL$^4$]** 26 μM; [HSA] 9.4 μM, log K = 5.16(03), assuming a 1:1 binding isotherm, $\lambda_{ex}$ = 390 nm, 298 K, pH = 7.40).

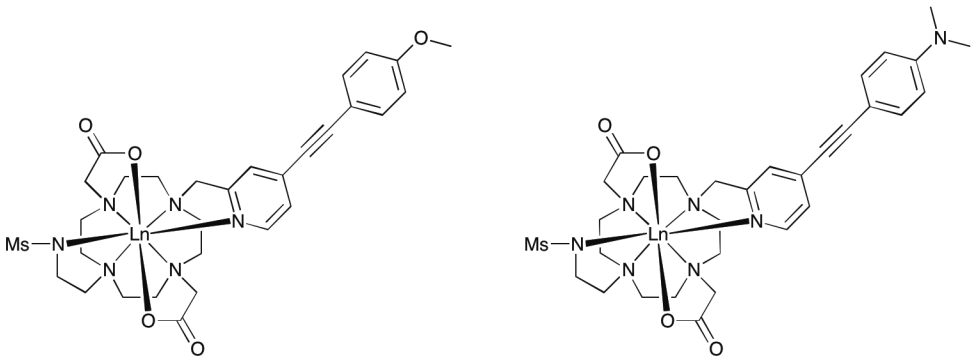


**Fig. III.11** Molecular structures of **[EuL$^1$]** (*left*) and **[EuL$^4$]** (*right*)

The structure of **[EuL$^4$]** is closely related to **[EuL$^1$]** (Fig. III.11), and therefore the p$K_a$ of the former is expected to be close to that obtained for **[EuL$^1$]** (p$K_a$ ~ 4.0 in 0.1 M NaCl aqueous solution) and probably slightly higher, due to the presence of a stronger donating $NMe_2$ group on top of the chromophore. However, direct measurement of the p$K_a$ of **[EuL$^4$]** in the absence of the protein was hampered by its low emission intensity, whilst the absorption spectrum did not show any noticeable

change. At the same time, the p$K_a$ value may experience a dramatic change upon binding to the protein, as has been shown in the number of examples[10], including **[EuL$^1$]**, where a p$K_a$ ~ 7.0 was observed in cell lysate.

A similar situation was observed in the case of **[EuL$^4$]** (Fig. III.12), where a p$K_a$ value of 7.2 (±0.1) was calculated in the presence of HSA, which is approximately 3 units higher than that expected in the absence of HSA. Moreover, nearly a complete quenching of the emission intensity was observed below pH 6.0, which can be explained by the replacement of the sulfonamide nitrogen by two water molecules. The spectral form of the emission spectrum showed a moderate change in the relative intensity of crystal field components upon varying solution pH. However, no change of the $\boldsymbol{B_0^2}$ sign was observed, as was the case for **[EuL$^1$]**. As mentioned before, no structural rearrangements of HSA occur at pH values above 6.0, and hence the observed p$K_a$ was attributed to the reversible binding of the sulfonamide arm. This process could be associated with the binding of an amino acid side chain, e.g. the carboxylate group in either Asp or Glu in the low pH regime. Unfortunately, the low emission intensity at reduced pH values inhibited acquisition of CPL spectra, which might have helped to characterise the local environment.

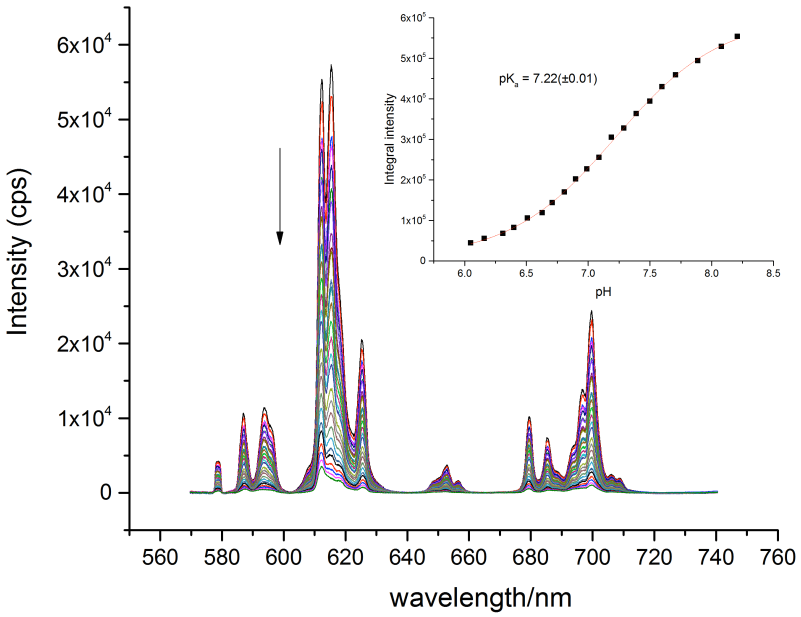


**Fig. III.12** The pH dependence of Eu emission in the human serum albumin bound complex (295K, 0.1 M NaCl, 10 μM **[EuL$^4$]**, $\lambda_{ex}$ = 390 nm) fitted as a Boltzmann sigmoid.

### *III.2.3 Binding of [EuL$^4$] to bovine , rabbit and goat serum albumins*

Although human serum albumin shares 76% sequence homology[11] with bovine serum albumin, changes in the remaining 24% of amino-acids can give rise to significantly different drug-binding properties. The analysis of amino-acid sequences in Sudlow's DS-1 and DS-2 (Fig. III.13) reveals a significant variation of amino acids capable of drug binding. As it is hypothesised that **[EuL$^4$]** primarily binds to DS-1, a more detailed consideration of the amino-acids lining this binding pocket has been performed. Substitution of Val-122 with Thr-121, as well as Thr-125 with Asp-124 and Ala-126 with Gly-125 increase the hydrophilicity of this binding pocket in BSA and reduce the number of functional groups which can be involved in hydrogen bonding with drugs in HSA.

Since the hydrophobicity of the HSA binding pocket is believed to be the key factor in 'switching on' the emission from **[EuL$^4$]**, similar binding studies were attempted with bovine, rabbit (RSA) and goat (GSA) serum albumins. In none of the cases was a comparable 'turn-on' response observed, making **[EuL$^4$]** a 'species selective' probe towards HSA.

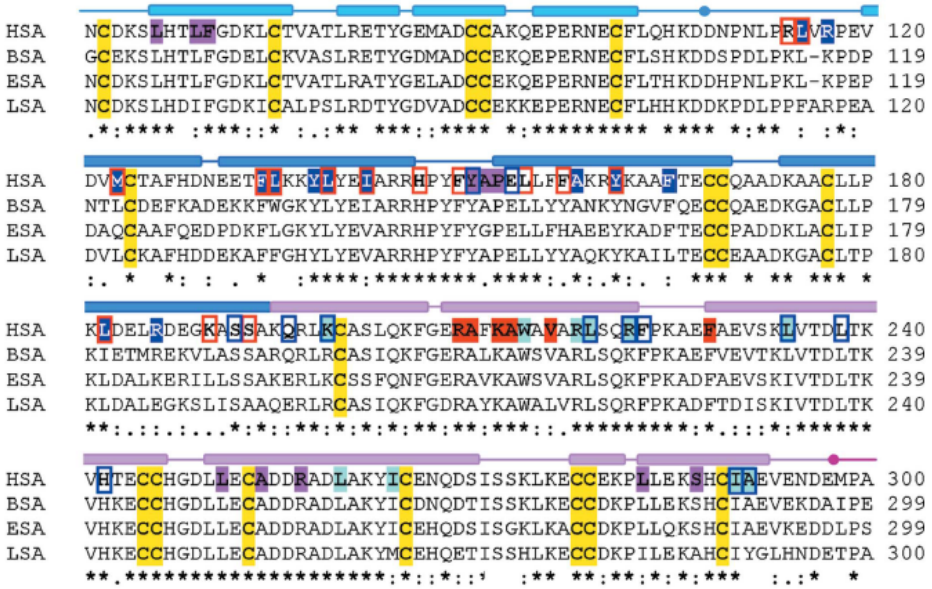


**Fig. III.13** Sequence alignment of HSA, BSA, equine SA and leporine SA. The amino acids in DS-1 are marked by dark blue and those in DS-2 are marked by cyan.[12]

The emission spectrum of **[EuL$^4$]** following addition of either HSA or BSA showed the same profile, suggesting a very similar coordination environment when protein

bound (Fig. III.14). Due to the low emission intensity of **[EuL$^4$]** in the presence of BSA, no CPL spectrum was able to be acquired to probe the immediate environment around $Eu^{3+}$. Analysis of the lifetimes of the europium excited state revealed a shorter lifetime for **[EuL$^4$]** when bound to BSA (0.18 ms), compared to HSA (0.30 ms). This observation is in line with the lower hydrophobicity of BSA and, as a consequence, with a more efficient back energy transfer rates from the resonance level of $Eu^{3+}$ to the ICT state of the ligand.

**Table III.1** Selected photophysical properties of **[EuL$^4$]** and **[EuL$^1$]** (295 K, $H_2O$)

| Complex | **[EuL$^4$]** | **[EuL$^1$]** |
|---|---|---|
| $\lambda_{abs}$/nm | 365 | 325 |
| $\varepsilon(H_2O)/M^{-1}cm^{-1}$ | 28,000 | 35,400 |
| $\tau_{H_2O}$/ms | c | 0.73 (pH 6) |
| $\tau_{D_2O}$/ms | c | 1.00 (pH 6) |
| $\tau_{H_2O}$ + HSA/ms[a] | 0.30<br>(0.18) | 0.79<br>(1.02) |
| $\phi_{Eu}$/% | 0 | 6.6 |
| $\phi_{Eu}$ + HSA/%[a] | 0.7 | 6.0 (4.3)[b] |

[a]Added protein concentration was 0.7 mM; [b] value in parenthesis is for added BSA; [c] No measurable emission in solution.

Analogous measurements performed in $D_2O$ showed a predictable increase of the total emission intensity in each case (HSA and BSA), and were consistent with the presence of the outer sphere water molecules, which contributed to the quenching of $^5D_0$ excited state (hydration number q equals zero in each case).

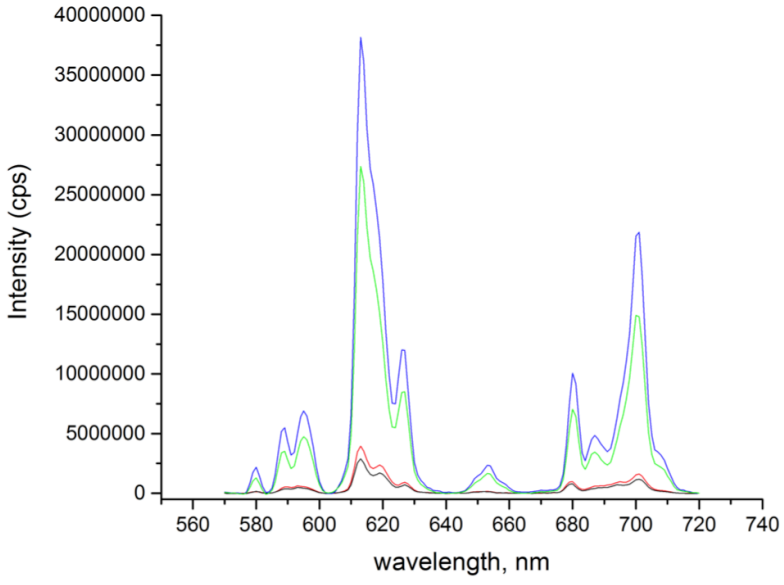


**Fig. III.14** Emission spectra of **[EuL$^4$]** (10 μM) in the presence of HSA (0.75 mM) in $H_2O$ (*green*) and $D_2O$ (*blue*), as well as in the presence of BSA (0.75 mM) in $H_2O$ (*black*) and $D_2O$ (*red*) (295 K, $\lambda_{ex}$ = 390 nm).

An important consequence of the observed specificity of **[EuL$^4$]** towards HSA is the impact of the selection of the type of the serum used as cell medium, in the performance of the luminescent probes studied. As a proof of concept, emission intensities of **[EuL$^4$]** with HSA, BSA and GSA were recorded, revealing a similar difference of the overall emission intensity as for *in vitro* studies (Fig. III.15). At the same time, analysis of the lifetimes was also in accord with *in vitro* experiments, showing lower lifetimes for BSA and GSA (0.19 ms and 0.22 ms, respectively) and a longer lifetime for HSA (0.47 ms). These results are again consistent with a more efficient back energy transfer from $Eu^{3+}$ to ICT state for the BSA- and GSA-bound species.

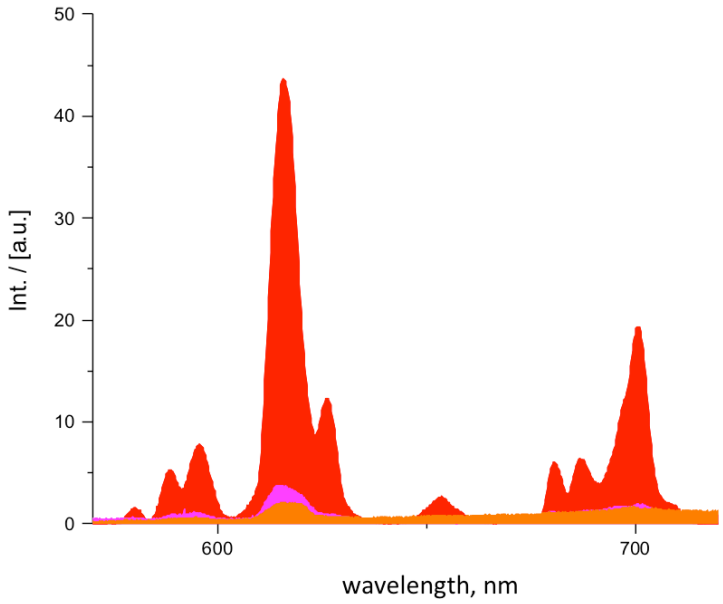


**Fig. III.15** Emission spectra of **[EuL$^4$]** in the growth medium (10 μM) with added HSA (*red*), BSA (*orange*) or GSA (*magenta*) respectively.

## *III.2.4 Cellular studies of [EuL$^4$] incubated in different serum albumins*

The complex **[EuL$^4$]** possesses an N-coordinated sulfonamide group with a p$K_a$ expected to be in the pH range of the lysosome. The presence of such a group usually promotes lysosomal uptake and is often referred as lysosomal trapping.[13] The **[EuL$^4$]** complex was examined as a luminescent cellular stain in living mouse fibroblast cells (NIH-3T3) using both live cell epi- and confocal microscopy. In the incubation medium, 10% foetal calf-serum (FCS) is normally added to promote cell growth; FCS contains BSA. Accordingly, different cell growth media were created

to replace FCS based on added heat inactivated, purified, culture grade human or goat serum. In the cell medium, the Eu emission could only be easily discerned by spectral imaging for the HSA-added preparation. Following an incubation of 4h in respective growth medium containing up to 100 µM **[EuL$^4$]** and keeping all experimental parameters constant, the Eu staining was 20 times brighter for the HS-medium vs FCS-medium.

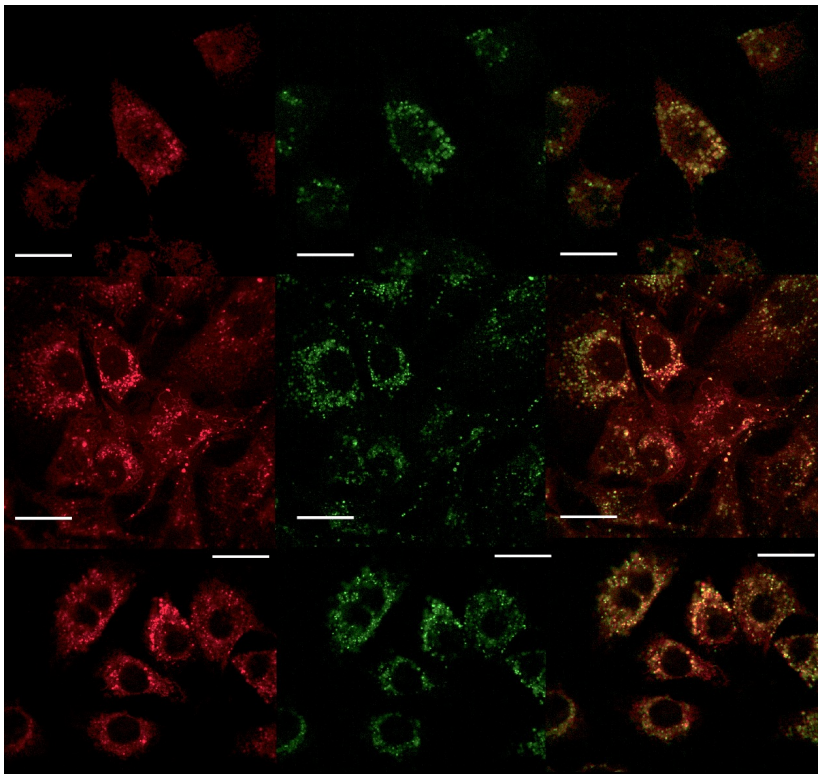

**Fig. III.16** LSCM images (1024 x 1024 pixel, 100Hz bidirectional) in NIH-3T3 cells showing: (upper) predominantly lysosomal staining following a 4 h incubation of 10 µM complex **[EuL$^4$]** ($\lambda_{ex}$ = 355 nm, $\lambda_{em}$ = 605-720 nm, 8 mW), and 5 min incubation of LysoTracker Green® ($\lambda_{ex}$ = 488 nm, $\lambda_{em}$ = 500-530 nm, 2 mW), (ambient lysosomal pH is *ca.* 4.5); (centre/lower): enhanced image intensity following a 5 min incubation with nigericin (200 nM) and LysoTracker Green® (central columns), RGB merge highlighting correspondence (scale bar 20 µM).

A study was initiated to allow consideration of the question as to whether it is enhanced intracellular uptake in the presence of HSA or enhanced complex brightness *in cellulo* that explains the variation of Eu emission intensity observed by microscopy. A lysosomal staining pattern was confirmed by co-staining with LysoTracker Green™ (P >0.83, Fig. III.16). The brightness of cell images was increased by 120% vs FCS medium when the local lysosomal pH (normally around 4.2-4.5) was adjusted to 6.5, following addition of nigericin (5 min, 200 nM)[14].

Independent measurement of the total Eu intracellular concentration for each incubation, was determined by ICP-MS measurements. No significant differences in Eu concentrations were observed between incubations of **[EuL$^4$]** with added HSA and BSA (62% and 60% accumulations, respectively). However, the sample incubated with GSA showed a siginificantly lower intracellular concentration (29%).

### *III.2.5 Serum albumin binding studies with [GdL$^4$]*

In order to answer the question if the observed 'turn-on' response was a result of a selective binding of the europium complex with HSA over BSA, the gadolinium analogue of **[EuL$^4$]** was synthesised, and its relaxivity measured as a function of added protein at 310 K and 1.4 T.

Water molecules in an aqueous solution of a paramagnetic complex are in constant exchange with each other. Of particular interest is the exchange between water molecules in the vicinity of the complex - either directly bound to the metal ion or in close proximity to it (the latter is usually referred as a second sphere water molecule) – and the bulk of an aqueous solution. Once an aqueous solution is brought into an external magnetic field, nuclear spins are aligned along the direction of this field (z axis). If a short RT pulse is applied perpendicular to the direction of an external magnetic field (i.e. along the x axis), a net magnetisation vector is tipped away from its initial position by a flip angle (determined by the duration of the pulse), nutating along the z axis giving rise to non-zero components of magnetisation vector $M_x$ and $M_y$ along x and y axis, respectively. After the RF pulse has ended, the net magnetisation vector recovers its initial direction along the z axis, with a characteristic decay time along x (y) axis $\mathbf{T_1}$, and a rise time along z axis $\mathbf{T_2}$.

The presence of the paramagnetic centre significantly changes the $\mathbf{T_1}$ value of water molecules. In these solutions the observed relaxation rate $\frac{\mathbf{1}}{\boldsymbol{T_{1,obs}}}$ can be expressed as a combination of diamagnetic and paramagnetic contributions:

$$\frac{1}{T_{1,obs}} = \frac{1}{T_{1,d}} + \frac{1}{T_{1,p}}.$$

In turn, the paramagnetic term is directly proportional to the concentration (*C*) of a paramagnetic ion (contrast agent) in the solution:

$$\frac{1}{T_{1,p}} = r_1 C$$

where $r_1$ is a characteristic of a contrast agent, showing how efficiently it reduces the observed relaxation rate $\frac{\mathbf{1}}{\boldsymbol{T_{1,obs}}}$.

There are several factors which determine the relaxivity of a given contrast agent. The number of directly bound water molecules $\boldsymbol{q}$ is the major parameter, varied by judicious ligand design. The interplay between maximising the $\boldsymbol{q}$ value and retaining stability of the complex towards decomplexation is the primary challenge in the design of new contrast agents. Another highly important parameter is the mean residence time of a directly bound water molecule $\boldsymbol{\tau_m}$ – the less time the water molecule remains bound to a paramagnetic metal ion, the faster is the exchange rate with bulk water and hence the more efficient the transfer of relaxation enhancement to the bulk solution (although the residence time should be long enough to accomplish full relaxation of the bound water molecule). The last parameter that can be altered by chemical design is the rotational correlation time $\boldsymbol{\tau_r}$ - reciprocal of the tumbling rate of the molecule in the solution. Enhancement of the tumbling rate is frequently exploited by increasing the molecular weight of the probe by attaching to macromolecules, for instance proteins.

Several examples on the improvement of the tumbling rate, and hence the observed relaxation rate have been reported, following binding of gadolinium complexes to serum albumins. In some cases, introducing molecular fragments known for their high affinity towards serum albumin may result in high affinity of the overall hybrid towards it. Bearing this in mind, Caravan showed that coupling an ibuprofen moiety – a well-known example of the drug transferred by HSA in human plasma - to the DO3A derivative **[Gd(7)($H_2O$)]**$^-$ via a primary amine arm (Fig. III.17) leads to a 5-fold increase of the observed relaxation rate (from 4.8 $mM^{-1}\,s^{-1}$ to 22.4 $mM^{-1}\,s^{-1}$, at 37 °C) upon addition of HSA, concomitant with displacement of one bound water molecule by an amino-acid side chain, e.g. Glu[15].

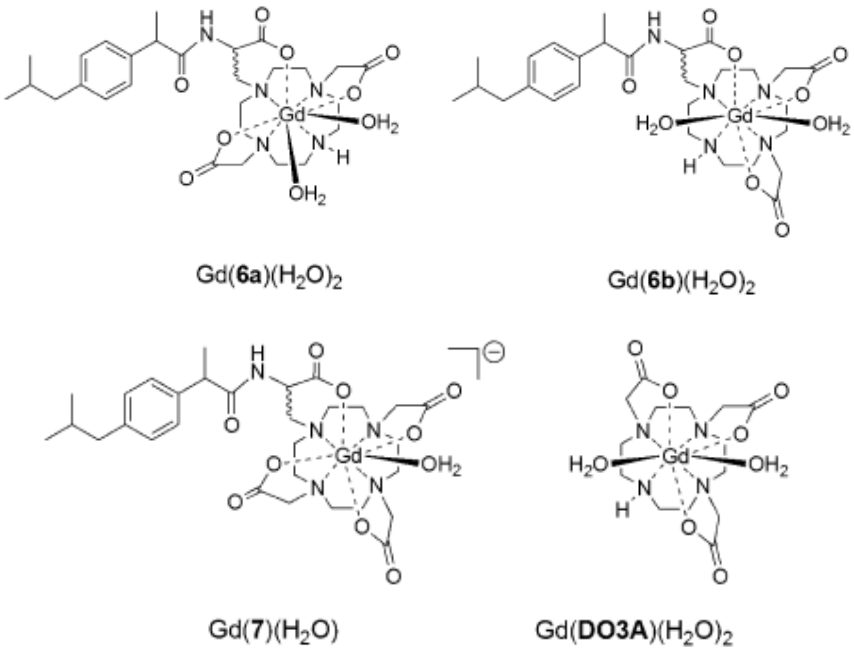


**Fig. III.17** Molecular structures of **[Gd(6a)(H$_2$O)$_2$]**, **[Gd(6b)(H$_2$O)$_2$]**, **[Gd(7)(H$_2$O)]$^-$** and the related **[Gd(DO3A)(H$_2$O)$_2$]**.[15]

A similar enhancement was observed in related DO2A structures, where two water molecules are bound in the absence of added protein, and therefore the overall gain in relaxivity rate upon protein binding was less pronounced (13.5 and 12.7 $mM^{-1}s^{-1}$ at 37 °C and 60 MHz for **[Gd(6a)(H$_2$O)$_2$]** and **[Gd(6b)(H$_2$O)$_2$]**, respectively), showing the competition before two aforementioned factors contributing to the observed relaxation rate – number of bound water molecules and the molecular weight of the aggregate.

Serum albumin proteins of different species are usually not distinguished and the more accessible bovine serum albumin is most commonly used for binding studies. However, deviations in amino-acid sequences between serum albumins of different species may give rise to differences in binding properies of the same drug. The only known example of such a study with a gadolinium contrast agent binding to different serum albumins was made by Caravan using **MS-325** (also known under its trade names Gadofosveset®, Vasovist® and Ablavar®)[16]. It was shown that plasma of different mammals showed different enhancement of the observed relaxivity upon binding to **MS-325**, along with significantly different binding affinities (Fig. III.18), following the order human > pig ~ rabbit > dog ~ rat ~ mouse.

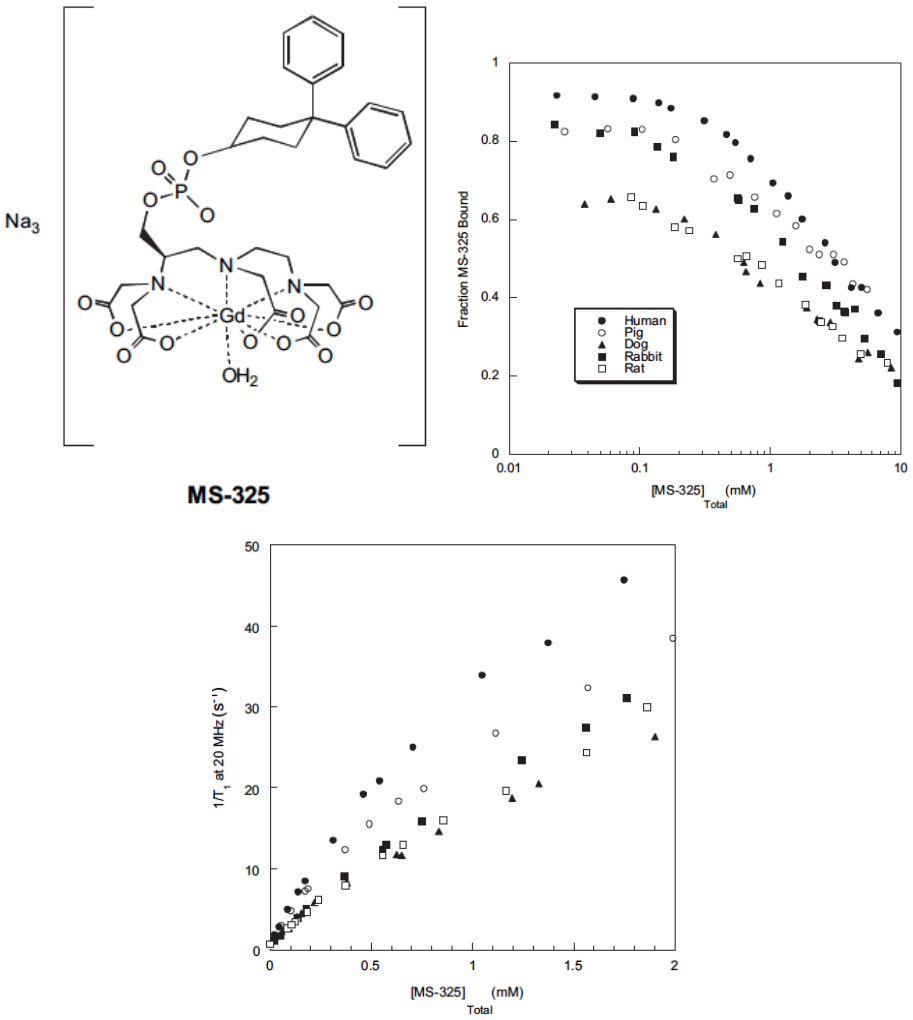


**Fig. III.18** Molecular structure of **MS-325** (*top left*), molecular fraction of bound **MS-325** as a function of added **MS-325** in different plasmas (*top right*) and change of the observed relaxivity as a function of added **MS-325** for different plasmas (*bottom*).[16]

Careful analysis revealed that these differences are largely caused by deviations in the albumin concentration in plasma among selected species, whilst titration with isolated serum albumins apparently showed only minor differences in affinity between species.

Binding studies using bovine and human serum albumins were carried out with **[GdL$^4$]**, revealing similar binding constants of 3.28 (±0.2) and 3.51 (±0.1) respectively, although the observed relaxivity at saturation for HSA and BSA was different – 6.8 $mM^{-1}s^{-1}$ and 4.2 $mM^{-1}s^{-1}$ at 37 °C and 60 MHz (Fig. III.19). This difference may be attributed to a differing fatty acid content in the commercially supplied serum albumins used for binding studies, and more detailed studies using albumins from different vendors are required to make a conclusion on the nature of

this discrepancy. At the same time, the observed relaxivity for the unbound **[GdL$^4$]** was unusually low (1.5 $mM^{-1}s^{-1}$ at 37 °C and 60 MHz), in line with the absence of bound water at pH 7.4, and apparently a minimal contribution of the second-sphere water to the observed relaxivity value.

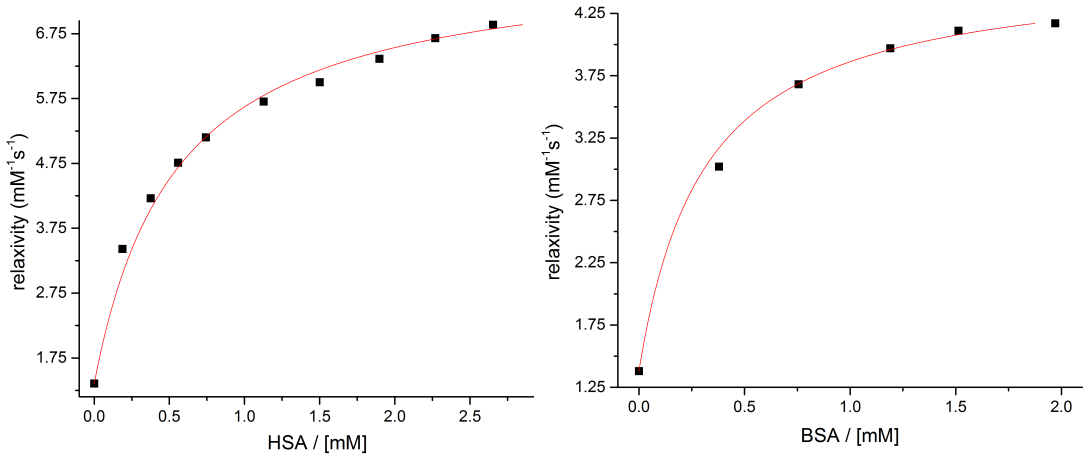


**Fig. III.19** Variation of the relaxivity of **[GdL$^4$]** following incremental addition of HSA (log$K_b$ = 3.28(0.2)) and BSA (log$K_b$ = 3.51(0.2)). The line shows the fit to the data points, using an iterative non-linear least-squares fitting to 1:1 binding model, 310 K, pH = 7.40 (PBS buffer).

Addition of three drugs, which are known to bind to the FA-1 and FA-2 pockets of HSA (see Chapter 1), ibuprofen, warfarin and iodipamide was made in large excess, but did not affect the relaxivity of **[GdL$^4$]*SA** aggregate. This finding along with lower binding constants obtained from relaxivity titration curves suggest that the primary binding site(s) in the cases of HSA and BSA are photophysically 'dark' sites, which do not induce a luminescent response, when **[EuL$^4$]** is bound to either of the proteins. The observed 'switch on' response of the europium complex can be attributed to binding to another site, with a two orders of magnitude higher affinity than the average value calculated from relaxivity data.

It was previously shown that a sulfonamide arm can reversibly bind to the lanthanide ion, changing the hydration number as a function of pH. Even though no change of hydration number was observed, when bound to a protein, pH variation may trigger conformational changes, and hence result in a change of relaxivity. The pH dependence of the relaxivity of **[GdL$^4$]** in the presence of 2.2 equivalents of HSA was analysed (Fig. III.20), revealing a p$K_a$ of 6.3, which is higher than the value observed for **[EuL$^1$]** in 0.1 M NaCl (p$K_a$ = 4.0), but lower than the p$K_a$ for **[EuL$^4$]** bound to HSA as observed from emission studies. The latter observation is consistent

with the assumption that the optically 'bright' binding site is different to the primary binding site, but this conclusion is not unambiguous.

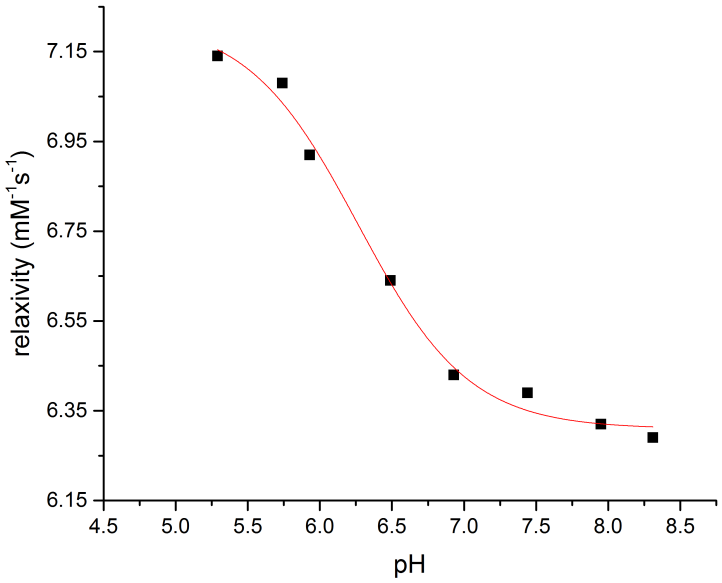


**Fig. III.20** Variation of the relaxivity of **[GdL$^4$]** as a function of pH, in the presence of 2.2 equivalents of HSA (p$K_a$ = 6.3(0.1), T = 37 °C, 0.1 M NaCl).

No ***q*** value could be obtained from **[EuL$^4$]*HSA,** when the sulfonamide moiety is unbound, due to the quenching of the emission at lower pH values. At the same time, only minor relaxivity changes as a function of pH were observed, suggesting that no water molecule is bound over the whole pH range analysed. In a paper of Helm and Caravan, gadolinium complexes with DO3A-derived ligands bearing a sulfonamide arm were added to a solution of HSA and the relaxivity was followed as a function of pH[17]. A p$K_a$ value of *ca.* 6.5 was observed for each complex (Fig. III.21), and no water molecules directly bound to the metal ion were observed from photophysical studies of the europium analogue.

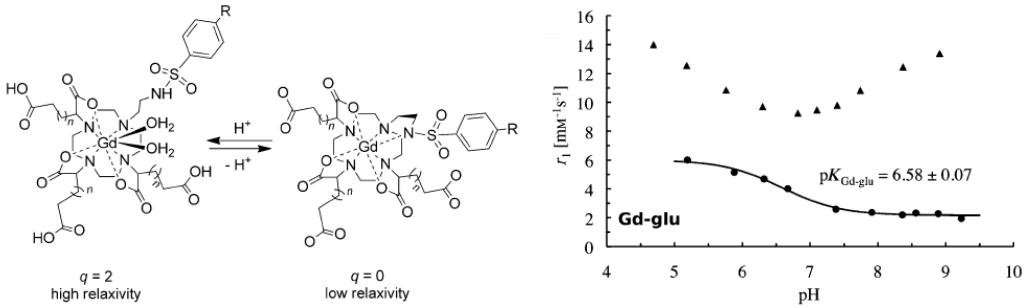


**Fig. III.21** Variation of q value as a function of pH in the absence of HSA and pH dependence of relaxivity in the absence (■) and in the presence (▲) of HSA for a glutarate derivative.[17]

Whilst reversible binding of a sulfonamide arm may well give rise to the observed change in the relaxivity upon varying pH (e.g. through replacing a protonated sulfonamide with an amino acid side chain of the protein), unravelling a more detailed explanation for pH dependent changes of relaxivity requires additional NMRD experiments. Helm and Caravan revealed that the distance between a long-lived water in the second sphere of hydration changed as a function of pH, allegedly due to reversible binding of sulfonamide arm. A similar explanation could be possible for **[GdL$^4$]**, although additional NMRD experiments are required to verify this assumption.

At the same time, a recent study showed that HSA unfolding is a pH driven process with a p$K_a$ of *ca.* 4.5[18]. This finding allows us to rule out the influence of any pH-driven rearrangement of HSA on the observed relaxivity change and attribute the observed variation to the reversible binding of the sulfonamide arm.

# II.3 [LnL$^5$] as $\alpha_1$-AGP sensing probe

## *III.3.1 Synthesis and photophysical studies*

$\alpha_1$-AGP is the second most abundant protein in human plasma after serum albumin, comprising up to 3-4% of the total serum protein contents. Its role in drug transport has attracted a lot of attention, as well as its concentrational changes in response to inflammatory processes in the body. In contrast to HSA, $\alpha_1$-AGP has only one drug binding site, which is known to accommodate a large variety of different endogenous and exogenous drugs[19].

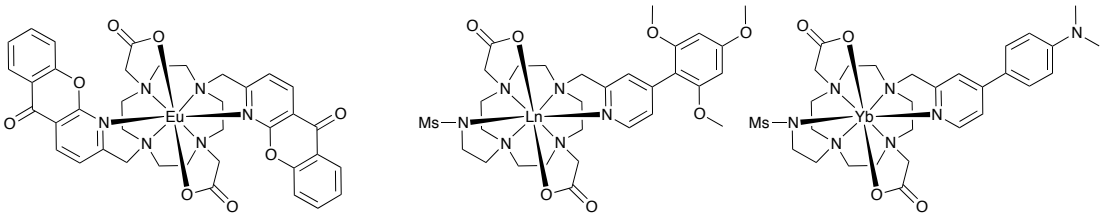


**Fig. III.22** Molecular structures of **[EuL$^{x1}$]** (*left*) described in ref. [5] along with **[LnL$^5$]** (*centre*) and **[YbL$^6$]** (*right*) described in the present work.

Change of the local polarity of an $\alpha_1$-AGP selective probe with a strong ICT component might be expected to give rise to a 'switch-on' response upon protein binding. Analysis of the literature showed that the only $\alpha_1$-AGP-selective luminescent probe was designed by Parker and was alluded to in Chapter 2[5]. Screening of several compounds resulted in the design of probes **[LnL$^5$]** and **[YbL$^6$]**, which are structurally related to both **[EuL$^4$]** and probe **[EuL$^{x1}$]** (Fig. III.22). In every case, a DO2A-based motif is used, along with a pyridine-based chromophore. In **[LnL$^5$]** and **[YbL$^6$]**[1] a sulfonamide arm was added to impart pH-sensitivity and give an additional functional group suitable for hydrogen bonding to amino-acids of the protein inside the binding pocket.

[1] Ytterbium complex **[YbL$^6$]** was only briefly studied and it revealed similar affinity towards $\alpha_1$-AGP. Two bands comprising the $^2F_{7/2} \rightarrow {}^2F_{5/2}$ transition showed change of their relative emission intensities upon binding to bovine $\alpha_1$-AGP, consistent with dissociation of the sulphonamide nitrogen and binding to an amino-acid of the protein side chain.

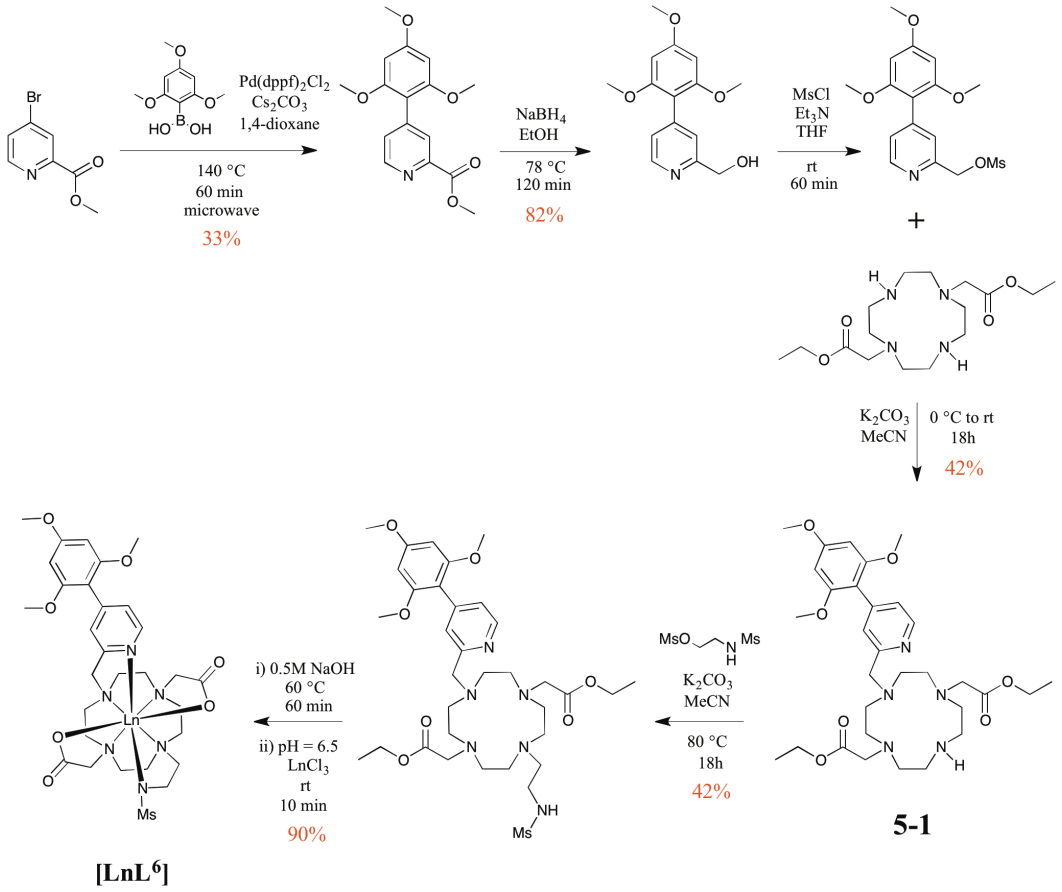


**Scheme III.1** Synthetic procedure for **[LnL$^5$]**. Yields for each step are given. An analagous synthetic procedure was used for **[YbL$^6$]** (see Experimental section).

The synthetic procedures for preparation of **[LnL$^5$]** and **[YbL$^6$]** complexes were analogous to those used to synthesise **[LnL$^1$]** and **[LnL$^5$]** (Scheme III.1). In the first step, a biaryl chromophore precursor was prepared via a Suzuki cross-coupling reaction in a microwave reactor, using $Pd(dppf)_2Cl_2$ for **[LnL$^5$]** and $Pd(TPP)_2Cl_2$ for **[YbL$^6$]** as the catalyst. An attempt to use $Pd(TPP)_4$ as a catalyst was made following the report of procedures[20],[21] for a closely related chormophore with diethyl 4-bromopyridine-2,6-dicarboxylate in anhydrous DMF, but only very low conversion was observed even after 48 h, using a conventional route and in a modified procedure undertaken in a microwave reactor with either anhydrous DMF or anhydrous 1,4-dioxane as a solvent at 140 °C for 1 h. When 2,4,6-trimethoxy (2,4,6-trimethoxyphenyl)boronic acid was coupled, a significant amount of by-product – 1,3,5-trimethoxybenzene – was observed, which hampered purification using RP-HPLC and required additional purification step using silica flash chromotography. On the other hand, reaction with (4-(dimethylamino)phenyl)boronic acid showed complete conversion according to LC-MS analysis and the product was readily

purified using silica flash chromotography. In each case, the isolated ester was reduced in EtOH within 2 h, using an excess of $NaBH_4$ under reflux.

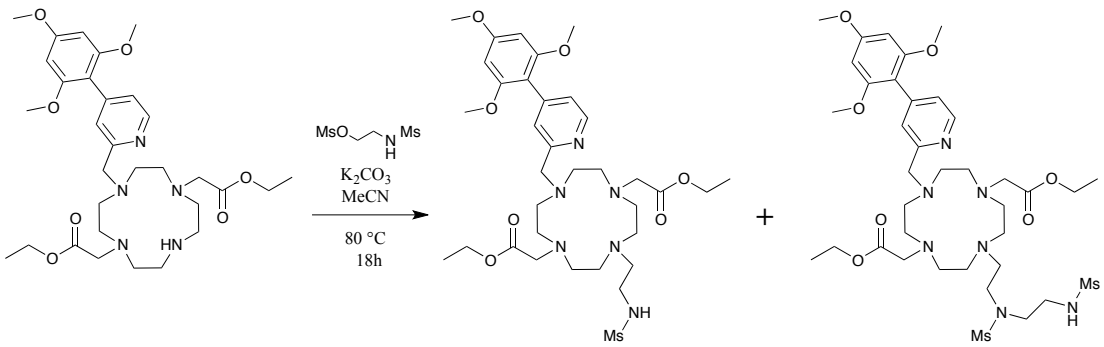


**Fig. III.23** Two products obtained in the reaction mixture upon addition of sulfonamide.

The alkylation of the diethyl ester of DO2A with the freshly prepared mesylate derivative of the aryl chromophore resulted in preferential formation of the desired trialkylated product, according to LC-MS analysis; subsequent purification of the product was performed using RP-HPLC. The next step – introducing of a sulfonamide arm – resulted in the mixture of the desired product as well as a by-product, where the generated aziridine had reacted twice (Fig. III.23). This step was not easily controlled, and the ratio between the desired product and the by-product varied significantly in different attempts. The mixture composition had a big impact on their ease of separation using RP-HPLC. A pure product was finally isolated for NMR characterisation. In other cases, the crude mixture was hydrolysed in 0.5 M aqueous NaOH solution, neutralised and the complex was synthesised by adding an excess of the corresponding $LnCl_3$ salt. The complexation reaction was accomplished in few minutes at rt. Any excess lanthanide salt was precipitated in a form of $Ln(OH)_3$ by raising the pH to 10 and separated on a centrifuge. The reaction mixture was purified using RP-HPLC with a Chromolith® C18 column without buffer, showing a single peak in the UV trace, which corresponded to the desired complex. The resulting complex, **[EuL$^5$]**, was characterised by $^1$H NMR (Fig. III.24) and $^1$H-$^1$H COSY spectroscopy (see Appendix). The yttrium analogue **[YL$^5$]** was also synthesised to determine the diamagnetic contribution to the observed shifts in the $^1$H NMR spectrum of **[EuL$^5$]**, and assisted in the assignment of the spectrum.

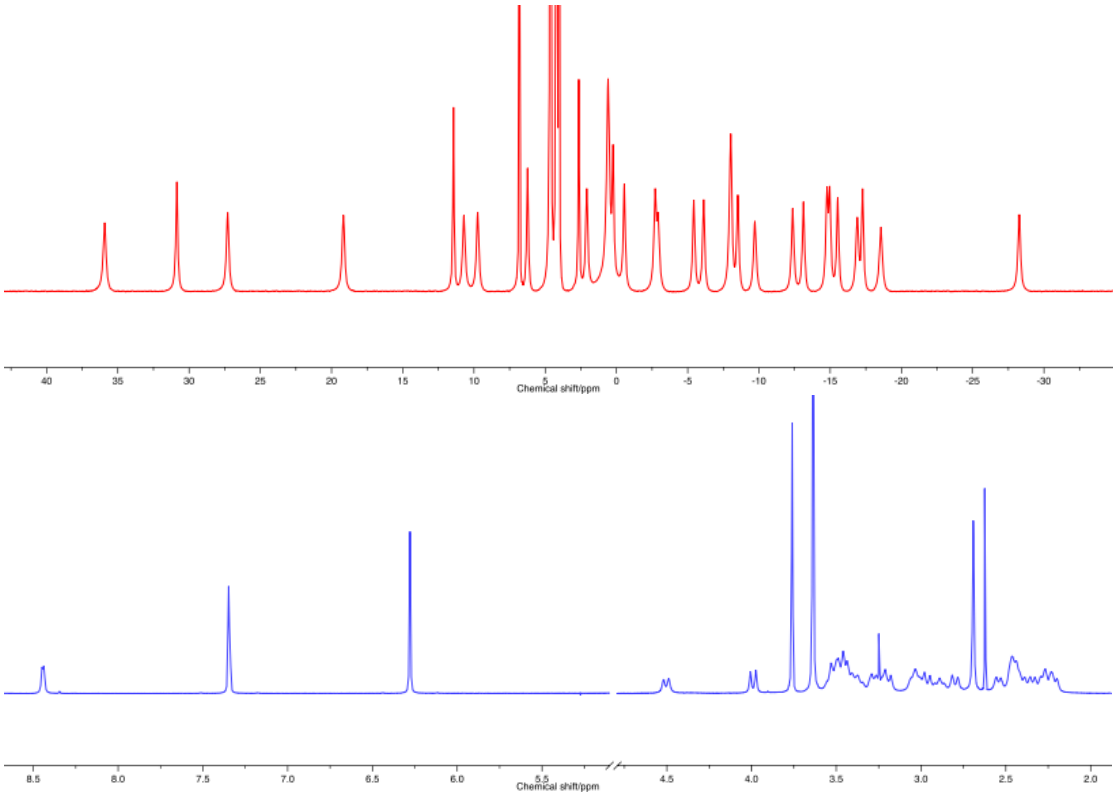


**Fig. III.24** $^{1}$H NMR spectra of **[EuL$^{5}$]** (*top*) and **[YL$^{5}$]** (*bottom*) ($D_2O$, 295 K, 9.4 T for **[EuL$^{5}$]** and 278 K, 11.7 T for **[YL$^{5}$]**).

Assignment of the signals for **[YL$^{5}$]** was carried out at 278 K to reduce the spectral broadening. As at least two species were in dynamic exchange, Nuclear Overhauser Effect Spectroscopy (NOESY, Fig. III.25) and Rotating-frame Overhauser Effect Spectroscopy (ROESY, Fig. III.26) experiments were carried to assign observed chemical shifts. The NOESY experiment allows assigning signals from protons that are close in space to be pinpointed. Moreover, the technique, commonly designated as EXSY (Exchange Spectroscopy), helps to assign protons that are in chemical and conformational exchange.

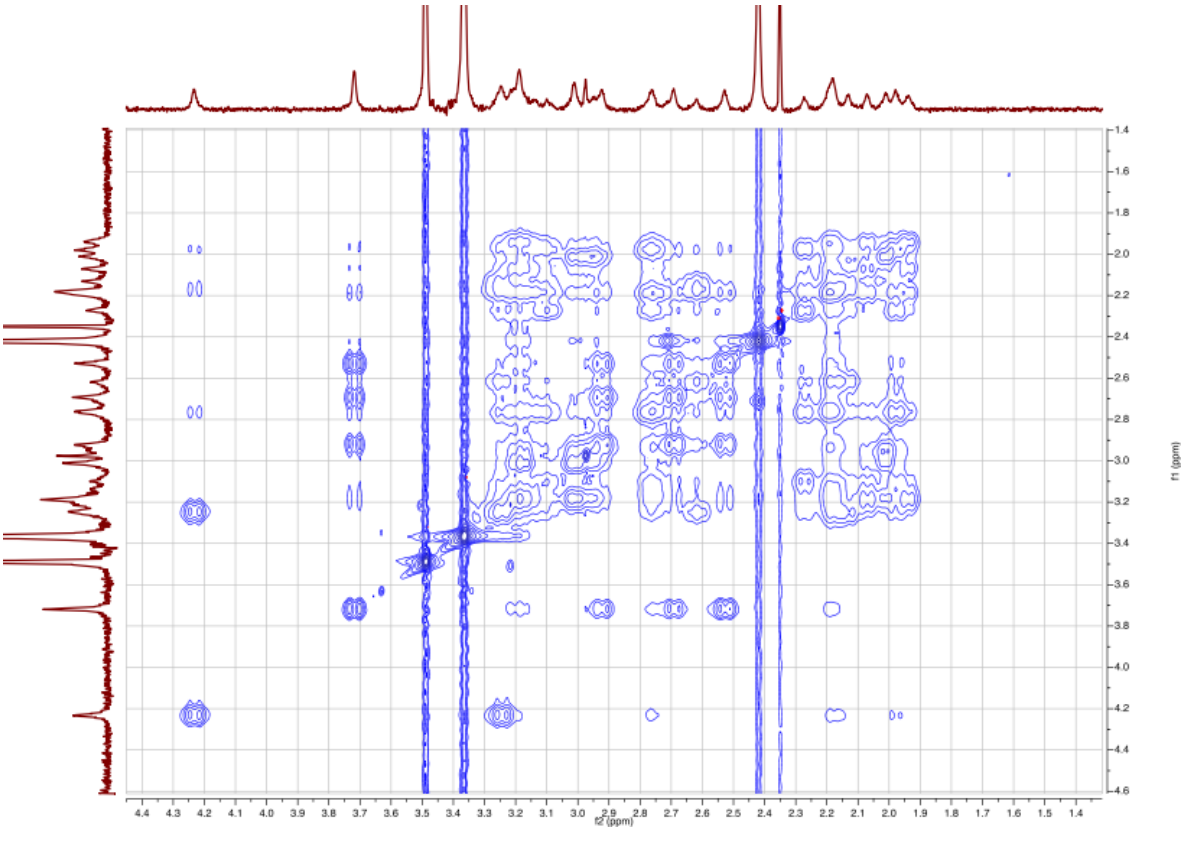

**Fig. III.25** $^{1}$H-$^{1}$H NOESY spectrum of **[YL$^{5}$]** ($D_2O$, 278 K, 11.7 T).

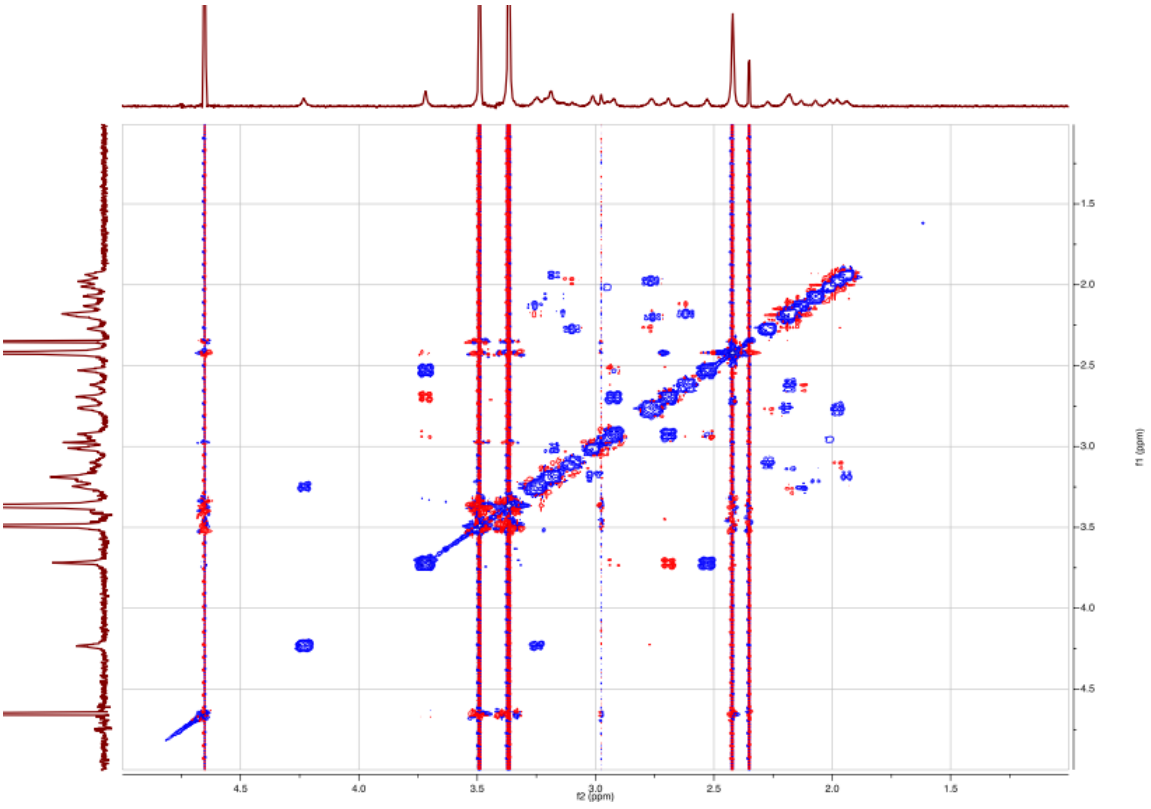

**Fig. III.26** $^{1}$H-$^{1}$H ROESY spectrum of **[YL$^{5}$]** ($D_2O$, 278 K, 11.7 T).

As the Nuclear Overhauser Effect (NOE) approaches zero for molecules with molecular masses of 700-1200 Da[22], the ROESY experiment is often used to

provide similar information on signals that are close in space or in exchange. In contrast with NOE, which is positive for small molecules and negative for macromolecules, the Rotating-frame Overhauser Effect (ROE) is always positive regardless of the molecular mass, and therefore turned out to be the better technique for assigning proton NMR signals in **[EuL$^5$]** (see Appendix).

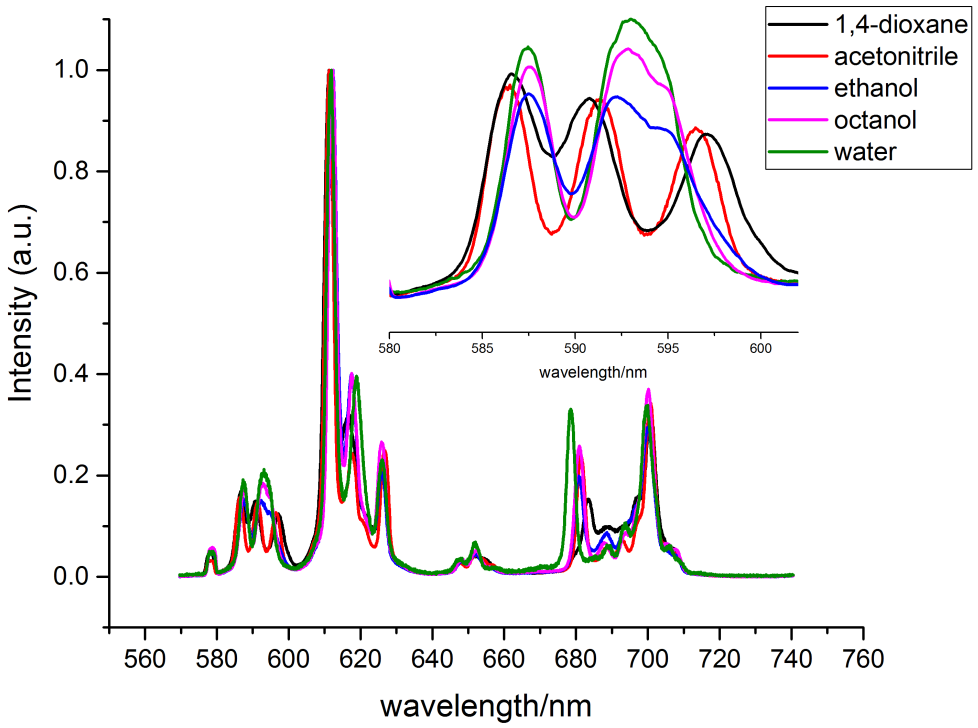


**Fig. III.27** Emission spectra of **[EuL$^5$]** in different organic solvents and water with a magnified region of $^5D_0 \rightarrow {}^7F_1$ manifold (298 K, $\lambda_{ex}$ = 390 nm).

The europium complex **[EuL$^5$]** showed very weak emission in aqueous solution, which was unaffected by degassing the solution, suggesting no triplet character in the quenching state. However, as in the case of **[EuL$^4$]**, the emission intensity was enhanced upon lowering the polarity of the solvent and was also accompanied by changes in the spectral signature (Fig. III.27). Similar changes of $^5D_0 \rightarrow {}^7F_1$ splitting (change of $\boldsymbol{B_0^2}$sign) were observed on going from water through acetonitrile to 1,4-dioxane, probably indicating the change of the coordination environment from a twisted square antiprism to a square antiprism. It was recently reported that free rotation around the C-C bond in a similar integral biaryl chromophore can give rise to a TICT state, which can efficiently quench the emission of lanthanide complexes[22]. However, no significant change in the emission intensity or lifetime of excited state was observed for both the europium and terbium complexes upon

changing solvent from pure methanol to the pure glycerol, which is *ca.* 200 times more viscous, ruling out the involvment of a TICT excited state, as a quenching mechanism in aqueous solution.

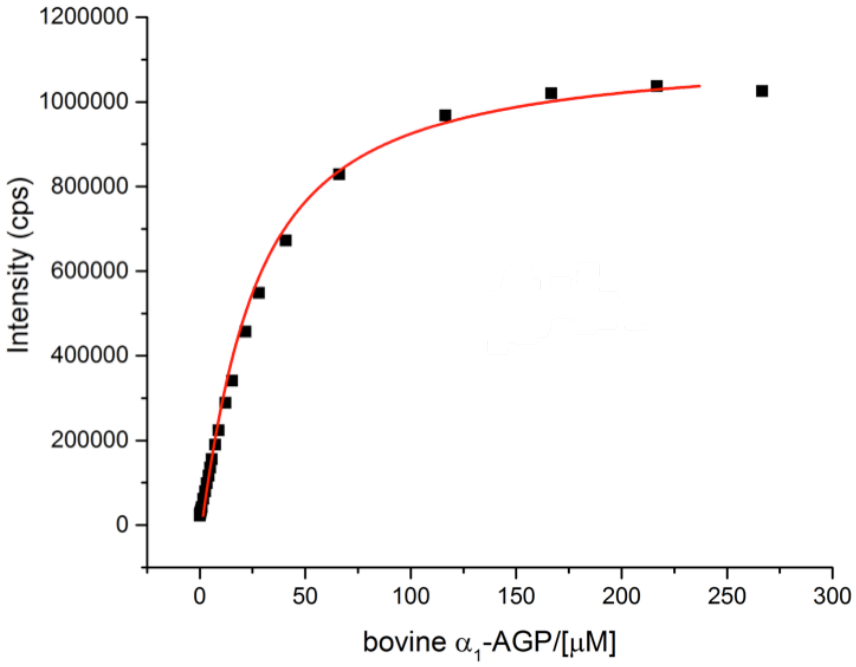


**Fig. III.28** Change of the total emission intensity upon addition of bovine $\alpha_1$-AGP to **[EuL$^5$]** (**[EuL$^5$]** 11 μM; log K = 4.71(0.1), assuming a 1:1 binding isotherm, $\lambda_{ex}$ = 310 nm, 298 K, 0.1 M HEPES, pH = 7.40).

A significant increase of the emission intensity upon addition of $\alpha_1$-AGP (Fig. III.28) suggests that an ICT state may be responsible for the observed quenching in aqueous solution. Substantially smaller changes of the observed emission intensity were observed upon addition of HSA, BSA, human antitrypsin, firbrinogen and ImG. Thus, this probe can be considered to be selective for $\alpha_1$-AGP sensing.

## *III.3.2 Protein binding studies of [LnL$^5$]*

Stepwise addition of bovine $\alpha_1$-AGP to **[EuL$^5$]** gave rise to a dramatic increase of the emission intensity, along with a change in spectral form (Fig. III.29). The pH-dependent behaviour was analysed and a very high p$K_a$ = 8.2 was estimated by following changes in the lifetime of the excited state with pH, attributed to a reversible binding of sulfonamide arm (Fig. III.30).

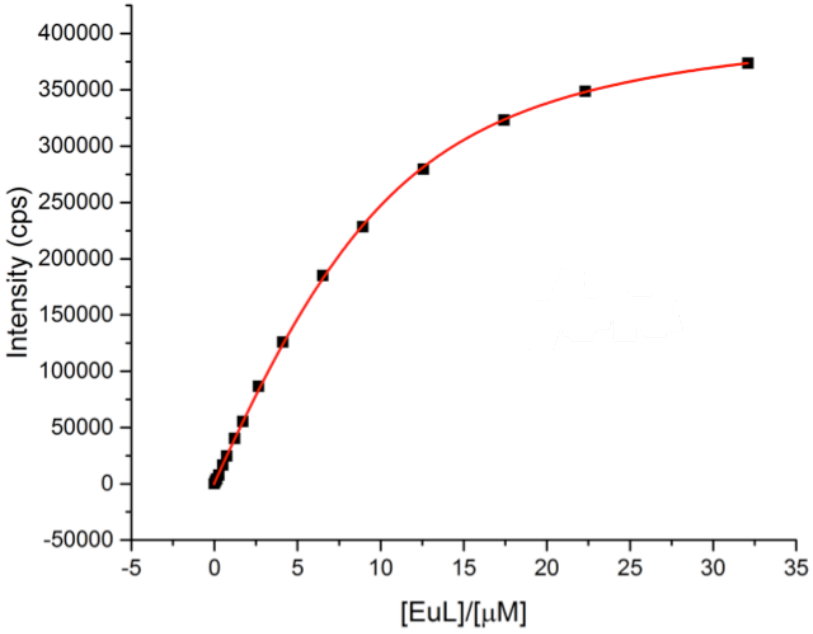


**Fig. III.29** Change of the total emission intensity upon addition of **[EuL$^5$]** to bovine $\alpha_1$-AGP ([bovine $\alpha_1$-AGP] 25 μM; log K = 5.52(0.1), assuming a 1:1 binding isotherm, $\lambda_{ex}$ = 310 nm, 298 K, 0.1 M HEPES, pH = 7.40).

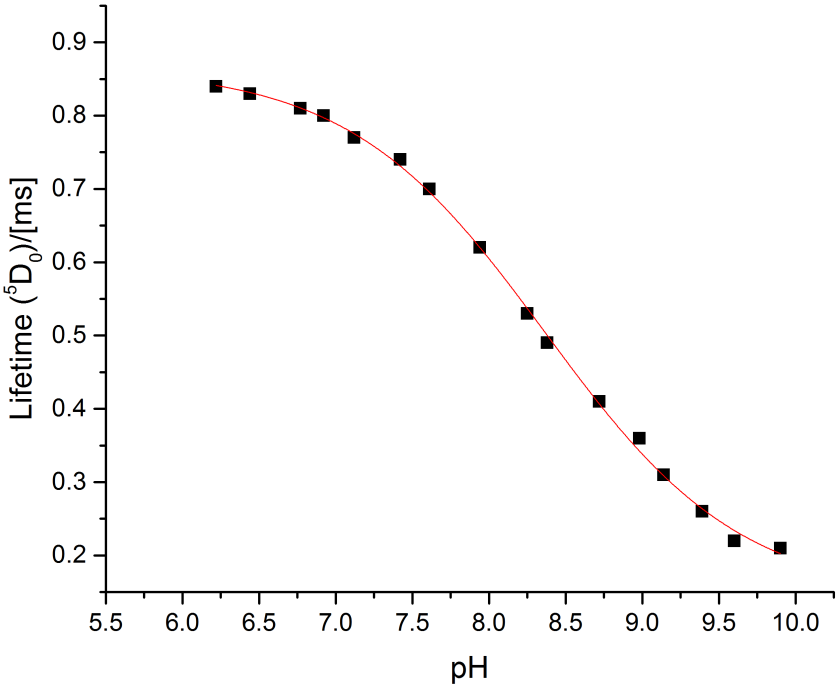


**Fig. III.30** pH calibration curves for **[EuL$^5$]** (18 μM) following the lifetime of the europium $^5D_0$ state with bovine $\alpha_1$-AGP ($\lambda_{ex}$ = 310 nm, $H_2O$, 295 K).

The induced CPL signal was also recorded, as a function of pH. At higher pH values when the sulfonamide arm is bound, a mirror image of the CPL signal of **[EuL$^4$]** with added HSA was observed. The total emission spectrum was also identical to **[EuL$^4$]** with a bound sulfonamide but without added protein. Moreover, analogous

binding studies with human $\alpha_1$-AGP showed a mirror-image CPL signal when compared to added bovine $\alpha_1$-AGP with an identical fingerprint to the **[EuL$^4$]*HSA** adduct (Fig. III.31). The opposite signs of the induced helicities for **[EuL$^4$]*HSA** and **[EuL$^5$]*[human $\alpha_1$-AGP]** on the one hand and **[EuL$^5$]*[bovine $\alpha_1$-AGP]** on the other, indicate a tightly bound complex inside the binding pocket, preserved even when the sulfonamide arm dissociates at lower pH values.

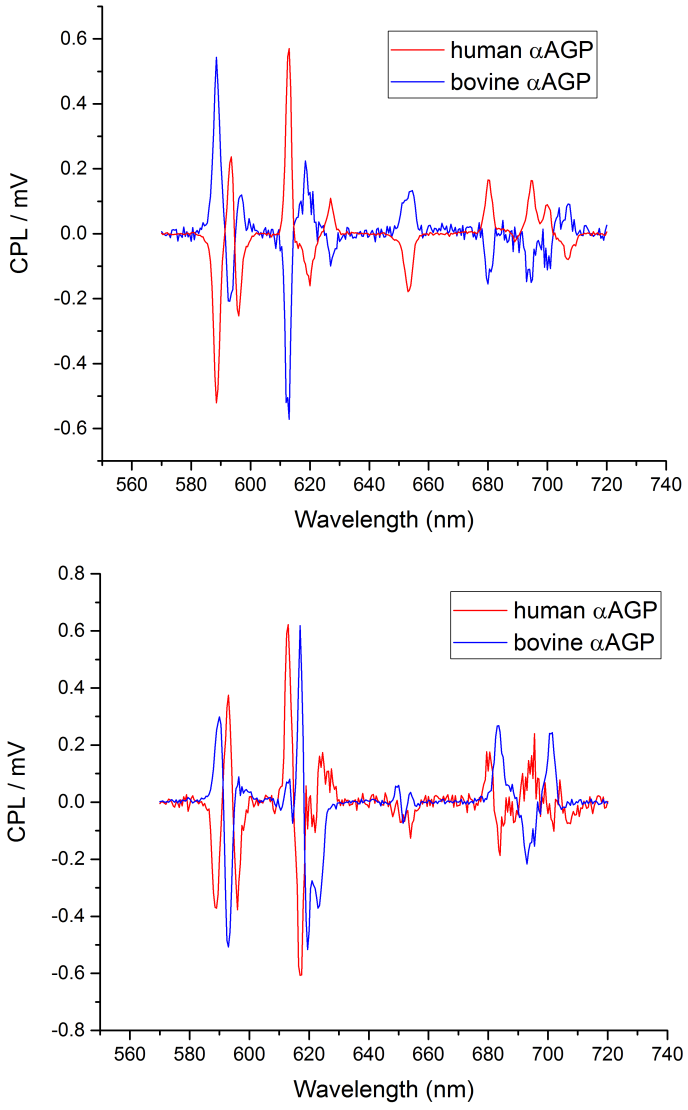


**Fig. III.31** Induced CPL spectra of **[EuL$^5$]** bound with human and bovine $\alpha_1$-AGP, when the sulfonamide arm is bound (pH = 9.3, *top*) and unbound (pH = 3.6, *bottom*) to $Eu^{3+}$ ion ($\lambda_{ex}$ = 310 nm, $D_2O$, 295 K).

The identical nature of the CPL spectra for **[EuL$^4$]*HSA** and **[EuL$^5$]*[human $\alpha_1$-AGP]**, as well as their total emission spectra is not surprising, bearing in mind their similar coordination environment, which is not significantly perturbed by structural variation of the top half of the biaryl chromophore. To support this assumption, $^1$H

NMR spectra of **[EuL$^1$]** and **[EuL$^5$]** were superimposed, showing a remarkable similarity in chemical shifts between two complexes, in the absence of added protein (Fig. III.32).

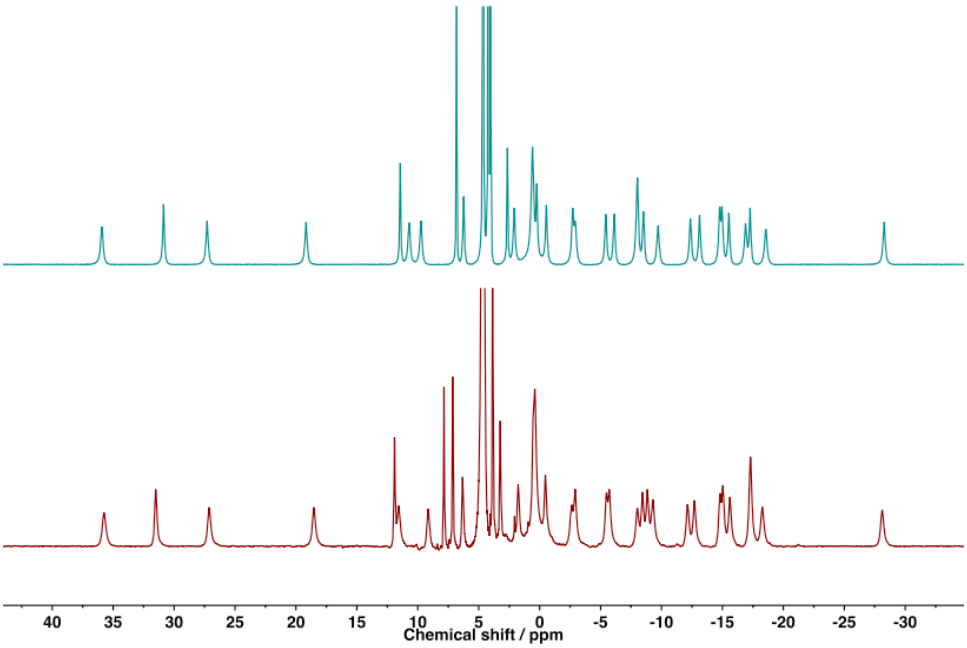


**Fig. III.32** $^1$H NMR spectra of **[EuL$^1$]** (maroon) and **[EuL$^5$]** (turquoise) ($D_2O$, 295 K, 9.4 T).

However, once the sulfonamide arm was protonated, the CPL signals were no longer mirror images and their total emission spectra were also different. This behaviour suggests that the sulfonamide arm was probably replaced by a carboxylate group from the side chain of a protein, that is different for the bovine and human species.

Similar titration experiments were performed with the human version of $\alpha_1$-AGP, which is comprised of two genetic variants, F1/S and A. It has been shown that there is a significant difference in binding affinities between these two modifications,[23] with the variant A having a considerably lower affinity than F1/S due to a smaller binding pocket and hence its contribution is usually ignored.[24]

The binding curve obtained (Fig. III.33) following addition of human $\alpha_1$-AGP to **[EuL$^5$]** showed a similar 1:1 binding constant (4.14(0.1) vs. 4.71(0.1)) when compared to bovine $\alpha_1$-AGP, even though the sulfonamide arm remained bound when the complex was added to a protein. In a reciprocal experiment, when the complex **[EuL$^5$]** was added to human $\alpha_1$-AGP (Fig. III.34), a close resemblance with

the behaviour of the bovine species was also observed (log K values were 5.85(0.1) vs. 5.52(0.1) respectively). This observation should not be surprising, given that the curve reached saturation after addition of two equivalents of **[EuL$^5$]**. At the same time, a lower binding constant K for human $\alpha_1$-AGP may either indicate the presence of a tighter binding pocket in the case of bovine $\alpha_1$-AGP, for instance by replacing a sulfonamide with a carboxylate of a protein side-chain.

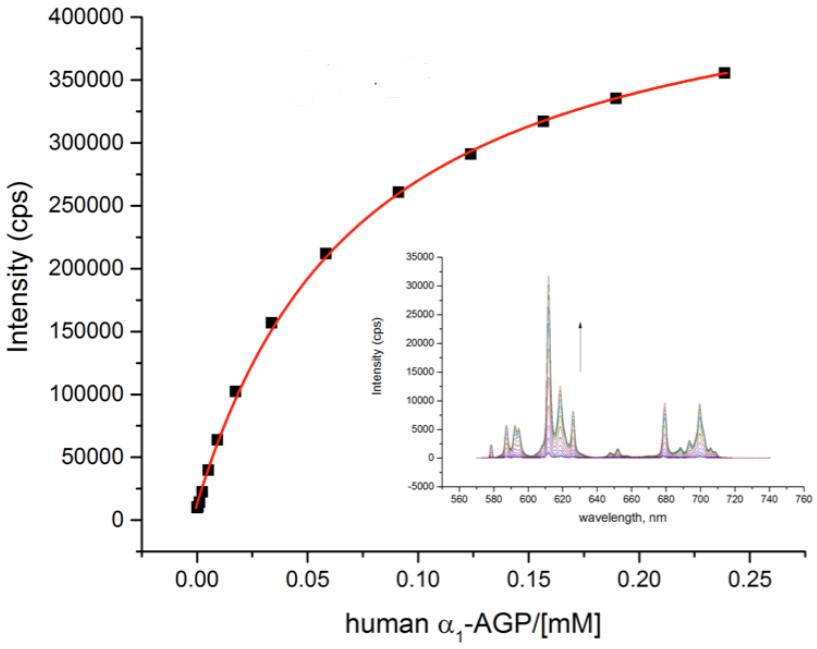


**Fig. III.33** Change of the total emission intensity upon addition of human $\alpha_1$-AGP to **[EuL$^5$]** (**[EuL$^5$]** 9 µM; log K = 4.14(0.1), assuming a 1:1 binding isotherm, $\lambda_{ex}$ = 310 nm, 298 K, 0.1 M HEPES, pH = 7.40).

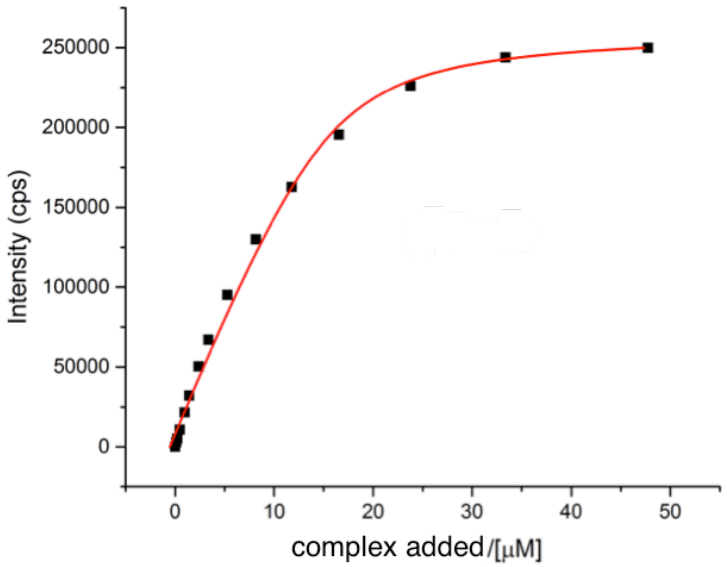


**Fig. III.34** Change of the total emission intensity upon addition of **[EuL$^5$]** to human $\alpha_1$-AGP ([human $\alpha_1$-AGP] 25 µM; log K = 5.85(0.1), assuming a 1:1 binding isotherm, $\lambda_{ex}$ = 310 nm, 298 K, 0.1 M HEPES, pH = 7.40).

The observed induced CPL signal following binding of **[LnL$^5$]** to $\alpha_1$-AGP is caused by preferential binding of one enantiomer, the enantiomers of **[EuL$^5$]** co-exist in dynamic equilibrium at ambient temperature in aqueous solution (Fig. III.35).

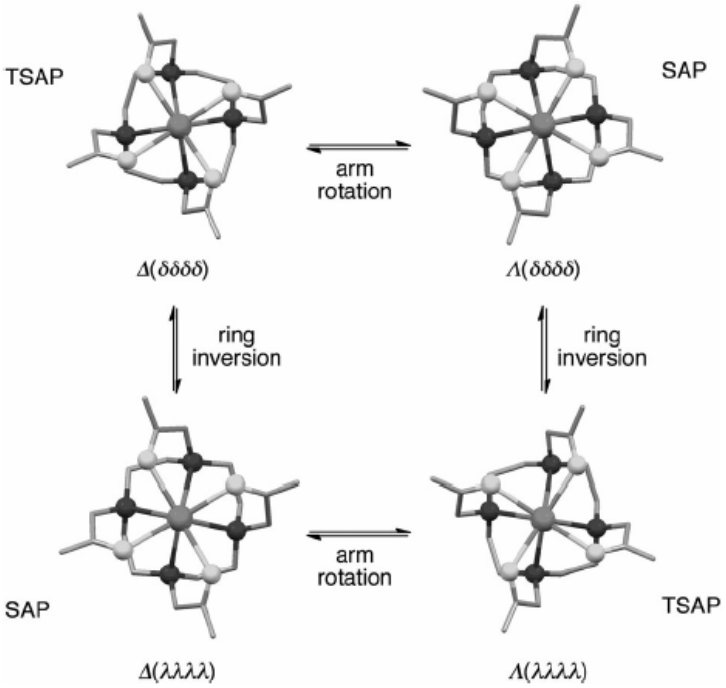


**Fig. III.35** Equilibrium between different isomers present in tetra-substitueted cyclen derivatives (SAP – square antiprism; TSAP – twisted square antiprism).[25]

Once the complex is bound to a protein, its conformational flexibility is restricted by steric constraints, and an induced CPL signal can be recorded. $\alpha_1$-AGP species differ in their drug binding pockets and therefore showed different binding preferences towards enantiomers – bovine $\alpha_1$-AGP preferentially stabilizes the *Δ*(*δδδδ*) enantiomer, whilst human selectively binds *Λ*(*λλλλ*). This assignment of configuration is based on previously reported emission spectra for structurally related enantiopure europium(III) complexes (Fig. III.36).[26]

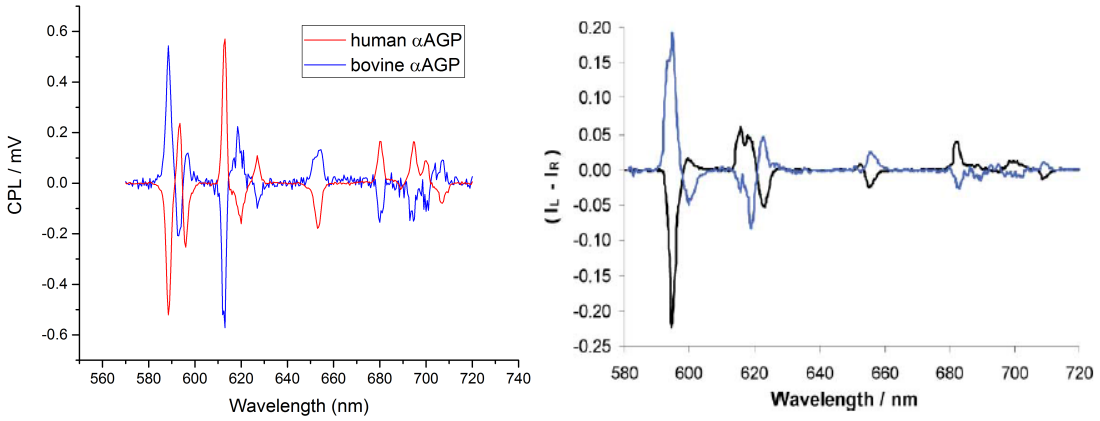


**Fig. III.36** Comparison between CPL spectra recorded for **[EuL$^5$]** in the presence of human and bovine $\alpha_1$-AGP at pH = 9.30 (*left*) and CPL spectra of complexes reported in [26], where *Δ(δδδδ)* enantiomer (blue) refers to **[EuL$^5$]** with added bovine $\alpha_1$-AGP and the *Λ(λλλλ)* enantiomer (black) is preferentially bound when **[EuL$^5$]** is added to human $\alpha_1$-AGP.

In order to further exemplify this selective binding process, the terbium complex **[TbL$^5$]** was synthesised, which showed a strong emission intensity in both the absence and presence of human and bovine $\alpha_1$-AGP. Only a minor enhancement of the total emission intensity was observed following addition of $\alpha_1$-AGP, and therefore the unbound racemic species, which were quenched in the case of **[EuL$^5$]**, are now emissive.

Very weak CPL signal was observed for **[TbL$^5$]** at higher pH with sulfonamide arms bound, when added to both human and bovine $\alpha_1$-AGP. In contrast, once the sulfonamide nitrogen dissociates at lower pH, a strong CPL signal was detected for both $\alpha_1$-AGP species (Fig. III.37). Similarly to **[EuL$^5$],** opposite helicities were observed following addition of human and bovine $\alpha_1$-AGP. The binding curve obtained for **[TbL$^5$]** (Fig. III.38) with added bovine $\alpha_1$-AGP showed a slightly higher binding affinity than in the case of **[EuL$^5$]** (log K = 5.14(0.1)). Such behaviour may be attributed to the existence of more than one binding site in the protein. As **[TbL$^5$]** was not quenched via an ICT state, those binding pockets which remained 'dark' upon binding **[EuL$^5$]** now may become visible.

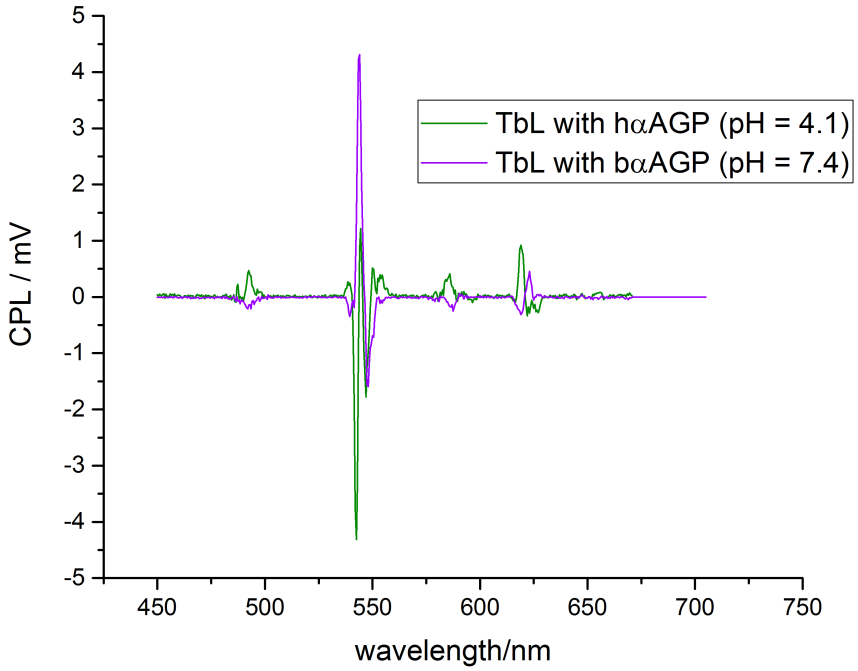


**Fig. III.37** Induced CPL spectra of **[TbL$^5$]** (8 μM) bound with human and bovine $\alpha_1$-AGP, when the sulfonamide arm is unbound ($\lambda_{ex}$ = 310 nm, 0.1 M HEPES, pH = 7.40, 298 K).

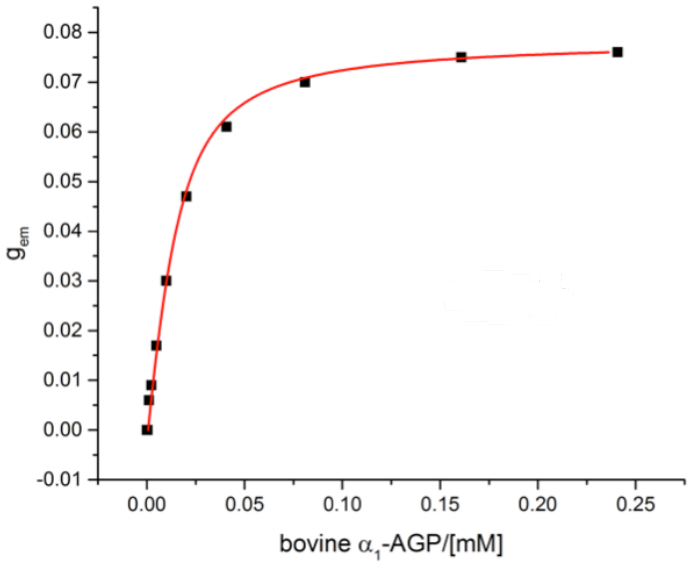


**Fig. III.38** Change of the emission dissymmetry factor upon addition of bovine $\alpha_1$-AGP to **[TbL$^5$]** (**[TbL$^6$]** 8μM; log K = 5.14(0.1), assuming a 1:1 binding isotherm, $\lambda_{ex}$ = 310 nm, $\lambda_{em}$ = 545 nm, 298 K, 0.1 M HEPES, pH = 7.40).

Lanthanide complexes with sterically small carboxylate arms tend to be prone to *Δ*/*Λ* racemisation, and therefore even if one of the enantiomers selectively binds to a protein, a dynamic equilbrium will be quickly established in the remaining solution, leading to racemisation of unbound complexes. Thus, the observed CPL signal can be produced only by complex that is bound to a protein. It was not possible to

establish the number of complexes bound per protein molecule and therefore the most emissive bound complex in the diastereomeric adducts determines the observed CPL. Therefore, it might be possible that there is no significant difference in binding enantioselectivity between bovine and human $\alpha_1$-AGP, but the different bound enantiomers have differing emission brightness, giving rise to opposite helicities in the CPL spectrum.

Analysis of the pH behaviour (Fig. III.38) of **[EuL$^5$]** with both human and bovine $\alpha_1$-AGP was performed and compared to the pH calibration curve for **[TbL$^5$]** in the absence of protein (Fig. III.40). A dramatic increase of p$K_a$ was observed only in the case of bovine $\alpha_1$-AGP (8.4(0.1) *vs.* 4.2(0.1) for **[TbL$^5$]** in 0.1M NaCl), whilst a more modest variation was observed for human $\alpha_1$-AGP (4.6(0.1)). Moreover, at pH values above 8.5 for both **[EuL$^5$]*[bovine $\alpha_1$-AGP]** and **[TbL$^5$]*[bovine $\alpha_1$-AGP]** a strong quenching of the emission intensity was observed, along with a very low lifetime of the $^5D_4$ state for **[EuL$^5$]*[bovine $\alpha_1$-AGP]** (0.20 ms). Such a short lifetime is consistent with the occurrence of an additional quenching pathway. The large difference in p$K_a$ values suggests the presence of a functional group inside the binding pocket, with a p$K_a$ around 8.5, which quenches strongly when it is deprotonated.

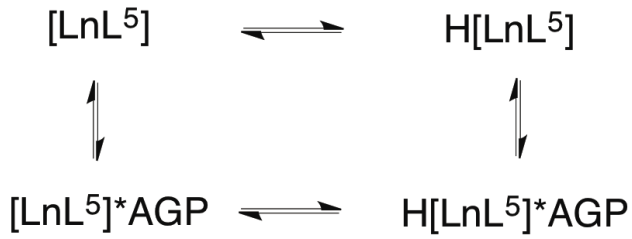


**Fig. III.38** Equilibria present in the **[LnL$^5$]**/ $\alpha_1$-AGP system, showing protonated and non-protonated forms.

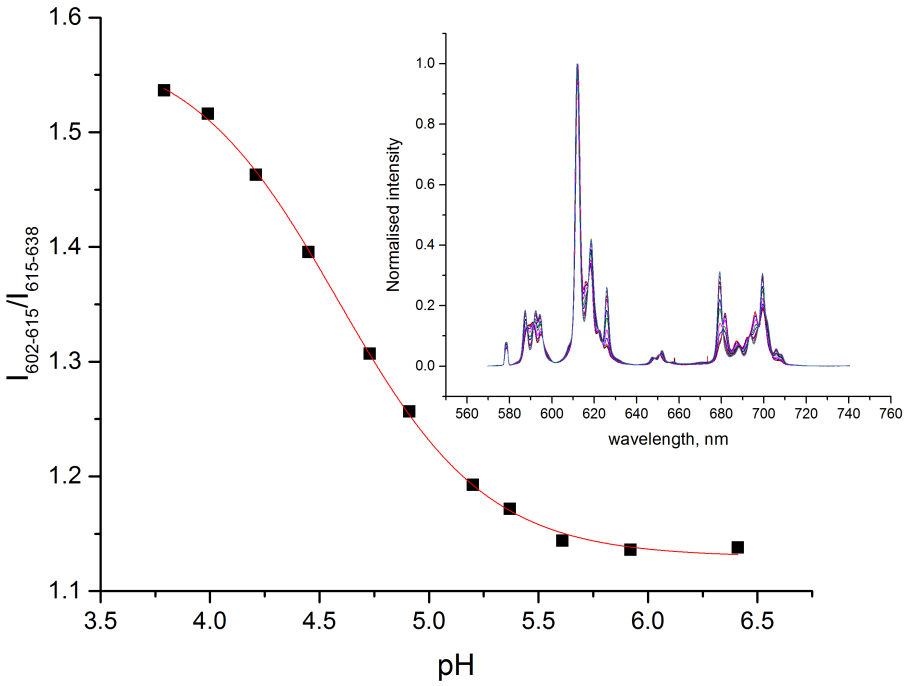


**Fig. III.39** pH calibration curves for **[EuL$^5$]** (6 μM) following the relative intensities of two bands (602-615 nm vs. 615-638 nm) of $^5D_0 \rightarrow {}^7F_2$ transition manifold in the emission spectrum with human α$_1$-AGP ($\lambda_{ex}$ = 310 nm, 298 K), τ(pH = 3.79) = 0.91 ms, τ(pH = 6.41) = 0.78 ms

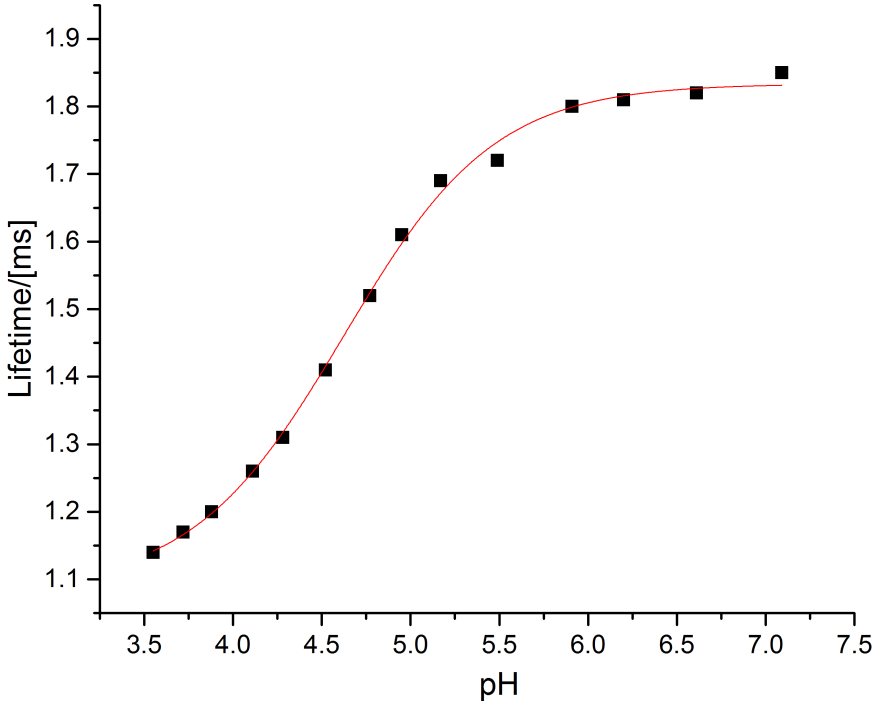


**Fig. III.40** pH calibration curves for **[TbL$^5$]** (5 μM) following the lifetime of an excited state $^5D_4$ (0.1M NaCl, $\lambda_{ex}$ = 310 nm, 298 K).

In order to provide a reasonable explanation of the difference in p$K_a$ values between human and bovine α$_1$-AGP, a more detailed analysis of the binding pocket of human and bovine α$_1$-AGP, as well as its comparison with DS-1 binding site in HSA (which

also showed a significant enhancement of p$K_a$ when compared to a free complex. However, the analysis of the amino acid sequence of bovine $\alpha_1$-AGP is hindered by the presence of different homologous proteins with substantial discrepancies in amino acid content[27]. Fortunately, several amino acids are preserved in selected homologous of bovine $\alpha_1$-AGP, particularly Trp25 (Trp26 in bovine $\alpha_1$-AGP), which has been shown to participate in binding incorporated drugs via hydrophobic interactions (Fig. III.41)[28].

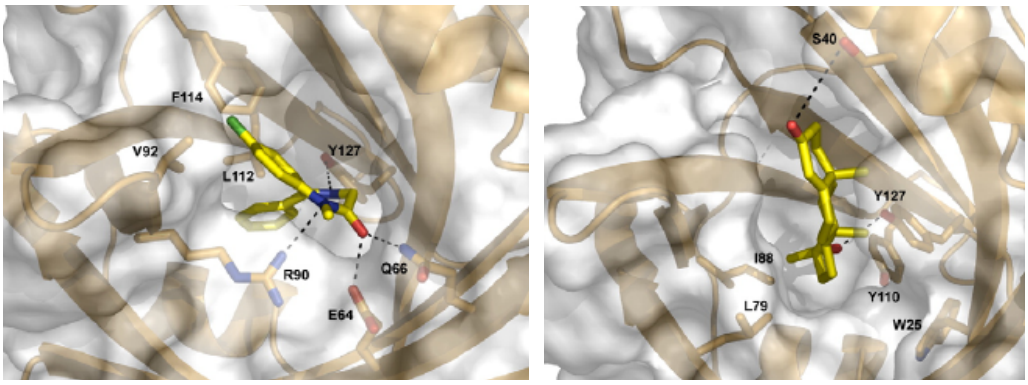


**Fig. III.41** Computer docking simulations of two human $\alpha_1$-AGP-bindings drugs – diazepam (*left*) and progesterone (*right*), showing interactions with side chain amino-acids.[28]

At the same time, by juxtaposing the amino acids in the drug binding pocket of bovine and human $\alpha_1$-AGP (Fig. III.42), several acidic residues can be identified which can potentially increase a p$K_a$ of a sulfonamide arm by stablising its protonated form.

```
P02763 A1AG1_HUMAN          1   MALSWVLTVLSLLPLLEAQIPLCANLVP-VPITNATLDQITGKWFYIASAFRNEEYNKSV      59
P19652 A1AG2_HUMAN          1   MALSWVLTVLSLLPLLEAQIPLCANLVP-VPITNATLDRITGKWFYIASAFRNEEYNKSV      59
Q5GN72 Q5GN72_BOVIN         1   MALLWALAVLSLLPLLDAQSPECANLMTVAPITNATMDLLSGKWFYIGSAFRNPEYNKSA      60
                                *** *.*:********:** * ****:  .******:* ::******.***** *****.

P02763 A1AG1_HUMAN         60   QEIQATFFYFTPNKTEDTIFLREYQTRQDQCIYNTTYLNVQRENGTISRYVGGQEHFAHL      119
P19652 A1AG2_HUMAN         60   QEIQATFFYFTPNKTEDTIFLREYQTRQNQCFYNSSYLNVQRENGTVSRYEGGREHVAHL      119
Q5GN72 Q5GN72_BOVIN        61   RAIQAAFFYLEPRHAEDKLITREYQTIEDKCVYNCSFIKIYRQNGTLSKVESDREHFVDL      120
                                : ***:***: *.::**.:: ***** :::*.** ::::: *:***:*:  ..:**...*

P02763 A1AG1_HUMAN        120   LILRDTKTYMLAFDVNDEKNWGLSVYADKPETTKEQLGEFYEALDCLRIPKSDVVYTDWK      179
P19652 A1AG2_HUMAN        120   LFLRDTKTLMFGSYLDDEKNWGLSFYADKPETTKEQLGEFYEALDCLCIPRSDVMYTDWK      179
Q5GN72 Q5GN72_BOVIN       121   LLSKHFRTFMLAASWNGTKNVGVSFYADKPEVTQEQKKEFLDVIKCIGIQESEIIYTDEK      180
                                *: :. :* *:.   :. ** *:*.******.*:**  ** :.:.*: * .*:::*** *

P02763 A1AG1_HUMAN        180   KDKCEPLEKQHEKERKQEEGES                                      201
P19652 A1AG2_HUMAN        180   KDKCEPLEKQHEKERKQEEGES                                      201
Q5GN72 Q5GN72_BOVIN       181   KDACGPLEKQHEEERKKETEAS                                      202
                                ** * *******:***:*   *
```

**Fig. III.42** Alignment of two homologues of human $\alpha_1$-AGP (ORM-1 and ORM-2) with bovine $\alpha_1$-AGP (*Bos Taurus*)

One of the potential candidates is Tyr101 which is replaced with Gln100 in both modifications of human $\alpha_1$-AGP (ORM-1 and ORM-2). Tyr84 can preferentially bind a sulphonamide oxygen via hydrogen bonding in the phenolic moiety (Fig.

III.43). Once the phenolic moiety of tyrosine is deprotonated, this hydrogen bonding interaction disappears and the sulfonamide nitrogen can bind to $Eu^{3+}$. The p$K_a$ observed then relates to proton transfer to the phenol, and not protonation of the sulphonamide nitrogen in **[EuL$^5$]**. In turn, glutamine residue present in both human modifications of $\alpha_1$-AGP is a worse hydrogen bond donor than a phenolic OH-group in tyrosine and therefore it cannot stabilise the mesylate group on a sulfonamide in its unbound form. However, this assumption requires docking simulations, which are currently not possible, since no crystal structure of any of bovine $\alpha_1$-AGP homologues has been reported so far.

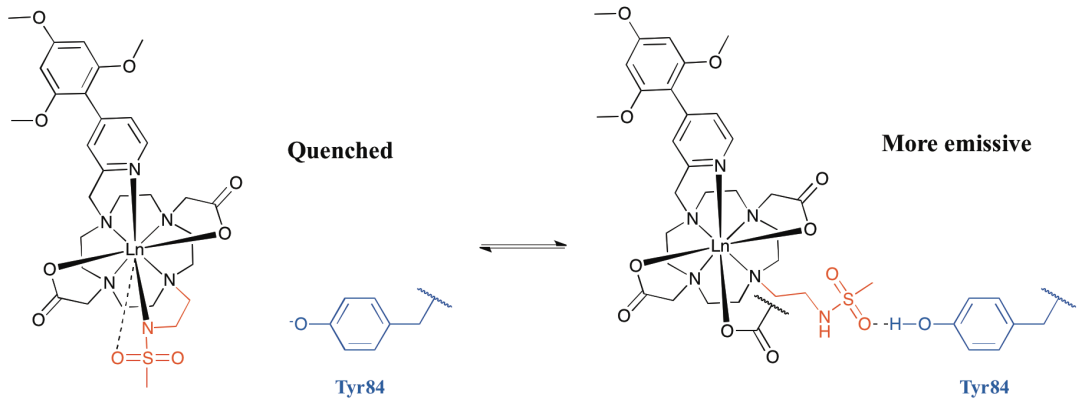


**Fig. III.43** Putative mechanism behind an enhanced p$K_a$ of **[LnL$^5$]** with bovine $\alpha_1$-AGP in the sulphonamide bound complex, the proximate phenolate quenches the luminescence by electron transfer.

## *III.3.3 Competitive drug-binding studies of [EuL$^5$]*$\alpha_1$-AGP*

$\alpha_1$-AGP along with serum albumin plays a crucial role in drug delivery, and multiple studies have been carried out to establish its binding properties with essential drugs. Since the concentration of $\alpha_1$-AGP varies in response to inflammatory processes, the dosage of prescribed drugs should be changed accordingly, and therefore a detailed knowledge of drug binding affinities to $\alpha_1$-AGP is required. Unfortunately, very little data is avaliable on systematic comparison of drug binding affinities between human and animal $\alpha_1$-AGP. However, the number of approved drugs is constantly rising, and therefore the data on drug binding properties is expected to be in demand.

In the present work, three drugs - lidocaine, bupivacaine and imatinib – were chosen for their different binding affinities, spanning the affinity range from log K =

4.4(0.1) for lidocaine (Fig. III.45, III.46) to log K = 6.4(0.1) for imatinib. Competitive binding studies were performed for the europium complex, **[EuL$^5$]**, bound to both human and bovine $\alpha_1$-AGP. The full recovery of the initial weak metal-centred emission was observed in every case, after an excess of the drug was added.

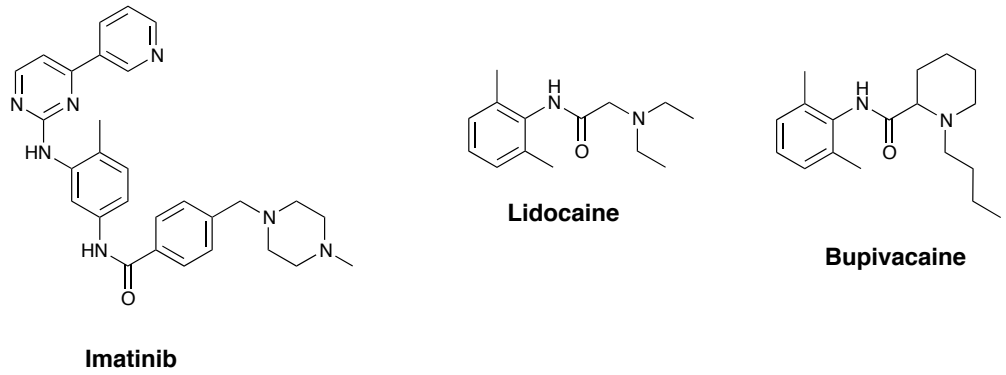


**Fig. III.44** $\alpha_1$-AGP-selective drugs discussed in the present work.

In the case of **[EuL$^5$]*[bovine $\alpha_1$-AGP]** with added lidocaine and bupivacaine, a change of the spectral form was also observed, as the sulfonamide arm was protonated at pH = 7.40, when the complex is bound to a protein. At the same time, the spectral signature of **[EuL$^5$]*[human $\alpha_1$-AGP]** did not change following the displacement of the complex from the protein by added drug. However, following the addition of imatinib to both $\alpha_1$-AGP species, the emission intensity was lower than the intensity of **[EuL$^5$]** without an added protein. Moreover, no change of the spectral form was observed in the case of **[EuL$^5$]*[bovine $\alpha_1$-AGP]**, suggesting that in **[EuL$^5$]** the sulphonamide nitrogen was still protonated, and the complex was apparently still in the binding pocket. To further support this hypothesis, a similar experiment was carried out using **[TbL$^5$]**, which had also revealed a strong quenching of the emission intensity with an unchanged $g_{em}$ value. The efficient quenching of the emission intensity observed for both (**[EuL$^5$]** and **[TbL$^5$]**) indicates that a new ICT state may have been introduced that quenches the singlet excited state of the chromophore.

The fact that imatinib did not displace **[EuL$^5$]** from $\alpha_1$-AGP was reflected in lower values of the observed binding constants for both human and bovine species (log K = 5.6(0.1) and log K = 4.8(0.1), respectively), than was expected (log K = 6.4(0.1)). The observed quenching constant corresponds to a charge-transfer quenching process

within the binding pocket, rather than to the quenching due to displacement. In the case of bupivacaine, very similar binding constants were observed (log K = 5.6(0.1) for human $\alpha_1$-AGP and log K = 5.9(0.1) for bovine $\alpha_1$-AGP), whilst binding constants for lidocaine were also very close (log K = 4.4(0.1) for human $\alpha_1$-AGP and log K = 4.5(0.1) for bovine $\alpha_1$-AGP). Both values observed for human $\alpha_1$-AGP are in a good agreement with previously reported data (log K = 4.4(0.1) for lidocaine and log K = 5.7(0.1) for bupivacaine)[29], whilst very close values observed for two species suggests similar binding motifs. Drug binding data are summarised in Table III.2.

**Table III.2** Binding affinities of **[EuL$^5$]**, lidocaine, bupivacaine and imatinib to bovine and human $\alpha_1$-AGP (pH = 7.40, 298 K). Literature values are given in parentheses[29]

| | **[EuL$^5$]** | lidocaine | bupivacaine | imatinib |
|---|---|---|---|---|
| human $\alpha_1$-AGP | 4.1 | 4.4 (4.4) | 5.6 (5.7) | 5.6 (6.4) |
| bovine $\alpha_1$-AGP | 4.7 | 4.5 | 5.9 | 4.8 |

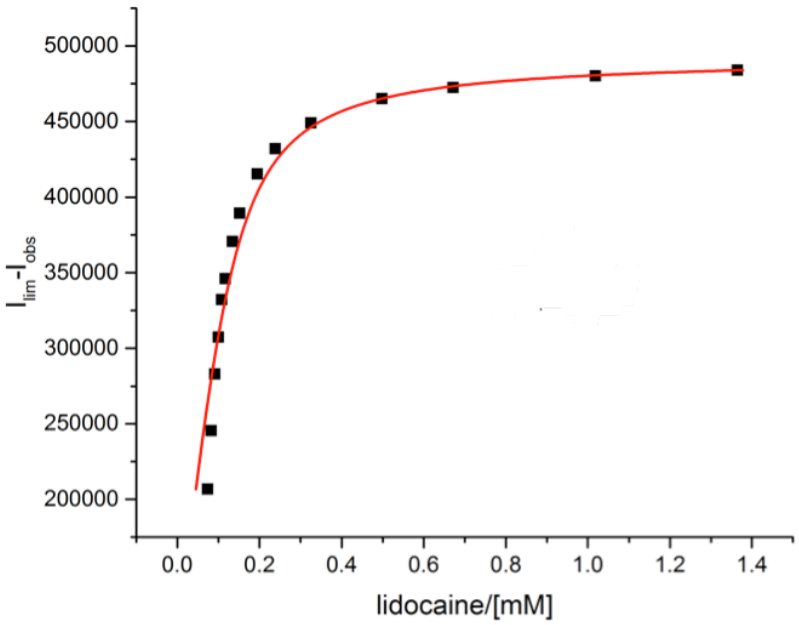


**Fig. III.45** Variation of europium emission intensity in the presence of bovine $\alpha_1$-AGP showing the fit (line) to the data points with added lidocaine (**[EuL$^5$]** 3 μM; [bovine $\alpha_1$-AGP] 122.0 μM, log K = 4.54(0.1), assuming a 1:1 binding isotherm, pH = 7.40, $\lambda_{ex}$ = 310 nm, 0.1 M HEPES, 298 K).

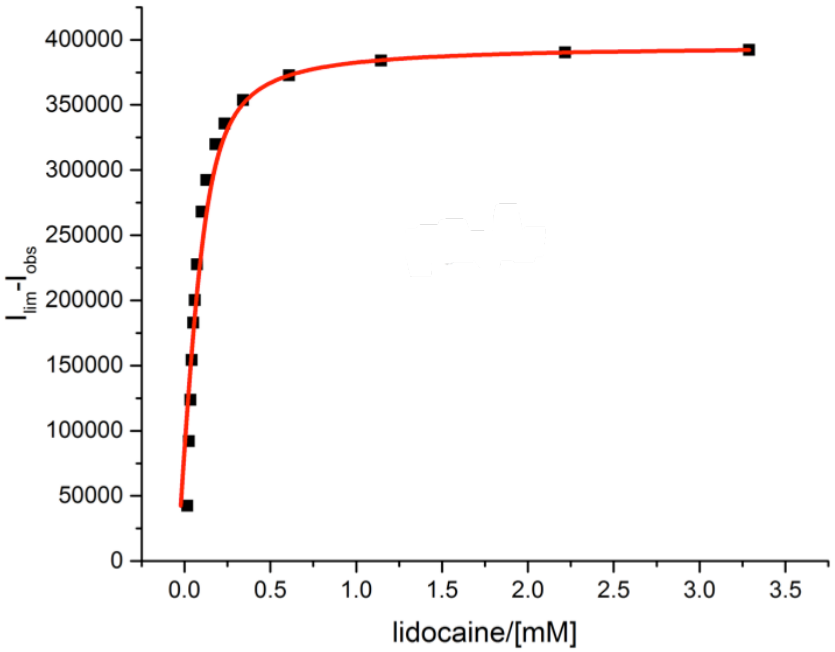


**Fig. III.46** Variation of europium emission intensity in the presence of bovine $\alpha_1$-AGP showing the fit (line) to the data points with added lidocaine (**[EuL$^5$]** 3 μM; [human $\alpha_1$-AGP] 122.0 μM, log K = 4.39(0.1), assuming a 1:1 binding isotherm, pH = 7.40, $\lambda_{ex}$ = 310 nm, 0.1 M HEPES, 298 K).

Acute phase proteins, including $\alpha_1$-AGP, derive their name from their concentration dependence in response to external acute processes, primarily inflammation. Elevated levels of $\alpha_1$-AGP in human plasma may indicate the occurrence of inflamation processes in a body and can rise up to 5-fold, compared to a normal concentration in serum[30]. Therefore, monitoring the level of $\alpha_1$-AGP in human serum can be a useful tool for diagnosing the onset or occurrence of inflammatory processes in patients.

The development of the emission probe is associated with several difficulties, such as the presence of different proteins, which can compete with $\alpha_1$-AGP for binding the probe, as well as residual emission from conjugated amino acids. Moreover, it is highly desirable to have a ratiometric response, as the precise determination of the probe concentration in the sample is not always possible. The suggested probe **[EuL$^5$]** was succesfully tested *in vitro* and time-gating the europium emission response provides effective subtraction of any residual emission from emissive organic moieties. However, this 'turn-on' probe did not show a change of the emission spectral form, and also showed a very limited change in the lifetime of the excited $^5D_0$ state.

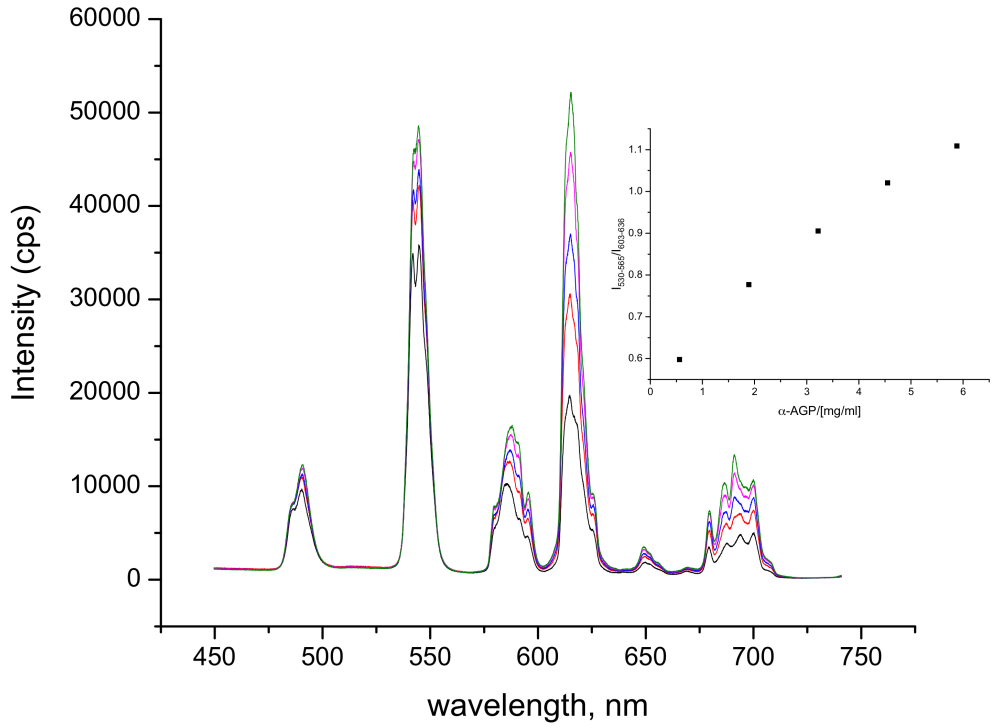


**Fig. III.47** Change of the total emission spectrum of **[EuL$^5$]/[TbL$^5$]** (22 μM/2 μM) 'cocktail' upon addition of bovine $\alpha_1$-AGP to bovine serum (pH = 7.40, $\lambda_{ex}$ = 310 nm, 298 K).

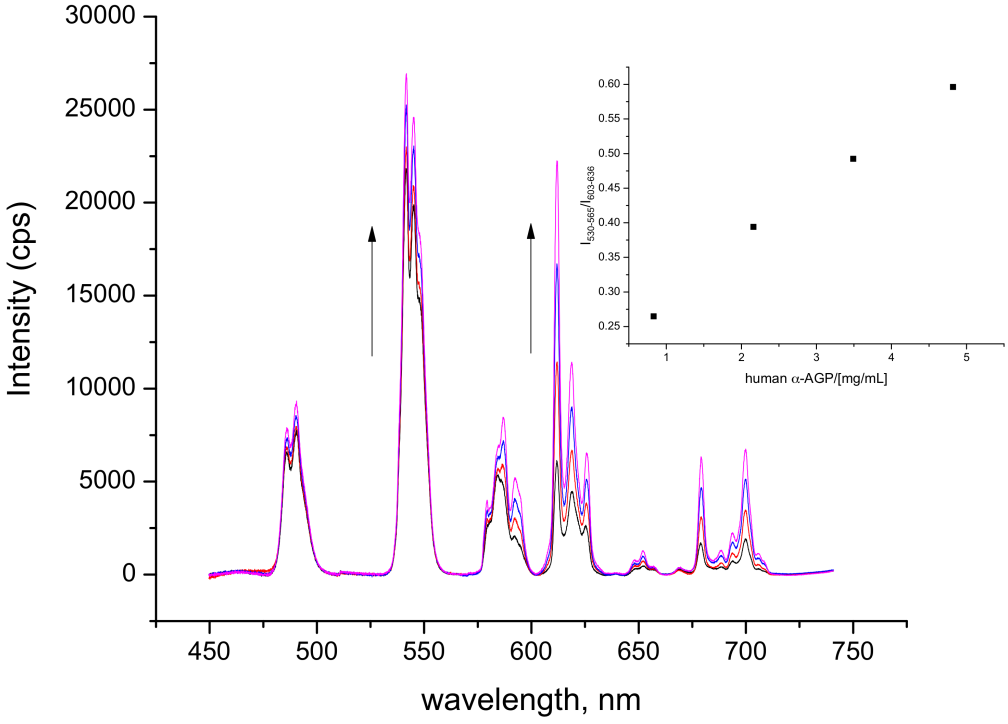


**Fig. III.48** Change of the total emission spectrum of **[EuL$^5$]/[TbL$^5$]** (22 μM/2 μM) 'cocktail' upon addition of human $\alpha_1$-AGP to human serum (pH = 7.40, $\lambda_{ex}$ = 310 nm, 298 K).

A possible solution to these problems is the use of a so-called 'cocktail' mixture – a combination of **[EuL$^5$]** and **[TbL$^5$]** complexes with a certain ratio between them (**[EuL$^5$]/[TbL$^5$]** = 22μM/2μM). Since the total emission of **[TbL$^5$]** was only weakly

dependent on the amount of added $\alpha_1$-AGP, the relative intensities of the $^5D_4 \rightarrow {}^7F_5$ transition in the $Tb^{3+}$ complex and the $^5D_0 \rightarrow {}^7F_2$ hypersensitive transition of $Eu^{3+}$ complex were monitored as a function of added $\alpha_1$-AGP in a serum background. The concentration was varied between 0.5-6 mg/mL, covering a 10-fold rise of $\alpha_1$-AGP concentration (Fig. III.47-III.48). No time-gating was performed for recording the emission spectrum, since negligible protein-based emission was observed in each case. A quasi-linear dependence was observed in both human and bovine serum, whilst the binding constant was lower than that observed during *in vitro* experiments. In addition, the total emission intensity of the 'cocktail' in serum was lower than for the same concentration of **[EuL$^5$]** and **[TbL$^5$]** in aqueous solution for the same concentration of added $\alpha_1$-AGP. Taken together, these observations indicate that competitive binding with other proteins does take place, and leads to a reduced emission intensity. To evaluate quantitatively the impact of the emission quenching by other proteins, the change of the total emission intensity was monitored upon binding **[TbL$^5$]** to both human (Fig. III.49) and bovine (Fig. III.50) serum albumins. The choice of terbium was made because **[EuL$^5$]** did not show a strong luminescence signal in the absence and presence of serum albumin.

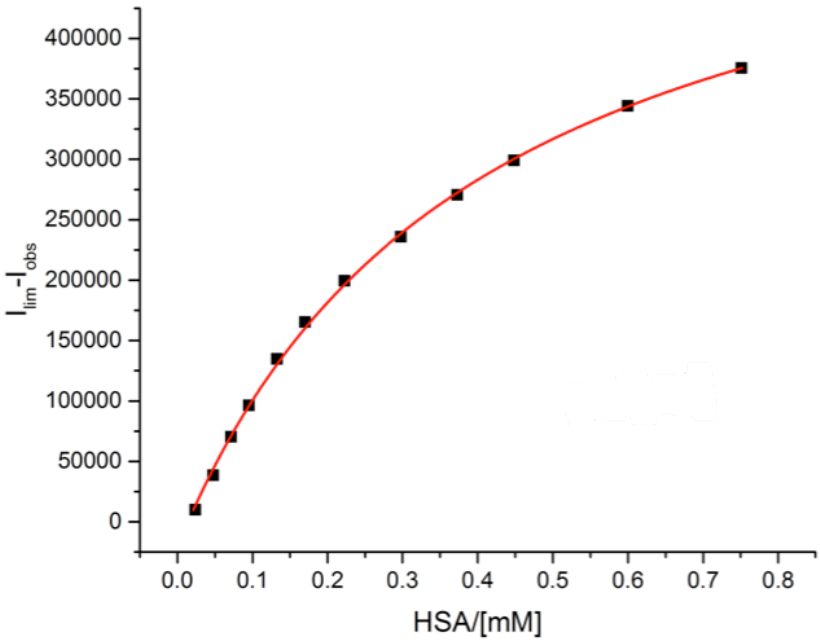


**Fig. III.49** Quenching of the total emission intensity of **[TbL$^5$]** (8 μM) upon addition of HSA. The apparent binding constant is logK = 3.41(0.1) (pH = 7.40, 0.1 M HEPES, $\lambda_{ex}$ = 310 nm, 298 K).

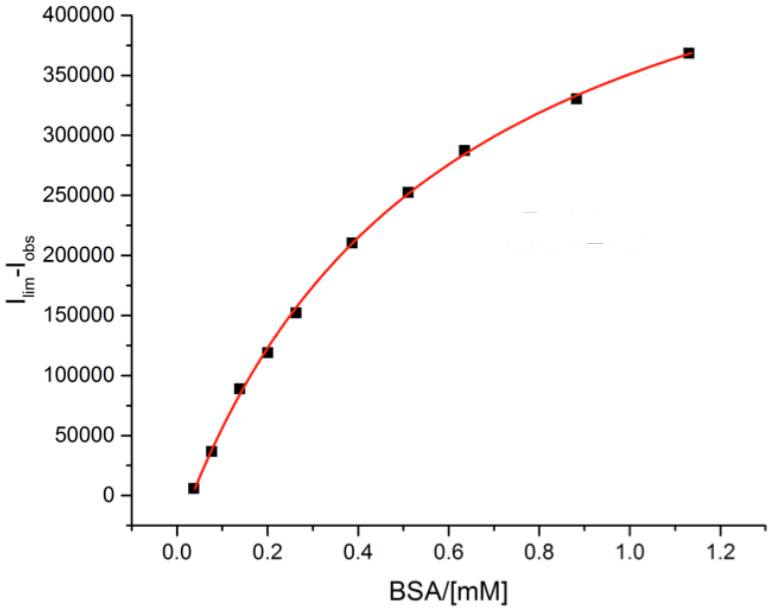


**Fig. III.50** Quenching of the total emission intensity of **[TbL$^5$]** (8 μM) upon addition of BSA. The apparent binding constant is logK = 3.24(0.1) (pH = 7.40, 0.1 M HEPES, $\lambda_{ex}$ = 310 nm, 298 K).

Following addition of serum albumin to **[TbL$^5$]**, quenching of the total emission intensity was observed. A similar effect was observed upon addition of BSA. Analysis of both binding curves revealed a rather low binding constant, similar for both human and bovine serum albumin and lower than those measured for $\alpha_1$-AGP. However, since the concentration of HSA is approximately one order of magnitude higher than the concentration of $\alpha_1$-AGP in human plasma, this effect will potentially hamper determination of $\alpha_1$-AGP, especially if its concentration changes significantly. Even though HSA is not usually considered as an acute phase protein, its concentration can still vary in response to different external factors. For instance, ageing is accompanied by a decrease of HSA concentration, whilst the concentration of $\alpha_1$-AGP remains the same.[31] At the same time, both proteins were shown to be useful markers in predicting the survival in post-operative patients. A low concentration of HSA suggested a poorer outcome.[32] With all these factors in mind, the effect of varying both HSA and $\alpha_1$-AGP was monitored by following the change of the total emission intensity of the **[EuL$^5$]**/**[TbL$^5$]** 'cocktail' (21μM/ 0.8μM) following separate incremental additional of each protein (Fig. III.51).

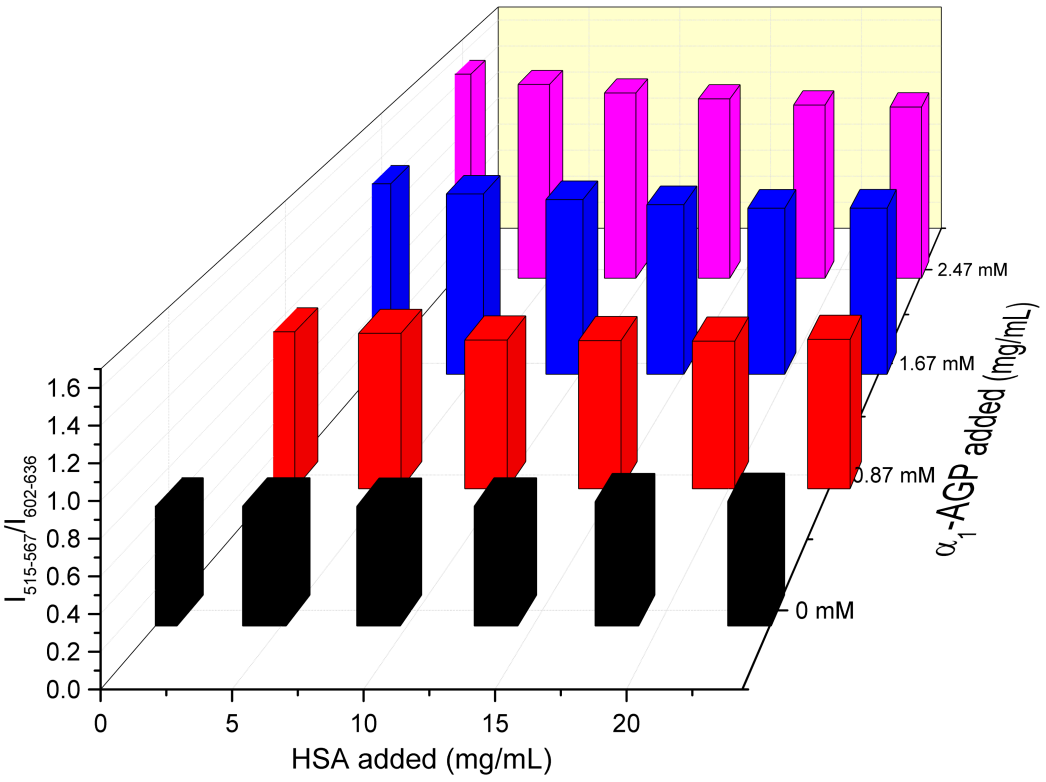


**Fig. III.51** Variation of the ratio of the terbium $^5D_4 \rightarrow {}^7F_5$ and the europium $^5D_0 \rightarrow {}^7F_2$ transitions in **[LnL$^5$]** as a function of added HSA and $\alpha_1$-AGP ($\lambda_{ex}$ = 310 nm, 298 K)

The concentration of human $\alpha_1$-AGP was varied 4-fold compared to its normal value, whilst the concentration of HSA was increased up to a factor of 2. The relative intensities of the $^5D_4 \rightarrow {}^7F_5$ transition of $Tb^{3+}$ and the $^5D_0 \rightarrow {}^7F_2$ hypersensitive transition of $Eu^{3+}$ were monitored as a function of added $\alpha_1$-AGP and HSA in serum. At no added $\alpha_1$-AGP, only a minor change in the emission intensity was observed in response to addition of HSA. However, at higher concentration of added $\alpha_1$-AGP, a drop of the relative emission intensity was observed. Moreover, the overall intensity of the emission spectra also gradually decreased for both europium and terbium components, in line with previously reported experiments involving addition of HSA.

The observed changes of the binding curve for different concentrations of added HSA at elevated concentrations of $\alpha_1$-AGP may be due to more complicated regulatory processes in human blood, and the simple addition of lyophilised protein to serum is probably a gross simplification. Real serum samples from patients with different levels of $\alpha_1$-AGP and HSA should be analysed and their concentrations

determined by independent methods. At the same time, the proposed $\alpha_1$-AGP probe can be developed further, by adding an additional reference compound, which does not bind to either of two proteins. The resulting system may by used to monitor concentrations of two proteins simultaneously, since the responses of **[EuL$^5$]** and **[TbL$^5$]** towards each of the two proteins are different. The proposed system can be employed to monitor the deviation of both $\alpha_1$-AGP and HSA in serum, over a broad range of physiologically relevant concentrations.

### *III.3.4 $\alpha_1$-AGP binding of [DyL$^5$]*

Dysprosium complexes have attracted much less attention as bio-imaging probes than their europium and terbium counterparts, primarily due to their lower emission quantum yields. On the other hand, dysprosium complexes are the most attractive among 'secondary' lanthanides emitting in the visible range – samarium, thulium and praseodymium. The lowest excited state of $Dy^{3+}$ is $^4F_{9/2}$, which is close in energy to the $^5D_4$ level of $Tb^{3+}$, and therefore ligands sensitising terbium emission are also often good sensitisers for dysprosium emission. However, compared to other lanthanide ions, lower lying energy states are spanning a wider range of values up to 12000 cm$^{-1}$, making an energy gap of only 10000 cm$^{-1}$ between the lowest excited and the highest 'ground' state. It is not surprising therefore that the $Dy^{3+}$ excited state in complexes is prone to vibrational quenching *via* energy transfer to proximate O-H oscillators. Another feature of such an energy diagram is the presence of luminescence signals in both the visible and near-IR part of the emission spectrum, even though the potential of dysprosium complexes as IR-emitters has not been fully recognised.

In the visible part of the spectrum, three transition manifolds are usually observed – $^4F_{9/2} \rightarrow {}^6H_J$, J = 13/2, 11/2, 9/2. The latter transition is usually significantly weaker than the other two and is often observed just as a weak broad band. With regard to susceptibility of the emission spectrum in response to perturbation of coordination environment, none of these three transitions can strictly be classified as hypersensative and this is probably another reason why dysprosium complexes have found such a limited application in ratiometric bio-imaging.[33]

In the present study, the dysprosium complex **[DyL$^5$]** was synthesised and its photophysical behaviour was investigated. The complex showed an increase of the total emission intensity upon addition of human $\alpha_1$-AGP (Fig. III.52), which might be attributed to an expulsion of the second sphere water molecules, when bound to the protein. No change of the spectral form was observed upon addition of the protein, in line with previous findings. Such behaviour corresponds to an absence of change in the coordination environment when human $\alpha_1$-AGP is added to **[DyL$^5$]** in HEPES (0.1M, pH = 7.40). When the sulfonamide hydrogen is protonated, the observed emission profile underwent a drop in intensity.

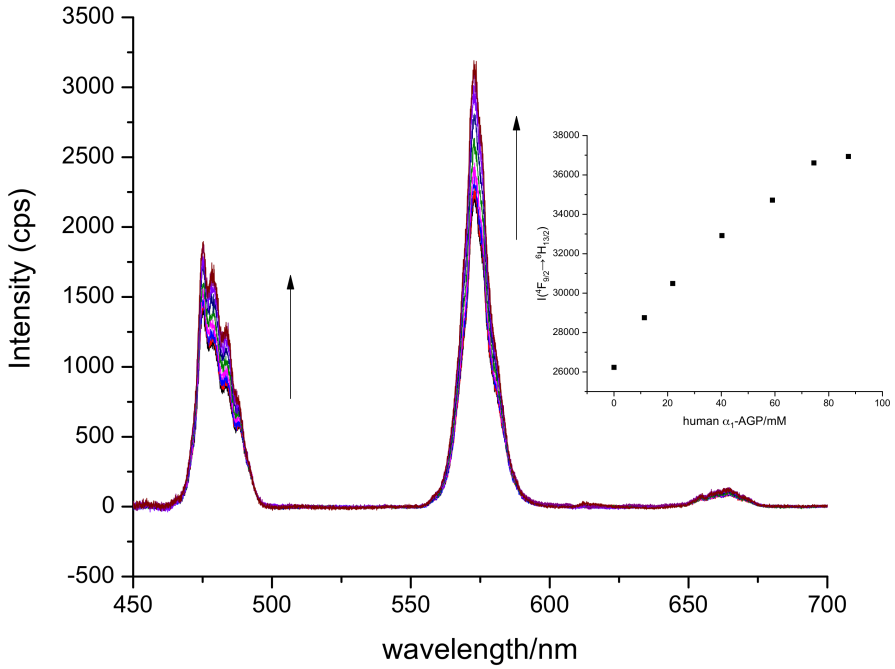


**Fig. III.52** Variation of the total emission intensity of **[DyL$^5$]** (6 μM) as a function of added human $\alpha_1$-AGP (pH = 7.40, 0.1 M HEPES, $\lambda_{ex}$ = 310 nm, 298 K).

## III.4 Conclusion and future studies

In the present study, two europium-based luminescent 'turn-on' probes **[EuL$^4$]** and **[EuL$^5$]** have been synthesised for the selective detection of HSA and $\alpha_1$-AGP, respectively, both of which showed high protein selectivity. Their principle of action is based on the efficient quenching of the ligand singlet excited state by an ICT state. The energy of the ICT is dependent on the polarity of the local environment. Once each of the complexes is bound to a protein, the local polarity is decreased. At the same time, the ICT state energy is elevated and can no longer quench the $Eu^{3+}$-centred emission as efficiently, as it is in a less polar medium. This observation may

allow these probes to be used in studies of protein conformations, as the degree of of the exposure of the binding pocket to water should modulate the observed total emission intensity.

Circularly-polarised luminescence spectroscopy has been used to probe the chiral environment in binding pockets of both proteins, resulting in a very unexpected opposite handednesses of the CPL spectrum of **[EuL$^5$]**, when bound to human and bovine $\alpha_1$-AGP, respectively. This indicated that different enantiomers have been locked in binding pockets of different variants of the protein, even though their different amino-acid content resulted in similar binding affinities. Furthemore, this discrepancy in amino-acide sequence around the binding pocket led to a considerable change of the p$K_a$ of **[EuL$^5$]**, which was explained by an interaction between sulphonamide arm and Tyr-84, which is present in bovine version, but not in human. Such a detailed analysis of the difference between binding pockets in human and bovine $\alpha_1$-AGP has not been performed before, and provides a better understanding of possible interactions between molecular probes and amino-acid lining up the binding pocket.

These differences were analysed further by running competitive binding experiments of **[EuL$^5$]*$\alpha_1$-AGP** with popular drugs, which are know to be carried in blood by $\alpha_1$-AGP. Similar values were obtained for lidocaine and bupivacaine despite the difference in amino-acid content of two proteins. This series can be extended further by using other drugs, which can provide a better insight into binding essential drugs to $\alpha_1$-AGP, and hence its metabolism in livestock.

As terbium and europium complexes, due to the different redox potential and resonance levels of the excited state, showed significantly different dependence on the solvent polarity, their mixture produced a ratiometric response. This 'cocktail' has been used to monitor the concentration of $\alpha_1$-AGP in bovine and human serum, which may find practical application for monitoring its level in patients with inflammation diseases.

The induced CPL signal in both **[EuL$^4$]** and **[EuL$^5$]** can be used to elucidate structural changes in the proteins, as even subtle changes of conformation around the binding pocket are very likely to cause changes in their CPL spectral signature. To

improve the observed dissymmetry ratio, bulkier substituents, e.g. phosphinate arms, can be introduced to lock the conformation of the *Δ* or *Λ* enantiomer (Fig. III.53). Moreover, it is interesting to compare the changes in the coordination polyhedron upon binding/dissociation of the sulphonamide nitrogen in a diphosphinate analogue with **[EuL$^5$]**, and check if the postulated TSAP⇆SAP transition is also observed.

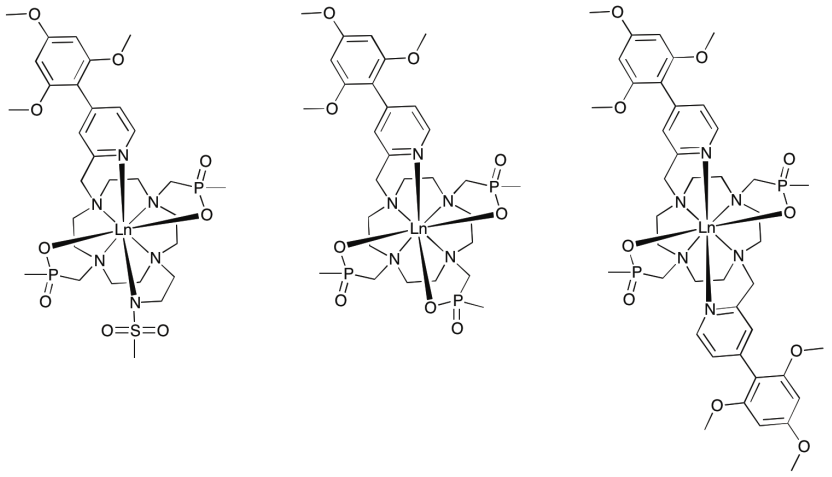

**Fig. III.53** Molecular structure of proposed $\alpha_1$-AGP-selective probes, with enhanced $g_{em}$ values.

The competitive binding studies between **[EuL$^5$]*[human α$_1$-AGP]** or **[EuL$^5$]*[bovine α$_1$-AGP]** and common drugs showed similar binding affinities, irrespective of the nature of the $\alpha_1$-AGP species used. These studies can be extended further, by expanding the number of species studied and should be followed by both total emission intensity and CPL. Furthermore, the p$K_a$ values of the complex in the presence of different $\alpha_1$-AGP species should be measured, and their comparison with amino-acid composition could shed the light on the residues directly involved in binding to the complex.

# III.5 References


[1] C. Reichardt, *Chem. Rev.* **1994**, *94*, 2319–2358.

[2] C. Reichardt, *Green Chem.* **2005**, *7*, 339-351.

[3] G. S. Loving, M. Sainlos, B. Imperiali, *Trends Biotechnol.* **2010**, *28*, 73–83.

[4] M. Vonci, K. Mason, E. A. Suturina, A. T. Frawley, S. G. Worswick, I. Kuprov, D. Parker, E. J. L. McInnes, N. F. Chilton, *J. Am. Chem. Soc.* **2017**, *139*, 14166-14172

[5] R. Carr, L. Di Bari, S. Lo Piano, D. Parker, R. D. Peacock, J. M. Sanderson, *Dalton Trans.* **2012**, *41*, 13154-13158.

[6] U. Rösch, S. Yao, R. Wortmann, F. Würthner, *Angew. Chem. - Int. Ed.* **2006**, *45*, 7026–7030.

[7] M. Fasano, S. Curry, E. Terreno, M. Galliano, G. Fanali, P. Narciso, S. Notari, P. Ascenzi, *Life* **2005**, *57*, 787–796.

[8] S. R. Berenberg, Ed. , *Liver Diseases in Infancy and Childhood*, Springer Netherlands, Dordrecht, **1976**.

[9] L. Lu, H. Z. He, H. J. Zhong, L. J. Liu, D. S. H. Chan, C. H. Leung, D. L. Ma, *Sensors Actuators, B Chem.* **2014**, *201*, 177–184.

[10] A. V. Onufriev, E. Alexov, *Q. Rev. Biophys.* **2013**, *46*, 181–209.

[11] B. X. Huang, H. Y. Kim, C. Dass, *J. Am. Soc. Mass Spectrom.* **2004**, *15*, 1237–1247.

[12] A. Bujacz, *Acta Crystallogr. Sect. D Biol. Crystallogr.* **2012**, *68*, 1278–1289.

[13] S. D. B. Goldman, R. S. Funk, R. A. Rajewski, J. P. Krise, *Bioanalysis* **2009**, *1*, 1445–59.

[14] D. G. Smith, B. K. McMahon, R. Pal, D. Parker, *Chem. Commun.* **2012**, *48*, 8520-8522.

[15] E. Boros, P. Caravan, *Inorg. Chem.* **2015**, *54*, 2403–2410.

[16] H. B. Eldredge, M. Spiller, J. M. Chasse, M. T. Greenwood, P. Caravan, *Invest. Radiol.* **2006**, *41*, 229–243.

[17] L. Moriggi, M. A. Yaseen, L. Helm, P. Caravan, *Chem. - Eur. J.* **2012**, *18*, 3675–3686.

[18] J. Ghuman, P. A. Zunszain, I. Petitpas, A. A. Bhattacharya, M. Otagiri, S. Curry, *J. Mol. Biol.* **2005**, *353*, 38–52.

[19] F. Zsila, Y. Iwao, *Biochim. Biophys. Acta - Gen. Subj.* **2007**, *1770*, 797–809.

[20] J. Hovinen, M. Veli-Matti, H. Hakala, J. Peuralahti, *Novel Chelating Agents And Highly Luminescent And Stable Chelates And Their Use*, **2005**, WO 2005/058877 A1.

[21] T. Nakamura, S. Mizukami, M. Tanaka, K. Kikuchi, *Chem. - Asian J.* **2013**, *8*, 2685–2690.

[22] C. M. Thiele, K. Petzold, J. Schleucher, *Chem. - A Eur. J.* **2009**, *15*, 585–588.

[23] A. T. Bui, A. Grichine, A. Duperray, P. Lidon, F. Riobé, C. Andraud, O. Maury, *J. Am. Chem. Soc.* **2017**, *139*, 7693–7696.

[24] F. Herve, G. Caron, J. C. Duche, P. Gaillard, N. Abd Rahman, A. Tsantili-

Kakoulidou, P. A. Carrupt, P. d'Athis, J. P. Tillement, B. Testa, *Mol Pharmacol* **1998**, *54*, 129–138.

[25] E. Hazai, J. Visy, I. Fitos, Z. Bikádi, M. Simonyi, *Bioorganic Med. Chem.* **2006**, *14*, 1959–1965.

[26] S. Shinoda, *Chem. Soc. Rev.* **2013**, *42*, 1825–1835.

[27] E. J. New, D. Parker, R. D. Peacock, *Dalton Trans.* **2009**, 672–679.

[28] M. Baldassarre, R. Galeazzi, B. Maggiore, F. Tanfani, A. Scirè, *Biochimie* **2014**, *102*, 19–28.

[29] D. L. Schönfeld, R. B. G. Ravelli, U. Mueller, A. Skerra, *J. Mol. Biol.* **2008**, *384*, 393–405.

[30] L. Jennings, R. S. Waters, R. Pal, D. Parker, *ChemMedChem* **2017**, *12*, 271–277.

[31] T. Hochepied, F. G. Berger, H. Baumann, C. Libert, *Cytokine Growth Factor Rev.* **2003**, *14*, 25–34.

[32] B. Veering, A. Burm, J. Souverijn, J. Serree, J. Spierdijk, *Br. J. Clin. Pharmacol.* **1990**, *29*, 201–206.

[33] D. G. Levitt, M. D. Levitt, *Int. J. Gen. Med.* **2016**, *9*, 229–255.

[34] D. M. Gruen, C. W. Dekock, R. L. McBeth, in *Lanthanide/Actinide Chem.*, **1967**, pp. 102–121.

# Chapter Four

# Europium probes for nucleotide and zinc(II) sensing

# IV.1 Luminescent probes for biologically relevant anions

The selective detection of biologically relevant anions in complex mixtures is a challenging task, given the typically narrow concentration range of target species and the presence of chemically related and hence competing anions. In order to create a probe with a high signal-to-noise ratio, an amplification of the signal is needed to allow discrimination between the resting state of the probe and the state with the analyte bound. When luminescent probes are taken into consideration, a change of the total emission intensity and/or shift of the emission/excitation bands are the usual 'read-outs' to signal the binding event, and their magnitude can be altered by judicious design of the probe.

Concentrations of biologically important anions, e.g. carbonate, citrate, lactate, phosphate, AMP, ADP, ATP, can be monitored in aqueous media through reversible binding involving electrostatic, H-bonding and weaker non-bonding interactions. In some cases, a common luminescent platform can be employed, which is customised depending on the required species to be analysed. For instance, a 3,3'-bipyridyl-modified ruthenium(II) complex has been used as a platform, to which different functional groups can be attached for sensing either $Zn^{2+}$ or oxo-anions (Fig. IV.1)[1]. Anions were reversibly bound by H-bonding and Coulombic interactions of the attached guanidinium and ammonium moieties.

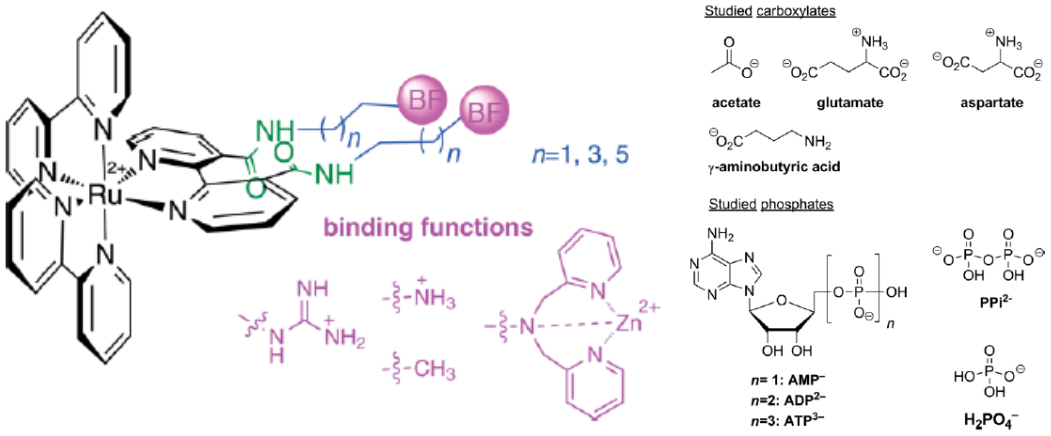


**Fig. IV.1** Molecular structure of 3,3'-bipyridyl-modified ruthenium(II) complex with different sensing moieties attached and the list of anions used for binding studies.[1]

In contrast to metal ions, anions more often possess both different shapes and sizes, making their selective recognition slightly easier by designing complementary binding pockets in the molecular probes. For example, a chiral receptor featuring two [9]aneN$_3$ moieties bridged by an (*S*)-BINOL linker showed selectivity towards (*S*,*S*)-tartaric acid over the (*R*,*R*)/*meso* forms (Fig. IV.2)[2]. Six nitrogens of two [9]aneN$_3$ rings stabilised two carboxylate groups of tartaric acid by H- and electrostatic-bonding, whilst binding of the hydroxyl groups of tartrate with tertiary amines provided for enantioselectivity towards the (*R*,*R*)/*meso* forms of tartaric acid. Once the analyte was bound, the emission intensity experienced a significant rise due to the removal of PET quenching of the BINOL linker.

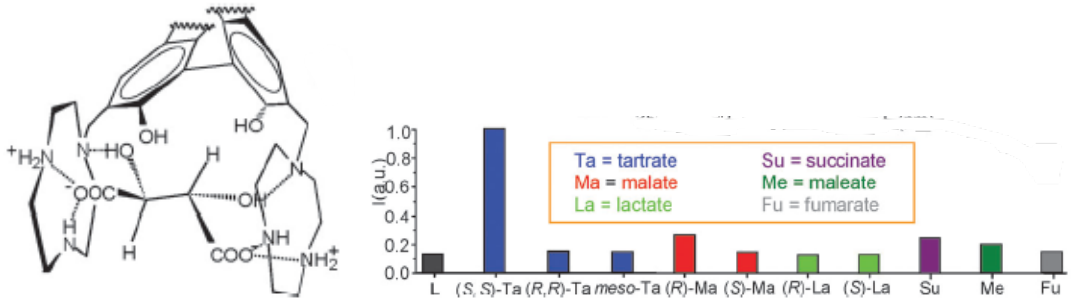


**Fig. IV.2** Binding mode of the probe and its selectivity towards different anions after adding 10 equivalents of each substrate (pH = 7.0, water).[2]

In a similar fashion, a bis-pyridinium calix[4]pyrrole derivative was used for the selective detection of pyrophosphate through displacement of a chromenolate anion, giving rise to an enhancement of the emission intensity upon elimination of PET quenching (Fig. IV.3)[3]. The size of the pyrophosphate anion matched that of the cavity formed inside the calix[4]pyrrole between two pyridinium moieties and was stabilised by H-bonding with pyrrole hydrogens and a Coulombic interaction with the pyridinium nitrogen atoms.

However, purely organic systems usually show low binding affinities in water, as a result of relatively low H-bond energies. Anions in aqueous solution are strongly solvated and are stabilised via a network of H-bonds. Therefore, a large binding energy must compensate for the enthalpy of hydration in order for binding to the molecular probe to occur. One of the possible solutions to this problem is to bind the anion to a metal centre, leading to formation of a strong metal-oxygen bond.

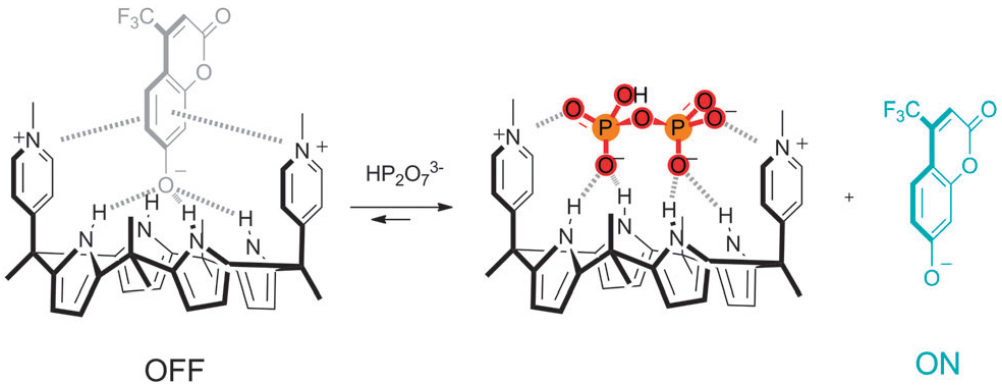


**Fig. IV.3** Proposed switching-on mechanism upon addition of pyrophosphate in acetonitrile.[4]

A dipicolylamine-appended sensor **Zinpyr-1**, initially proposed by Lippard for zinc sensing *in cellulo*, was used for the selective binding of the pyrophosphate anion involving two coordinated zinc ions (Fig. IV.4)[5]. Gradual addition of pyrophosphate led to an increase of the total emission intensity, along with a bathochromic shift of emission. The bridging binding mode to two metal centres ensured high selectivity towards bidentate pyrophosphate over monodentate hydrogenphosphate.

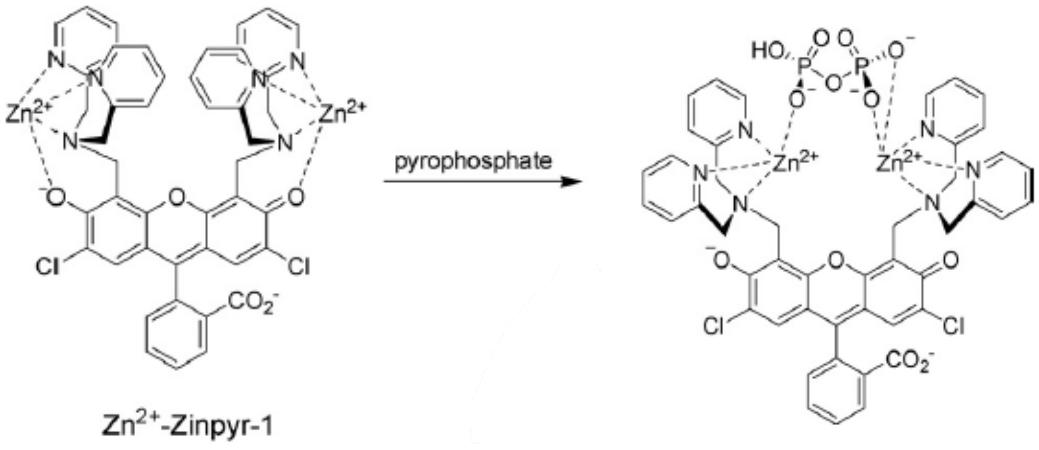


**Fig. IV.4** Putative binding mechanism of pyrophosphate by a bimetallic zinc complex **$Zn^{2+}$-Zinpyr-1** ($H_2O$, pH = 7.40).[5]

The primary limitation of most reports of anion binding to transition metal ion centres is the absence of a ratiometric response and the presence of residual emission from other fluorophores in the reaction mixture. Even though a shift of the emission intensity is sometimes observed upon binding of the analyte in these systems, its magnitude is usually small and prevents efficient ratiometric read-outs. Certain lanthanide complexes do not have these drawbacks and can provide a strong

ratiometric response if suitably designed, with millisecond lifetimes, allowing efficient time-gating of the emission intensity signal.

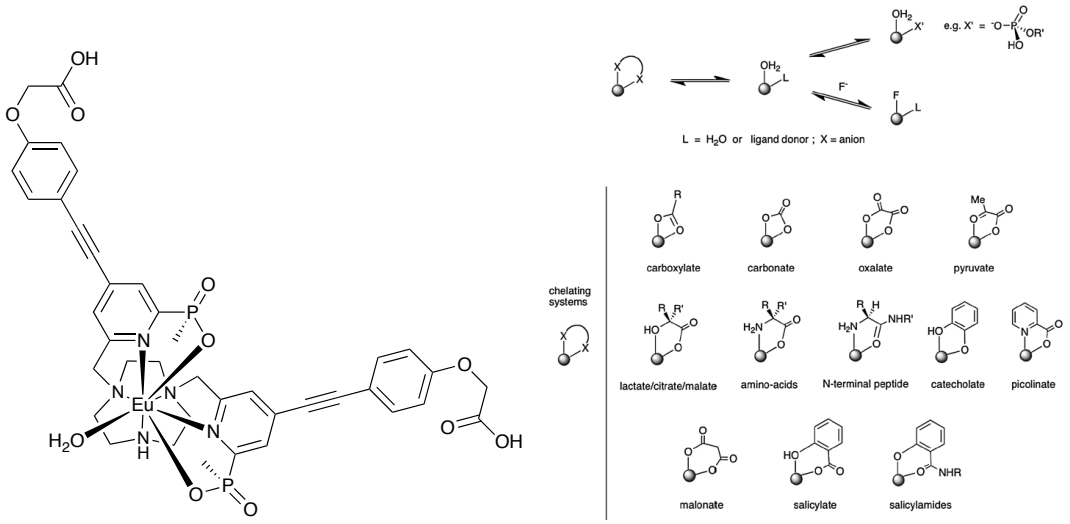


**Fig. IV.5** Molecular structure of **EuroTracker®** probe used for anion binding studies and putative binding modes for different anions.[6]

A series of **EuroTracker®** probes with rod-like alkynyl-pyridine chromophores based on [9]ane$N_3$ platform has been used for anion-binding studies (Fig. IV.5)[7]. A coordinated water molecule was displaced by a bound analyte, increasing the overall emission intensity along with a significant change of the spectral fingerprint. By following the relative intensitiy of the hypersensitive, electric-dipole allowed $^5D_0 \rightarrow {}^7F_2$ transition, the concentration of the bound analyte could be monitored.

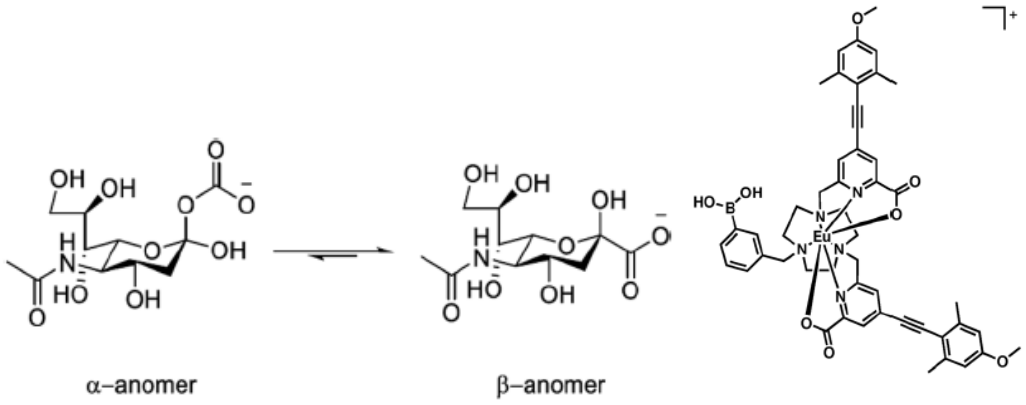


**Fig. IV.6** Molecular structure of sialic acid with two pyranose forms and the probe used for its sensing.[8]

Additional stabilisation and selectivity can be achieved if metal binding is augmented by weaker interactions, e.g. H-bond formation or boron-carbohydrate interactions. Bearing this in mind, a phenylboronic acid moiety was attached to the

[9]ane$N_3$ platform with two alkynyl-pyridine chromophores and binding studies with sialic acid were carried out (Fig. IV.6)[8]. By comparing binding data for this complex and its analogue without the phenylboronic acid moiety, the cooperative binding of a terminal diol group of sialic acid to the boronic acid residue and an amide carbonyl oxygen to europium was hypothesised.

This concept was developed further, and the reversible intramolecular binding of a pyridine moiety in response to external stimuli was suggested. It has been previously reported by Pope, that a pyridine with an appended dipicolylamine moiety on a DO3A platform could efficiently sense zinc ions by significantly perturbing the europium emission profile[9]. The same principle can be employed for sensing anions, assuming that apart from direct binding to the lanthanide metal, an anion molecule can be stabilised by H-bonding with three pyridine moieties and a protonated tertiary amine nitrogen. With this in mind, the initial structure proposed by Pope was modified and a chromophore arm was added to provide sensitisation using a 355 nm diode laser, whilst the substituents at the tertiary amine centre were varied in order to modulate affinity.

## IV.2 Novel anion-binding probes [EuL$^{7-9}$]

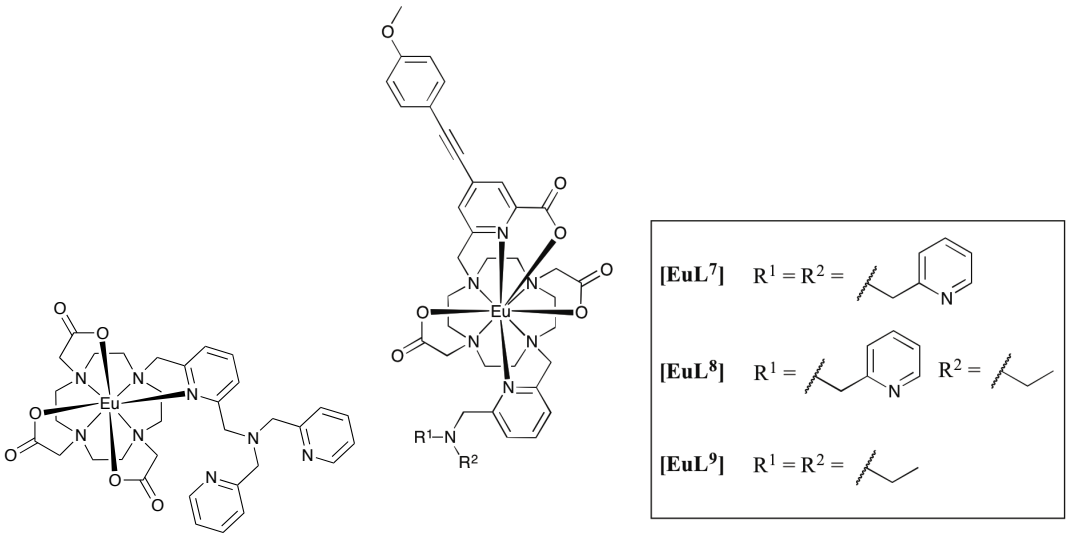


**Fig. IV.7** Molecular structure of the probe proposed by Pope[9] (*left*) and the series of probes **[EuL$^{7-9}$]** discussed in the present study (*right*).

The complexes **[EuL$^{7-9}$]** (Fig. IV.7) were synthesised as shown on Scheme IV.1. The alkynyl-pyridine chromophore was synthesised in accord with a previously reported

procedure[7]. In this sequence, the freshly prepared mesylate was slowly added to a DO2A ester intermediate, yielding mostly a *tri*-substituted product. A picolylamine arm was prepared by mixing three equivalents of 2,6-*bis*(chloromethyl)pyridine with the corresponding secondary amine. The resulting chloride was reacted with a *tri*-substituted 12-ane N4 platform, giving the ester derivatives of the ligands $\mathbf{L^{7\text{-}9}}$, which were hydrolysed in aqueous base overnight at 60°C, neutralised and complexed with $EuCl_3$ to give the desired complexes $\mathbf{[EuL^{7\text{-}9}]}$.

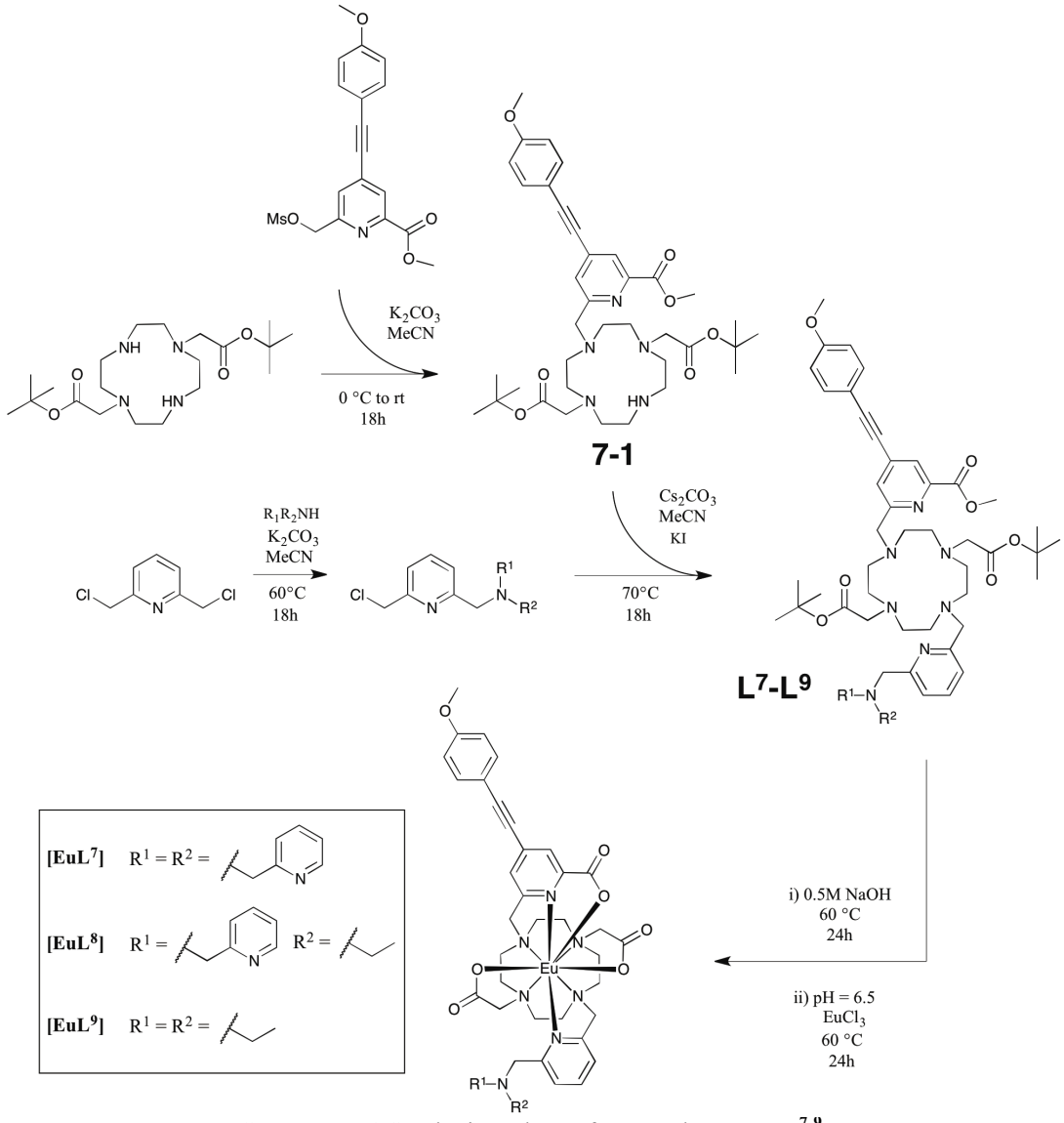


**Scheme IV.1** Synthetic pathway for complexes $\mathbf{[EuL^{7\text{-}9}]}$.

Any excess metal ion was precipitated in the form of $Eu(OH)_3$ by adding aqueous ammonia solution, followed by neutralisation with 1M HCl. All attempts to purify the desired complex on RP-HPLC failed, either due to extremely broad and unresolved bands in the UV-trace when no buffer was used, or a change of the emission spectrum of the resulting complex when ammonium bicarbonate or formic

acid were used as a buffer, indicating binding of bicarbonate or formate to the complex. Therefore, no further purification steps were attempted and the complexes studied were used as proposed, with an uncontrolled amount of NaCl.

Preliminary studies revealed the high affinity of the parent probe, **[EuL$^7$]**, towards phosphate and glyphosate - *N*-(phosphonomethyl)glycine – one of the most extensively used herbicides in the world. At physiological pH in HEPES buffer (0.1 M, pH = 7.4) phosphate is present as an almost equal mixture of $H_2PO_4^-$ and $HPO_4^{2-}$, whilst the glyphosate phosphonate OH-group (p$K_a$ = 5.6) is mostly deprotonated[10]. At this pH, very similar binding curves were observed for both phosphate and glyphosate, suggesting that a similar binding mechanism was occurring in each case. However, once the pH was lowered to 5.9 in 0.1M MES buffer, the phosphate was mainly present in the $H_2PO_4^-$ form, whilst the glyphosate phosphonate OH was still partially deprotonated, giving higher electrostatic affinity, and hence stronger overall binding (Fig. IV.8).

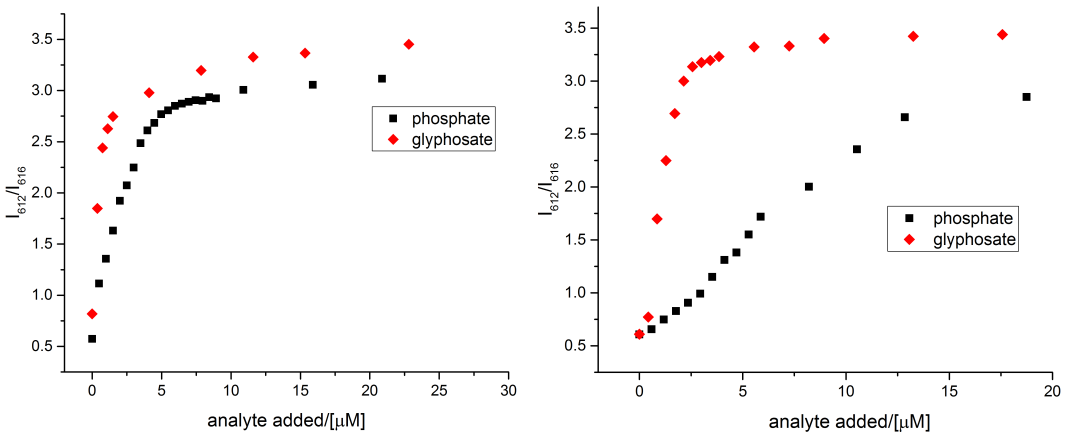


**Fig. IV.8** Binding curves of **[EuL$^7$]** for phosphate and glyphosate binding in HEPES (0.1 M, pH = 7.40; *left*) and MES (0.1 M, pH = 5.90; *right*).

Analogous measurements were carried out for various carboxylates (e.g. citrate, lactate, acetate), although binding affinities turned out to be considerably lower than for phosphate and glyphosate. This trend is normally observed for lanthanide complexes, with a bidentate binding mode normally observed for carboxylate anions and monodentate for phosphates[6].

## IV.3 Binding of nucleotides

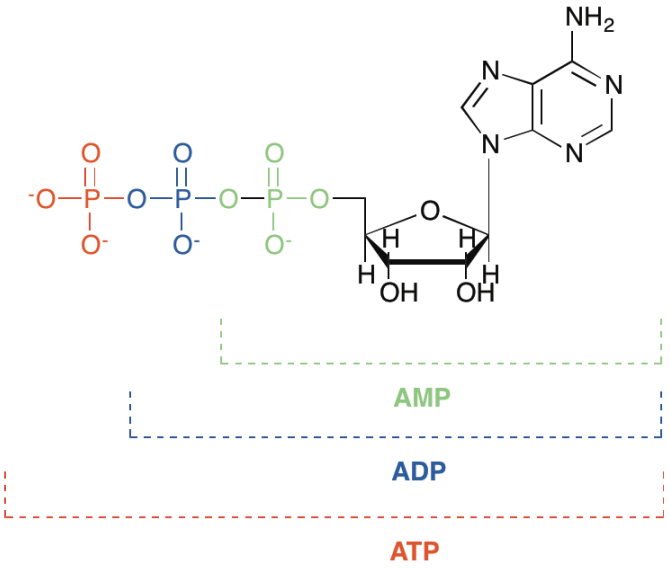


**Fig. IV.9** Molecular structure of the nucleosides AMP, ADP and ATP.

Adenosine triphosphate (ATP) plays an essential role in biological processes, supplying energy by transferring a phosphate group from adenosine triphosphate to a target molecule (e.g. glucose) and subsequent reduction to adenosine diphosphate (ADP, Fig. IV.9 - IV.10). The high energy of the phosphoester bond is released upon cleavage (30.5 kJ/mol at physiological conditions) and varies depending on the concentration of $Mg^{2+}$ ions, which promote hydrolysis by activating the P-O bond. Further hydrolysis of ADP to AMP is also possible, releasing a second phosphate molecule.

**Fig. IV.10** A simplified hydrolysis scheme of ATP to ADP with release of the hydrogenphosphate anion.

The ratio between the concentrations of ADP and ATP is of significant importance for cellular metabolism and determines the direction of multiple reactions. For example, in the citric acid cycle, a lowered ATP/ADP ratio triggers oxidation of a substrate by isocitrate dehydrogenase[11]. Therefore, easily accessible tools for

monitoring the ATP/ADP ratio on a cellular level are important and have commercial significance, with new sensors appearing regularly.

A recent example, which has been reported is Perceval, which involves a fusion protein, consisting of a bacterial regulatory protein GInK1 and a modified green fluorescent protein GFP, originally developed by Yellen (Fig. IV.11)[12]. The GInK1 protein possesses three nucleotide binding sites for binding both ADP and ATP, but only binding of ATP causes a local conformational change, giving rise to changes of fluorescent signal of the coupled GFP.

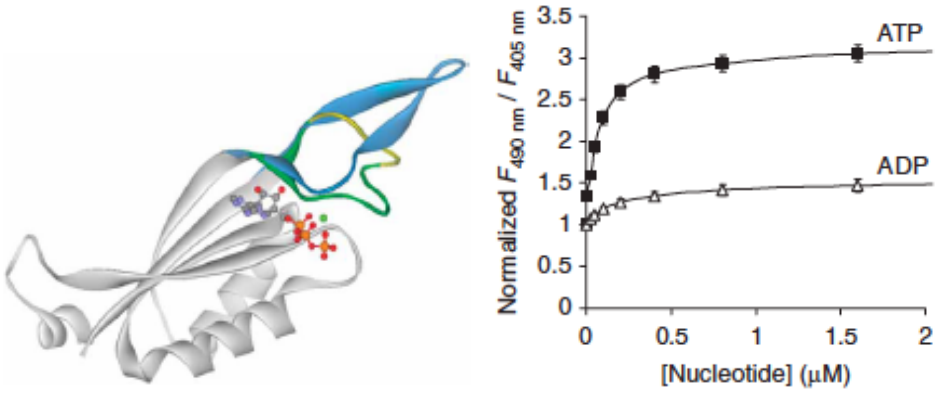


**Fig. IV.11** Ribbon representation of one subunit of the GlnK1 protein without a ligand (gray and blue) or with $Mg^{2+}$-ATP (grey, green and yellow, with the ligand in ball- and-stick form) and the ratio between fluorescent intensities upon excitation at 490 nm vs 405 nm and addition of ADP and ATP molecules. [12]

In the present study, three nucleotides – AMP, ADP and ATP – were added to **[EuL$^{7\text{-}10}$]** and the corresponding change of emission intensity and lifetime was monitored. To follow the changes in the emission spectrum upon addition of a nucleotide, the electric-dipole transition $^5D_0 \rightarrow {}^7F_2$ resolved into two bands and their relative intensity was monitored.

As no reliable fitting to a 1:1 binding model was possible, only an approximate evaluation of the affinity order was carried out. The highest affinity was observed for **[EuL$^7$]** with a pyridine moiety bearing a dipicolylamine substituent. After addition of 1.0 equivalent of AMP and ADP, saturation of the binding curve was observed, suggesting a 1:1 binding mode with a nucleotide molecule (Fig. IV.12). A higher affinity was observed for AMP, which also gave rise to the biggest spectral change reflected in the highest value of the ratio between the two bands. A rise of the total

emission intensity was observed, in line with displacing one water molecule from coordination sphere.

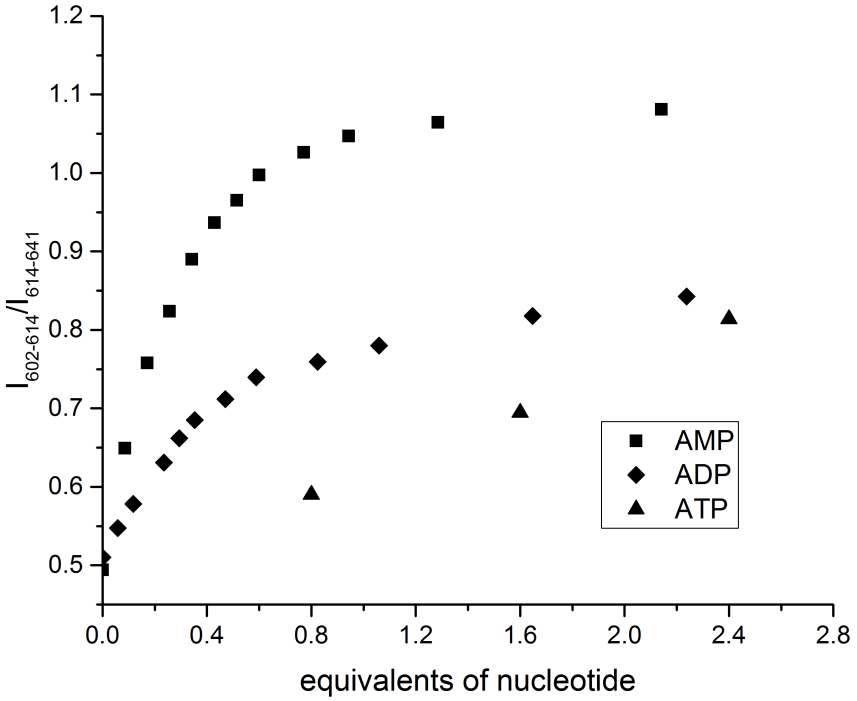


**Fig. IV.12** Binding curves for **[EuL$^7$]** upon addition of AMP, ADP and ATP (**[EuL$^7$]** 5 μM, 0.1 M HEPES, pH = 7.40, 298 K, $\lambda_{ex}$ = 335 nm). No satisfactory fitting to a 1:1 model was possible.

Addition of ADP led to smaller spectral changes, even though the binding affinity was nearly the same. The lifetime of an excited state experienced a two-fold rise – in accord with a reduced PET quenching of the chromophore by the tertiary amine . Similarly to AMP addition, the total emission intensity exhibited a 14-fold increase, reaching a plateau at ca. 1.0 equivalent of ADP added. In the case of the bulkiest nucleotide studied – ATP – a shallower binding curve was observed, approaching a plateau only after three equivalents of ATP was added, suggestive of a 1:1 binding mode. A similar rise in the lifetime and overall emission intensity was observed in this case as well, whilst the spectral change was close to that observed for ADP. In all three cases, the total emission intensity was enhanced after addition of $Zn^{2+}$, accompanied by minor changes of the spectral form. This rise of the emission intensity may be again attributed to a reduced PET quenching of the chromophore, consistent with the increase of the observed europium lifetime in each case.

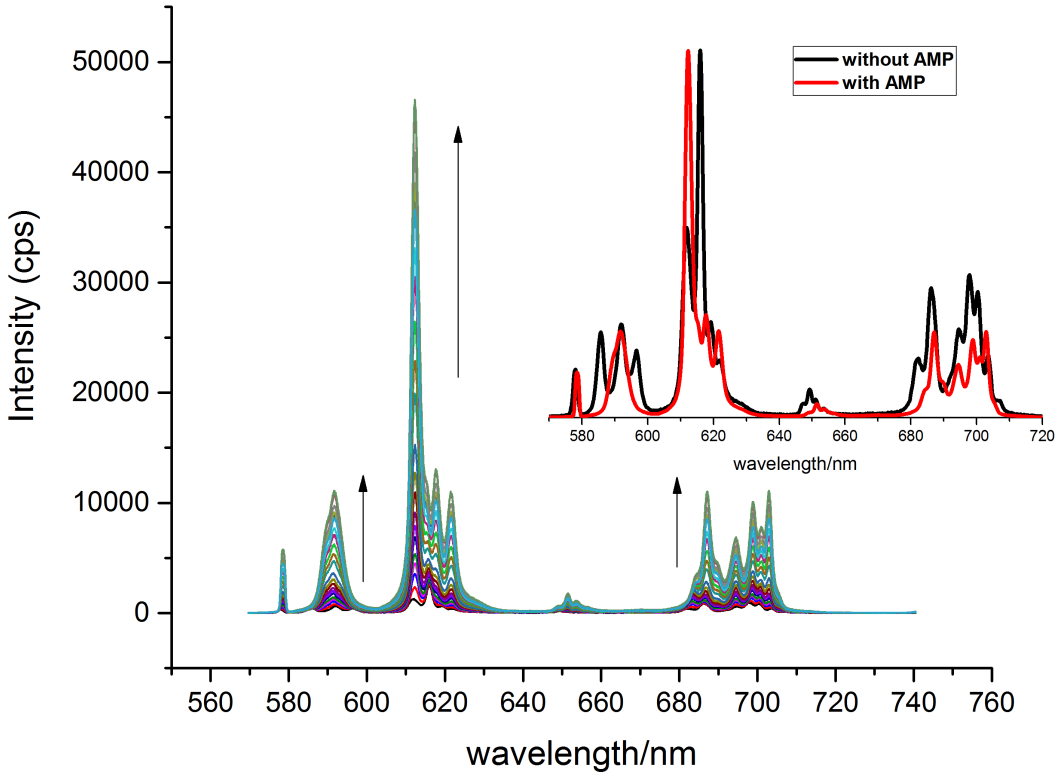


**Fig. IV.13** Spectral change of **[EuL$^7$]** upon addition of AMP (**[EuL$^7$]** 5 μM, 0.1 M HEPES, pH = 7.40, 298 K, $\lambda_{ex}$ = 335 nm).

Upon addition of nucleotides, all four primary transitions $^5D_0 \rightarrow {}^7F_j$ (j = 1-4) experienced considerable changes (Fig. IV.13). In the magnetic dipole allowed transition $^5D_0 \rightarrow {}^7F_1$ two Stark components replaced the three seen in the initial complexes, suggesting a change in the local ligand field. The ligand field splitting defined as the distance between the Stark splitting components also reduced in size in accord with a change in the coordination environment upon binding a phosphate group. Analysis of the number of Stark components for other transitions is more complicated and was not carried out.

The most striking change in spectral behaviour was revealed after recording CPL spectra for **[EuL$^7$]** with each of the nucleotides bound. Zinc ions were added in each case to increase the total emission intensity, and allowed faster acquisition of data with enhanced resolution, although the spectral signature were the same with and without added $Zn^{2+}$. The spectra of the complexes with AMP and ADP showed identical CPL spectra, whilst the CPL spectrum of the complex with ATP revealed an inversed helicity (Fig. IV.14). Moreover, the intensity of CPL signal decreased in the order AMP ($g_{em}$ = 0.070) >ATP ($g_{em}$ = 0.042) > ADP ($g_{em}$ = 0.032).

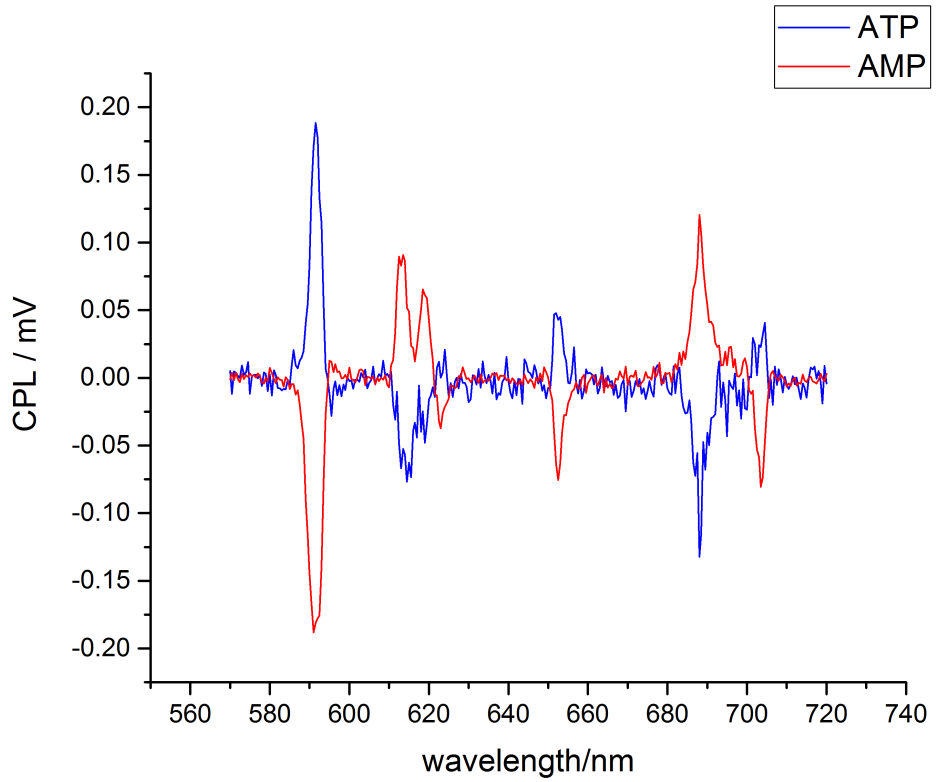


**Fig. IV.14** CPL spectra of **[EuL$^7$]** with added AMP and ATP (**[EuL$^7$]** 5 μM, 0.1 M HEPES, pH = 7.40, 298 K, $\lambda_{ex}$ = 335 nm).

The aforementioned photophysical data allow a binding mode of nucleotides to **[EuL$^7$]** to be hypothesised. As will be shown later, the presence of two picolyl moieties is essential for attaining high binding affinity. Therefore, the synchronous involvement of both pyridine rings in H-bonding with a nucleotide seems to be a reasonable assumption. The similarity of both the lifetime of the excited state and the emission spectral form in each case suggests that binding occurs via the terminal phosphonate group. The adenine residue is located further away from the metal on going from AMP to ADP, whilst different binding modes in the case of ADP and ATP probably account for the observed inverse order of $g_{em}$ values ($g_{em}$ (ADP) < $g_{em}$ (ATP)). However, in all the cases a 1:1 binding mode is expected (Fig. IV.15).

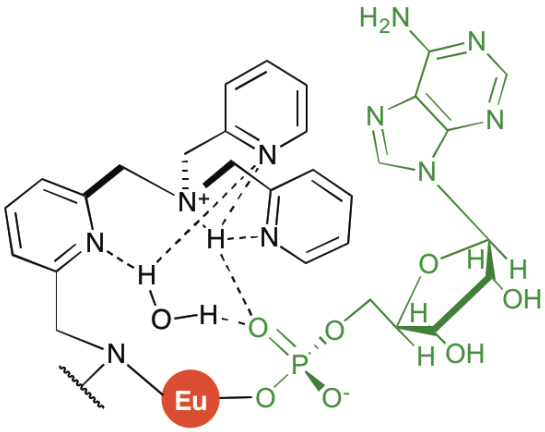


**Fig. IV.15** Proposed binding modes of AMP to **[EuL$^7$]**.

In both cases, it is highly likely that two picolyl moieties bind at least one water molecule through H-bonding, which in turn form H-bonds with a phosphonate oxygen of the nucleotide. A synergistic effect of multiple hydrogen bonds and direct binding to the metal centre leads to a very high affinity for the probe.

**Table IV.1** Lifetimes (in $H_2O$ and $D_2O$), q values and QY for **[EuL$^7$]**

| | **$\tau(H_2O)$, ms** | **$\tau(D_2O)$, ms** | **q** |
|---|---|---|---|
| **water** | 0.46 | 0.79 | 0.8 |
| **$Zn^{2+}$** | 0.45 | 1.28 | 1.4 |
| **$Zn^{2+}$+AMP** | 0.97 | 1.48 | 0 |
| **$Zn^{2+}$+ADP** | 0.99 | 1.45 | 0 |
| **$Zn^{2+}$+ATP** | 0.97 | 1.56 | 0 |

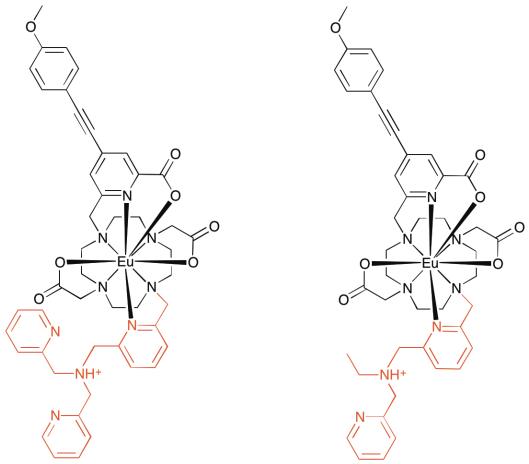


**Fig. IV.16** Molecular structures of **[EuL$^7$]** (*left*) and **[EuL$^8$]** (*right*). Nucleotide binding moieties are depicted in red.

The complex **[EuL$^8$]** has one of the picolyl arms replaced by an ethyl group (Fig. IV.16), compared to the parent complex **[EuL$^7$]**. This change resulted in a considerably lower affinity towards nucleotides (ca. 2-3 orders of magnitude lower), emphasizing the significance of both picolyl arms in phosphate binding (Fig. IV.17). Moreover, a two-fold shorter lifetime (0.2 ms vs 0.4 ms) was observed in the absence of nucleotide, suggesting the presence of a more efficient quenching pathway upon replacing one of picolyl arms with an ethyl group. It is possible that the lower steric demand imposed by an ethyl group allows more efficient O-H quenching through formation of a more well-defined second and outer hydration sphere.

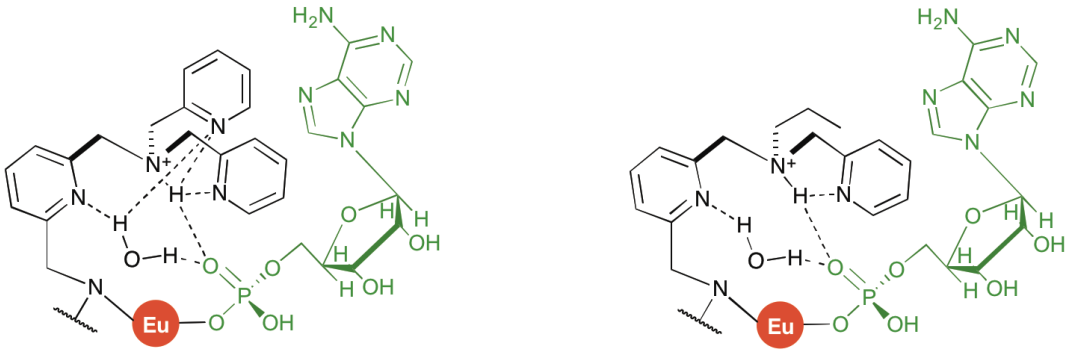

**Fig. IV.17** Comparison in proposed binding modes of AMP between **[EuL$^7$]** (*left*) and **[EuL$^8$]** (*right*).

At the same time, analysis of the emission spectra revealed spectral signatures in the presence and in the absence of AMP very close to those obtained for **[EuL$^7$]**, in line with the proposed similar binding mode for both complexes. Indeed, in the absence of the bound anion, a pyridine nitrogen is bound to $Eu^{3+}$, leading to a coordination number of [8+1]. Once the anion binds to europium, the triaza moiety dissociates and is replaced by phosphonate oxygen, retaining the coordination number [8+1]. Therefore, for both **[EuL$^7$]** and **[EuL$^8$]**, the spectral form should be unaffected by change of the substituents at the tertiary nitrogen atom.

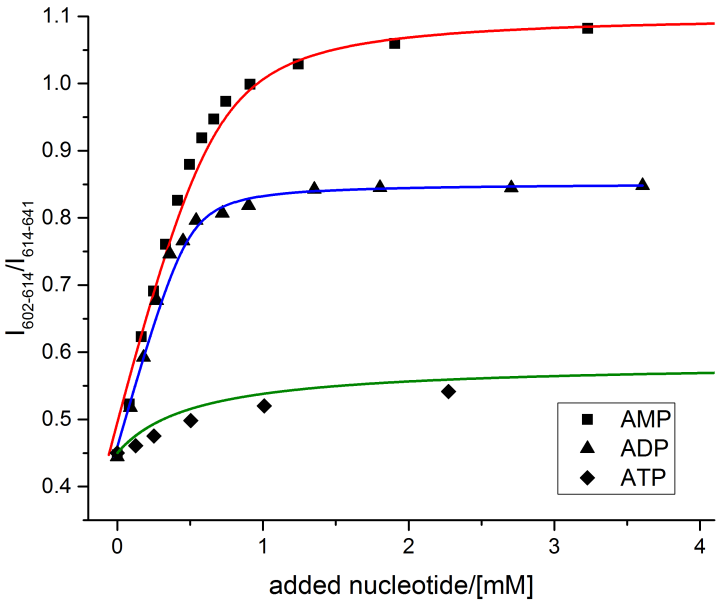


**Fig. IV.18** Binding curves for **[EuL$^8$]** upon addition of AMP, ADP and ATP (**[EuL$^8$]** 5 μM, 0.1 M HEPES, pH = 7.40, 298 K, $\lambda_{ex}$ = 335 nm). Binding constants obtained assuming 1:1 binding mechanism were as follows: log K = 4.1 for AMP, log K = 4.6 for ADP and log K = 3.3 for ATP.

However, a closer inspection of the emission spectra of **[EuL$^8$]** with different bound nucleotides revealed significant differences in their spectral form (Fig. IV.18-IV.19). If the situation upon addition of AMP was similar to that observed for **[EuL$^7$]** with all three nucleotides, addition of ADP and ATP caused smaller spectral changes. It might be possible that the bulkier nucleotides cannot cause sufficient conformational change to encourage dissociation of the $NCH_2Py$ moiety from $Eu^{3+}$, leaving it in between an initial unbound conformation and an idealised final conformation where the pyridine ring has dissociated. At the same time, binding affinities in each case were of similar magnitude. Unfortunately, no indications of binding stoichiometry can be inferred confidently from these binding curves due to their low affinities. However, analysis of the CPL spectra and the similarity of each molecular structure suggest a binding mode analogous to that observed for **[EuL$^7$]**, which bind each nucleotide in 1:1 stoichiometry.

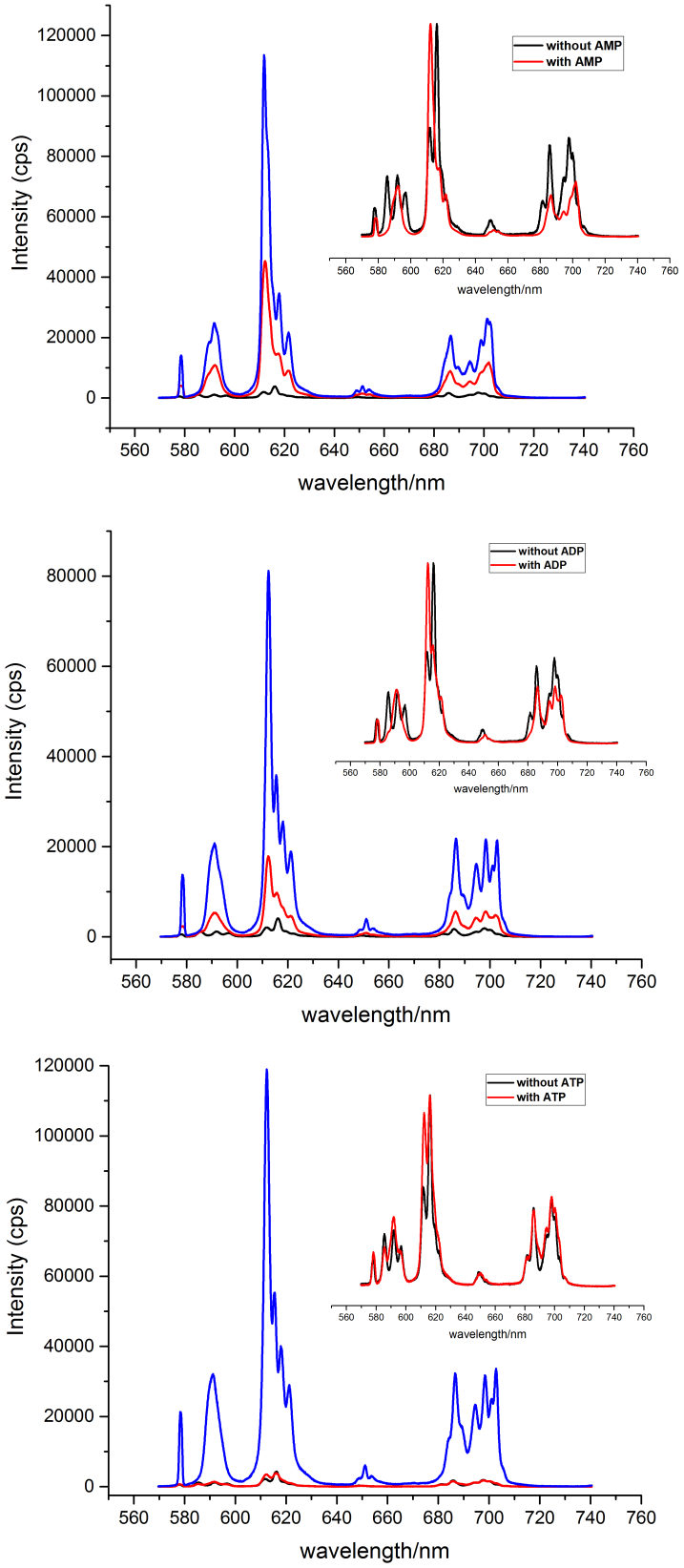


**Fig. IV.19** Emission spectra of **[EuL$^8$]** (black), upon addition of nucleotides (red) - AMP (*top*), ADP (*centre*) and ATP (*bottom*). $ZnCl_2$ was added after every experiment (blue) increasing the total emission intensity (**[EuL$^8$]** 5 μM, $\lambda_{ex}$ = 335 nm, 0.1 M HEPES, pH = 7.40, 298 K).

Despite changes in the emission spectra for three nucleotides once the binding curve reached a plateau, addition of $Zn^{2+}$ (ca. 60 μM) dramatically changed the spectrum of **[EuL$^8$]*ADP** and especially **[EuL$^8$]*ATP**, making their spectral signature very similar. Furthermore, the overall emission intensity in every case was also similar, indicating a close resemblance of their coordination polyhedra. A tentative binding motif following addition of $Zn^{2+}$ was proposed (Fig. IV.20), which involves binding of the $Zn^{2+}$ ion by two pyridine nitrogen atoms, a tertiary nitrogen and a hydroxyl ion. The latter was suggested to participate in H-bonding with phosphonate oxygen, providing a high affinity of the resulting aggregate.

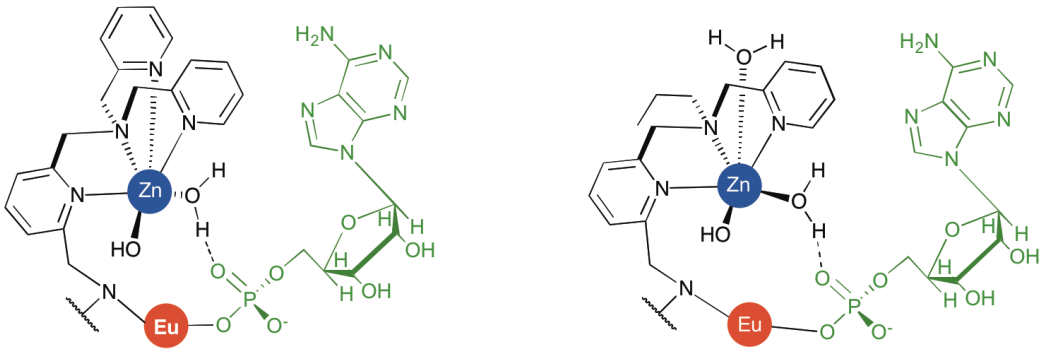


**Fig. IV.20** Schematic showing proposed binding for **[EuL$^7$]** and **[EuL$^8$]** with AMP following addition of $Zn^{2+}$.

To verify the proposed binding mode, zinc chloride was added to the complex first, forming **[EuL$^8$]*Zn** and then ADP or ATP was added. In both cases, similar binding constants were calculated (Fig. IV.21), which were two orders of magnitude higher than those estimated for binding ADP and ATP without pre-added zinc. The observed difference, which is consistent with the proposed binding model, corresponds to additional stabilization of a bound phosphonate group by a coordinated zinc ion. In each case, more than a two-fold rise of the $Eu^{3+}$ lifetime was observed, although a significant (three-fold) rise of the emission intensity was observed only upon addition of ADP, whilst adding ATP did not change the total emission intensity of the complex.

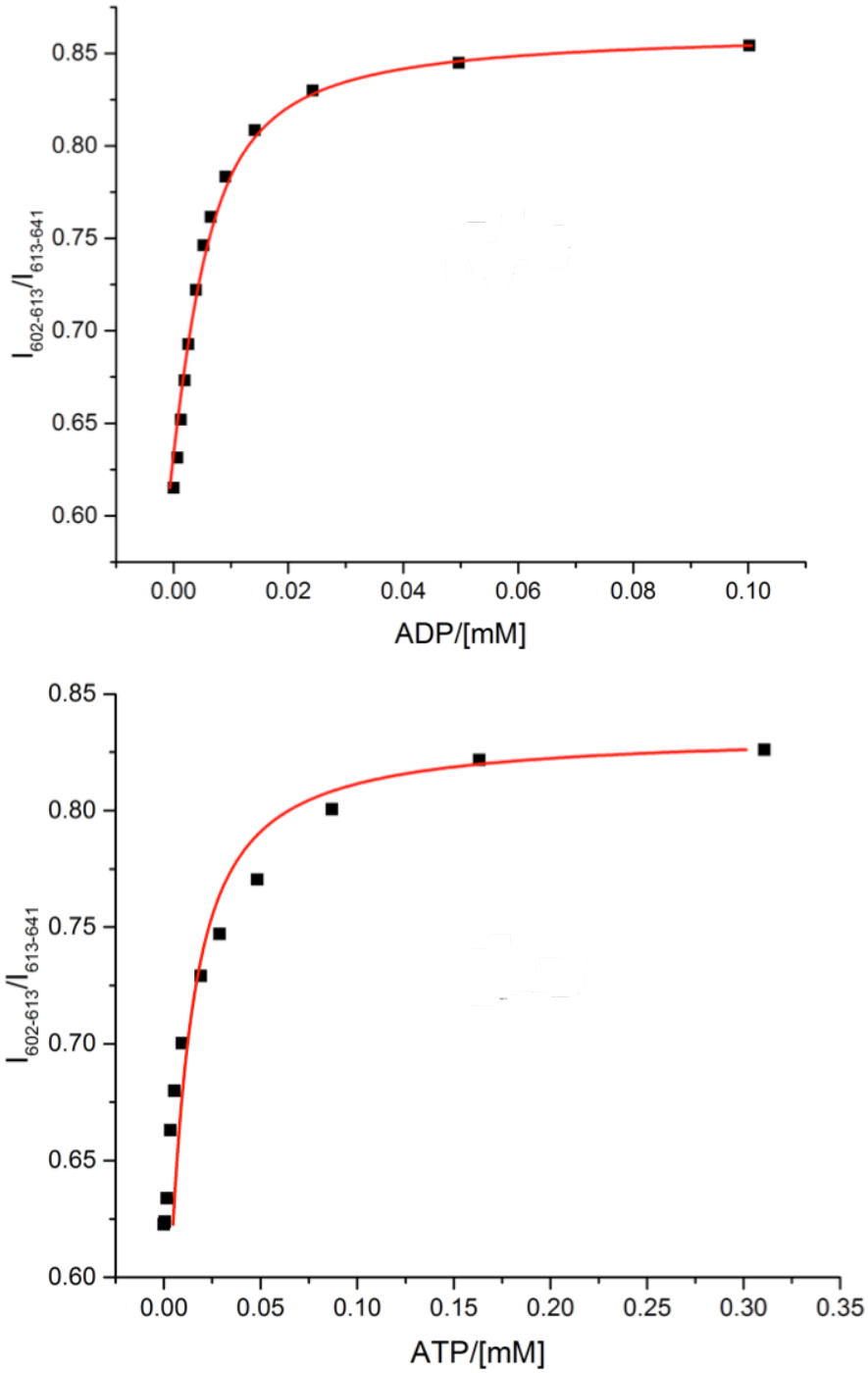


**Fig. IV.21** Binding curves for **[EuL$^8$]*Zn** upon addition of ADP (*top*, log K = 5.5(0.1)) and ATP (*bottom*, log K = 5.1(0.1)) (**[EuL$^8$]** 5 µM, 0.1 M HEPES, pH = 7.40, 298 K, $\lambda_{ex}$ = 335 nm).

However, detailed analysis of the three spectra revealed that the emission spectra for **[EuL$^8$]*ADP** and **[EuL$^8$]*ATP** were identical, whilst that of **[EuL$^8$]*AMP** was slightly different. As with **[EuL$^7$]**, the crystal field splitting parameter decreased upon binding the nucleotide with zinc, whilst the number of Stark splitting components also reduced. The latter observation again may indicate the higher point symmetry of $Eu^{3+}$ with bound nucleotides. In every case, the lifetime of the

europium excited state rose from 0.2 ms to 1.1 ms, in line with the removal of a PET quenching of the chromophore excited state.

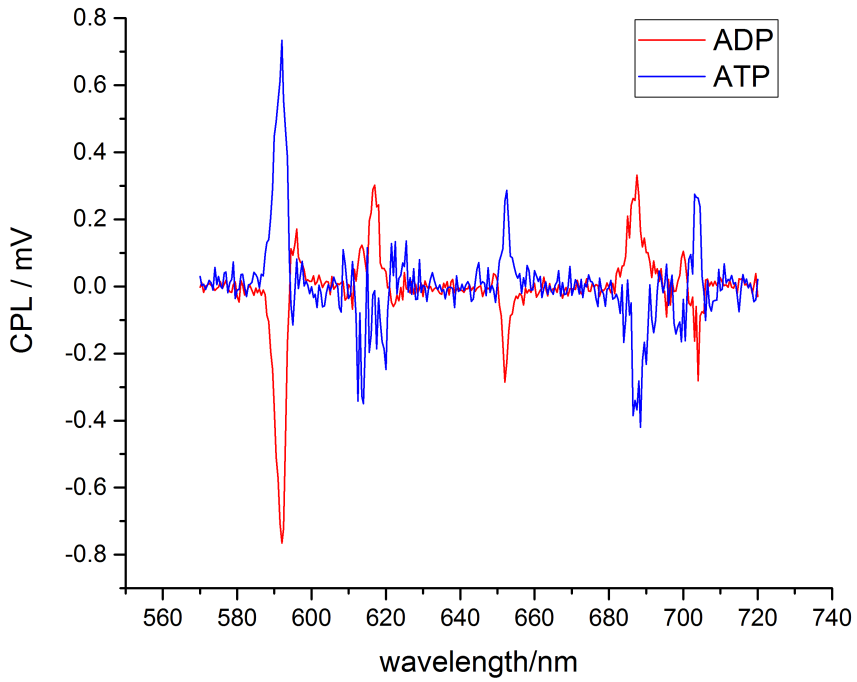


**Fig. IV.22** CPL spectra of **[EuL$^8$]** with added ADP and ATP (**[EuL$^8$]** 5 μM, $ZnCl_2$ 60 μM, 0.1 M HEPES, pH = 7.40, 298 K, $\lambda_{ex}$ = 335 nm).

Analysis of the CPL spectra of the three adducts revealed behaviour identical to **[EuL$^7$]**, with **[EuL$^8$]*AMP** and **[EuL$^8$]*ADP** having the same helicity, whilst the complex **[EuL$^8$]*ATP** exhibited the opposite chirality (Fig. IV.22). The intensity of the CPL signal was similar for AMP and ATP ($g_{em}$ = 0.012) and three times higher for ADP ($g_{em}$ = 0.038), suggesting a slightly different binding mode for ADP.

**Table 2** Lifetimes (in $H_2O$ and $D_2O$), q values and QY for **[EuL$^8$]**

| | **τ($H_2O$), ms** | **τ($D_2O$), ms** | **q** |
|---|---|---|---|
| **water** | 0.22 | 0.29 | 1.0 |
| **$Zn^{2+}$** | 0.47 | 1.30 | 1.3 |
| **$Zn^{2+}$+AMP** | 1.09 | 1.47 | 0 |
| **$Zn^{2+}$+ADP** | 1.09 | 1.51 | 0 |
| **$Zn^{2+}$+ATP** | 1.10 | 1.49 | 0 |

Since the complex **[EuL$^8$]*$Zn^{2+}$** showed higher binding affinity towards ADP over ATP, its potential for monitoring the ADP/ATP ratio was assessed by recording CPL spectra at different stoichiometries (Fig. IV.23). Samples with ADP/ATP ratios

ranging from 4:1 to 1:2 were prepared, their CPL spectra analysed and the observed $g_{em}$ value ($\lambda$ = 592 nm) were plotted as a function of the concentration of added ATP. The observed quasi-linear curve showed a gradual decay from $g_{em}$ = 0.36 for pure ADP to $g_{em}$ = 0.05 for two equivalents of ATP added. Even though a significant change of the dissymmetry factor was observed, the total emission intensity decreased upon increasing the total nucleotide concentration. In a separate experiment, the total concentration of nucleotides was kept constant and similar values for $g_{em}$ as a function of ADP/ATP ratio were observed. Apparently, the observed quenching of the complex at elevated concentration of nucleotides is explained by a $\pi$-$\pi$ interaction between the chromophore and the nitrogenous base of the nucleotide. This problem can be potentially overcome by using a less electron-rich chromophore, for example one with a biaryl chromophore, as reported in the previous chapter.

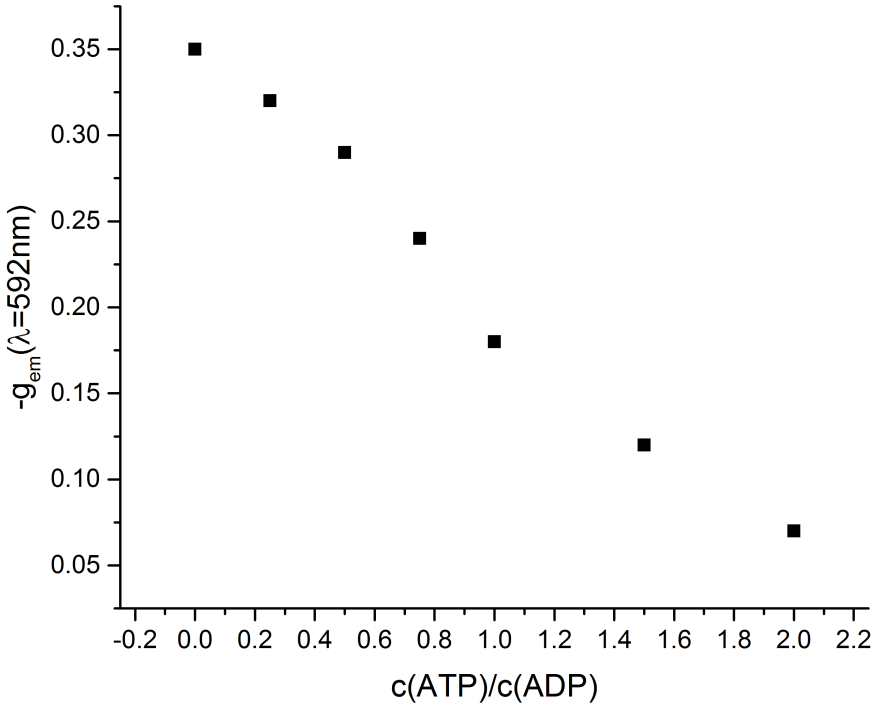


**Fig. IV.23** Variation of -$g_{em}$ ($\lambda$ = 592 nm) as a function the ADP/ATP ratio for **[EuL$^8$]** (**[EuL$^8$]** 10 μM, $ZnCl_2$ 100 μM, 0.1 M HEPES, pH = 7.40, 298 K, $\lambda_{ex}$ = 335 nm).

To complete the structural variation of this series of complexes, the complex **[EuL$^9$]** bearing a diethylamine substituent (Fig. IV.24) was synthesised and its binding properties were analysed. A very weak binding affinity was observed for each nucleotide, accompanied by only minor changes in their $Eu^{3+}$ emission spectra. Subsequent addition of $ZnCl_2$ changed neither the spectral fingerprint, nor the total

emission intensity. Due to a relatively weak emission intensity signal, no CPL signal could be recorded over a 2 h acquisition timescale, whilst low binding affinities limited quantitative studies. Indeed, the maximum water solubility of these nucleotides is ca. 50 mg/mL, and was not sufficient to reach saturation. Nonetheless, similarly to previously discussed complexes a very similar emission fingerprint was observed for the initial complex with no added nucleotide, whilst a similar increase of the relative intensity of the first Stark component in the $^5D_0 \rightarrow {}^7F_2$ transition was observed.

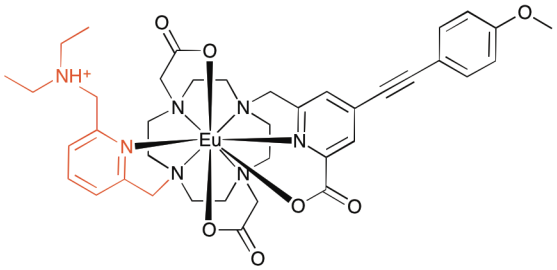


**Fig. IV.24** Molecular structure of **[EuL$^9$]**. Putative anion-binding moieties are depicted in red.

These findings support the assumption of the cooperative involvement of both picolyl arms in binding the nucleotide through a H-bonded array. Removal of both pyridine groups decreased the binding affinity to values expected for a neutral 8-coordinate lanthanide complex. On the other hand, the protonated tertiary amine on its own does not seem to be sufficient to stabilise bound nucleotides via H-bonding, as shown in the behaviour of **[EuL$^9$]**. Generally speaking, it is not necessary for a bound atom to dissociate in order to produce a significant change of the emission spectrum. It is also possible to modulate the spectral form by varying the electron density and/or polarisability of donor atoms. With this in mind, the complex **[EuL$^{10}$]** was designed and synthesised, featuring a 1,2,3-triazole moiety with an attached dipicolylamine arm in the 4-position. The same arm has already been used by Liu in **TPETH-2Zn** to detect zinc ions *in cellulo*, with a putative coordination motif involving binding to two pyridine nitrogen atoms, the tertiary nitrogen and the 3-nitrogen atom of triazole moiety (Fig. IV.25)[13]. Therefore, it was assumed that a triazole moiety could bind to $Eu^{3+}$ through its 1-nitrogen, whilst the 3-nitrogen atom can participate in hydrogen bonding along with the dipicolylamino group. Binding to the 3-nitrogen should change the electronic distribution within the heterocyclic ring and henceforth alter the emission spectrum of the complex.

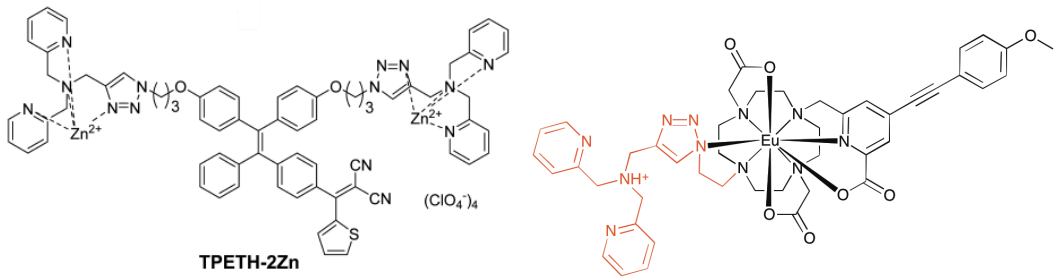


**Fig. IV.25** Molecular structure of **TPETH-2Zn** (*left*) and **[EuL$^{10}$]** (*right*). Putative anion-binding moieties are depicted in red.[13]

The complex **[EuL$^{10}$]** was synthesised in accordance with a multi-step procedure (Scheme IV.2). First, commercially available 2-azidoethanol was converted to its mesylate and was reacted with the DO2A *bis t*-butyl ester. The resulting mixture consisted of the desired tri- and a tetra-substituted product. The crude mixture was reacted with *N*,*N*-*bis*(pyridin-2-ylmethyl)prop-2-yn-1-amine, which was synthesised in accordance with a literature procedure[14]. The resulting crude mixture was purified using RP-HPLC, yielding a mixture of two products – the desired tri-substituted moiety and a tetra-substituted by-product with two triazole arms.

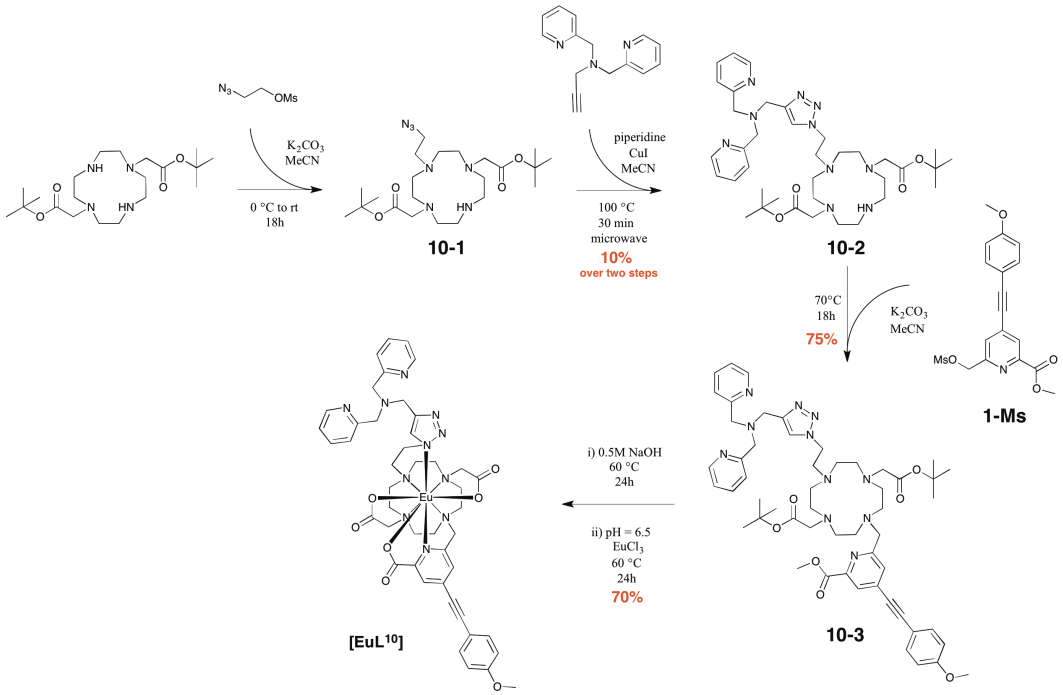


**Scheme IV.2** Synthetic pathway for complexes **[EuL$^{10}$]**.

The desired product **10-1** were separated on an alumina column and a freshly prepared sample of the chromophore mesylate **1-Ms** was added to give a tetra-substituted ligand, which was purified using RP-HPLC. The resulting ligand was

hydrolysed in 0.5M NaOH, neutralised and purified using RP-HPLC with ammonium bicarbonate buffer. The buffer was removed by freeze-drying. The resulting colourless hydrolysed ligand was complexed with $EuCl_3$ and precipitated as an off-white solid upon storing in a fridge at 4°C overnight.

Anion-binding studies with **[EuL$^{10}$]** and selected nucleotides were carried out, and spectral changes were monitored (Fig. IV.26). Although a similar binding affinity to that observed for **[EuL$^{7}$]** was expected, a much lower binding constant was observed in each case (all K are of the order $10^2$ vs. $10^{6\text{-}7}$ for **[EuL$^{7}$]** and $10^4$ for **[EuL$^{8}$]**). Different spectral changes were observed upon binding different nucleotides. Again, the biggest change was observed upon binding of AMP, followed by ADP and ATP. The binding constants were calculated for each nucleotide by fitting the variation in relative emission intensities, using non-linear iterative least squares analysis.

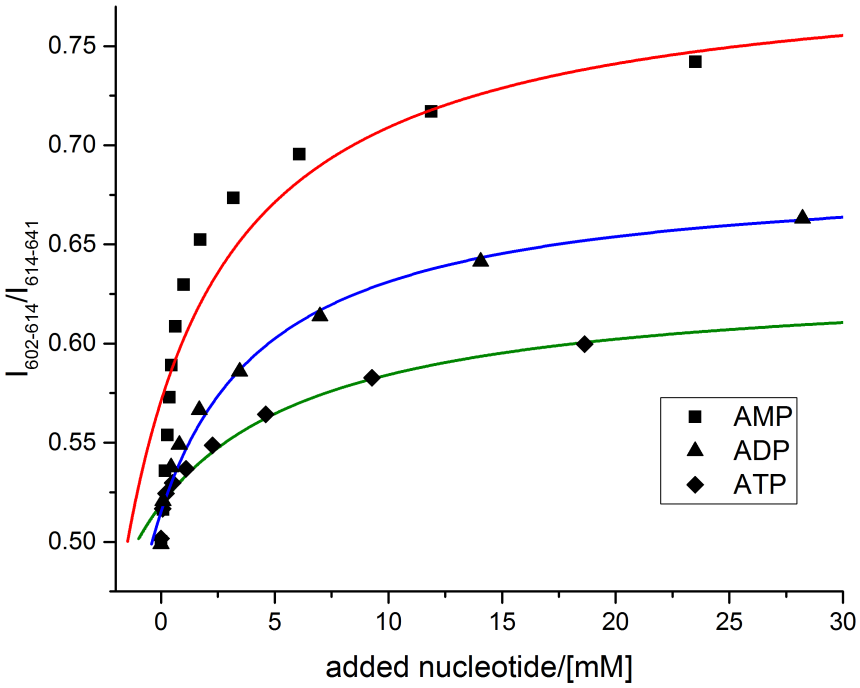


**Fig. IV.26** Binding curves for **[EuL$^{10}$]** upon addition of AMP, ADP and ATP (**[EuL$^{10}$]** 8 μM, 0.1M HEPES, 0.1 M HEPES, pH = 7.40, 298 K, $\lambda_{ex}$ = 335 nm). log K = 2.2 for AMP, log K = 2.3 for ADP and log K = 2.1 for ATP.

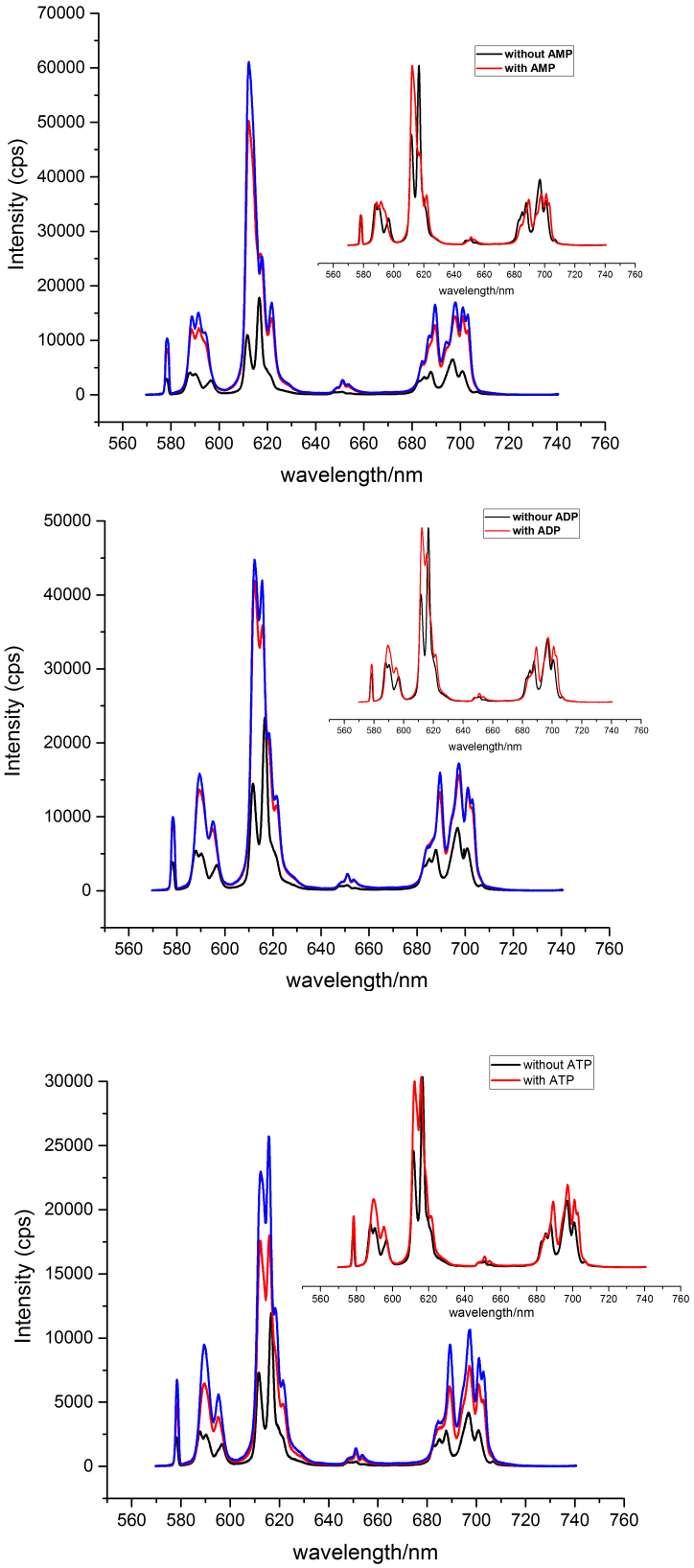


**Fig. IV.27** Emission spectra of **[EuL$^{10}$]** (black) and following addition of nucleotides (red) - AMP (*top left*), ADP (*top right*) and ATP (*bottom*). $ZnCl_2$ was added after every experiment (blue) and slightly increased the total emission intensity (**[EuL$^{10}$]** 8 μM, 0.1 M HEPES, $\lambda_{ex}$ = 335 nm, pH = 7.40, 298 K).

In each case, a rise of the total emission intensity was observed – highest with AMP and lowest with ATP (Fig. IV.27). Addition of $ZnCl_2$ (up to a 10-fold excess) only slightly increased the emission intensity, without changing the form of the spectral signature. Addition of extra zinc (II) ions led to a gradual decrease of the emission intensity, probably due to competitive binding to the nucleotide. In every case, the emission lifetime increased up to a limit of 1.0-1.1 ms, consistent with replacing a coordinated water molecule and partially eliminating PET quenching.

**Table 3** Lifetimes (in $H_2O$ and $D_2O$), q values and QY for **[EuL$^{10}$]**

| | **$\tau(H_2O)$, ms** | **$\tau(D_2O)$, ms** | **q** |
|---|---|---|---|
| **water** | 0.51 | 1.12 | 0.97 |
| **AMP** | 0.86 | 1.54 | 0.3 |
| **ADP** | 0.94 | 1.48 | 0.2 |
| **ATP** | 0.80 | 1.44 | 0.4 |

Regarding the changes in the coordination environment, no significant change in the number of Stark splitting components was observed, in line with the assumption that the 1,2,3-triazole moiety is bound to $Eu^{3+}$ with and without added nucleotide. An observed variation of the ligand field splitting can be explained by elongation of $Eu^{3+}$-X (X = O, N) bonds upon increasing coordination number, e.g. when a nucleotide phosphate moiety binds to europium. The fact that addition of $Zn^{2+}$ ions did not change the emission pattern, in contrast with previously discussed complexes, suggests the inaccessibility of the bound nucleotide towards $Zn^{2+}$ binding (Fig. IV.28). On the other hand it could be a result of a more rigid structure, which cannot be easily perturbed by addition of Lewis acids.

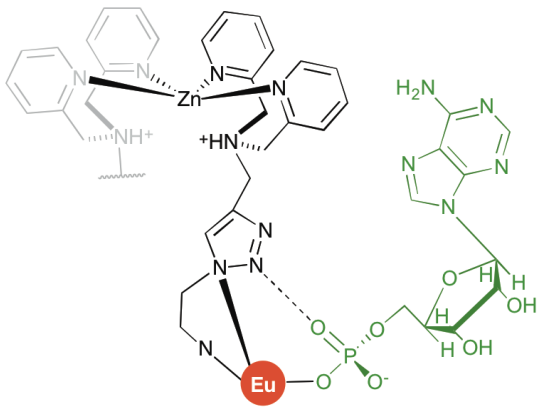


**Fig. IV.28** Schematic showing proposed binding **[EuL$^{10}$]** with AMP following addition of $Zn^{2+}$.

In every case a strong CPL signal was recorded, with the same spectral signature for each nucleotide (Fig. IV.29). In contrast to the behaviour of complexes **[EuL$^{7}$]** and **[EuL$^{8}$]**, the same sign of $g_{em}$ was found indicating the same helicity for AMP, ADP and ATP. The asymmetry ratio rose in the order AMP ($g_{em}$ (591 nm) = 0.24) < ADP ($g_{em}$ (591 nm) = 0.29) < ATP ($g_{em}$ (591 nm) = 0.50). This finding is consistent with an increasing distance between $Eu^{3+}$ and the nearest stereogenic centre of the nucleotide from ATP to AMP. This conclusion is counterintuitive, as a reducing length of a phosphate chain should bring them closer together and give rise to higher $g_{em}$ values. The only plausible explanation for this phenomenon is that a different binding mode exists for ATP, compared to AMP and ADP, that allows the chiral sugar moiety to approach the europium ion more closely, and hence give rise to a higher $g_{em}$ value.

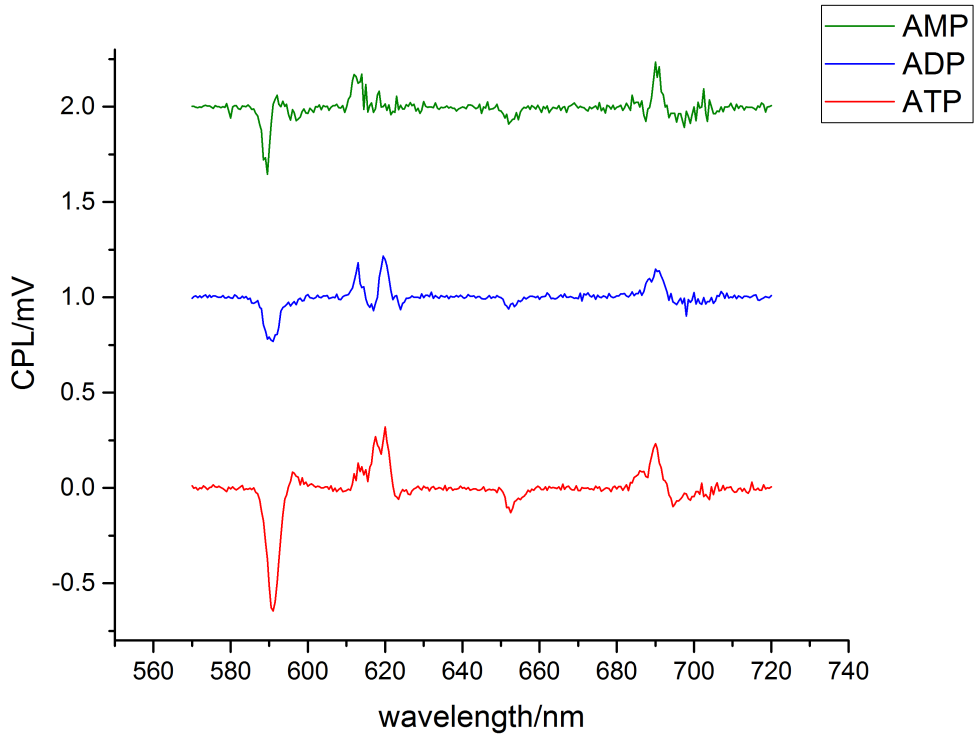


**Fig. IV.29** CPL spectra of **[EuL$^{10}$]** with added AMP, ADP and ATP (**[EuL$^{10}$]** 8 μM, $ZnCl_2$ 60 μM, 0.1 M HEPES, pH = 7.40, 298 K, $\lambda_{ex}$ = 335 nm).

To evaluate the impact of complex charge on anion binding and $Zn^{2+}$ behaviour, a positively charged complex **[EuL$^{11}$]$^{+}$** (Fig. IV.30) was synthesised according to a procedure employed for the synthesis of **[EuL$^{7\text{-}9}$]**, the only difference being that a chromophore without a carboxylate group was used.

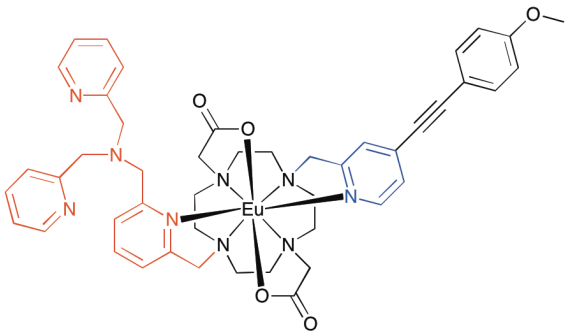


**Fig. IV.30** Molecular structure of **[EuL$^{11}$]**$^{+}$. Putative anion-binding moieties are depicted in red and monodentate pyridine ring is depicted in blue.

The resulting complex was expected to have a coordination number of 8 and an overall positive charge (doubly positive charge if protonation of a tertiary amine of a sensing moiety is also considered). However, isolation of the complex proved difficult, as all attempts to raise the pH of the solution above 8.0 resulted in irreversible chemical transformation of the complex, causing a significantly decreased emission intensity. Competitive and apparently irreversible bicarbonate binding was suggested to be responsible for this change, although displacing of the bicarbonate by bubbling argon through the solution did not restore the initial emission spectrum. Therefore, it was not possible to remove any excess free $Eu^{3+}$ and the complex was used without any further purification.

A very high affinity towards phosphate and glyphosate was observed, which was accompanied by changes in the relative emission intensity and lifetime. However, due to problems with handling and storage, no more detailed analyses of **[EuL$^{11}$]**$^{+}$ were carried out.

## IV.4 Binding of $Zn^{2+}$ ions to [EuL$^{7-8}$]

Zinc is the second most abundant transition metal in our bodies after iron, participating in multiple biological processes, including gene expression, stabilisation of DNA, signaling between cells, and wound healing. The zinc-deficiency in childhood and adolescence due to low dietary zinc intake often leads to severe pathologies, such as anaemia, hypogonadism and dwarfism[15]. Even though significant progress has been made in unraveling the biological role of zinc in living cells, the monitoring of its concentration and flux might help to address the remaining questions. Despite a relatively high concentration of zinc in human cells

(0.2-0.3 mM), the concentration of 'free' zinc, which is not bound to a protein and available for binding with a molecular probe, is usually several orders of magnitude lower.

However, there are a few exceptional cases, when the concentration of 'free' (labile) $Zn^{2+}$ is unusually high, as for example in prostatic fluid. The reason for such a high concentration of $Zn^{2+}$ ions in prostatic fluid (ca. 3 mM in healthy individuals[16]) is still debatable, but is connected to the secretory function of the prostate gland[17]. It was established that prostate malignancies are usually accompanied by low concentrations of both $Zn^{2+}$ and citrate anions in secreted prostate fluid and can be potentially used to detect early stages of prostate cancer. One of the possible ways to analyse prostatic fluid samples is to use fluorescent probes, which can produce a change in the emission signal as a function of zinc concentration. However, the primary requirement for these probes is their insensitivity towards citrate anions, whose concentration also usually changes in the presence of cancerous cells.

A series of lanthanide complexes was developed for the selective binding of citrate ions[18], which was deemed a simpler strategy to monitor the presence of malignancies in prostate fluid, as the emission signal from lanthanide complexes is usually unaffected by the concentration of $Zn^{2+}$, unless special zinc-binding groups are introduced. By varying the charge of a series of complexes with 12-$N_4$ based heptadentate ligands along with the steric demand associated with the nature of the ring substituents, selectivity and binding affinity towards citrate was modulated. Upon addition of citrate the relative intensities of $Eu^{3+}$ emission bands changed and this change was followed as a function of citrate concentration. The best results were obtained for a singly charged complex with two amide arms and an azaxanthone ligand. The accuracy of the probe was verified by comparing readings obtained with this probe and by independent ELISA assay measurements (Fig. IV.31).

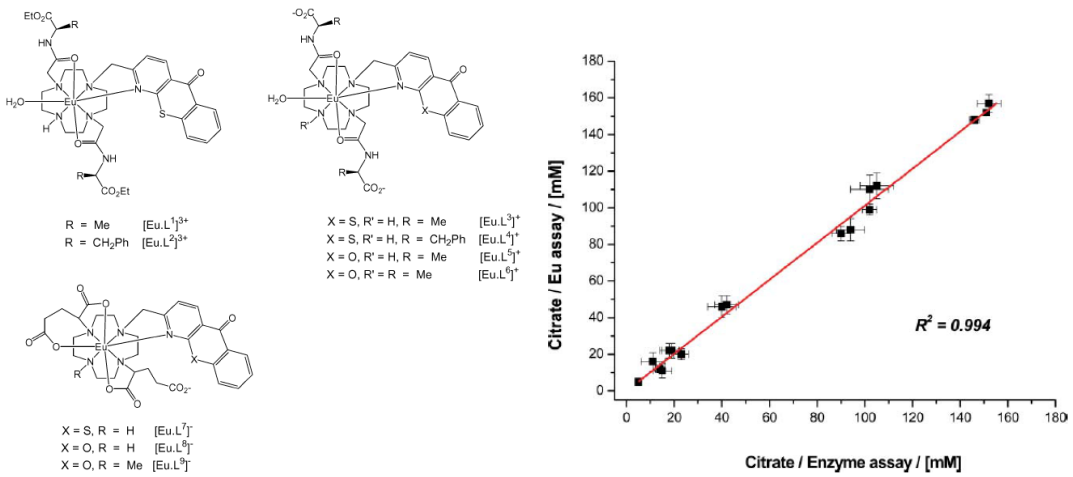


**Fig. IV.31** Molecular structures of complexes studied as citrate-binding probes and comparison between concentration determination by using probe **[Eu.L$^3$]**$^+$.[18]

Although the proposed citrate probe showed encouraging results for determination of citrate levels in real prostate fluid samples, the need to improve the magnitude of the spectral change, as well as to induce a significant change of the lifetime of the $Eu^{3+}$ excited state upon binding the analyte, stimulated a search for alternatives. The complexes **[EuL$^{7-8}$]** were thus assessed as potential probes, as they can detect zinc by modulating a significant change of the emission spectrum (Fig. IV.32) and show a two-fold increase of the lifetime upon binding $Zn^{2+}$ in the case of **[EuL$^8$]**.

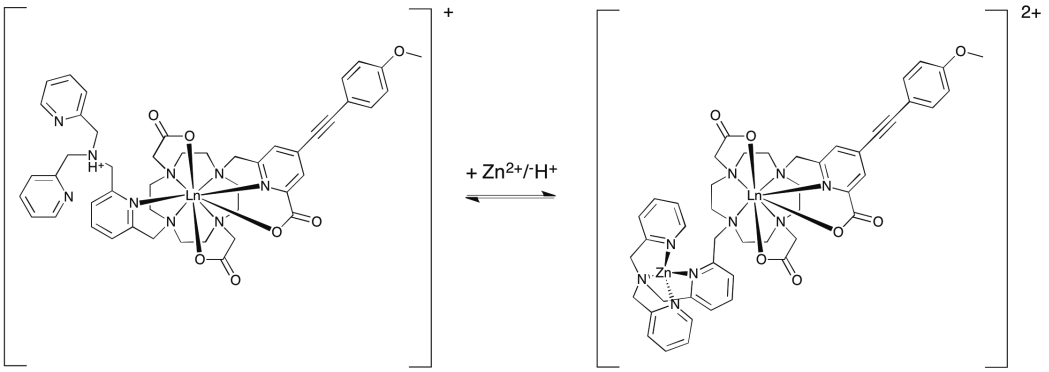


**Fig. IV.32** Assumed binding mode of $Zn^{2+}$ to **[EuL$^7$]**.

The analysis of the binding curve of **[EuL$^7$]** with added $Zn^{2+}$ revealed 1:2 binding stoichiometry (Fig. IV.33-IV.34), suggesting that $Zn^{2+}$ bridges two europium complexes with 6 nitrogen atoms of the pyridine moieties comprising an octahedral coordination environment. A very high binding affinity to $Zn^{2+}$ ions was observed (log K = 7.5) accompanied by no change in the $Eu^{3+}$ emission lifetime ($\tau$ = 0.46 ms). However, this value should be treated with extra caution, as it was calculated

assuming 1:1 binding model, and therefore can be considered only as an approximation.

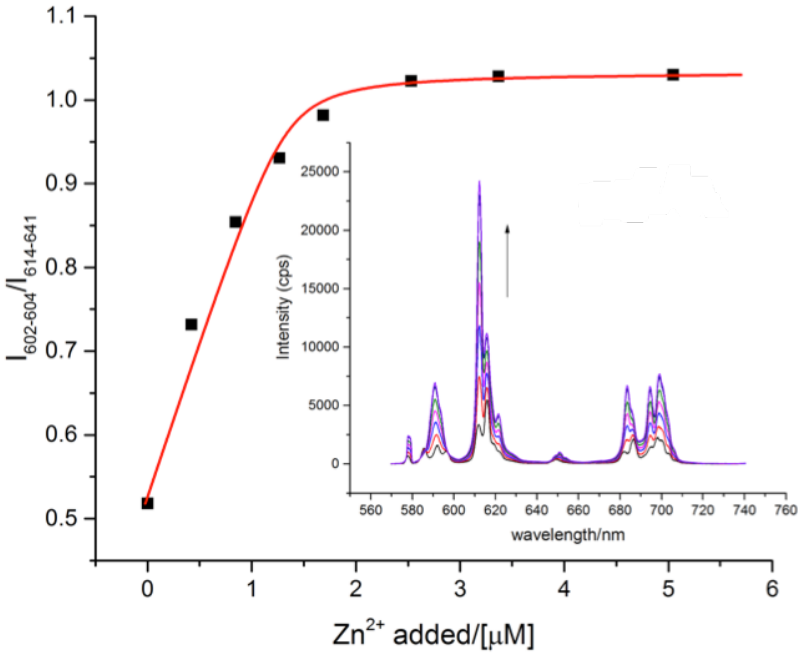


**Fig. IV.33** Change of the emission spectrum upon binding $Zn^{2+}$ to **[EuL$^7$]** (**[EuL$^7$]** 5 μM, 0.1 M HEPES, pH = 7.40, 298 K, $\lambda_{ex}$ = 335 nm). The binding affinity (log K = 7.5) was fitted in 1:1 binding model.

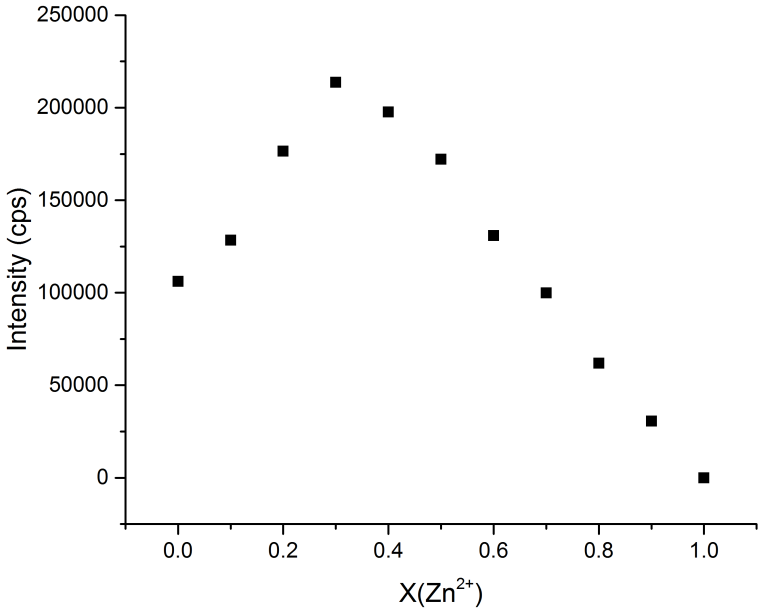


**Fig. IV.34** Job plot for **[EuL$^7$]** following the addition of $Zn^{2+}$ (**[EuL$^7$]** 5 μM, 0.1 M HEPES, pH = 7.40, 298 K, $\lambda_{ex}$ = 335 nm).

A similar binding stoichiometry and affinity were observed for $Ni^{2+}$, whilst no binding curve could be obtained for $Cu^{2+}$ due to severe PET quenching of the

europium emission. Addition of a large excess of alkali-earth metals, such as $Ca^{2+}$ and $Mg^{2+}$ and transition metals, such as $Cr^{3+}$ and $Mn^{2+}$ only slightly changed the total emission intensity, and did not affect the spectral signature.

Complex **[EuL$^8$]** showed a similar form of binding curve, but it was not possible to assess the binding stoichiometry using a Job plot due to an insufficiently high binding affinity. The total emission intensity underwent a significant 10-fold rise, along with a change of the spectral pattern, whilst the lifetime of the excited state doubled upon addition of $Zn^{2+}$ from 0.22 ms to 0.46 ms (Fig. IV.35-IV.36).

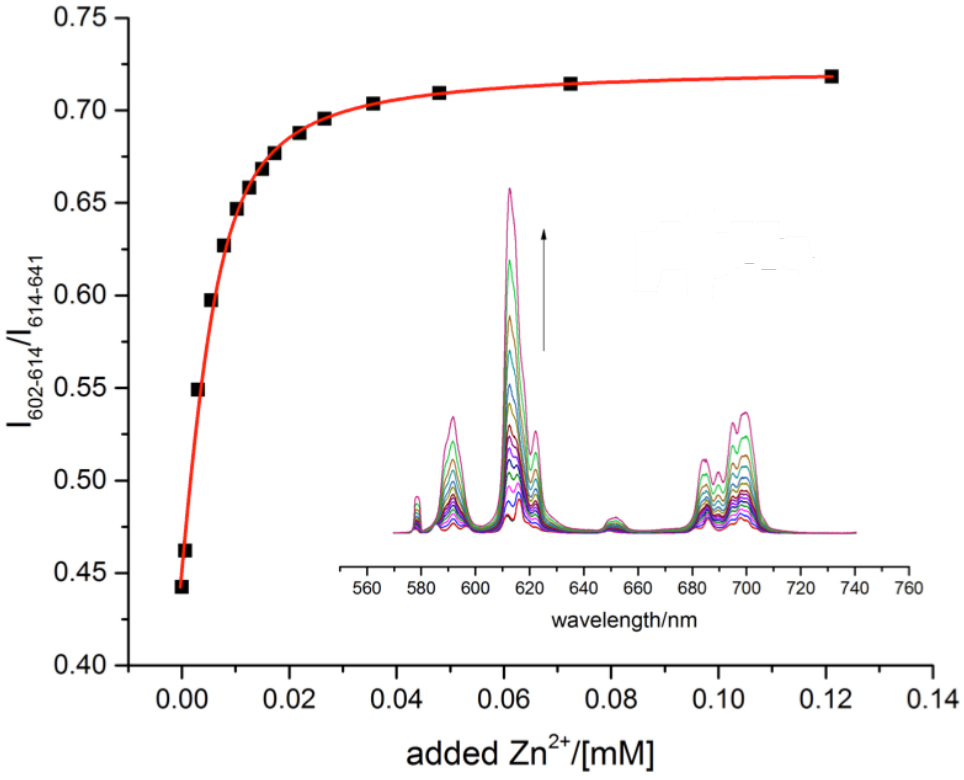


**Fig. IV.35** Change of the emission spectrum upon binding $Zn^{2+}$ to **[EuL$^8$]** (**[EuL$^8$]** 8 μM, 0.1 M HEPES, pH = 7.40, 298 K, $\lambda_{ex}$ = 335 nm). The binding affinity (log K = 5.6) was fitted in 1:1 binding model.

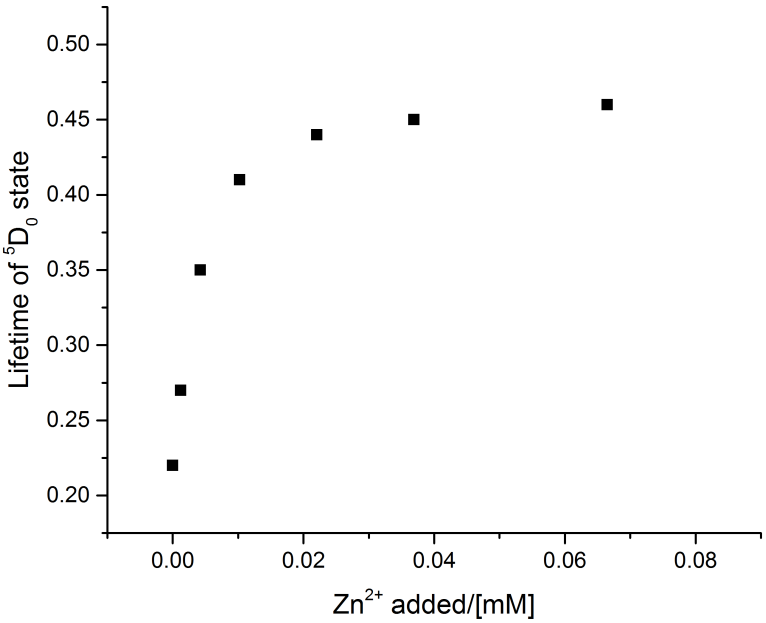


**Fig. IV.36** Change of the lifetime of an excited state $^5D_0$ upon binding $Zn^{2+}$ to **[EuL$^8$]** (**[EuL$^8$]** 5 μM, 0.1 M HEPES, pH = 7.40, 298 K, $\lambda_{ex}$ = 335 nm, $\lambda_{em}$ = 613 nm).

The analysis of binding stoichiometries of **[EuL$^7$]** and lower affinity of **[EuL$^8$]** allowed the proposed structures (Fig. IV.37) to be promulgated.

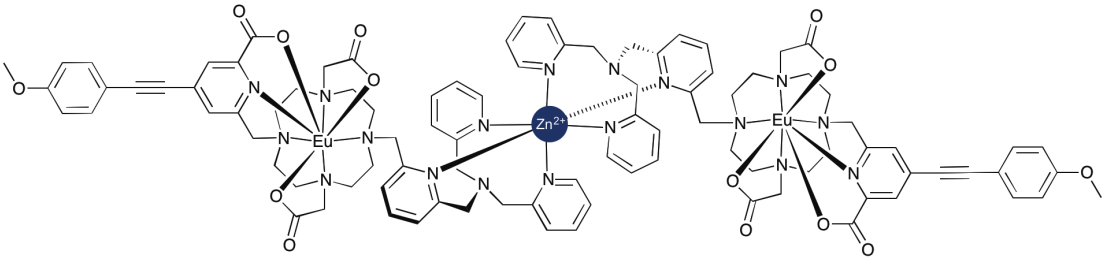


**Fig. IV.37** Putative binding motifs of $Zn^{2+}$ for **[EuL$^7$]**, showing 2:1 complexation mode.

In the case of **[EuL$^7$]**, the most likely binding mode involves six pyridine nitrogens, defining an octahedron. The two tertiary nitrogen centres are further away from the coordinated $Zn^{2+}$ and do not participate in binding. A similar binding motif with a zinc atom coordinated by two dipicolylamine moieties has been reported previously with a $Zn^{2+}$ complex bearing a btpa ligand (Fig. IV.38)[19]. However, in that structure the high steric demand encouraged the two tertiary nitrogen atoms to bind to the zinc atom, leaving two picolyl arms unbound. In contrast with **[EuL$^7$]**, a tetrahedral configuration is proposed involving two picolyl nitrogens, a tertiary amine nitrogen atom and a bound water molecule is suggested for **[EuL$^8$]** (Fig. IV.39), in line with 1:1 binding stoichiometry evidenced from the obtained Job plot (see Appendix).

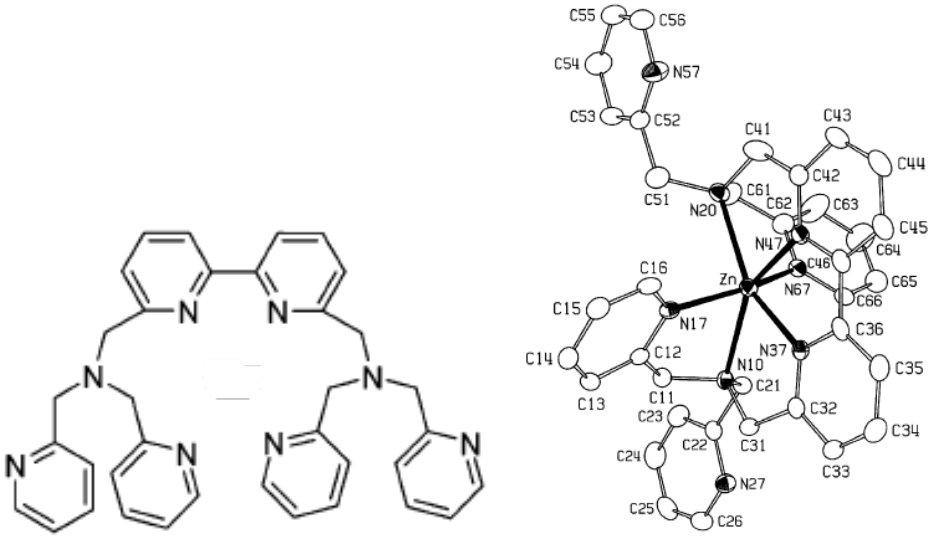


**Fig. IV.38** Molecular structure of btpa ligand and the structure of its complex with $Zn^{2+}$.[19]

Another potential tetrahedral binding mode can be considered involving two picolyl nitrogen atoms and two water molecules without direct participation of the tertiary amine nitrogen.

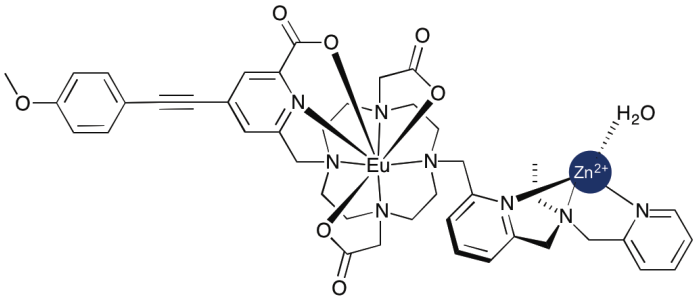


**Fig. IV.39** Putative binding motifs of $Zn^{2+}$ for **[EuL$^8$]**, showing 1:1 complexation mode.

In order to establish the potential use of these probes in sensing zinc (II) ions in prostatic fluid, a titration of **[EuL$^8$]** vs. added $Zn^{2+}$ was performed, in the presence of 40 mM citrate at pH=7.40. A much shallower binding curve was observed in this case (Fig. IV.40), and the spectral signature was unaffected by the presence of the citrate. This behaviour indicates that citrate ions compete with **[EuL$^8$]** for binding zinc ions to same extent. It has been shown that citrate form stable complexes (primarily $[Zn(cit)]^-$ with with log $\beta$ = 5.02 (3))[20] with first row transition metals, including zinc, over a the wide range of pH values. As both the concentration of $Zn^{2+}$

and citrate anions is lowered in patients with prostate cancer, this can interfere with interpretation of the data obtained.

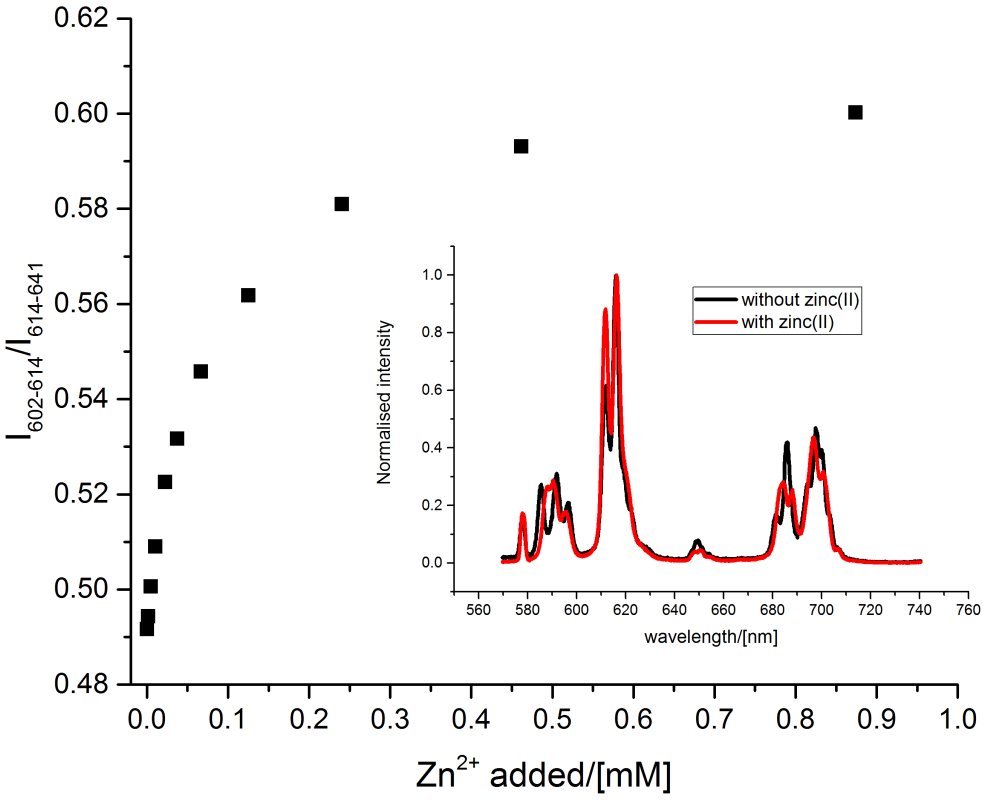


**Fig. IV.40** Change of the emission spectrum of **[EuL$^{8}$]** upon binding $Zn^{2+}$ in the presence of trisodium citrate (**[EuL$^{8}$]** 8 μM, citrate 40 mM, 0.1 M HEPES, pH = 7.40, 298 K, $\lambda_{ex}$ = 335 nm).

## IV.5 Conclusions and future work

The selective binding of target anions by lanthanide complexes is governed by the combined effects of steric complementarity, overall charge and the presence of certain functional groups that participate in electrostatic or H-bond interactions. In the present study, it was demonstrated with **[EuL$^{7\text{-}11}$]** that by subtle structural alterations, a significant change in nucleotide affinity can be gained. On the other hand, steric factors may also be responsible for discrimination e.g. with ADP and ATP, which produced CPL signals of opposite signs upon binding to **[EuL$^{7\text{-}8}$]**. Furthermore, different levels of signal amplification (i.e. total emission intensity) were observed across the nucleotide series, which was also attributed to size exclusion. It was also shown that the binding of $Zn^{2+}$ ions resulted in the formation of bimetallic complexes **[EuL$^{7}$]$_2$*Zn$^{2+}$** and **[EuL$^{8}$]*Zn$^{2+}$**, which showed an enhanced affinity to the nucleotides. At the same time, variation in the number of

donor atoms in the $Zn^{2+}$ binding site, provided an efficient means for tuning $Zn^{2+}$ binding affinity.

The selective detection observed for ADP over ATP, makes further development of probes based on **[EuL$^{7\text{-}8}$]** highly attractive. They have potential applications as cellular probes for tracking the ADP/ATP ratio using chiral confocal luminescence microscopy. The major drawback of proposed systems, is their rather low brightness and the quenching of the chromophore by protein binding and other electron-rich molecules. One possible solution to overcome these issues is to use a biaryl chromophore, which is able to sensitise $Tb^{3+}$ emission with a significantly higher quantum yield. Such a complex should require less time to acquire a high CPL signal (Fig. IV.41).

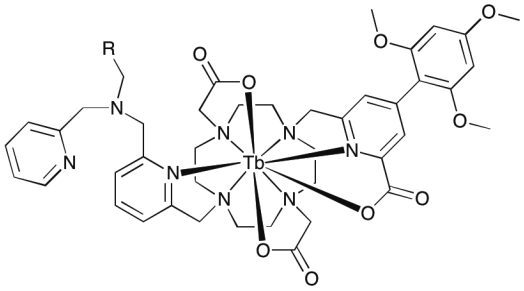


**Fig. IV.41** Proposed molecular probe for detecting the ratio between ADP and ATP *in cellulo* (R = Py, Et).

Further structural alterations should be also aimed at increasing the dissymmetry factor, $g_{em}$, by rigidifying the structure. It has been reported that introducing phosphinate arms can significantly increase the rigidity of lanthanide complexes based on macrocyclic ring platforms[21]. Therefore, by substituting carboxylate arms in both the chromophore and cyclen ring, higher $g_{em}$ values may be achieved, thereby enhancing the sensitivity of the ADP/ATP probe (Fig. IV.42). Furthermore, substitution of the carboxylate arm with a phosphinate should bathochromically shift the excitation wavelength of the complex by approximately 10 nm, making it brighter under the 355 nm laser that is often used in a confocal microscope.

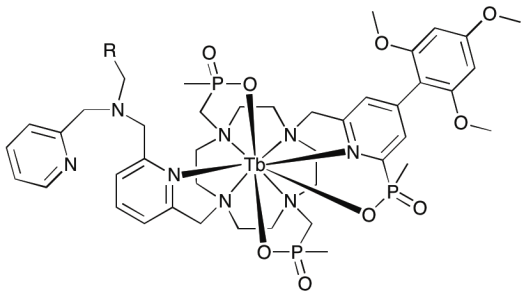


**Fig. IV.42** Proposed molecular probe with phosphinate arms for detecting the ratio between ADP and ATP *in cellulo* (R = Py, Et).

Even though probes **[EuL$^{7\text{-}8}$]** combine both an affinity towards nucleotides and $Zn^{2+}$ ions, the utility of these probes for detecting $Zn^{2+}$ *in cellulo* is significantly hampered by their high affinity towards different bioactive anions. The intrinsic drawback of these systems for binding metal ions is a close proximity of the binding pocket to the lanthanide ion, notwithstanding the benefit for high anion affinity. At the same time, a relatively short distance between $Zn^{2+}$ ion and lanthanide is usually necessary to provide a significant perturbation of the coordination environment, which causes a concomitant photophysical change. Therefore, the ideal $Zn^{2+}$-sensitive probe should be designed in such a way that on the one hand, metal binding causes sufficient alteration of the coordination environment of the lanthanide to track these changes spectroscopically, and on the other, it is not hindered by competitive binding of interfering anionic species.

Recently, Mishra reported gadolinium probes for relaxometric detection of calcium and zinc ions, where an amide arm bearing a metal-sensitive moiety was attached to the DO3A moiety[22]. Photophysical studies of the $Eu^{3+}$ analogue revealed that despite a relatively long distance between $Eu^{3+}$ and the carbonyl group, its reversible binding as a function of added metal produced a noticeable change of the spectral signature that can be followed ratiometrically. In addition, a relatively long distance between the binding moiety and $Ln^{3+}$ should exclude any competitive binding with anions at biologically relevant concentrations.

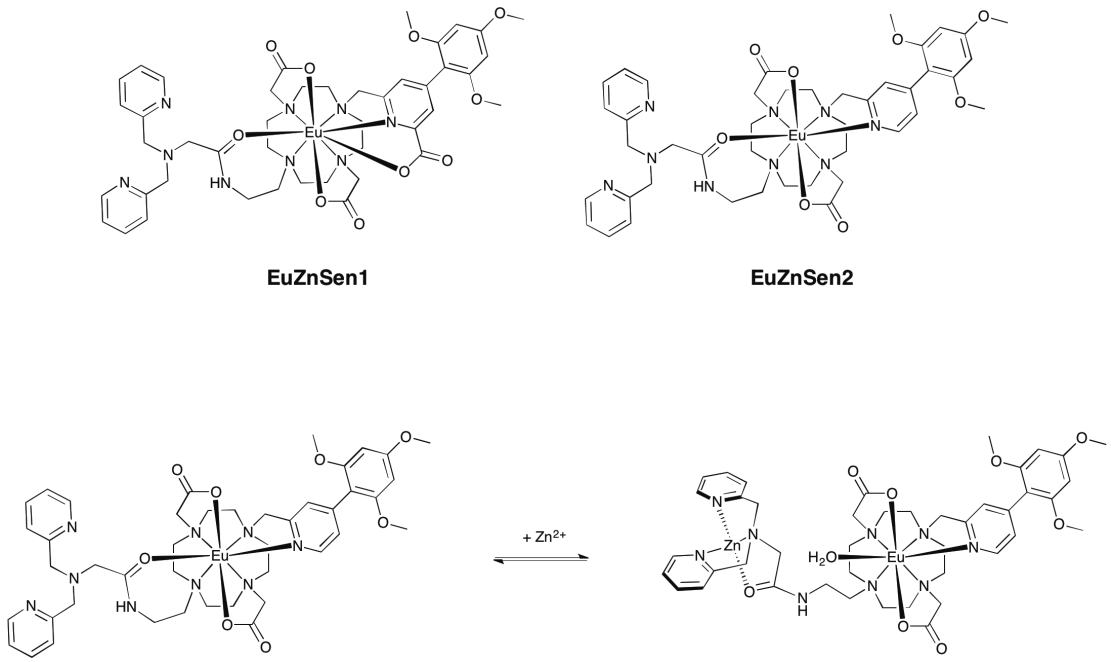


**Fig. IV.43** Proposed zinc (II) sensors **EuZnSen1** and **EuZnSen2** and the schematic of the reversible $Zn^{2+}$-binding mechanism for **EuZnSen2**.

With this structure in mind, novel luminescent zinc-selective probes for cellular imaging based on a DO2A platform are proposed here (Fig. IV.43), which employ the biaryl chromophore and an amide arm bearing a dipicolylamine moiety. Two complexes with different charges and coordination numbers along with their synthetic pathway are suggested below (Scheme IV.3). The complex with an overall positive charge and coordination number 8 should have a lower affinity than the corresponding neutral complex with a coordination number of 9.

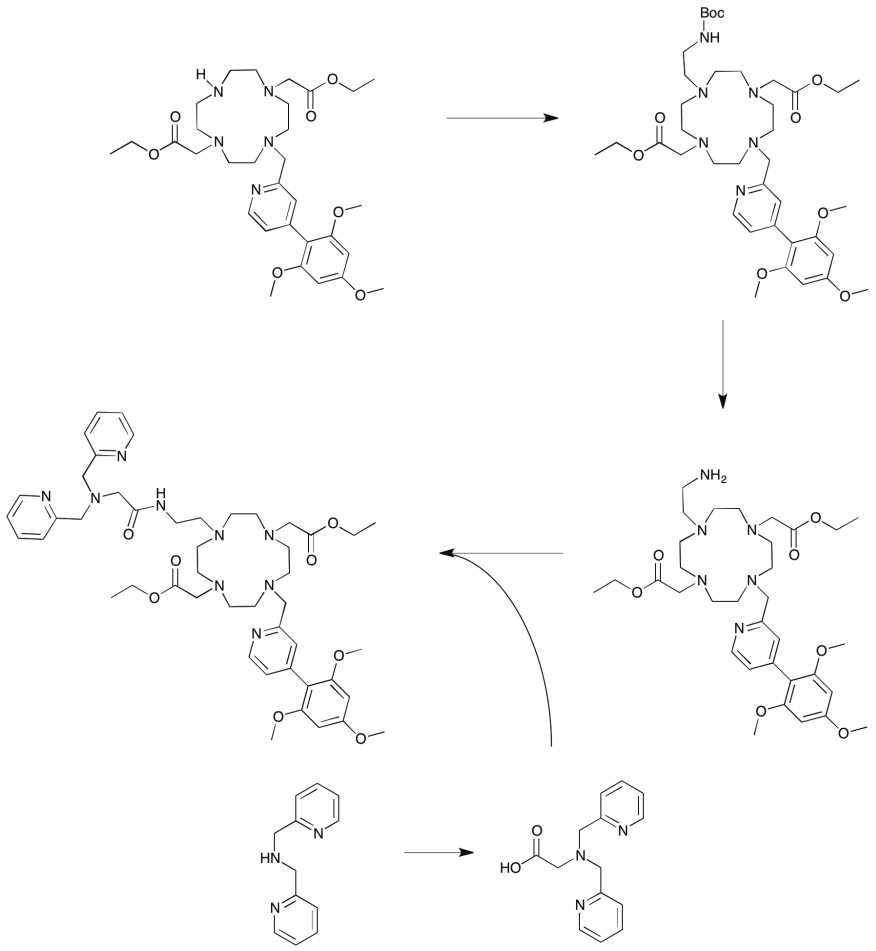

**Scheme IV.3** Suggested synthetic pathway for **EuZnSen1**.

To modulate significant changes in the emission spectrum of $Eu^{3+}$ as a function of added analyte, alterations in the coordination sphere of $Eu^{3+}$ are usually involved. However, in order to perturb the electronic distribution on the lanthanide ion, it is sufficient to alter the polarisability or partial charge on the already ligated atoms without their dissociation. Pyridine-containing moieties are often used as a binding arm in lanthanide complexes, due to the ease of their functionalisation. Although, a high partial charge on the nitrogen atom makes electrophilic substitutions into the ring a challenging task, even subtle alterations of the electronic distribution in the ring should give rise to considerable changes in the emission spectrum of the bound lanthanide ion. Henceforth, introduction of the dipicolylamine moiety in a *para*-position should result in a zinc-responsive probe, which can modulate spectral changes in response to added $Zn^{2+}$ (Fig. IV.44).

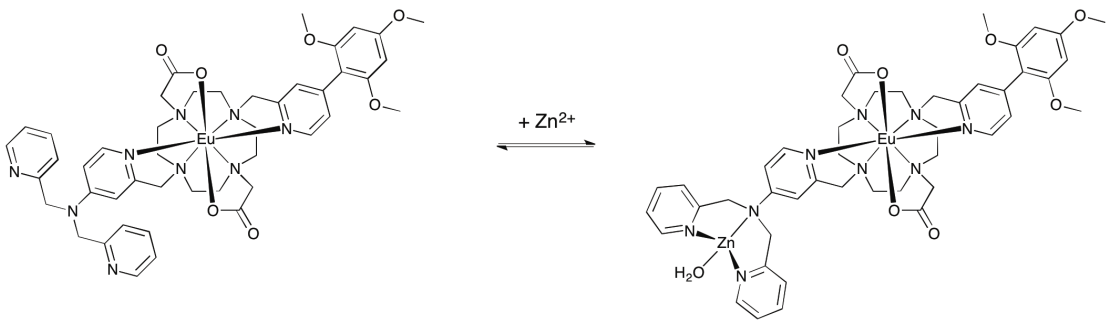


**Fig. IV.44** Reversible $Zn^{2+}$-sensing for the proposed molecular probe.

# IV.6 References


[1] E. Berni, L. Le Henaff, L. Jarrige, E. Girard, G. Jonusauskas, I. Gosse, S. Pinet, *Eur. J. Org. Chem.* **2017**, *2017*, 3620–3630.

[2] A. Bencini, C. Coluccini, A. Garau, C. Giorgi, V. Lippolis, L. Messori, D. Pasini, S. Puccioni, *Chem. Commun.* **2012**, *48*, 10428-10430.

[3] P. Sokkalingam, D. S. Kim, H. Hwang, J. L. Sessler, C.-H. Lee, *Chem. Sci.* **2012**, *3*, 1819-1824.

[4] P. A. Gale, N. Busschaert, C. J. E. Haynes, L. E. Karagiannidis, I. L. Kirby, *Chem. Soc. Rev.* **2014**, *43*, 205–241.

[5] Y. J. Jang, E. J. Jun, Y. J. Lee, Y. S. Kim, J. S. Kim, J. Yoon, *J. Org. Chem.* **2005**, *70*, 9603–9606.

[6] S. J. Butler, D. Parker, *Chem. Soc. Rev.* **2013**, *42*, 1652–1666.

[7] S. J. Butler, B. K. McMahon, R. Pal, D. Parker, J. W. Walton, *Chem. - Eur. J.* **2013**, *19*, 9511–9517.

[8] E. R. Neil, D. Parker, *RSC Adv.* **2017**, *7*, 4531–4540.

[9] S. J. A. Pope, R. H. Laye, *Dalton Trans.* **2006**, *44*, 3108-3113.

[10] M. M. Peixoto, G. F. Bauerfeldt, M. H. Herbst, M. S. Pereira, C. O. Da Silva, *J. Phys. Chem. A* **2015**, *119*, 5241–5249.

[11] M. Tantama, J. R. Martínez-François, R. Mongeon, G. Yellen, *Nat. Commun.* **2013**, *4*, 2550-.

[12] J. Berg, Y. P. Hung, G. Yellen, *Nat. Methods* **2009**, *6*, 161–166.

[13] G. Feng, C. J. Zhang, X. Lu, B. Liu, *ACS Omega* **2017**, *2*, 546–553.

[14] J. T. Simmons, J. R. Allen, D. R. Morris, R. J. Clark, C. W. Levenson, M. W. Davidson, L. Zhu, *Inorg. Chem.* **2013**, *52*, 5838–5850.

[15] C. F. Mills, *Zinc in Human Biology*, Springer Verlag, Berlin, **1989**.

[16] L. C. Costello, R. B. Franklin, *Prostate Cancer Prostatic Dis.* **2009**, *12*, 17–24.

[17] V. Y. Zaichick, T. V. Sviridova, S. V. Zaichick, *Int. Urol. Nephrol.* **1996**, *28*, 687–694.

[18] R. Pal, D. Parker, L. C. Costello, *Org. Biomol. Chem.* **2009**, *7*, 1525–1528.

[19] C. Brady, P. L. Callaghan, Z. Ciunik, C. G. Coates, A. Døssing, A. Hazell, J. J. McGarvey, S. Schenker, H. Toftlund, A. X. Trautwein, et al., *Inorg. Chem.* **2004**, *43*, 4289–99.

[20] D. E. Stefano, *Talanta* **1986**, *33*, 763–767.

[21] A. T. Frawley, R. Pal, D. Parker, *Chem. Commun.* **2016**, *52*, 13349–13352.

[22] A. Mishra, N. K. Logothetis, D. Parker, *Chem. - Eur. J.* **2011**, *17*, 1529–1537.

# Chapter five

# Experimental part

# V.1 Materials and Methods

All solvents used were laboratory grade and anhydrous solvents, when required, were freshly distilled over the appropriate drying agent. Water was purified by the 'PuriteSTILLplus' system, with conductivity of ≤4 μS $cm^{-1}$. All reagents used were purchased from commercial suppliers (Aldrich, Fisher Scientific, Fluorochem, Apollo Scientific) and were used without further purification unless otherwise stated. Reactions requiring anhydrous conditions were carried out using Schlenk-line techniques under an atmosphere of argon. DO2A-*tret*-butyl ester[1], DO2A-ethyl ester[2], methyl 6-(hydroxymethyl)-4-((4-methoxyphenyl)ethynyl)picolinate[3], 1-(6-(Chloromethyl)pyridin-2-yl)-*N*,*N*-*bis*(pyridin-2-ylmethyl)methanamine[4] and (4-bromopyridin-2-yl)methanol[5] were synthesised according to previously reported procedures'. A synthesis of sulphonamide arm is performed in accordance with literature procedure[6]. Synthesis of di-substituted cyclen with chiral amide arms was described elsewhere[7],[8].

## *V.1.1 Optical measurements*

**Absorption spectroscopy**

UV/Vis absorption measurements were recorded using a Perkin-Elmer Lambda 900 absorption spectrophotometer, using matched quartz cells.

**Luminescence**

Emission spectra were measured using a Horiba-Jobin Yvon Fluorolog-3® and Horiba-Jobin Yvon Fluoromax-3®. The steady-state luminescence was excited by unpolarised light from a 450W xenon CW lamp and detected at an angle of 90° for diluted solution measurements (10 mm quartz cell) by a red-sensitive Hamamatsu R928 photomultiplier tube. Spectra were reference corrected for both the excitation source light intensity variation (lamp and grating) and the emission spectral response (detector and grating). Phosphorescence lifetimes (> 30 μs) were obtained by pulsed excitation using a FL-1040 UP Xenon Lamp. Luminescence decay curves were fitted by least-squares analysis using Origin®. Luminescence quantum yields $\phi$ were measured in diluted aqueous solution with an absorbance lower than 0.3, using an integrating sphere. The apparent binding constant of the selected anion was

calculated according to equation, using Origin2015™ software and non-linear iterative least squares regression.

$$[X] = \frac{\frac{(F - F_0)/(F_1 - F_0)}{K} + [Eu] * (F - F_0)/(F_1 - F_0) - [Eu] * \left((F - F_0)/(F_1 - F_0)\right)^2}{1 - (F - F_0)/(F_1 - F_0)}$$

$$\mathrm{Eu} + \mathrm{X} \leftrightarrow \mathrm{EuX} \qquad K = \frac{[EuX]}{[X_f][Eu_f]}$$

**[X]:** the total concentration of protein in the solution

**[Eu]:** the total concentration of the complex

**K:** the binding constant

**F:** the ratio of selected peaks

**$F_0$:** the ratio at the beginning

**$F_1$:** the final ratio

**[EuX]:** the concentration of the appropriate SA or drug -coordinated complex

**[$X_f$]:** the concentration of free SA or drug in the mixture

**[$Eu_f$]:** the concentration of the free complex

**Circularly Polarised Luminescence**

CPL spectra were recorded on a custom built spectrometer consisting of a laser driven light source (Energetiq EQ-99 LDLS, spectral range 170 to 2100 nm) coupled to an Acton SP2150 monochromator (600 g/nm, 300 nm Blaze) allowing excitation wavelengths to be selected with a 6 nm FWHM band-pass. The collection of the emitted light was facilitated (90° angle set up, 1 cm path length quartz cuvette) by a Lock-In Amplifier (Hinds Instruments Signaloc 2100) and Photoelastic Modulator (Hinds Series II/FS2AA). The differentiated light was focused onto an Acton SP2150 monochromator (1200 g/nm, 500 nm Blaze) equipped with a high sensitivity cooled Photo Multiplier Tube (Hamamatsu H10723-20 PhotoSensor red corrected). The detection of the CPL signal was achieved using the field modulation lock-in technique. The electronic signal from the PMT was fed into the lock-in amplifier (Hinds Instruments Signaloc 2100). The reference signal for the lock-in detection was provided by the PEM control unit. The monochromators, PEM control unit and

lock-in amplifier were interfaced with a desktop PC and controlled by Labview2011 code.

### *V.1.2 Confocal Microscopy*

Cell microscopy imaging of the complexes studied in cells was achieved using a custom built epiflorescence microscope (modified Zeiss Axiovert 200M), using a Zeiss APOCHROMAT 63x/1.40 NA objective, combined with a low voltage 365 nm pulsed UV LED focused and collimated excitation source (1.2W). For rapid spectral acquisition, the microscope was equipped at the X1 port with a Peltier cooled 2D-CCD detector (Ocean Optics), used in an inverse 100 Hz time gated sequence. The spectrum was recorded from 400-800 nm with a resolution of 0.24 nm and the final spectrum was acquired using an averaged 10,000 scan duty cycle.

Probe lifetimes were measured on the same microscope platform using a cooled PMT detector (Hamamatsu H7155), mounted on the X2 port. Both the control and detection algorithm were written in LabView2014. Time gated images were recorded using a high resolution cooled EO-1312M CCD camera (Thor labs). All duty cycle and gating sequences were established and controlled by in house LabView software[4].

High resolution Laser Scanning Confocal Microscopy (LSCM) images were recorded on a modified Leica SP5 II microscope, equipped with a new SIM technique called PhMoNa[4]. In order to achieve excitation with maximal probe emission, the microscope was coupled by an optical fibre to a Coherent CW laser (Nd:YAG, 355 nm), operating at 8 mW power. A He/Ne or Ar ion laser was used when commercially available organelle-specific stains (e.g. LysoTrackerGreenTM) were used to corroborate cellular compartmentalisation profiles.

The microscope was equipped with a triple channel imaging detector, comprising two conventional PMT systems and a HyD hybrid avalanche photodiode detector. The latter part of the detection system, when operated in the BrightRed mode, is capable of improving imaging sensitivity above 550 nm by 25%, reducing signal to noise by a factor of 5. The pinhole was always determined by the Airy disc size, calculated from the objective in use (HCX PL APO 63x/1.40 NA αBlue), using the

lowest excitation wavelength (355 nm). Scanning speed was adjusted to 200 Hz in a unidirectional mode, to ensure both sufficient light exposure and enough time to collect the emitted light from the lanthanide based optical probes (2048 x 2048 frame size, a pixel size of 62 x 62 nm and depth of 298 nm). Spectral imaging on this Leica system is possible with the xyλ-scan function, using the smallest allowed spectral band-pass (5 nm) and step-size (3 nm) settings. However, much improved spectral imaging in cells was achieved using a custom built and Peltier cooled CCD detector (Ocean Optics, HR2000plus) synchronised to the X1 port.

The europium complexes (10 μM) were incubated with NIH-3T3 cells for up to 24h to allow complex uptake within the lysosomes; this localisation profile was verified by co-incubation with LysoTrackerGreen.

**Live cell cultures studies**

A detailed investigation of the cellular behaviour of each complex was conducted using NIH 3T3 mouse skin fibroblast cell using epi-fluorescence and laser scanning confocal microscopy. Initial cell line was sourced from American Type Culture Collection (NIH 3T3 CRL-1658) and have been established and maintained in a category 2 cell culture facility according to established standardised protocol for 12 months; they have been periodically monitored for mycoplasma contamination. Cells were maintained in exponential growth as monolayers in F-12/DMEM (Dulbecco's Modified Eagle Medium) 1:1 that was supplemented with 10% fetal bovine serum (FBS) or human or goat serum where appropriate. Cells were grown in 75 $cm^2$ plastic culture flasks, with no prior surface treatment. Cultures were incubated at 37 °C, 10% average humidity and 5% (v/v) $CO_2$. Cells were harvested by treatment with 0.25% (v/v) trypsin solution for 5 min at 37 ºC. Cell suspensions were pelleted by centrifugation at 1000 rpm for 3 min, and were re-suspended in fresh medium by repeated aspiration with a sterile plastic pipette. Microscopy cells were seeded in untreated iBibi 100 μL live cell channels and allowed to grow to 40% to 60% confluence, at 37 ºC in 5% $CO_2$. At this stage, the medium was replaced and cells were treated with the studied Eu-complex and co-stains as appropriate, present in the final imaging medium. For live cell imaging, DMEM/F12 media lacking phenol red was used from this point onwards using a purpose build incubator housing the microscope maintaining 37 ºC, 5% $CO_2$ and 10% humidity.

### *V.1.3 HPLC analysis*

HPLC analysis and purification were performed at 295 K using a Shimadzu system (degassing unit DGU-20A5R, Prominence semi-preparative liquid chromatograph LC-20AP, Prominence UV/Vis detector SPD-20A and communications bus module CBM-20A). The solvent system used was ammonium bicarbonate buffer (25 mM, pH = 7) / methanol [isocratic 10 % methanol in buffer (3 min), linear gradient to 100% methanol (10 min), isocratic 100 % methanol (5 min)] or formic acid buffer (0.1%) / Acetonitrile [isocratic 10 % acetonitrile in buffer (3 min), linear gradient to 100% Acetonitrile (10 min), isocratic 100 % acetonitrile (5 min)] flow: 2 ml / min for analytical mode on XBridge C18 column, 4.6 x 100 mm, i.d. 5 µm, and 17 ml / min for preparative mode on XBridge C18 column, 19 x 100 mm, i.d. 5 µm.

### *V.1.4 Electrospray mass spectral analysis and accurate mass determinations*

Electrospray mass spectra and accurate masses were recorded on a TQD mass spectrometer or a QTOF Premier mass spectrometer respectively, both equipped with an Acquity UPLC, a lock-mass electrospray ion source and an Acquity photodiode array detector (Waters Ltd, UK), acetonitrile was used as the carrier solvent. Solvent system used for TQD was water (0.1 % formic acid) / Acetonitrile (0.1 % formic acid) [5 % acetonitrile (0.2 min), linear gradient to 95 % Acetonitrile (3.8 min), isocratic 95 % acetonitrile (0.5 min), linear gradient to 5% acetonitrile (0.5 min)], flow: 0.6 ml / min on Acquity UPLC BEH C18 column, 2.1 x 50 mm, i.d. 1.7 µm. Solvent system used for QTOF was ammonium bicarbonate buffer (25 mM, pH = 7) / Acetonitrile [2 % acetonitrile in buffer (3 min), linear gradient to 40% Acetonitrile (6 min), linear gradient to 100% Acetonitrile (4 min), isocratic 100 % acetonitrile (2 min)] or water (0.1 % formic acid) / Acetonitrile (0.1 % formic acid) [linear gradient to 99 % Acetonitrile (5 min), isocratic 99 % acetonitrile (1 min), linear gradient to 100 % water (0.1 min), isocratic 100 % water (0.9 min)], flow: 0.6 ml / min on an Acquity UPLC BEH C18 column, 2.1 x 50 mm, i.d. 1.7 µm.

### *V.1.5 NMR Analysis*

$^{1}H$ and $^{13}C$ NMR spectra were recorded on a Bruker Avance-400 ($^{1}H$ 400.052 MHz and $^{13}C$ 100.603 MHz) spectrometer. Spectra were recorded in commercially available deuteriated solvents. $^{13}C$ and $^{1}H$ chemical shift values are quoted in ppm relative to trimethylsilane and all coupling constants are given in Hz. Assignment of the spectra was achieved using COSY, NOESY, ROESY, HSQC and HMBC experiments. The operating temperature of the spectrometers (usually 295 K) was measured with the aid of an internal calibration solution of ethylene glycol.

Relaxivity measurements were carried out at 310 K, 60 MHz (1.4 T) on a Bruker Minispec mq60 instrument. The mean value of three independent measurements was recorded. The relaxivities of the compounds were calculated as the slope of the function shown in the eqn (1) below,

$$\frac{1}{T_{1,obs}} = \frac{1}{T_{1,d}} + r_1[GdL^1] \qquad (1)$$

where $T_{1,obs}$ is the measured $T_1$, $T_{1,d}$ is the diamagnetic contribution of the solvent (calculated to be 4.0 ms) and **[GdL$^4$]** is the concentration in mM of the appropriate $Gd^{3+}$ complex (n = 1–6). Errors for all relaxivity values were less than 0.3 $mM^{-1}s^{-1}$.

The apparent binding constant for the interaction of the $Gd^{3+}$ complexes with Human Serum Albumin (HSA), Bovine Serum Albumin (BSA), iodipamide and ibuprofen was calculated using eq. (2) below:

$$[X] = \frac{\frac{(R-R_0)/(R_1-R_0)}{K} + [GdL^1] \times \frac{R-R_0}{R_1-R_0} - [GdL^1] \times \left(\frac{R-R_0}{R_1-R_0}\right)^2}{1-\frac{(R-R_0)}{(R_1-R_0)}}$$

$$K = \frac{[Gd \cdot X]}{[X_f][Gd_f]} \qquad (2)$$

where [X] is the total concentration of serum albumin in the solution; [Gd.L$^1$]: the total concentration of the complex; *K*: the binding constant; *R*: relaxation rate of a given concentration of *X*; $R_0$: the initial relaxation rate; $R_1$: final relaxation rate; [Gd.X]: the concentration of the serum albumin-coordinated complex; [$X_f$]: the

concentration of free serum albumin in the mixture; [$Gd_f$]: the concentration of the free complex.

## V.2. Synthesis

**(4-((4-Methoxyphenyl)ethynyl)pyridin-2-yl)methanol, 1**

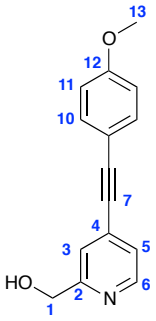


(4-Bromopyridin-2-yl)methanol (0.67 g, 3.56 mmol) and 4-ethynylanisole (0.70 mL, 5.40 mmol) were dissolved in anhydrous THF (15 mL) under argon, followed by addition pyrrolidine (0.40 mL) and $Pd(TPP)_2Cl_2$ (0.25 g, 0.36 mmol). The reaction mixture was stirred at 50 °C for 18 h and the solvent was removed under reduced pressure. The crude material was purified on a silica column (100% DCM to 50%DCM-50%EtOAc), giving an orange solid (0.85 g, 100% yield); $^1$H NMR (295 K, 400 MHz, $CDCl_3$) $\delta_H$ 8.50 (1H, d, $^3J_{H\text{-}H}$ = 5.0 Hz, $H^6$), 7.48 (2H, d, $^3J_{H\text{-}H}$ = 9.0 Hz, $H^{10}$), 7.38 (1H, br s, $H^3$), 7.25 (1H, d, $^3J_{H\text{-}H}$ 5.0, $H^5$), 6.90 (2H, d, $^3J_{H\text{-}H}$ = 9.0 Hz, $H^{11}$), 4.76 (2H, s, $H^1$), 3.83 (3H, s, $H^{13}$); $^{13}$C NMR (295 K, 100 MHz, $CDCl_3$) $\delta_C$ 160.4 ($C^{12}$), 159.5 ($C^2$), 148.4 ($C^6$), 133.5 ($C^4$), 132.6 ($C^{10}$), 124.0 ($C^3$), 122.2 ($C^5$), 114.2 ($C^9$), 114.0 ($C^{11}$), 94.4 ($C^8$), 85.7 ($C^7$), 64.2 ($C^1$), 55.3 ($C^{13}$); *m/z* (HRMS$^+$) 240.1027 $[M+H^+]^+$ ($C_{15}H_{14}N_2O$ requires 240.1025).

**Di-*tert*-butyl 2,2'-(4-((4-((4-methoxyphenyl)ethynyl)pyridin-2-yl)methyl)-1,4,7,10-tetraazacyclododecane-1,7-diyl)diacetate, 1-1**

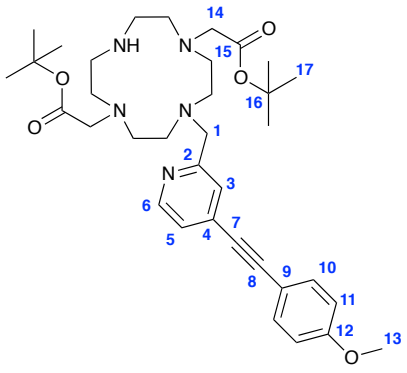


(4-((4-Methoxyphenyl)ethynyl)pyridin-2-yl)methanol, **1** (103 mg, 0.43 mmol) was dissolved in anhydrous THF (5 mL) under argon, followed by addition of anhydrous triethylamine (130 μL, 0.90 mmol) and methenesulfonyl chloride (55 μL, 0.70 mmol). The reaction mixture was stirred for 2 h at rt and the solvent was removed at reduced pressure. The crude material was dissolved in dichloromethane (20 mL) and washed with water (2 x 10 mL). The organic phase was dried over $MgSO_4$ and the solvent was removed under reduced pressure. The crude yellow oil of **1-Ms** was dissolved in anhydrous acetonitrile (5 mL) and was slowly added upon cooling (ice/acetone bath) and vigorous stirring to the solution of DO2A-tBu ester (172 mg, 0.43 mmol) and $K_2CO_3$ (83 mg, 0.60 mmol) in dry acetonitrile (10 mL). The reaction mixture was stirred for 18 h allowing the reaction mixture to reach rt and was purified using reverse phase HPLC (10% water to 100% water in MeOH over 9 min, 0.1% formic acid). Collected fractions were neutralised using ammonia solution, the solvent was removed under reduced pressure and acetonitrile (20 mL) was added. The insoluble ammonium formate was filtered off and the filtrate was collected. The solvent was removed under reduced pressure giving clear oil (60 mg, 37% yield); $^1$H NMR (295 K, 400 MHz, $CDCl_3$) $\delta_H$ 8.41 (1H, d, $^3J_{H\text{-}H}$ = 5.0 Hz, $H^6$), 7.51 (2H, d, $^3J_{H\text{-}H}$ = 9.0 Hz, $H^{10}$), 7.47 (1H, br s, $H^3$), 7.37 (1H, d, $^3J_{H\text{-}H}$ = 5.0 Hz, $H^5$), 6.92 (2H, d, $^3J_{H\text{-}H}$ = 9.0 Hz, $H^{11}$), 3.97-2.52 (22H, m br, $H^1$, $H^{14}$, cyclen), 3.85 (3H, s, $H^{13}$), 3.16-2.62 (20H, m, $H^{14}$, cyclen), 1.48 (18H, s, $H^{17}$); $^{13}$C NMR (295 K, 100 MHz, $CDCl_3$) 160.9 ($C^{12}$), 157.5 ($C^2$), 147.9 ($C^6$), 135.2 ($C^{10}$), 133.8 ($C^4$), 125.4 ($C^3$), 124.9 ($C^5$), 114.4 ($C^9$), 113.2 ($C^{11}$), 97.8 ($C^8$), 86.6 ($C^{16}$), 84.8 ($C^7$), 58.7 ($C^1$, $C^{14}$), 55.5 ($C^{13}$), 51.6-43.3 (cyclen), 28.5 ($C^{17}$); m/z (HRMS$^+$) 622.3965 $[M+H^+]^+$ ($C_{35}H_{52}N_5O_5$ requires 622.3968).

**[EuL$^1$]**

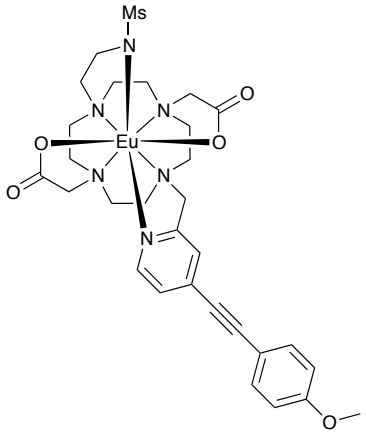


Di-*tert*-butyl 2,2'-(4-((4-((4-methoxyphenyl)ethynyl)pyridin-2-yl)methyl)-1,4,7,10-tetraazacyclododecane-1,7-diyl)diacetate, **1-1** (57 mg, 0.09 mmol) was dissolved in dry acetonitrile (10 mL), followed by addition of $K_2CO_3$ (25 mg, 0.18 mmol) and 2-(methylsulfonamido)ethyl methanesulfonate (20 mg) was added. The oil bath was heated up to 80 °C and the reaction flask was immersed inside the bath. The reaction mixture was stirred for 18 h and the formation of the desired product was confirmed by LC-MS analysis. The solvent was removed under reduced pressure and dichloromethane (15 mL) was added, filtered and the solvent was removed under reduced pressure. The crude was dissolved in methanol (4 mL) and aqueous NaOH solution (2.5 M, 2 mL) was added. The mixture was stirred at 60 °C for 3 h. The reaction mixture was neutralised by careful addition of concentrated HCl and $EuCl_3$ (52 mg, 0.2 mmol) was added. The reaction mixture was stirred at 60 °C for 3 h and the product was purified using reverse phase HPLC (0-3 min 10% water, 3-13 min 10% water to 100% water in MeOH, $NH_4HCO_3$ buffer (2 g/L), $t_r$ = 10.5 min), yielding a white powder (22 mg, 36% yield over 2 steps); *m*/*z* (HRMS$^+$) 779.1898 $[M+H^+]^+$ ($C_{30}H_{40}N_6O_7S^{151}Eu$ requires 779.1878); $\lambda_{abs}$ = 325 nm; $\varepsilon(H_2O)$ = 35400 $M^{-1}cm^{-1}$; $\tau(H_2O)$ = 0.73 ms (pH = 6), $\tau(D_2O)$ = 1.00 ms (pD = 6.4); $\phi_{Eu}$ = 6.6%.

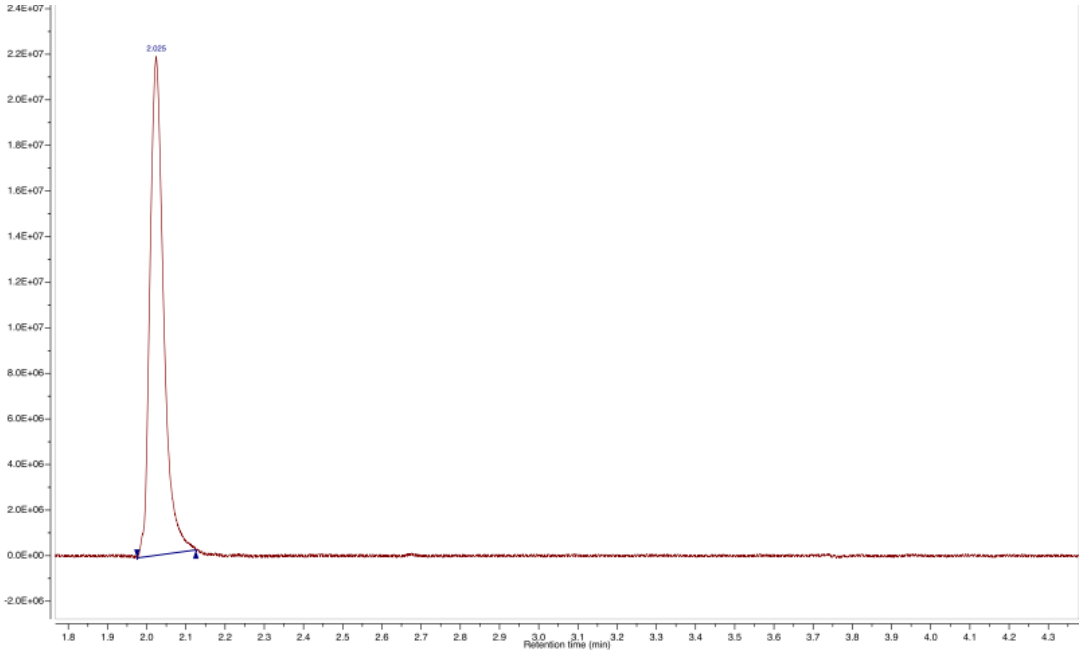


LC-MS UV trace of **[EuL$^1$]** (5% $H_2O$ (+0.1% v/v formic acid) in MeOH (+0.1% v/v formic acid) to 95% $H_2O$ (+0.1% v/v formic acid) in MeOH (+0.1% v/v formic acid) over 3.8 min

**2,2'-(4-((4-((4-Methoxyphenyl)ethynyl)pyridin-2-yl)methyl)-1,4,7,10-tetraazacyclododecane-1,7-diyl)*bis*(*N*-((S)-1-phenylethyl)acetamide), 2-1**

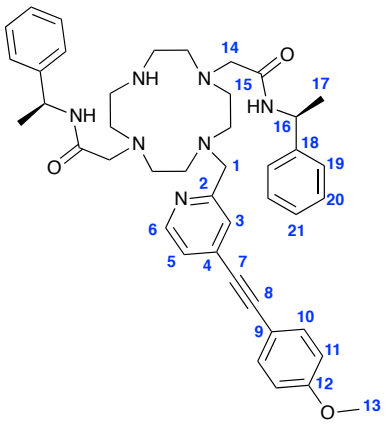

(4-((4-Methoxyphenyl)ethynyl)pyridin-2-yl)methanol, **1** (39 mg, 0.16 mmol) was dissolved in anhydrous THF (4 mL) under argon, followed by addition of anhydrous triethylamine (30 µL, 0.21 mmol) and methanesulfonyl chloride (15 µL, 0.19 mmol). The reaction mixture was stirred for 2 h at rt and the solvent was removed at reduced pressure. The crude material was dissolved in dichloromethane (20 mL) and washed with water (2 x 10 mL). The organic phase was dried over $MgSO_4$ and the solvent was removed under reduced pressure. The crude yellow oil of **1-Ms** was dissolved in anhydrous acetonitrile (5 mL) and was slowly added upon cooling (ice/acetone bath)

and vigorous stirring to the solution of 2,2'-(1,4,7,10-tetraazacyclododecane-1,7-diyl)*bis*(N-((S)-1-phenylethyl)acetamide) (80 mg, 0.16 mmol) and $K_2CO_3$ (83 mg, 0.60 mmol) in dry acetonitrile (10 mL). The reaction mixture was stirred for 18 h allowing to reach rt and was purified using reverse phase HPLC (10% water to 100% water in MeOH over 9 min, 0.1% formic acid). Collected fractions were neutralised using ammonia solution and the solvent was removed under reduced pressure. The residue was dissolved in water (10 mL) and the pH was increased up to 14 by addition of 1M NaOH solution. The aqueous solution was washed with DCM (3 x 10 mL), organic fractions were combined and dried over $MgSO_4$. The solvent was removed under reduced pressure to give a desired product as a thick yellow oil (28 mg, 24% yield); $^1$H NMR (295 K, 700 MHz, $CDCl_3$) $\delta_H$ 8.46 (1H, m, $H^6$), 7.50 (2H, d, $^3J_{H\text{-}H}$ = 9.0 Hz, $H^{10}$), 7.30 (4H, d, $^3J_{H\text{-}H}$ = 8.0 Hz, $H^{19}$), 7.25 (4H, t, $^3J_{H\text{-}H}$ = 8.0 Hz, $H^{20}$), 7.20 (1H, m, $H^5$), 7.18 (2H, m, $H^{21}$), 7.14 (1H, m, $H^3$), 6.89 (2H, d, $^3J_{H\text{-}H}$ = 9.0 Hz, $H^{11}$), 5.13 (2H, m, $H^{16}$), 3.83 (3H, s, $H^{13}$), 3.52 (2H, m, N**H**), 3.11 (4H, m, $H^{14}$), 2.87-2.53 (18H, m, $H^1$, cyclen), 1.47 (6H, d, $^3J_{H\text{-}H}$ = 7.0 Hz, $H^{17}$); $^{13}$C NMR (295 K, 176 MHz, $CDCl_3$) $\delta_C$ 170.3 ($C^{15}$), 160.3 ($C^{12}$), 157.5 ($C^2$), 149.2 ($C^6$), 143.7 ($C^4$), 143.3 ($C^{18}$), 133.5 ($C^{10}$), 128.5 ($C^{20}$), 127.2 ($C^{21}$), 126.4 ($C^{19}$), 125.3 ($C^3$), 124.0 ($C^5$), 114.1 ($C^{11}$), 114.0 ($C^9$), 94.5 ($C^8$), 85.6 ($C^7$), 59.9 ($C^{14}$), 55.3 ($C^{13}$), 53.1-51.3 ($C^1$, cyclen), 48.3 ($C^{16}$), 21.4 ($C^{17}$); *m/z* (HRMS$^+$) 716.4290 $[M+H^+]^+$ ($C_{43}H_{54}N_7O_3$ requires 716.4288).

**[EuL$^2$]Cl$_2$**

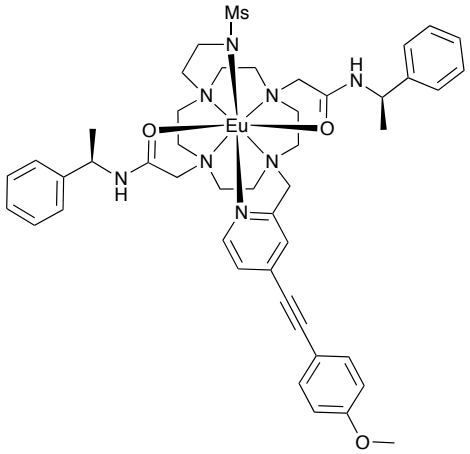


2,2'-(4-((4-((4-Methoxyphenyl)ethynyl)pyridin-2-yl)methyl)-1,4,7,10-tetraazacyclo-dodecane-1,7-diyl)bis(N-((S)-1-phenylethyl)acetamide), **2-1** (28 mg, 0.039 mmol)

was dissolved in dry acetonitrile (7 mL), followed by addition of $K_2CO_3$ (20 mg, 0.25 mmol) and 2-(methylsulfonamido)ethyl methanesulfonate (8 mg, 0.039 mmol). The reaction mixture was immersed into an oil bath preliminary heated up to 80°C and stirred at this temperature for 18 h. The reaction mixture was filtered off and $EuCl_3$ (37 mg, 0.14 mmol) was suspended and the reaction mixture was stirred at 70 °C for 18 h. The solution was decanted and the solid was washed three times with DCM and then dissolved in 4 mL of water. Any excess of $Eu^{3+}$ was precipitated in the form of $Eu(OH)_3$ by adjusting the pH up to 10 with 0.1 M NaOH. The solid was separated by centrifugation, the solution was neutralised by addition of 0.1M HCl and freeze-dried to give a desired complex as an off-white solid; *m/z* ($HRMS^+$) 985.3461 $[M+H^+]^+$ ($C_{46}H_{58}N_8O_5S^{151}Eu$ requires 985.3449); $\lambda_{abs}$ = 325 nm; $\varepsilon(H_2O)$ = 35400 $M^{-1}cm^{-1}$; $\tau(H_2O)$ = 0.54 ms (pH = 8), $\tau(D_2O)$ = 0.68 ms (pD = 8.4); $\phi_{Eu}$ = 1.9%.

**(*S*)-Ethyl 2-(2-(7-(2-(((R)-1-ethoxyethyl)amino)-2-oxoethyl)-4-((4-((4-methoxyphenyl)ethynyl)pyridin-2-yl)methyl)-1,4,7,10-tetraazacyclododecan-1-yl) acetamido)propanoate, 3-1**

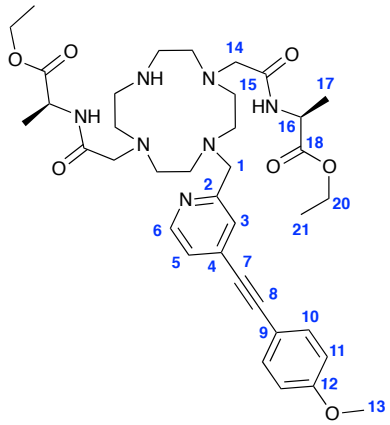


Methyl 6-(hydroxymethyl)-4-((4-methoxyphenyl)ethynyl)picolinate, **1** (196 mg, 0.82 mmol) was dissolved in dry THF (5 mL), followed by addition of dry triethylamine (0.1 mL, 0.72 mmol) and MsCl (45 mL, 0.57 mmol). The reaction mixture was stirred at rt for 1 h and the solvent was removed under reduced pressure. The crude material was redissolved in 15 mL of DCM and was washed with water (2 x 15 mL). The organic fraction was dried over $MgSO_4$ and the solvent was removed under reduced pressure, dried and redissolved in dry acetonitrile (5 mL). (*S*)-ethyl 2-(2-(7-(2-(((R)-1-ethoxyethyl)amino)-2-oxoethyl)-1,4,7,10-tetraazacyclododecan-1-

yl)acetamido) pro-panoate (400 mg, 0.82 mmol) was dissolved in dry acetonitrile (15 mL) and $K_2CO_3$ (100 mg, 0.72 mmol) was added. The reaction was cooled down using ice bath and stirred for 5 min. The **1-Ms** solution was added dropwise within 5 min. The reaction mixture was allowed to reach rt and stirred for 18 h. The reaction mixture was filtered and purified on RP-HPLC (10% to 100% acetonitrile (+0.1% formic acid) in water (+0.1% formic acid) over 9 min). The fractions containing the desired product were combined and neutralised with aqueous ammonia solution. The solvent was removed under reduced pressure, dried and redissolved in acetonitrile. Ammonium formate was filtered off and the solvent was removed under reduced pressure, giving a colourless oil (169 mg, 30% yield); $^1$H NMR (295 K, 400 MHz, $CDCl_3$) $\delta_H$ 8.60 (1H, m, $H^6$), 7.51 (2H, d, $^3J_{H\text{-}H}$ = 9.0 Hz, $H^{10}$), 7.45 (1H, d, $^3J_{H\text{-}H}$ = 7.0 Hz, $H^5$), 7.32 (1H, m, $H^3$), 6.92 (2H, d, $^3J_{H\text{-}H}$ = 9.0 Hz, $H^{11}$), 4.47 (2H, p, $^3J_{H\text{-}H}$ = 7.0 Hz, $H^{16}$), 4.15 (4H, t, $^3J_{H\text{-}H}$ = 7.0 Hz, $H^{20}$), 3.97 (2H, m, N**H**), 3.85 (3H, s, $H^{13}$), 3.34-2.79 (22H, m, $H^1$, $H^{14}$, cyclen), 1.32 (6H, d, $^3J_{H\text{-}H}$ = 7.0 Hz, $H^{17}$), 1.25 (6H, t, $^3J_{H\text{-}H}$ = 7.0 Hz, $H^{21}$); $^{13}$C NMR (295 K, 100 MHz, $CDCl_3$) $\delta_C$ 172.9 ($C^{18}$), 170.5 ($C^{15}$), 160.6 ($C^{12}$), 156.9 ($C^2$), 149.7 ($C^6$), 133.6 ($C^{10}$), 133.1 ($C^4$), 125.7 ($C^3$), 124.6 ($C^5$), 114.2 ($C^{11}$), 113.7 ($C^9$), 95.6 ($C^8$), 85.2 ($C^7$), 61.4 ($C^{20}$), 58.6 ($C^{14}$), 57.8 ($C^1$), 55.4 ($C^{13}$), 54.2-45.9 (cyclen), 48.1 ($C^{16}$), 17.5 ($C^{17}$), 14.1 ($C^{21}$); *m/z* (HRMS$^+$) 708.4106 $[M+H^+]^+$ ($C_{37}H_{54}N_7O_7$ requires 708.4085).

**[EuL$^3$]**

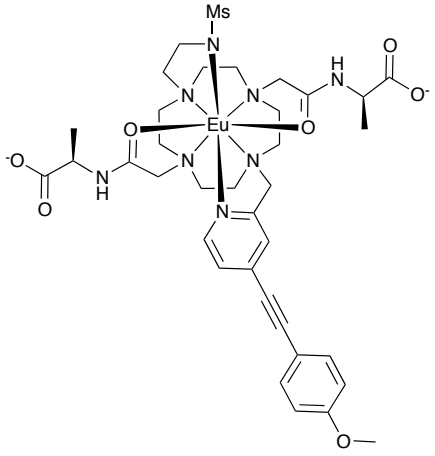


(S)-Ethyl 2-(2-(7-(2-(((R)-1-ethoxyethyl)amino)-2-oxoethyl)-4-((4-((4-methoxy-phenyl)ethynyl)pyridin-2-yl)methyl)-1,4,7,10-tetraazacyclododecan-1-yl) acetamido) propanoate, **3-1** (92 mg, 0.14 mmol) was dissolved in dry acetonitrile (10 mL),

followed by addition of $K_2CO_3$ (50 mg, 0.63 mmol) and 2-(methylsulfonamido)ethyl methanesulfonate (28 mg, 0.137 mmol). The reaction mixture was immersed into an oil bath preliminary heated up to 80 °C and stirred at this temperature for 18 h. The solution was filtered off and the solvent was removed under reduced pressure and the residue was redissolved in 0.1 M NaOH (4 mL) and stirred at 60 °C for 2 h. The solution was neutralised and $EuCl_3$ (37 mg, 0.14 mmol) was dissolved and the reaction mixture was stirred at 60 °C for 18 h. Any excess of $Eu^{3+}$ was precipitated in the form of $Eu(OH)_3$ by adjusting the pH up to 10 with 0.1 M NaOH. The solid was separated by centrifugation, the solution was neutralised by addition of 0.1M HCl and the residue was purified using reverse phase HPLC (0-3 min 10% water, 3-13 min 10% water to 100% water in MeOH, $NH_4HCO_3$ buffer (2 g/L)), yielding white powder (15 mg, 11% yield over 2 steps); *m/z* (HRMS$^+$) 921.2625 $[M+H^+]^+$ ($C_{36}H_{50}N_8O_9S^{151}Eu$ requires 921.2620); $\lambda_{abs}$ = 325 nm; $\varepsilon(H_2O)$ = 35400 $M^{-1}cm^{-1}$; $\tau(H_2O)$ = 0.48 ms (pH = 8), $\tau(D_2O)$ = 0.58 ms (pD = 8.4); $\phi_{Eu}$ = 1.3%.

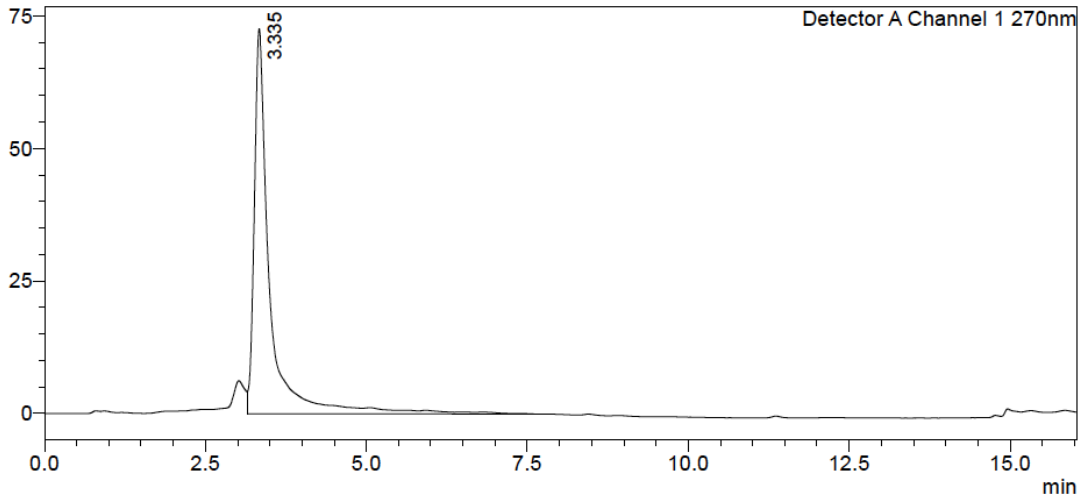


HPLC UV trace of **[EuL$^3$]** (10% $H_2O$ (+0.1% v/v formic acid) in MeOH (+0.1% v/v formic acid) to 100% $H_2O$ (+0.1% v/v formic acid) in MeOH (+0.1% v/v formic acid) over 10 min

**(4-((4-(Dimethylamino)phenyl)ethynyl)pyridin-2-yl)methanol, 2**

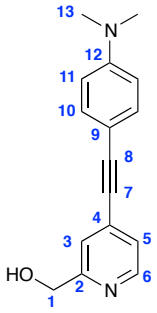

(4-Bromopyridin-2-yl)methanol (0.22 g, 1.18 mmol) and 4-ethynyl-N,N-dimethylaniline (0.20 g, 1.40 mmol) were dissolved in anhydrous THF (10 mL) under argon, followed by addition of pyrrolidine (0.50 mL) and $Pd(TPP)_2Cl_2$ (0.10 g, 0.14 mmol). The reaction mixture was stirred at 50 °C for 24 h and the solvent was removed under reduced pressure. The crude material was purified on a silica column (100% DCM to 50%DCM-50%EtOAc), giving a pale brown oil (0.23 g, 77% yield); $^1$H NMR (295 K, 400 MHz, $CDCl_3$) $\delta_H$ 8.49 (1H, d, $^3J_{H\text{-}H}$ = 6.0 Hz, $H^6$), 7.44 (2H, d, $^3J_{H\text{-}H}$ = 9.0 Hz, $H^{10}$), 7.34 (1H, br s, $H^3$), 7.26 (1H, d, $^3J_{H\text{-}H}$ = 6.0 Hz, $H^5$), 6.67 (2H, d, $^3J_{H\text{-}H}$ = 9.0 Hz, $H^{11}$), 4.77 (2H, s, $H^1$), 3.03 (6H, s, $H^{13}$); $^{13}$C NMR (295 K, 100 MHz, $CDCl_3$) $\delta_C$ 159.1 ($C^2$), 151.0 ($C^{12}$), 148.3 ($C^6$), 133.2 ($C^{10}$, $C^4$), 123.9 ($C^3$), 122.0 ($C^5$), 111.7 ($C^9$), 108.4 ($C^{11}$), 96.3 ($C^8$), 85.3 ($C^7$), 64.1 ($C^1$), 40.1 ($C^{13}$); *m/z* (HRMS$^+$) 253.1344 $[M+H^+]^+$ ($C_{16}H_{17}N_2O$ requires 253.1341).

**Di-*tert*-butyl 2,2'-(4-((4-((4-(dimethylamino)phenyl)ethynyl)pyridin-2-yl)methyl)-1,4,7,10-tetraazacyclododecane-1,7-diyl)diacetate, 4-1**

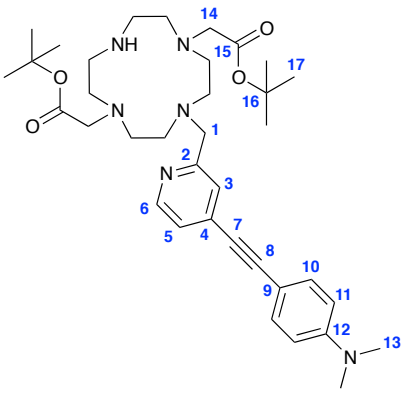

(4-((4-(Dimethylamino)phenyl)ethynyl)pyridin-2-yl)methanol, **2** (64 mg, 0.25 mmol) was dissolved in anhydrous THF (5 mL) under argon, followed by addition of anhydrous triethylamine (30 μL, 0.21 mmol) and methanesulfonyl chloride (15 μL, 0.19 mmol). The reaction mixture was stirred for 2 h at rt and the solvent was removed under reduced pressure. The crude material was dissolved in dichloromethane (20 mL) and washed with water (2 x 10 mL). The organic phase was dried over $MgSO_4$ and the solvent was removed under reduced pressure. The crude yellow oil of **2-Ms** was dissolved in anhydrous acetonitrile (5 mL) and was slowly added upon cooling (ice/acetone bath) and vigorous stirring to the solution of DO2A-$^t$Bu (102 mg, 0.26 mmol) and $K_2CO_3$ (50 mg, 0.36 mmol) in dry acetonitrile (10 mL). The reaction mixture was stirred for 18 h allowed to reach rt and was purified using reverse phase HPLC (10% water to 100% water in MeOH over 9 min, 0.1% formic acid). Collected fractions were neutralised using aqueous ammonia solution, the solvent was removed under reduced pressure and acetonitrile (20 mL) was added. The insoluble ammonium formate was filtered off and the filtrate was collected. The solvent was removed under reduced pressure to afford a clear oil (60 mg, 37% yield); $^1$H NMR (295 K, 400 MHz, $CDCl_3$) $\delta_H$ 8.62 (1H, d, $^3J_{H\text{-}H}$ = 5.0 Hz, $H^6$), 7.44 (2H, d, $^3J_{H\text{-}H}$ = 9.0 Hz, $H^{10}$), 7.34 (1H, br s, $H^3$), 7.27 (1H, d, $^3J_{H\text{-}H}$ = 5.0 Hz, $H^5$), 6.68 (2H, d, $^3J_{H\text{-}H}$ = 9.0 Hz, $H^{11}$), 3.73 (2H, s, $H^1$), 3.04 (6H, s, $H^{13}$), 3.16-2.62 (20H, m, $H^{14}$, cyclen), 1.45 (18H, s, $H^{17}$); $^{13}$C NMR (295 K, 100 MHz, $CDCl_3$) $\delta_C$ 170.6 ($C^{15}$), 157.6 ($C^2$), 150.7 ($C^{12}$), 149.5 ($C^6$), 133.2 ($C^{10}$, $C^4$), 125.2 ($C^3$), 123.9 ($C^5$), 111.7 ($C^9$), 108.2 ($C^{11}$), 96.4 ($C^8$), 85.3 ($C^7$), 81.5 ($C^{16}$), 56.6 ($C^1$), 54.6-46.6 ($C^{14}$, cyclen), 40.1 ($C^{13}$), 28.2 ($C^{17}$); *m/z* (HRMS$^+$) 635.4282 $[M+H^+]^+$ ($C_{36}H_{55}N_6O_4$ requires 635.4285).

**[LnL$^4$] (Ln = Eu, Gd)**

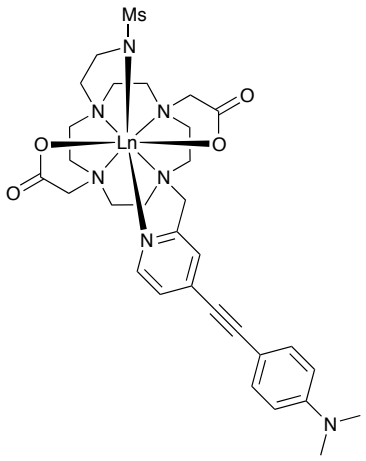

Di-*tert*-butyl 2,2'-(4-((4-((4-(dimethylamino)phenyl)ethynyl)pyridin-2-yl)methyl)-1,4,7,10-tetraazacyclododecane-1,7-diyl)diacetate, **4-1** (54 mg, 0.09 mmol) was dissolved in dry acetonitrile (10 mL), followed by addition of $K_2CO_3$ (40 mg, 0.29 mmol) and 2-(methylsulfonamido)ethyl methanesulfonate (17 mg) was added. The oil bath was heated up to 80 °C and the reaction flask was immersed into the bath. The reaction mixture was stirred for 18 h and the formation of the product was confirmed by LC-MS analysis (m/z (HRMS$^+$) 756.4459 $[M+H^+]^+$ ($C_{39}H_{62}N_7O_6S$ requires 756.4482)). The solvent was removed under reduced pressure and dichloromethane (15 mL) was added, filtered and the solvent was removed under reduced pressure. The crude was dissolved in methanol (4 mL) and aqueous NaOH solution (2.5 M, 2 mL) was added. The mixture was stirred at 60 °C for 3 h. The reaction mixture was neutralised by careful addition of concentrated HCl and $LnCl_3$ (0.2 mmol) was added. The reaction mixture was stirred at 60 °C for 3 h and the product was purified using reverse phase HPLC (10% water to 100% water in MeOH over 9 min, $NH_4HCO_3$ buffer (2 g/L), $t_r$ = 7.6 min), yielding the desired complex as yellow powder (16 mg for **[EuL$^4$]** and 18 mg for **[GdL$^4$]**, 24% and 27% yield over 2 steps, respectively); m/z (HRMS$^+$) 792.2199 $[M+H^+]^+$ ($C_{31}H_{43}N_7O_6S^{151}Eu$ requires 792.2194), m/z (HRMS$^+$) 795.2204 $[M+H^+]^+$ ($C_{31}H_{43}N_7O_6S^{154}Gd$ requires 795.2204); $\tau_{1r}$ (**[GdL$^4$]**) = 1.43 $mM^{-1}s^{-1}$ (pH = 7.0); $\lambda_{abs}$ (**[EuL$^4$]**) = 365 nm, $\varepsilon(H_2O)$ = 28000 $M^{-1}cm^{-1}$, $\tau_{H_2O}$ = 0.30 ms (with HSA).

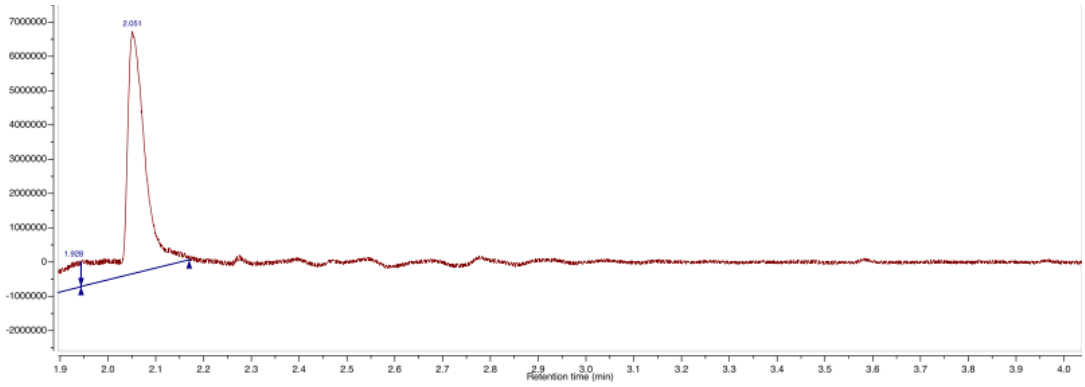


LC-MS UV trace of **[EuL$^4$]** (5% $H_2O$ (+0.1% v/v formic acid) in MeOH (+0.1% v/v formic acid) to 95% $H_2O$ (+0.1% v/v formic acid) in MeOH (+0.1% v/v formic acid) over 3.8 min

**Methyl 4-(2,4,6-trimethoxyphenyl)picolinate, 3**

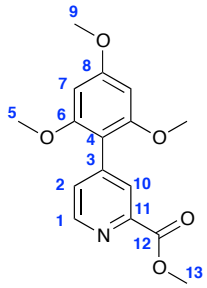


2,4,6-Trimethoxyphenyl boronic acid (200 mg, 0.94 mmol), methyl 4-bromopicolinate (160 mg, 0.74 mmol), caesium carbonate (350 mg, 1.07 mmol) and $Pd(dppf)_2Cl_2$ (20 mg, 0.027 mmol) were placed into a microwaveable vial, sealed, evacuated and refilled with argon. Dry 1,4-dioxane (1.5 mL) was added and two freeze-pump-thaw cycles were carried out to degas the solution. The reaction mixture was microwaved at 150 °C for 40 min. The crude product was purified on a silica column (0% to 5% of MeOH in DCM), giving a mixture of the desired product and 2,4,6-trimethoxybenzene as a side product. The fractions containing both compounds were combined and purified on RP-HPLC (10% to 100% acetonitrile (+0.1% formic acid) in water (+0.1% formic acid) over 10 min). The fractions containing the desired product were combined and neutralised with aqueous ammonia solution. The solvent was removed under reduced pressure, dried and redissolved in acetonitrile. Ammonium formate was filtered off and the solvent was removed under reduced pressure, giving an off-white solid (75 mg, 33% yield); $^1$H NMR (295 K, 400 MHz, $CDCl_3$) $\delta_H$ 8.72 (1H, d, $^3J_{H\text{-}H}$ = 4.5 Hz, $H^1$), 8.18 (1H, m, $H^{10}$), 7.50 (1H, dd, $^3J_{H\text{-}H}$ = 4.5 Hz, $^4J_{H\text{-}H}$ = 1.5 Hz, $H^2$), 6.24 (2H, s, $H^7$), 4.03 (3H, s, $H^{13}$), 3.90 (3H, s, $H^9$), 3.76 (6H, s, $H^5$); $^{13}$C NMR (295 K, 100 MHz, $CDCl_3$) 165.9 ($C^{12}$), 161.8 ($C^8$), 158.2 ($C^6$), 148.6 ($C^1$), 129.8 ($C^2$), 128.2 ($C^{10}$), 108.4 ($C^4$), 90.8 ($C^7$), 55.8 ($C^5$), 55.4 ($C^9$), 52.8 ($C^{13}$); *m/z* (HRMS$^+$) 304.1187 $[M+H^+]^+$ ($C_{16}H_{18}NO_5$ requires 304.1185).

**(4-(2,4,6-Trimethoxyphenyl)pyridin-2-yl)methanol, 4**

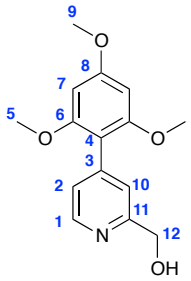

Methyl 4-(2,4,6-trimethoxyphenyl)picolinate, **3** (150 mg, 0.50 mmol) was dissolved in 5 mL of ethanol (200 proof) and $NaBH_4$ (130 mg, 3.42 mmol) was added. The reaction mixture was boiled under reflux at 78 °C for 2 h and the reaction mixture was quenched by adding water (35 mL). The solution was washed with DCM (3 x 40 mL), organic fractions were combined and dried over $MgSO_4$ and the solvent was removed under reduced pressure giving a desired product as an off-white solid (112 mg, 82% yield). $^{1}$H NMR (295 K, 400 MHz, $CDCl_3$) $\delta_H$ 8.55 (1H, $^{3}J_{H\text{-}H}$ = 5.0 Hz, $H^{1}$), 7.25 (1H, m, $H^{10}$), 7.23 (1H, dd, $^{3}J_{H\text{-}H}$ = 5.0 Hz, $^{4}J_{H\text{-}H}$ = 1.4 Hz), 6.24 (2H, s, $H^{7}$), 4.80 (2H, s, $H^{12}$), 3.89 (3H, s, $H^{9}$), 3.75 (6H, s, $H^{5}$); $^{13}$C NMR (295 K, 100 MHz, $CDCl_3$) $\delta_C$ 161.6 ($C^{8}$), 158.2 ($C^{6}$), 158.0 ($C^{11}$), 147.5 ($C^{1}$), 143.7 ($C^{3}$), 125.4 ($C^{2}$), 123.4 ($C^{10}$), 109.4 ($C^{4}$), 90.9 ($C^{7}$), 64.2 ($C^{12}$), 55.8 ($C^{5}$), 55.4 ($C^{9}$); *m/z* (HRMS$^{+}$) 276.1245 $[M+H^{+}]^{+}$ ($C_{15}H_{18}NO_4$ requires 276.1236).

**Diethyl 2,2'-(4-((4-(2,4,6-trimethoxyphenyl)pyridin-2-yl)methyl)-1,4,7,10-tetraazacyclododecane-1,7-diyl)diacetate, 5-1**

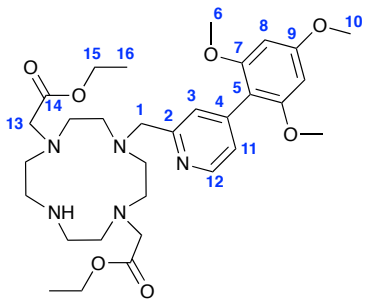

(4-(2,4,6-Trimethoxyphenyl)pyridin-2-yl)methanol, **4** (56 mg, 0.20 mmol) was dissolved in 5 mL of dry THF, followed by addition of 0.1 mL of dry triethylamine (0.72 mmol) and 0.045 mL of MsCl (0.58 mmol). The reaction mixture was stirred for 1 h at rt and the solvent was removed under reduced pressure. The crude material

was dissolved in DCM (25 mL), washed with water (2 x 25 mL) and dried over $MgSO_4$. The solvent was removed under reduced pressure, dried and dissolved in dry acetonitrile (3 mL). DO2A-ethyl ester (100 mg, 0.29 mmol) was dissolved in dry acetonitrile (9 mL) and $K_2CO_3$ was added (150 mg, 1.09 mmol). The reaction mixture was cooled down using an ice bath and stirred for 5 minutes, followed by dropwise addition of the **4-Ms** within 5 min. The reaction mixture was allowed to reach rt and stirred for 18h. The reaction mixture was filtered and purified on RP-HPLC (10% to 100% acetonitrile (+0.1% formic acid) in water (+0.1% formic acid) over 10 min). The fractions containing the desired product were combined and neutralised with aqueous ammonia solution. The solvent was removed under reduced pressure, dried and redissolved in acetonitrile. Ammonium formate was filtered off and the solvent was removed under reduced pressure, giving a transparent oil (50 mg, 42% yield); $^1$H NMR (295 K, 700 MHz, $CDCl_3$) $\delta_H$ 8.60 (1H, $^3J_{H-H}$ = 5.5 Hz, $H^{12}$), 7.19 (2H, m, $H^3$, $H^{11}$), 6.20 (2H, s, $H^8$), 4.11 (4H, t, $^3J_{H-H}$ = 7.0 Hz, $H^{15}$), 3.85 (3H, s, $H^{10}$), 3.72 (2H, m, $H^1$), 3.70 (6H, s, $H^6$), 3.23 (4H, s, $H^{13}$), 3.11-2.62 (16H, m, cyclen), 1.23 (6H, $^3J_{H-H}$ = 7.0 Hz, $H^{16}$); $^{13}$C NMR (295 K, 176 MHz, $CDCl_3$) $\delta_C$ 171.4 ($C^{14}$), 161.6 ($C^9$), 158.0 ($C^7$), 156.2 ($C^2$), 148.7 ($C^{12}$), 143.5 ($C^4$), 126.8 ($C^{11}$), 125.5 ($C^3$), 109.3 ($C^5$), 90.8 ($C^8$), 60.5 ($C^{15}$), 57.1 ($C^1$), 55.7 ($C^6$), 55.6 ($C^{13}$), 55.4 ($C^{10}$), 54.7, 51.0, 50.5, 46.3 (cyclen), 14.2 ($C^{16}$); *m/z* (HRMS$^+$) 602.3557 $[M+H^+]^+$ ($C_{31}H_{48}N_5O_7$ requires 602.3554).

**Diethyl 2,2'-(4-(2-(methylsulfonamido)ethyl)-10-((4-(2,4,6-trimethoxyphenyl)pyridin-2-yl)methyl)-1,4,7,10-tetraazacyclododecane-1,7-diyl)diacetate ($L^5$)**

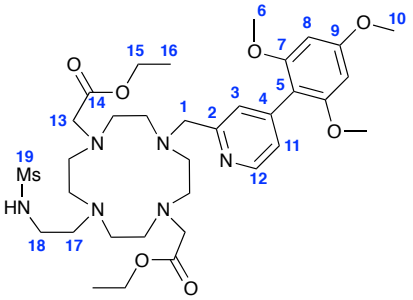


Diethyl 2,2'-(4-((4-(2,4,6-trimethoxyphenyl)pyridin-2-yl)methyl)-1,4,7,10-tetraazacyclo-dodecane-1,7-diyl)diacetate, **5-1** (50 mg, 0.083 mmol) was dissolved in dry acetonitrile (5 mL), followed by addition of $K_2CO_3$ (28 mg, 0.20 mmol) and 2-

(methylsulfonamido)ethyl methanesulfonate (18 mg, 0.083 mmol). The reaction mixture was immersed into an oil bath and heated up initially to 80 °C and stirred at this temperature for 18 h. The reaction mixture was filtered and purified on RP-HPLC (10% to 100% acetonitrile (+0.1% formic acid) in water (+0.1% formic acid) over 10 min). The fractions containing the desired product were combined and neutralised with aqueous ammonia solution. The solvent was removed under reduced pressure, dried and redissolved in acetonitrile. Ammonium formate was filtered off and the solvent was removed under reduced pressure, giving a transparent oil (25 mg, 42% yield); $^{1}$H NMR (295 K, 700 MHz, $CDCl_3$) $\delta_H$ 8.53 (1H, $^{3}J_{H\text{-}H}$ = 5.0 Hz, $H^{12}$), 7.30 (1H, m, $H^{3}$), 7.27 (1H, dd, $^{3}J_{H\text{-}H}$ = 5.0 Hz, $^{4}J_{H\text{-}H}$ = 1.5 Hz, $H^{11}$), 6.19 (2H, s, $H^{8}$), 4.14 (2H, m, $H^{1}$), 4.13 (4H, q, $^{3}J_{H\text{-}H}$ = 7.0 Hz, $H^{15}$), 3.85 (3H, s, $H^{10}$), 3.72 (6H, s, $H^{6}$), 3.48 (2H, m, $H^{18}$), 3.40 (4H, s, $H^{13}$), 3.30 (2H, m, $H^{17}$), 3.22 – 2.92 (16H, m, cyclen), 2.96 (3H, s, $H^{19}$), 1.24 (6H, t, $^{3}J_{H\text{-}H}$ = 7.0 Hz, $H^{16}$); $^{13}$C NMR (295 K, 176 MHz, $CDCl_3$) $\delta_C$ 170.7 ($C^{14}$), 166.6 ($C^{9}$), 161.8 ($C^{7}$), 153.1 ($C^{2}$), 148.7 ($C^{12}$), 144.0 ($C^{4}$), 128.0 ($C^{3}$), 126.2 ($C^{11}$), 90.9 ($C^{8}$), 108.6 ($C^{6}$), 60.8 ($C^{15}$), 59.1 ($C^{1}$), 56.0 ($C^{13}$), 55.8 ($C^{6}$), 55.4 ($C^{10}$), 53.4 ($C^{18}$), 53.1, 52.8, 49.9, 49.8 (cyclen), 39.1 ($C^{19}$), 38.7 ($C^{17}$), 14.1 ($C^{16}$); *m/z* (HRMS$^{+}$) 723.3771 $[M+H^{+}]^{+}$ ($C_{34}H_{55}N_6O_9S$ requires 723.3751).

**[LnL$^{5}$] (Ln = Eu, Tb, Dy, Y)**

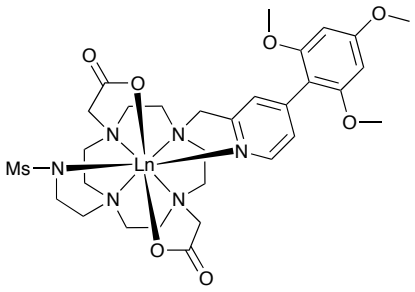


The ligand, **L$^{5}$**, (0.020 mmol) was dissolved in aqueous NaOH solution (0.5 M, 4 mL) and stirred at 60 °C for 2 h. The solution was neutralised by addition of 1 M HCl and $LnCl_3$ (0.030 mmol) was added. The reaction mixture was stirred at rt for 1 h and pH was adjusted to 6.5. The reaction mixture was stirred for another hour and a desired complex was purified on RP-HPLC (Chromolith® column, 0% to 100% acetonitrile in water). The combined fractions were freeze-dried to give a desired complex as an off-white solid in quantitative yield.

**[EuL$^5$]**: *m/z* (HRMS$^+$) 815.2113 [M+H$^+$]$^+$ ($C_{30}H_{44}N_6O_9S^{151}Eu$ requires 815.2089).

**[TbL$^5$]**: *m/z* (HRMS$^+$) 823.2137 [M+H$^+$]$^+$ ($C_{30}H_{44}N_6O_9STb$ requires 823.2144); ε($H_2O$) = 12800 $M^{-1}cm^{-1}$; τ($H_2O$) = 1.14 ms (pH = 8), τ($D_2O$) = 1.92 ms (pD = 8.4)

**[DyL$^5$]**: *m/z* (HRMS$^+$) 824.2172 [M+H$^+$]$^+$ ($C_{30}H_{44}N_6O_9SDy$ requires 824.2143).

**[YL$^5$]**: *m/z* (HRMS$^+$) 753.1941 [M+H$^+$]$^+$ ($C_{30}H_{44}N_6O_9SYb$ requires 753.1949).

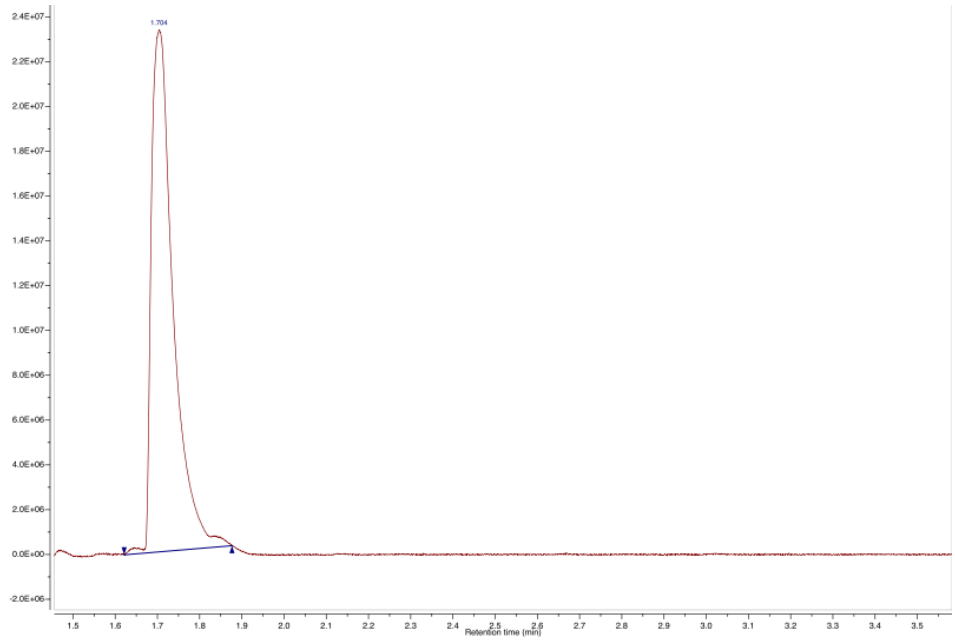


LC-MS UV trace of **[YL$^5$]** (0% $H_2O$ (+0.1% v/v formic acid) in MeOH (+0.1% v/v formic acid) to 99% $H_2O$ (+0.1% v/v formic acid) in MeOH (+0.1% v/v formic acid) over 5.0 min

**Methyl 4-(4-(dimethylamino)phenyl)picolinate, 5**

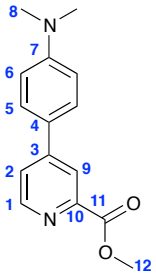


4-Dimethylaminephenyl boronic acid (200 mg, 1.21 mmol), methyl 4-bromopicolinate (200 mg, 0.93 mmol), caesium carbonate (350 mg, 1.07 mmol) and $Pd(TPP)_2Cl_2$ (25 mg, 0.036 mmol) were placed into a microwaveable vial, sealed, evacuated and refilled with argon. Dry 1,4-dioxane (1.3 mL) was added and two freeze-pump-thaw cycles were carried out to degas the solution. The reaction mixture was microwaved at 150 °C for 60 minutes. The crude product was purified on a silica column (0% to 10% of EtOAc in DCM), giving a desired product as a yellow solid

(72 mg, 30% yield); $^{1}$H NMR (295 K, 700 MHz, $CDCl_3$) $\delta_H$ 8.64 (1H, d, $^{3}J_{H\text{-}H}$ = 5.0 Hz, $H^{1}$), 8.32 (1H, m, $H^{9}$), 7.61 (2H, d, $^{3}J_{H\text{-}H}$ = 8.50 Hz, $H^{5}$), 7.60 (1H, m, $H^{2}$), 6.76 (2H, s, d, $^{3}J_{H\text{-}H}$ = 8.50 Hz, $H^{6}$), 4.00 (3H, s, $H^{12}$), 3.01 (6H, s, $H^{8}$); $^{13}$C NMR (295 K, 176 MHz, $CDCl_3$) $\delta_C$ 166.1 ($C^{11}$), 151.3 ($C^{7}$), 150.0 ($C^{1}$), 149.3 ($C^{10}$), 148.2 ($C^{3}$), 127.7 ($C^{5}$), 123.7 ($C^{4}$), 123.0 ($C^{2}$), 121.6 ($C^{9}$), 112.4 ($C^{6}$), 52.9 ($C^{12}$), 40.2 ($C^{8}$); *m/z* (HRMS$^{+}$) 257.1297 $[M+H^{+}]^{+}$ ($C_{15}H_{17}N_2O_2$ requires 257.1290).

**(4-(4-(Dimethylamino)phenyl)pyridin-2-yl)methanol, 6**

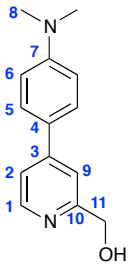


Methyl 4-(4-(dimethylamino)phenyl)picolinate, **5** (64 mg, 0.25 mmol) was dissolved in ethanol (7 mL, 200 proof) and $NaBH_4$ (122 mg, 3.21 mmol) was added. The reaction mixture was boiled under reflux at 78 °C for 2 h and the reaction mixture was quenched by adding water (35 mL). The solution was washed with DCM (3 x 40 mL), organic fractions were combined and dried over $MgSO_4$ and the solvent was removed under reduced pressure giving a desired product as an off-white solid (44 mg, 77% yield). $^{1}$H NMR (295 K, 700 MHz, $CDCl_3$) $\delta_H$ 8.49 (1H, m, $H^{1}$), 7.57 (2H, d, $^{3}J_{H\text{-}H}$ = 9.0 Hz, $H^{5}$), 7.43 (1H, m, $H^{2}$), 7.38 (1H, m, $H^{9}$), 6.77 (2H, d, $^{3}J_{H\text{-}H}$ = 9.0 Hz, $H^{6}$), 4.78 (2H, s, $H^{11}$), 3.01 (6H, s, $H^{8}$); $^{13}$C NMR (295 K, 176 MHz, $CDCl_3$) $\delta_C$ 159.3 ($C^{10}$), 151.1 ($C^{3}$), 148.9 ($C^{7}$), 148.6 ($C^{1}$), 127.7 ($C^{5}$), 124.9 ($C^{4}$), 119.2 ($C^{9}$), 116.9 ($C^{2}$), 112.4 ($C^{6}$), 64.4 ($C^{11}$), 40.2 ($C^{8}$); *m/z* (HRMS$^{+}$) 229.1340 $[M+H^{+}]^{+}$ ($C_{14}H_{17}N_2O$ requires 229.1341).

**Diethyl 2,2'-(4-((4-(4-(dimethylamino)phenyl)pyridin-2-yl)methyl)-1,4,7,10-tetraazacyclododecane-1,7-diyl)diacetate, 6-1**

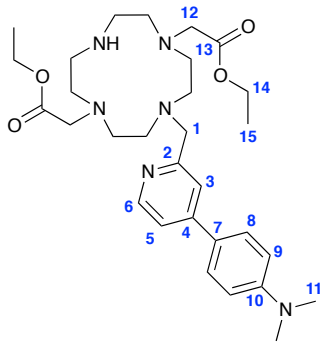


(4-(4-(Dimethylamino)phenyl)pyridin-2-yl)methanol, **6** (44 mg, 0.19 mmol) was dissolved in 4 mL of dry THF, followed by addition of 0.1 mL of dry triethylamine (0.72 mmol) and 0.025 mL of MsCl (0.32 mmol). The reaction mixture was stirred for 1 h at rt and the solvent was removed under reduced pressure. The crude material was dissolved in DCM (25 mL), washed with water (2 x 25 mL) and dried over $MgSO_4$. The solvent was removed under reduced pressure, dried and dissolved in dry acetonitrile (3 mL). DO2A-ethyl ester (68 mg, 0.20 mmol) was dissolved in dry acetonitrile (9 mL) and $K_2CO_3$ was added (96 mg, 0.70 mmol). The reaction mixture was cooled down using ice bath and stirred for 5 min, followed by dropwise addition of the **6-Ms** within 5 min. The reaction mixture was allowed to reach rt and stirred for 18 h. The reaction mixture was filtered and purified on RP-HPLC (10% to 100% acetonitrile (+0.1% formic acid) in water (+0.1% formic acid) over 10 min). The fractions containing the desired product were combined and neutralised with aqueous ammonia solution. The solvent was removed under reduced pressure, dried and redissolved in acetonitrile. Ammonium formate was filtered off and the solvent was removed under reduced pressure, giving a colourless oil (27 mg, 26% yield); $^1$H NMR (295 K, 700 MHz, $CDCl_3$) $\delta_H$ 8.59 (1H, d, $^3J_{H\text{-}H}$ = 5.0 Hz, $H^6$), 7.55 (2H, d, $^3J_{H\text{-}H}$ = 9.0 Hz, $H^8$), 7.40 (1H, dd, $^3J_{H\text{-}H}$ = 5.0 Hz, $^4J_{H\text{-}H}$ = 2.0 Hz, $H^5$), 7.38 (1H, m, $H^3$), 6.77 (2H, d, $^3J_{H\text{-}H}$ = 9.0 Hz, $H^9$), 4.10 (4H, q, $^3J_{H\text{-}H}$ = 7.0 Hz, $H^{14}$), 3.75 (2H, s, $H^1$), 3.25 (4H, s, $H^{12}$), 3.19-2.60 (16H, m, cyclen), 3.02 (6H, s, $H^{11}$), 1.22 (6H, t, $^3J_{H\text{-}H}$ = 7.0 Hz, $H^{15}$); $^{13}$C NMR (295 K, 176 MHz, $CDCl_3$) $\delta_C$ 171.3 ($C^{13}$), 157.5 ($C^2$), 151.2 ($C^{10}$), 149.8 ($C^6$), 148.8 ($C^4$), 127.6 ($C^8$), 124.4 ($C^7$), 120.2 ($C^3$), 119.2 ($C^5$), 112.4 ($C^9$), 60.5 ($C^{14}$), 57.6 ($C^1$), 55.6 ($C^{12}$), 54.7-46.2 (cyclen), 40.2 ($C^{11}$), 14.2 ($C^{15}$); *m/z* (HRMS$^+$) 555.3663 $[M+H^+]^+$ ($C_{30}H_{47}N_6O_4$ requires 555.3659).

**[YbL$^6$]**

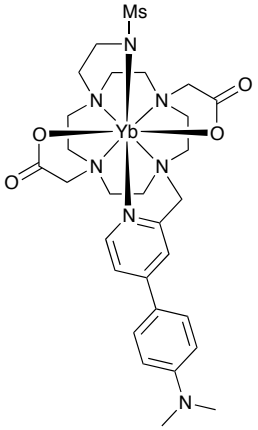


Diethyl 2,2'-(4-((4-(4-(dimethylamino)phenyl)pyridin-2-yl)methyl)-1,4,7,10-tetraazacyclododecane-1,7-diyl)diacetate, **6-1** (27 mg, 0.049 mmol) was dissolved in dry acetonitrile (5mL), followed by addition of $K_2CO_3$ (11 mg, 0.14 mmol) and 2-(methylsulfonamido)ethyl methanesulfonate (18 mg, 0.049 mmol). The reaction mixture was immersed into an oil bath initially heated to 80 °C and stirred at this temperature for 18 h. The reaction mixture was filtered and on purified on RP-HPLC (0% to 100% acetonitrile (+0.1% formic acid) in water (+0.1% formic acid) over 10 min). The fractions containing the desired product and the compound with two sulfonamide arms were combined and neutralised with aqueous ammonia solution. The solvent was removed under reduced pressure, dried and redissolved in acetonitrile. Ammonium formate was filtered off and the solvent was removed under reduced pressure, giving a transparent oil. The mixture of two products was dissolved in 0.5M NaOH (4 mL) and stirred at 60°C for 2h. The solution was neutralised by addition of 1 M HCl and $YbCl_3$ (0.060 mmol) was added. The reaction mixture was stirred at rt for 1 h and pH was adjusted to 6.5. The reaction mixture was stirred for another hour and excess of $Yb^{3+}$ was precipitated in the form of $Yb(OH)_3$ by adjusting the pH up to 10 with 0.5 M NaOH, followed by neutralization by addition of 0.5 M HCl. The mixture was purified on RP-HPLC (Chromolith® column, 10% to 100% acetonitrile in water). The fractions containing the desired product were combined and freeze-dried to give a desired complex as an off-white solid; *m*/*z* (HRMS$^+$) 753.1941 $[M+H^+]^+$ ($C_{30}H_{44}N_6O_9S^{89}Yb$ requires 753.1949).

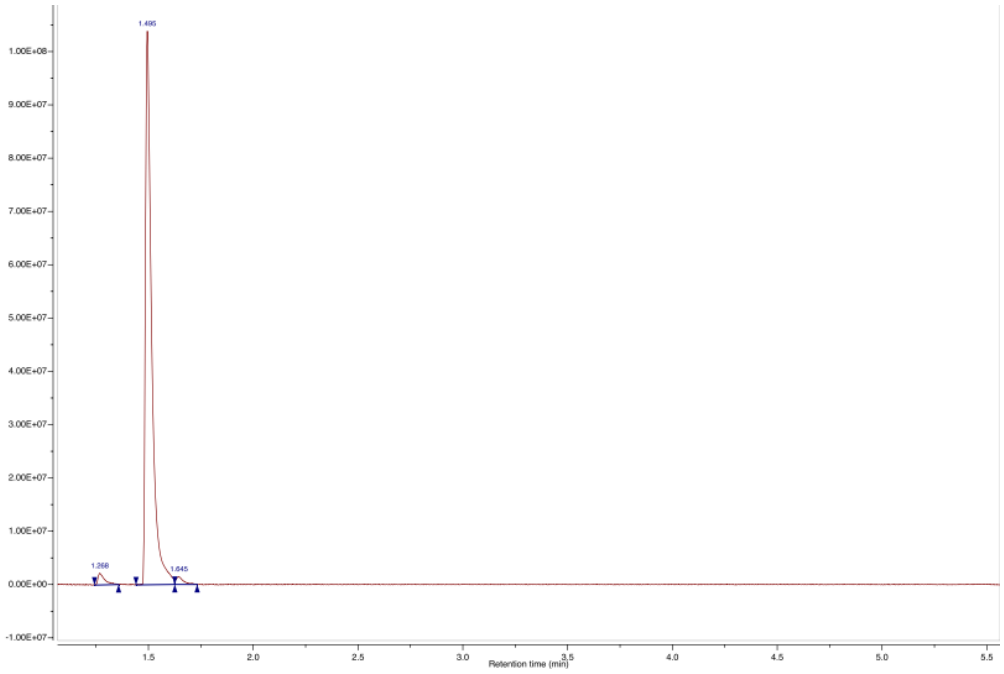


LC-MS UV trace of **[YbL$^6$]** (0% $H_2O$ (+0.1% v/v formic acid) in MeOH (+0.1% v/v formic acid) to 99% $H_2O$ (+0.1% v/v formic acid) in MeOH (+0.1% v/v formic acid) over 5.0 min

**Di-*tert*-butyl 2,2'-(4-((6-(methoxycarbonyl)-4-((4-methoxyphenyl)ethynyl)pyridine -2-yl)methyl)-1,4,7,10-tetraazacyclododecane-1,7-diyl)diacetate, 7-1**

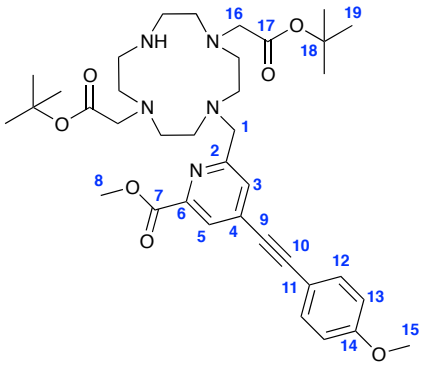

Methyl 6-(hydroxymethyl)-4-((4-methoxyphenyl)ethynyl)picolinate (60 mg, 0.20 mmol) was dissolved in dry THF (3 mL), followed by addition of dry triethylamine (0.1 mL, 0.72 mmol) and MsCl (30 mL, 0.38 mmol). The reaction mixture was stirred at rt for 1 h and the solvent was removed under reduced pressure. The crude material was redissolved in DCM (15 mL) and was washed with water (2 x 15 mL). The organic fraction was dried over $MgSO_4$ and the solvent was removed under reduced pressure, dried and redissolved in dry acetonitrile (3 mL). DO2A-tBu ester (101 mg, 0.25 mmol) was dissolved in dry acetonitrile (10 mL) and $K_2CO_3$ (100 mg, 0.72 mmol) was added. The reaction was cooled down using an ice bath and stirred

for 5 min. The mesylate solution was added dropwise within 5 min. The reaction mixture was allowed to reach rt and stirred for 18 h. The reaction mixture was filtered and purified on RP-HPLC (10% to 100% acetonitrile (+0.1% formic acid) in water (+0.1% formic acid) over 9 min). The fractions containing the desired product were combined and neutralised with aqueous ammonia solution. The solvent was removed under reduced pressure, dried and redissolved in acetonitrile. Ammonium formate was filtered off and the solvent was removed under reduced pressure, giving a transparent oil (63 mg, 46% yield); $^{1}$H NMR (295 K, 700 MHz, $CDCl_3$) $\delta_H$ 8.05 (1H, s, $H^5$), 7.54 (1H, s, $H^3$), 7.49 (2H, d, $^{3}J_{H\text{-}H}$ = 9.0 Hz, $H^{12}$), 6.90 (2H, d, $^{3}J_{H\text{-}H}$ = 9.0 Hz, $H^{12}$), 3.99 (3H, s, $H^8$), 3.83 (3H, s, $H^{15}$), 3.79 (2H, m, $H^1$), 3.19-2.64 (16H, m, cyclen), 3.13 (4H, s, $H^{16}$), 1.41 (18H, s, $H^{19}$); $^{13}$C NMR (295 K, 176 MHz, $CDCl_3$) $\delta_C$ 170.4 ($C^{17}$), 165.4 ($C^7$), 160.7 ($C^{14}$), 158.8 ($C^2$), 147.7 ($C^6$), 133.9 ($C^4$), 133.6 ($C^{12}$), 128.3 ($C^3$), 125.7 ($C^5$), 114.4 ($C^{13}$), 113.4 ($C^{11}$), 96.5 ($C^{10}$), 84.9 ($C^9$), 81.5 ($C^{18}$), 57.9 ($C^1$), 56.5 ($C^{16}$), 55.4 ($C^{15}$), 55.0-46.2 (cyclen), 53.2 ($C^8$), 28.1 ($C^{19}$); *m/z* (HRMS$^+$) 680.4027 $[M+H^+]^+$ ($C_{37}H_{54}N_5O_7$ requires 680.4023).

**Di-*tert*-butyl 2,2'-(4-((6-((bis(pyridin-2-ylmethyl)amino)methyl)pyridin-2-yl)methyl)-10-((6-(methoxycarbonyl)-4-((4-methoxyphenyl)ethynyl)pyridin-2-yl)methyl)-1,4,7,10-tetraazacyclododecane-1,7-diyl)diacetate ($L^7$)**

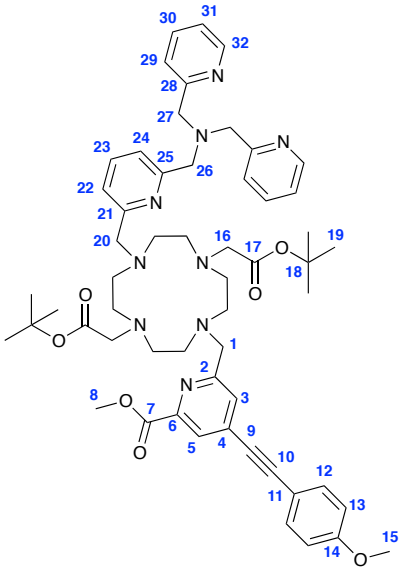

Di-tert-butyl 2,2'-(4-((6-(methoxycarbonyl)-4-((4-methoxyphenyl)ethynyl)pyridin-2-yl)methyl)-1,4,7,10-tetraazacyclododecane-1,7-diyl)diacetate, **7-1** (23 mg, 0.034 mmol) was dissolved in dry acetonitrile (5 mL), followed by addition of $Cs_2CO_3$ (20

mg, 0.06 mmol), 1-(6-(chloromethyl)pyridin-2-yl)-N,N-bis(pyridin-2-ylmethyl)methanamine (20 mg, 0.059 mmol) and KI (20 mg, 0.12 mmol) was added. The reaction mixture was stirred at 70 °C for 18 h. The reaction mixture was filtered and purified on RP-HPLC (10% to 100% acetonitrile (+0.1% formic acid) in water (+0.1% formic acid) over 10 min). The fractions containing the desired product were combined and neutralised with aqueous ammonia solution. The solvent was removed under reduced pressure, dried and redissolved in acetonitrile. Ammonium formate was filtered off and the solvent was removed under reduced pressure, giving a colourless oil (20 mg, 59% yield); $^{1}$H NMR (295 K, 600 MHz, $CDCl_3$) $\delta_H$ 8.51 (2H, m, $H^{32}$), 8.06 (1H, s, $H^{5}$), 7.66 (4H, m, $H^{3}$, $H^{23}$, $H^{30}$), 7.56-7.53 (3H, m, $H^{22}$, $H^{29}$), 7.47 (2H, d, $^{3}J_{H\text{-}H}$ = 9.0 Hz, $H^{12}$), 7.42 (1H, d, $^{3}J_{H\text{-}H}$ = 8.0 Hz, $H^{24}$), 7.14 (2H, m, $H^{31}$), 6.88 (2H, d, $^{3}J_{H\text{-}H}$ = 9.0 Hz, $H^{12}$), 4.54 (2H, s, $H^{20}$), 4.20 (2H, s, $H^{1}$), 3.95 (3H, s, $H^{8}$), 3.85 (6H, m, $H^{27}$, $H^{28}$), 3.82 (3H, s, $H^{15}$), 3.36 (4H, s, $H^{16}$), 3.34-2.92 (16H, m, cyclen), 1.39 (18H, s, $H^{19}$); $^{13}$C NMR (295 K, 151 MHz, $CDCl_3$) $\delta_C$ 169.8 ($C^{17}$), 165.1 ($C^{7}$), 160.7 ($C^{14}$), 159.4 ($C^{25}$), 159.0 ($C^{28}$), 157.6 ($C^{2}$), 152.6 ($C^{21}$), 149.0 ($C^{32}$), 147.4 ($C^{6}$), 137.6 ($C^{23}$), 136.6 ($C^{30}$), 134.0 ($C^{4}$), 133.6 ($C^{12}$), 128.7 ($C^{3}$), 125.8 ($C^{5}$), 123.8 ($C^{24}$), 122.9 ($C^{29}$), 122.5 ($C^{22}$), 122.1 ($C^{31}$), 114.2 ($C^{13}$), 113.5 ($C^{11}$), 96.4 ($C^{10}$), 85.0 ($C^{9}$), 81.8 ($C^{18}$), 60.2 ($C^{26}$, $C^{27}$), 59.20 ($C^{1}$), 57.20 ($C^{20}$), 56.8 ($C^{16}$), 55.3 ($C^{15}$), 53.1-49.6 (cyclen), 53.0 ($C^{8}$), 28.1 ($C^{19}$); *m*/*z* (HRMS$^{+}$) 982.5573 $[M+H^{+}]^{+}$ ($C_{56}H_{72}N_9O_7$ requires 982.5555).

**[EuL$^{7}$]**

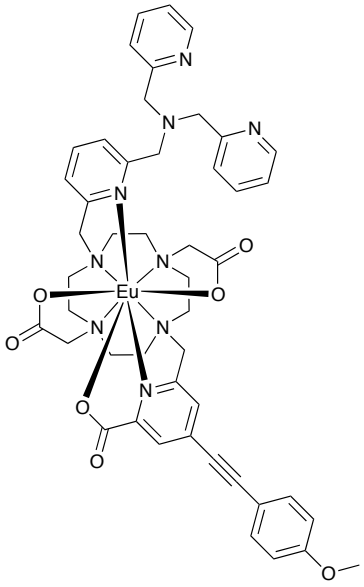

The ligand, $\mathbf{L}^7$, (20 mg, 0.020 mmol) was dissolved in aqueous NaOH (0.5 M, 4 mL) and stirred at 60 °C for 2 h. The solution was neutralised by addition of 1 M HCl and $EuCl_3$ (0.040 mmol) was added. The reaction mixture was stirred at rt for 1 h, pH was adjusted to 6.5 and the reaction mixture was stirred for another hour. Aqueous ammonia solution was added dropwise to pH 10 in order to precipitate excess europium in the form of $Eu(OH)_3$, which was separated by centrifugation. The solution was neutralised again and was left in the fridge, causing precipitation of the desired complex as an off-white solid, which was separated by decanting solution (8 mg, 40% yield); *m/z* (HRMS$^+$) 1004.3085 $[M+H^+]^+$ ($C_{47}H_{51}N_9O_7{}^{151}Eu$ requires 1004.3110); $\varepsilon(H_2O)$ = 20,000 $M^{-1}cm^{-1}$; $\tau(H_2O)$ = 0.54 ms (pH = 7.4), $\tau(D_2O)$ = 0.80 ms (pD = 7.8).

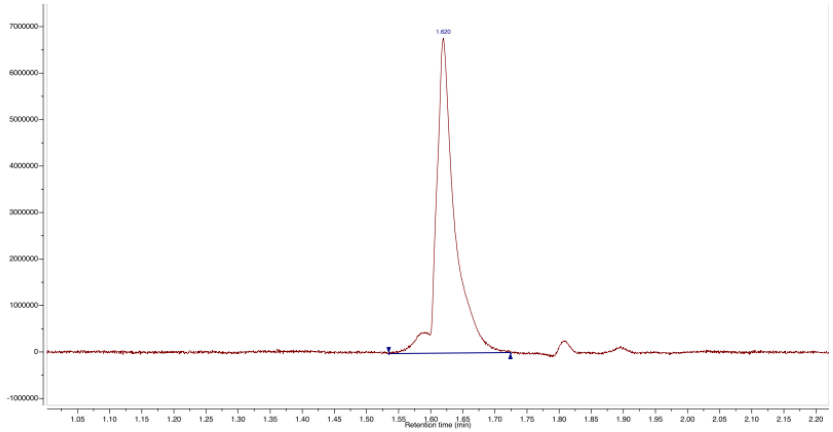

LC-MS UV trace of **[EuL$^7$]** (5% $H_2O$ (+0.1% v/v formic acid) in MeOH (+0.1% v/v formic acid) to 95% $H_2O$ (+0.1% v/v formic acid) in MeOH (+0.1% v/v formic acid) over 3.8 min

**_N_-((6-(Chloromethyl)pyridin-2-yl)methyl)-_N_-(pyridin-2-ylmethyl)ethanamine, 7**

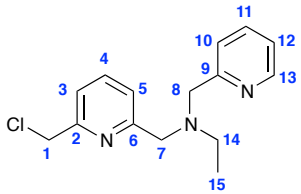


2,6-*Bis*(chloromethyl)pyridine (0.97 g, 5.51 mmol), *N*-(pyridin-2-ylmethyl)ethanamine (0.25 g, 1.84 mmol) and $K_2CO_3$ (0.25 g, 1.84 mmol) were dissolved in dry acetonitrile (15 mL) and the mixture was stirred at 70 °C for 18 h. The solution was filtered off, the solvent was removed under reduced pressure and the crude was purified on a silica column (0% to 66% of EtOAc in DCM), giving a

desired product as a pale yellow oil (110 mg, 22% yield); $^{1}$H NMR (295 K, 600 MHz, $CDCl_3$) $\delta_H$ 8.50 (1H, m, $H^{13}$), 7.66 (1H, t, $^{3}J_{H-H}$ = 8.0 Hz, $H^{4}$), 7.62 (1H, td, $^{3}J_{H-H}$ = 8.0 Hz, $^{4}J_{H-H}$ = 2.0 Hz, $H^{11}$), 7.51 (2H, m, $H^{10}$, $H^{5}$), 7.30 (1H, d, $^{3}J_{H-H}$ = 7.0 Hz, $H^{3}$), 7.11 (1H, m, $H^{12}$), 4.62 (2H, s, $H^{1}$), 3.81 (4H, s, $H^{7}$, $H^{8}$), 2.63 (2H, q, $^{3}J_{H-H}$ = 7.0 Hz, $H^{14}$), 1.09 (3H, t, $^{3}J_{H-H}$ = 7.0 Hz, $H^{15}$); $^{13}$C NMR (295 K, 151 MHz, $CDCl_3$) $\delta_C$ 160.1 ($C^{2}$), 159.9 ($C^{9}$), 155.7 ($C^{6}$), 149.0 ($C^{13}$), 137.3 ($C^{4}$), 136.3 ($C^{11}$), 122.8 ($C^{10}$), 122.0 ($C^{5}$), 121.8 ($C^{3}$), 120.8 ($C^{12}$), 59.9-59.7 ($C^{7}$, $C^{8}$), 48.3 ($C^{14}$), 46.8 ($C^{1}$), 12.0 ($C^{15}$); *m/z* (HRMS$^{+}$) 276.1269 $[M+H^{+}]^{+}$ ($C_{15}H_{19}N_3Cl$ requires 276.1269).

**Diethyl 2,2'-(4-((6-((ethyl(pyridin-2-ylmethyl)amino)methyl)pyridin-2-yl)methyl)-10-((6-(methoxycarbonyl)-4-((4-methoxyphenyl)ethynyl)pyridin-2-yl)methyl)-1,4,7,10-tetraazacyclododecane-1,7-diyl)diacetate ($L^{8}$)**

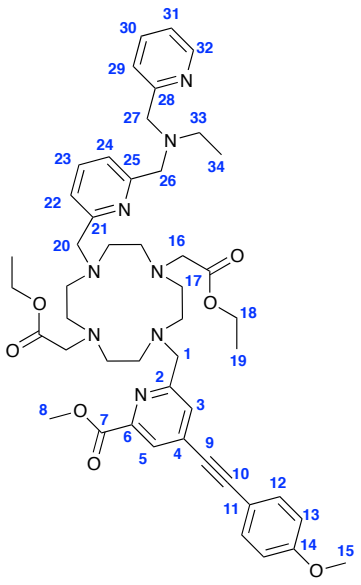

Diethyl 2,2'-(4-((6-(methoxycarbonyl)-4-((4-methoxyphenyl)ethynyl)pyridin-2-yl)methyl)-1,4,7,10-tetraazacyclododecane-1,7-diyl)diacetate (38 mg, 0.061 mmol) was dissolved in dry acetonitrile (10 mL), followed by addition of $Cs_2CO_3$ (30 mg, 0.09 mmol), N-((6-(chloromethyl)pyridin-2-yl)methyl)-N-(pyridin-2-ylmethyl)ethanamine, **7** (30 mg, 0.11 mmol) and KI (20 mg, 0.12 mmol) was added. The reaction mixture was stirred at 70 °C for 18 h. The reaction mixture was filtered and purified on RP-HPLC (10% to 100% acetonitrile (+0.1% formic acid) in water (+0.1% formic acid) over 10 min). The fractions containing the desired product were combined and neutralised with aqueous ammonia solution. The solvent was removed under reduced pressure, dried and redissolved in acetonitrile. Ammonium formate

was filtered off and the solvent was removed under reduced pressure, giving a colourless oil (15 mg, 28% yield); $^{1}$H NMR (295 K, 700 MHz, $CDCl_3$) $\delta_H$ 8.51 (1H, m, $^{3}J_{H\text{-}H}$ = 5.0 Hz, $H^{32}$), 7.68 (2H, t, $^{3}J_{H\text{-}H}$ = 8.0 Hz, $H^{23}$, $H^{30}$), 7.64 (1H, br s, $H^{3}$), 7.52 (2H, d, $^{3}J_{H\text{-}H}$ = 6.0 Hz, $H^{22}$, $H^{29}$), 7.48 (2H, d, $^{3}J_{H\text{-}H}$ = 8.0 Hz, $H^{12}$), 7.44 (1H, d, $^{3}J_{H\text{-}H}$ = 8.0 Hz, $H^{24}$), 7.17 (1H, m, $H^{31}$), 6.89 (2H, d, $^{3}J_{H\text{-}H}$ = 8.0 Hz, $H^{13}$), 4.66 (2H, s, $H^{20}$), 4.29 (2H, s, $H^{1}$), 4.11 (2H, q, $^{3}J_{H\text{-}H}$ = 7.0 Hz, $H^{18}$), 3.97 (3H, s, $H^{8}$), 3.86 (2H, s, $H^{27}$), 3.83 (5H, m, $H^{15}$, $H^{26}$), 3.54 (4, s, $H^{16}$), 3.45-2.97 (16H, m, cyclen), 2.66 (2H, q, $^{3}J_{H\text{-}H}$ = 7.0 Hz, $H^{33}$), 1.21 (6H, q, $^{3}J_{H\text{-}H}$ = 7.0 Hz, $H^{19}$), 1.12 (3H, q, $^{3}J_{H\text{-}H}$ = 7.0 Hz, $H^{34}$); $^{13}$C NMR (295 K, 176 MHz, $CDCl_3$) $\delta_C$ 170.5 ($C^{17}$), 165.0 ($C^{7}$), 160.7 ($C^{14}$), 159.6 ($C^{25}$), 158.9 ($C^{28}$), 157.2 ($C^{2}$), 151.8 ($C^{21}$), 148.6 ($C^{32}$), 147.7 ($C^{6}$), 137.6 ($C^{23}$), 136.9 ($C^{30}$), 134.1 ($C^{4}$), 133.7 ($C^{12}$), 128.9 ($C^{3}$), 125.9 ($C^{5}$), 124.2 ($C^{24}$), 123.1 ($C^{29}$), 122.8 ($C^{22}$), 122.3 ($C^{31}$), 114.2 ($C^{13}$), 113.5 ($C^{11}$), 96.6 ($C^{10}$), 84.9 ($C^{9}$), 61.0 ($C^{18}$), 59.6 ($C^{27}$), 59.4 ($C^{26}$), 59.1 ($C^{1}$), 57.0 ($C^{20}$), 56.1 ($C^{16}$), 55.4 ($C^{15}$), 53.0-49.3 (cyclen), 53.0 ($C^{8}$), 48.4 ($C^{33}$), 14.1 ($C^{19}$), 11.9 ($C^{34}$); *m/z* (HRMS$^{+}$) 863.4849 $[M+H^{+}]^{+}$ ($C_{48}H_{63}N_8O_7$ requires 863.4820).

**[EuL$^{8}$]**

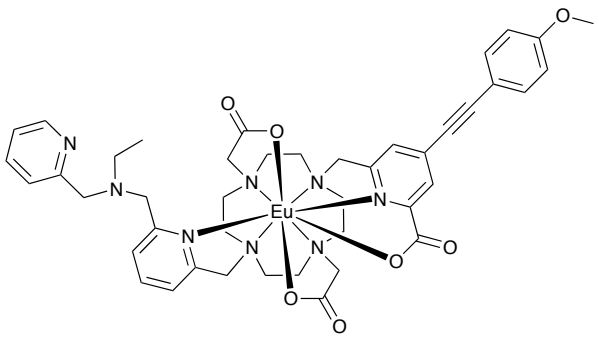


The ligand, **L$^{8}$**, (15 mg, 0.017 mmol) was dissolved in aqueous NaOH (0.5M, 4 mL) and stirred at 60 °C for 2 h. The solution was neutralised by addition of 1 M HCl and $EuCl_3$ (0.040 mmol) was added. The reaction mixture was stirred at rt for 1 h, pH was adjusted to 6.5 and the reaction mixture was stirred for another hour. Aqueous ammonia solution was added dropwise to pH 10 in order to precipitate an excess of europium in the form of $Eu(OH)_3$, which was separated by centrifugation. The solution was neutralised again, the solvent was removed under reduced pressure and the product was extracted several times with methanol. The methanol extracts were combined and the solvent was removed under reduced pressure giving a desired

product as an off-white solid in quantitative yield; *m/z* (HRMS$^{+}$) 941.3011 $[M+H^{+}]^{+}$ ($C_{43}H_{50}N_8O_7{}^{151}Eu$ requires 941.3001), ε($H_2O$) = 20,000 $M^{-1}cm^{-1}$; τ($H_2O$) = 0.22 ms (pH = 7.4), τ($D_2O$) = 0.29 ms (pD = 7.8).

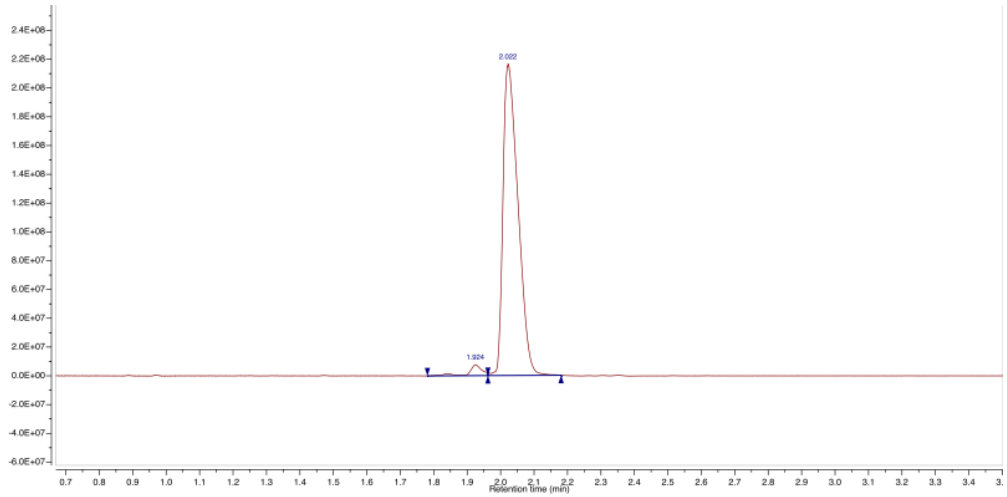

LC-MS UV trace of **[EuL$^{8}$]** (5% $H_2O$ (+0.1% v/v formic acid) in MeOH (+0.1% v/v formic acid) to 95% $H_2O$ (+0.1% v/v formic acid) in MeOH (+0.1% v/v formic acid) over 3.8 min

### *N*-((6-(Chloromethyl)pyridin-2-yl)methyl)-*N*-ethylethanamine, 8

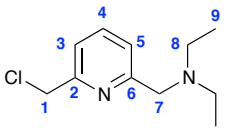


2,6-*Bis*(chloromethyl)pyridine (1.00 g, 5.67 mmol), diethylamine (0.6 mL, 5.67 mmol) and $K_2CO_3$ (0.80 g, 5.67 mmol) were dissolved in dry acetonitrile (20 mL) and the mixture was stirred at rt. After 2 h the temperature was increased up to 45 °C and the reaction mixture was stirred for 18 h The solution was filtered off, the solvent was removed under reduced pressure and the crude was purified on a silica column (0% to 66% of EtOAc in DCM), giving a desired product as a yellow oil (42 mg, 4% yield); $^{1}$H NMR (295 K, 600 MHz, $CDCl_3$) $\delta_H$ 7.66 (1H, t, $^{3}J_{H\text{-}H}$ = 8.0 Hz, $H^{4}$), 7.45 (1H, d, $^{3}J_{H\text{-}H}$ = 8.0 Hz, $H^{5}$), 7.32 (1H, d, $^{3}J_{H\text{-}H}$ = 7.0 Hz, $H^{3}$), 4.64 (2H, s, $H^{1}$), 3.72 (2H, s, $H^{7}$), 2.58 (4H, q, $^{3}J_{H\text{-}H}$ = 7.0 Hz, $H^{8}$), 1.04 (6H, t, $^{3}J_{H\text{-}H}$ = 7.0 Hz, $H^{9}$); $^{13}$C NMR (295 K, 176 MHz, $CDCl_3$) $\delta_C$ 160.3 ($C^{2}$), 155.7 ($C^{6}$), 137.3 ($C^{4}$), 122.1 ($C^{5}$), 120.7 ($C^{3}$), 59.3 ($C^{7}$), 47.4 ($C^{8}$), 46.8 ($C^{1}$), 11.8 ($C^{9}$); *m/z* (HRMS$^{+}$) 213.1165 $[M+H^{+}]^{+}$ ($C_{11}H_{18}N_2Cl$ requires 213.1159).

**Di-*tert*-butyl 2,2'-(4-((6-((diethylamino)methyl)pyridin-2-yl)methyl)-10-((6-(methoxycarbonyl)-4-((4-methoxyphenyl)ethynyl)pyridin-2-yl)methyl)-1,4,7,10-tetraazacyclododecane-1,7-diyl)diacetate ($L^9$)**

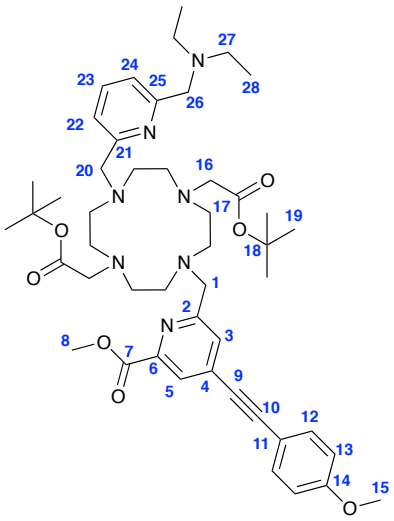

Di-tert-butyl 2,2'-(4-((6-(methoxycarbonyl)-4-((4-methoxyphenyl)ethynyl)pyridin-2-yl)methyl)-1,4,7,10-tetraazacyclododecane-1,7-diyl)diacetate, **7-1** (30 mg, 0.04 mmol) was dissolved in dry acetonitrile (9 mL), followed by addition of $Cs_2CO_3$ (30 mg, 0.09 mmol), N-((6-(chloromethyl)pyridin-2-yl)methyl)-N-ethylethanamine, **8** (20 mg, 0.09 mmol) and KI (20 mg, 0.12 mmol) was added. The reaction mixture was stirred at 70 °C for 18 h. The reaction mixture was filtered and purified on RP-HPLC (10% to 100% acetonitrile (+0.1% formic acid) in water (+0.1% formic acid) over 10 min). The fractions containing the desired product were combined and neutralised with aqueous ammonia solution. The solvent was removed under reduced pressure, dried and redissolved in acetonitrile. Ammonium formate was filtered off and the solvent was removed under reduced pressure, giving a colourless oil (20 mg, 52% yield); $^1$H NMR (295 K, 600 MHz, $CDCl_3$) $\delta_H$ 8.08 (1H, d, $^4J_{H\text{-}H}$ = 1.0 Hz, $H^5$), 7.74 (1H, t, $^3J_{H\text{-}H}$ = 8.0 Hz, $H^{23}$), 7.64 (1H, m, $H^3$), 7.58 (1H, d, $^3J_{H\text{-}H}$ = 8.0 Hz, $H^{22}$), 7.48 (2H, d, $^3J_{H\text{-}H}$ = 9.0 Hz, $H^{12}$), 7.46 (1H, d, $^3J_{H\text{-}H}$ = 8.0 Hz, $H^{24}$), 6.90 (2H, d, $^3J_{H\text{-}H}$ = 9.0 Hz, $H^{13}$), 4.59 (2H, s, $H^{20}$), 4.26 (2H, s, $H^1$), 4.14 (2H, $H^{26}$), 3.97 (3H, s, $H^8$), 3.84 (3H, s, $H^{15}$), 3.41 (4H, s, $H^{16}$), 3.37-2.97 (20H, cyclen, $H^{27}$), 1.42 (18H, s, $H^{19}$), 1.24 (6H, t, $^3J_{H\text{-}H}$ = 7.0 Hz, $H^{28}$); $^{13}$C NMR (295 K, 151 MHz, $CDCl_3$) $\delta_C$ 169.7 ($C^{17}$), 164.9 ($C^7$), 160.8 ($C^{14}$), 157.1 ($C^2$), 154.4 ($C^{25}$), 153.4 ($C^{21}$), 147.7 ($C^6$), 138.0 ($C^{23}$), 134.2 ($C^4$), 133.7 ($C^{12}$), 128.8 ($C^3$), 126.1 ($C^5$), 124.8 ($C^{24}$), 124.4 ($C^{22}$), 114.2 ($C^{13}$),

113.4 ($C^{11}$), 96.7 ($C^{10}$), 84.9 ($C^{9}$), 82.0 ($C^{18}$), 57.2 ($C^{20}$), 56.9 ($C^{26}$), 59.8 ($C^{16}$), 55.4 ($C^{15}$), 52.9 ($C^{8}$), 52.9-49.6 (cyclen), 46.7 ($C^{27}$), 28.1 ($C^{19}$), 9.7 ($C^{28}$); *m/z* (HRMS$^+$) 856.5364 $[M+H^+]^+$ ($C_{48}H_{70}N_7O_7$ requires 856.5337).

**[EuL$^9$]**

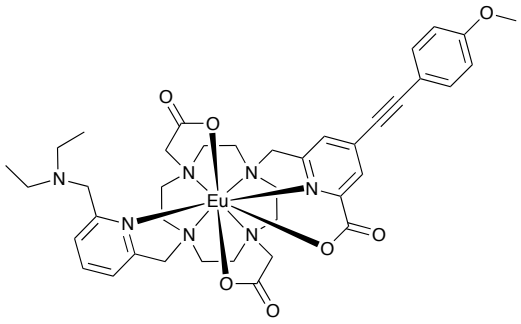


The ligand, **L$^9$**, (15 mg, 0.017 mmol) was dissolved in aqueous NaOH (0.5M, 4 mL) and stirred at 60°C for 2 h. The solution was neutralised by addition of 1 M HCl and $EuCl_3$ (0.040 mmol) was added. The reaction mixture was stirred at rt for 1 h, pH was adjusted to 6.5 and the reaction mixture was stirred for another hour. Aqueous ammonia solution was added dropwise to pH 10 in order to precipitate an excess of europium chloride in a form of $Eu(OH)_3$, which was separated by centrifugation. The solution was neutralized again, the solvent was removed under reduced pressure and the product was extracted several times with methanol. Methanol extracts were combined and the solvent was removed under reduced pressure giving a desired product as an off-white solid in quantitative yield; *m/z* (HRMS$^+$) 878.2879 $[M+H^+]^+$ ($C_{39}H_{49}N_7O_7{}^{151}Eu$ requires 878.2892), $\varepsilon(H_2O)$ = 20,000 $M^{-1}cm^{-1}$; $\tau(H_2O)$ = 0.61 ms (pH = 7.4), $\tau(D_2O)$ = 0.80 ms (pD = 7.8).

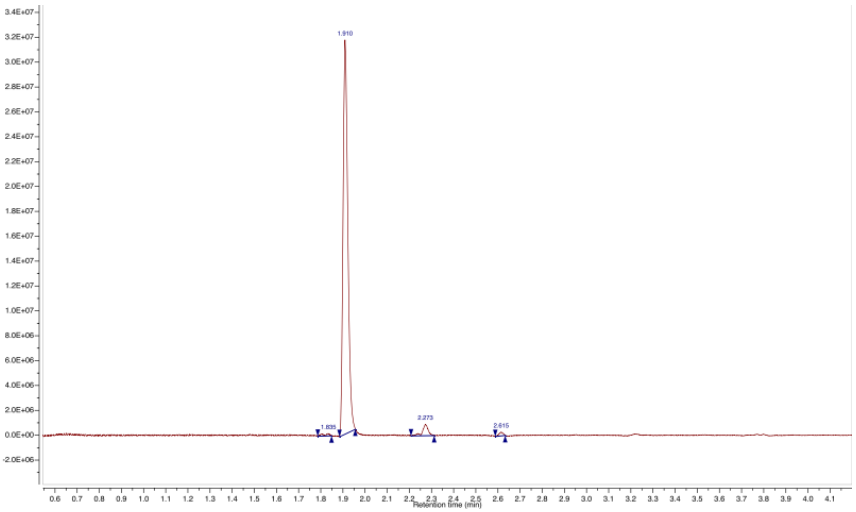


LC-MS UV trace of **[EuL$^9$]** (5% $H_2O$ (+0.1% v/v formic acid) in MeOH (+0.1% v/v formic acid) to 95% $H_2O$ (+0.1% v/v formic acid) in MeOH (+0.1% v/v formic acid) over 3.8 min

**1-(1-(2-Chloroethyl)-1H-1,2,3-triazol-4-yl)-N,N-*bis*(pyridin-2-ylmethyl) methanamine-DO2A-$^{t}$Bu, 10-2**

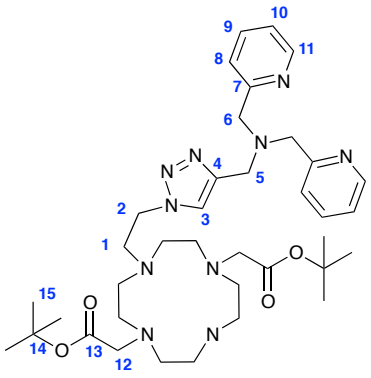

2-Azidoethanol (65 mg, 0.75 mmol) was dissolved in dry THF (3 mL), followed by addition of dry triethylamine (0.1 mL, 0.72 mmol) and MsCl (15 mL, 0.19 mmol). The reaction mixture was stirred at rt for 1h and the solvent was removed under reduced pressure. The crude material was redissolved in 15 mL of DCM and was washed with water (2 x 15 mL). The organic fraction was dried over $MgSO_4$ and the solvent was removed under reduced pressure, dried and redissolved in 3 mL of dry acetonitrile. DO2A-$^{t}$Bu ester (300 mg, 0.75 mmol) was dissolved in dry acetonitrile (10 mL) and $K_2CO_3$ was added (300 mg, 2.17 mmol) was added. The reaction mixture was cooled down with an ice bath and stirred for 5 min. The mesylate solution was added dropwise within 5 min and the reaction mixture was allowed to reach rt and stirred for 18 h. The solution was filtered, concentrated down to 4 mL, followed by addition of *N*,*N*-*bis*(pyridin-2-ylmethyl)prop-2-yn-1-amine (178 mg, 0.75 mmol), piperidine (1 mL) and CuI (10 mg, 0.05 mmol) were added. The reaction mixture was placed into a microwaveable vial, sealed and microwaved at 100 °C for 30 min. The reaction mixture was filtered and purified using RP-HPLC (10% to 100% of acetonitrile (+0.1% formic acid) in water (+0.1% formic acid) over 10 min). The fractions containing the desired product were combined and neutralised with aqueous ammonia solution. The solvent was removed under reduced pressure, dried and redissolved in acetonitrile. Ammonium formate was filtered off and the solvent was removed under reduced pressure, giving brown oil, containing the desired product and tetra-alkylated side-product. The components were separated using alumina column (0.5%→1% of MeOH in DCM), giving the desired product as a yellow oil (51 mg, 10% yield over two steps); $^{1}$H NMR (295 K, 400 MHz, $CDCl_3$) $\delta_H$ 8.54 (2H, d, $^{3}J_{H\text{-}H}$ = 5.0 Hz, $H^{11}$), 7.89 (1H, s, $H^{3}$), 7.73-7.62 (4H, m, $H^{8}$, $H^{9}$),

7.21-7.18 (2H, m, $H^{10}$), 4.51 (2H, m, $H^{1}$), 3.86 (2H, s, $H^{6}$), 3.85 (4H, s, $H^{6}$), 3.38 (4H, s, $H^{12}$), 3.11 (2H, m, $H^{2}$), 3.08-2.77 (16H, m, cyclen), 1.43 (18H, s, $H^{15}$); $^{13}C$ NMR (295 K, 100 MHz, $CDCl_3$) $\delta_C$ 170.4 ($C^{13}$), 158.6 ($C^{7}$), 148.5 ($C^{11}$), 143.9 ($C^{4}$), 137.1 ($C^{9}$), 124.0 ($C^{3}$), 123.5 ($C^{8}$), 122.3 ($C^{10}$), 81.7 ($C^{14}$), 59.1 ($C^{6}$), 57.8 ($C^{12}$), 52.7-45.8 ($C^{1}$, $C^{2}$, $C^{5}$, cyclen), 28.2 ($C^{15}$); *m/z* (HRMS$^{+}$) 707.4736 $[M+H^{+}]^{+}$ ($C_{37}H_{59}N_{10}O_4$ requires 707.4721).

**Di-*tert*-butyl 2,2'-(4-(2-(4-((bis(pyridin-2-ylmethyl)amino)methyl)-1H-1,2,3-triazol-1-yl)ethyl)-10-((6-(methoxycarbonyl)-4-((4-methoxyphenyl) ethynyl) pyridin-2-yl)methyl)-1,4,7,10-tetraazacyclododecane-1,7-diyl)diacetate ($L^{10}$)**

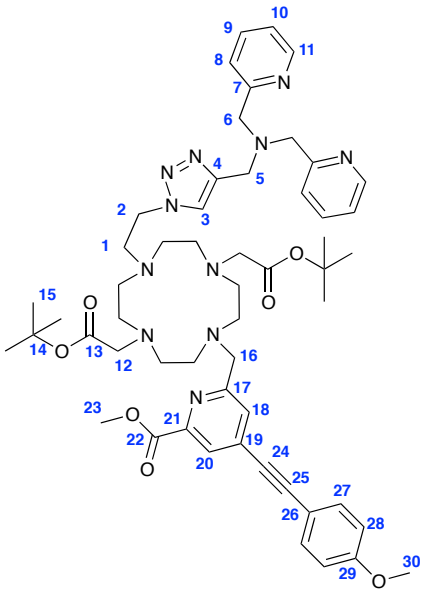

Methyl 6-(hydroxymethyl)-4-((4-methoxyphenyl)ethynyl)picolinate (30 mg, 0.10 mmol) was dissolved in dry THF (4 mL), followed by addition of dry triethylamine (0.1 mL, 0.72 mmol) and MsCl (15 mL, 0.19 mmol). The reaction mixture was stirred at rt for 1 h and the solvent was removed under reduced pressure. The crude material was redissolved in 15 mL of DCM and was washed with water (2 x 15 mL). The organic fraction was dried over $MgSO_4$ and the solvent was removed under reduced pressure, dried and redissolved in dry acetonitrile (3 mL). 1-(1-(2-Chloroethyl)-1H-1,2,3-triazol-4-yl)-N,N-bis(pyridin-2-ylmethyl)methanamine-DO2A-tBu ester, **10-2** (51 mg, 0.072 mmol) was dissolved in dry acetonitrile (8 mL) and $K_2CO_3$ (100 mg, 0.72 mmol) was added. The mesylate solution was added to the solution and the reaction mixture was stirred at 60 °C for 18 h. The reaction mixture was filtered and purified on RP-HPLC (10% to 100% acetonitrile (+0.1% formic

acid) in water (+0.1% formic acid) over 9 min). The fractions containing the desired product were combined and neutralised with aqueous ammonia solution. The solvent was removed under reduced pressure, dried and redissolved in acetonitrile. Ammonium formate was filtered off and the solvent was removed under reduced pressure, giving a colourless oil (53 mg, 75% yield); $^{1}$H NMR (295 K, 600 MHz, $CDCl_3$) $\delta_H$ 8.50 (2H, m, $H^{11}$), 8.06 (1H, $^{4}J_{H\text{-}H}$ = 1.5 Hz, $H^{20}$), 7.95 (1H, s, $H^{3}$), 7.69-7.66 (2H, m, $H^{9}$), 7.64 (1H, m, $H^{18}$), 7.61-7.60 (2H, m, $H^{8}$), 7.47 (2H, d, $^{3}J_{H\text{-}H}$ = 9.0 Hz, $H^{27}$), 7.15-7.13 (2H, m, $H^{10}$), 6.89 (2H, d, $^{3}J_{H\text{-}H}$ = 9.0 Hz, $H^{28}$), 4.64 (2H, t, $^{3}J_{H\text{-}H}$ = 7.0 Hz, $H^{1}$), 4.38 (2H, m, $H^{16}$), 3.95 (3H, s, $H^{30}$), 3.83 (4H, s, $H^{6}$), 3.82 (2H, s, $H^{5}$), 3.80 (3H, s, $H^{23}$), 3.52 (2H, t, $^{3}J_{H\text{-}H}$ = 7.0 Hz, $H^{2}$), 3.41 (4H, s, $H^{12}$), 3.12-2.98 (16H, m, cyclen), 1.39 (18H, s, $H^{15}$); $^{13}$C NMR (295 K, 151 MHz, $CDCl_3$) $\delta_C$ 169.4 ($C^{13}$), 164.7 ($C^{22}$), 160.7 ($C^{17}$), 159.0 ($C^{7}$), 148.6 ($C^{11}$), 147.8 ($C^{21}$), 144.6 ($C^{4}$), 136.9 ($C^{9}$), 134.5 ($C^{19}$), 133.7 ($C^{27}$), 128.9 ($C^{18}$), 126.2 ($C^{20}$), 124.1 ($C^{3}$), 123.2 ($C^{8}$), 122.2 ($C^{10}$), 114.2 ($C^{28}$), 113.3 ($C^{26}$), 97.0 ($C^{25}$), 84.7 ($C^{24}$), 82.3 ($C^{14}$), 59.3 ($C^{23}$), 58.1 ($C^{16}$), 56.4 ($C^{12}$), 55.4 ($C^{6}$), 53.8 ($C^{2}$), 53.0 ($C^{30}$), 52.0-50.2 (cyclen), 48.7 ($C^{5}$), 45.9 ($C^{1}$), 28.0 ($C^{15}$); *m/z* (HRMS$^{+}$) 986.5649 $[M+H^{+}]^{+}$ ($C_{54}H_{72}N_{11}O_7$ requires 986.5616).

**[EuL$^{10}$]**

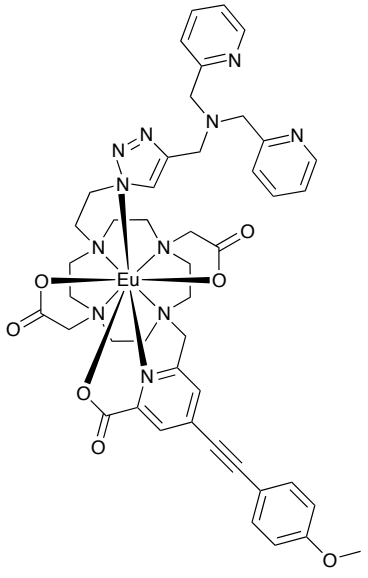


The ligand, **L$^{10}$**, (53 mg, 0.054 mmol) was dissolved in aqueous NaOH (0.5M, 4 mL) and stirred at 60 °C for 2 h. The solution was neutralised by addition of 1 M HCl and $EuCl_3$ (0.090 mmol) was added. The reaction mixture was stirred at rt for 1 h, pH was adjusted to 6.5 and the reaction mixture was stirred for another hour. Aqueous ammonia solution was added dropwise to pH 10 in order to precipitate an excess of

europium chloride in a form of $Eu(OH)_3$, which was separated by centrifugation. The solution was neutralised again and was left in the fridge, causing precipitation of the desired complex as an off-white solid, which was separated by decanting solution (20 mg, 37% yield); *m/z* (HRMS$^+$) 1008.3200 $[M+H^+]^+$ ($C_{45}H_{51}N_{11}O_7{}^{151}Eu$ requires 1008.3171), $\varepsilon(H_2O)$ = 20,000 $M^{-1}cm^{-1}$; $\tau(H_2O)$ = 0.51 ms (pH = 7.4), $\tau(D_2O)$ = 1.12 ms (pD = 7.8).

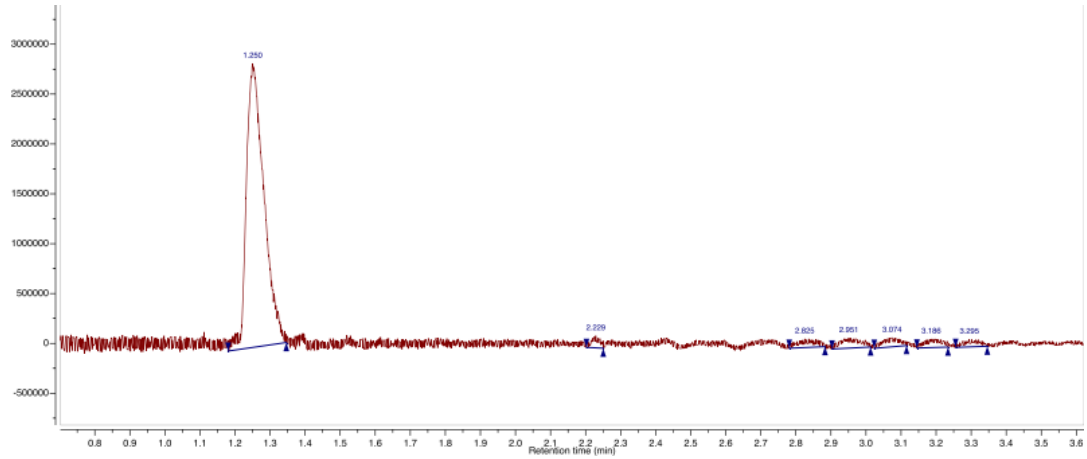


LC-MS UV trace of **[EuL$^{10}$]** (5% $H_2O$ (+0.1% v/v formic acid) in MeOH (+0.1% v/v formic acid) to 95% $H_2O$ (+0.1% v/v formic acid) in MeOH (+0.1% v/v formic acid) over 3.8 min

**Di-*tert*-butyl 2,2'-(4-((6-((*bis*(pyridin-2-ylmethyl)amino)methyl)pyridin-2-yl)methyl)-10-((4-((4-methoxyphenyl)ethynyl)pyridin-2-yl)methyl)-1,4,7,10-tetraazacyclododecane-1,7-diyl)diacetate (L$^{11}$)**

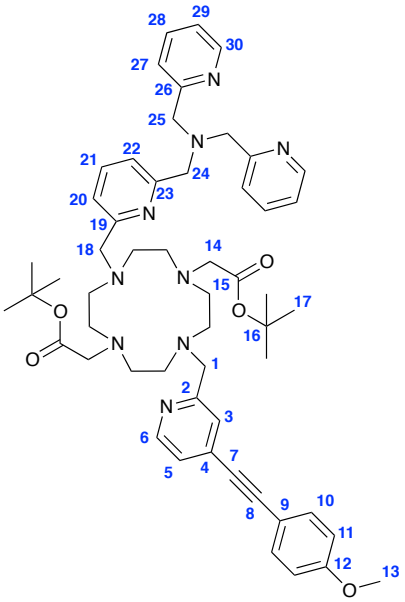

Di-tert-butyl 2,2'-(4-((4-((4-methoxyphenyl)ethynyl)pyridin-2-yl)methyl)-1,4,7,10-tetraazacyclododecane-1,7-diyl)diacetate, **1-1** (31 mg, 0.041 mmol) was dissolved in dry acetonitrile (10 mL), followed by addition of $K_2CO_3$ (50 mg, 0.36 mmol), 1-(6-(chloromethyl)pyridin-2-yl)-*N*,*N*-*bis*(pyridin-2-ylmethyl)methanamine (31 mg, 0.095 mmol) and KI (20 mg, 0.12 mmol) was added. The reaction mixture was stirred at 70 °C for 18 h. The reaction mixture was filtered and purified on RP-HPLC (10% to 100% acetonitrile (+0.1% formic acid) in water (+0.1% formic acid) over 10 min). The fractions containing the desired product were combined and neutralised with aqueous ammonia solution. The solvent was removed under reduced pressure, dried and redissolved in acetonitrile. Ammonium formate was filtered off and the solvent was removed under reduced pressure, giving a colourless oil (43 mg, 70% yield); $^1$H NMR (295 K, 600 MHz, $CDCl_3$) $\delta_H$ 8.54 (1H, d, $^3J_{H\text{-}H}$ = 8.0 Hz, $H^6$), 8.50 (2H, m, $^3J_{H\text{-}H}$ = 5.0 Hz, $H^{30}$), 7.66 (3H, m, $H^{21}$, $H^{28}$), 7.56-7.53 (3H, $H^{20}$, $H^{27}$), 7.46 (2H, d, $^3J_{H\text{-}H}$ = 9.0 Hz, $H^{10}$), 7.44 (1H, s, $H^3$), 7.39 (1H, d, $^3J_{H\text{-}H}$ = 8.0 Hz, $H^5$), 7.28 (1H, d, $^3J_{H\text{-}H}$ = 5.0 Hz, $H^{22}$), 7.14 (2H, m, $H^{29}$), 6.87 (2H, d, $^3J_{H\text{-}H}$ = 9.0 Hz, $H^{11}$), 4.38 (2H, s, $H^{18}$), 4.15 (2H, s, $H^1$), 3.85 (6H, br s, $H^{24}$, $H^{25}$), 3.36 (4H, s, $H^{14}$), 3.19-2.96 (16H, m, cyclen), 1.39 (18H, s, $H^{17}$); $^{13}$C NMR (295K, 151 MHz, $CDCl_3$) $\delta_C$ 169.8 ($C^{15}$), 160.4 ($C^{12}$), 159.5 ($C^{23}$), 159.1 ($C^{26}$), 156.0 ($C^2$), 153.2 ($C^{19}$), 149.4 ($C^6$), 149.0 ($C^{30}$), 137.5 ($C^{21}$), 136.6 ($C^{28}$), 133.5 ($C^{10}$), 132.7 ($C^4$), 126.1 ($C^3$), 124.5 ($C^{22}$), 123.6 ($C^5$), 122.8 ($C^{29}$), 122.3 ($C^{20}$), 122.1 ($C^{27}$), 114.1 ($C^{11}$), 113.9 ($C^9$), 95.1 ($C^8$), 85.4 ($C^7$), 81.8 ($C^{16}$), 60.2 ($C^{24}$, $C^{25}$), 58.7 ($C^1$), 57.8 ($C^{18}$), 56.6 ($C^{14}$), 55.3 ($C^{13}$), 52.5-50.0 (cyclen), 28.1 ($C^{17}$); *m/z* (HRMS$^+$) 924.5500 $[M+H^+]^+$ ($C_{54}H_{70}N_9O_5$ requires 924.5500).

**[EuL$^{11}$]**

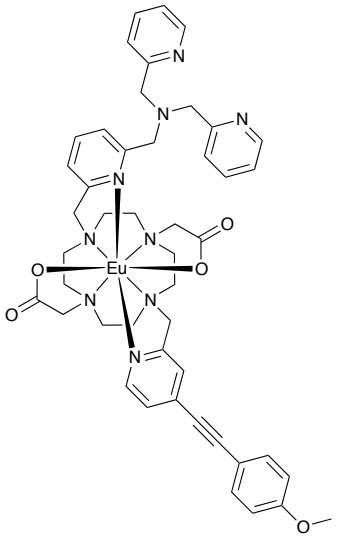

The ligand, $\mathbf{L^{11}}$, (43 mg, 0.046 mmol) was dissolved in aqueous NaOH (0.5 M, 4 mL) and stirred at 60 °C for 2 h. The solution was purified using RP-HPLC (10% to 100% MeOH in water (+25 mM $NH_4HCO_3$) over 10 min), fractions containing the desired product were combined and the solvent was removed under reduced pressure. $EuCl_3$ (0.046 mmol) was added and the reaction mixture was stirred at rt for 1 h, pH was adjusted to 6.5 and the reaction mixture was stirred for another hour. The compound was found to be extremely susceptible towards irreversible chemical transformation basic pH and the presence of anions, and therefore it was used without further purification (30 mg, 67% yield); *m/z* (HRMS$^+$) 960.3215 $[M+H^+]^+$ ($C_{46}H_{51}N_9O_5{}^{151}Eu$ requires 960.3212), $\varepsilon(H_2O)$ = 20,000 $M^{-1}cm^{-1}$; $\tau(H_2O)$ = 0.41 ms (pH = 7.4), $\tau(D_2O)$ = 0.99 ms (pD = 7.8).

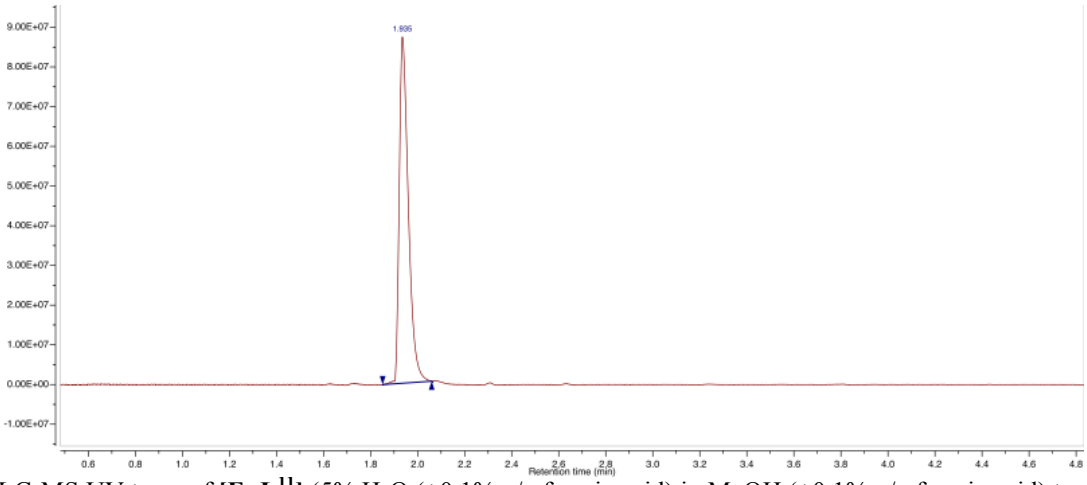


LC-MS UV trace of **[EuL$^{11}$]** (5% $H_2O$ (+0.1% v/v formic acid) in MeOH (+0.1% v/v formic acid) to 95% $H_2O$ (+0.1% v/v formic acid) in MeOH (+0.1% v/v formic acid) over 3.8 min

# V.3 References


[1] Y.-W. Yip, G.-L. Law, W.-T. Wong, *Dalton Trans.* **2016**, *45*, 928–935.
[2] Z. Kovacs, A. D. Sherry, *J. Chem. Soc. Chem. Comm.* **1995**, 185-186.
[3] J. W. Walton, A. Bourdolle, S. J. Butler, M. Soulie, M. Delbianco, B. K. McMahon, R. Pal, H. Puschmann, J. M. Zwier, L. Lamarque, et al., *Chem. Comm.* **2013**, *49*, 1600–1602.
[4] S. J. A. Pope, R. H. Laye, *Dalton Trans.* **2006**, *44*, 3108.
[5] H. Li, R. Lan, C.-F. Chan, L. Jiang, L. Dai, D. W. J. Kwong, M. H.-W. Lam, K.-L. Wong, *Chem. Comm.* **2015**, *51*, 14022–14025.
[6] R. Pal, D. Parker, *Chem. Comm.* **2007**, 474–476.
[7] C. P. Montgomery, E. J. New, L. O. Palsson, D. Parker, A. S. Batsanov, L. Lamarque, *Helv. Chim. Acta* **2009**, *92*, 2186–2213.
[8] L.-O. Pålsson, R. Pal, B. S. Murray, D. Parker, A. Beeby, *Dalton Trans.* **2007**, 5726-5734.

# VI. Conclusions

It has been shown in the present work that lanthanide complexes can find application as various luminescent probes, i.e. for pH-, protein-, metal- and anion-sensing. In each case a considerable spectral change can be modulated as a function of pH or analyte concentration, allowing unambiguous read-outs. Some of the described complexes have been tested *in cello*, demonstrating their potential for cellular studies. Rational design of the probes discussed herein tailored sensitivity and selectivity towards desired analytes, whilst macrocyclic nature of the ligands made corresponding chemical modifications easy to accomplish. A great potential of circularly polarised luminescence has been exemplified on numerous examples, where more conventional spectral techniques were unable to supply necessary data. High intensity of CPL signal even in the complexes with relatively low quantum yields, along with millisecond lifetimes and large Stokes shifts make lanthanide complexes ideal candidates for cellular imaging, whose potential will be unravelled even further with an advent of chiral fluorescent microscopy.

However, there are still certain obstacles, which hamper their wider application, even though lanthanide complexes as biological assays have been available on the market for the last decay. Some of these limitations have been encountered in the present work as well. First, targeting desired organelles with high selectivity of the cell remains an issue and requires further studies to be carried out. Second, despite a rich library of lanthanide complexes has been synthesised up to now, there are still synthetic limitations (especially in the chemistry of pyridine derivatives), which restrict availability of the ligands with desired substituents. To overcome this problem, a closer collaboration between organic and lanthanide chemists is required. Third, an exceptional sensitivity of emission spectra of europium complexes to even subtlest changes in the coordination environment can be exploited for refining simulated molecular structures. The reciprocal task – predicting luminescence spectrum based on structural considerations - may facilitate the search for the probes with highest spectral change in response to the external stimuli. This requires a more detailed and accurate theory of f-f transitions to be conceived.

## Appendix 1

## Assignment of $^{1}$H NMR spectrum of [YL$^{5}$], 298 K

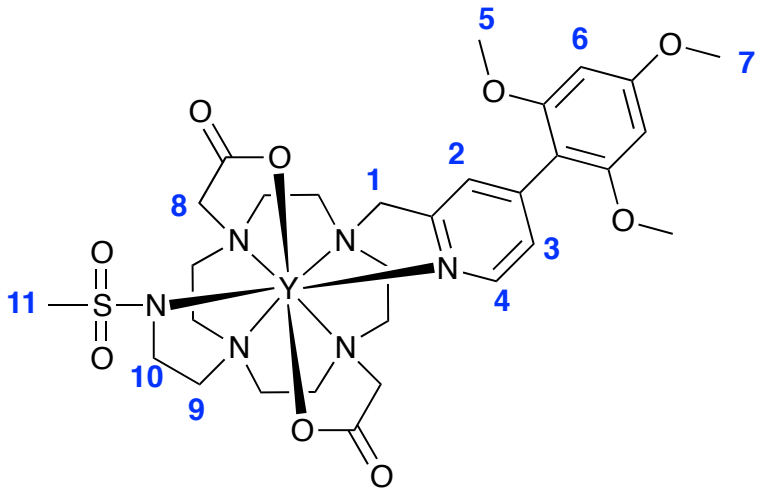


| | |
|---|---|
| **H$^{1}$** | 3.25 (eq), 4.23 (ax) |
| **H$^{2}$** | 7.07 |
| **H$^{3}$** | 7.07 |
| **H$^{4}$** | 8.17 |
| **H$^{5}$** | 3.37 |
| **H$^{6}$** | 6.01 |
| **H$^{7}$** | 3.49 |
| **H$^{8}$** | 2.53 (eq), 2.69 (eq), 2.92 (ax), 3.72 (ax) |
| **H$^{9}$** | |
| **H$^{10}$** | |
| **H$^{11}$** | 2.61 |

For H$^{8}$ equatorial protons of one arm are in exchange with an axial proton of the trans acetate arm and vice versa, suggesting exchange between two TSAP isomers.

## Appendix 2

## $^{1}H$-$^{1}H$ COSY of [EuL$^{5}$], 298 K

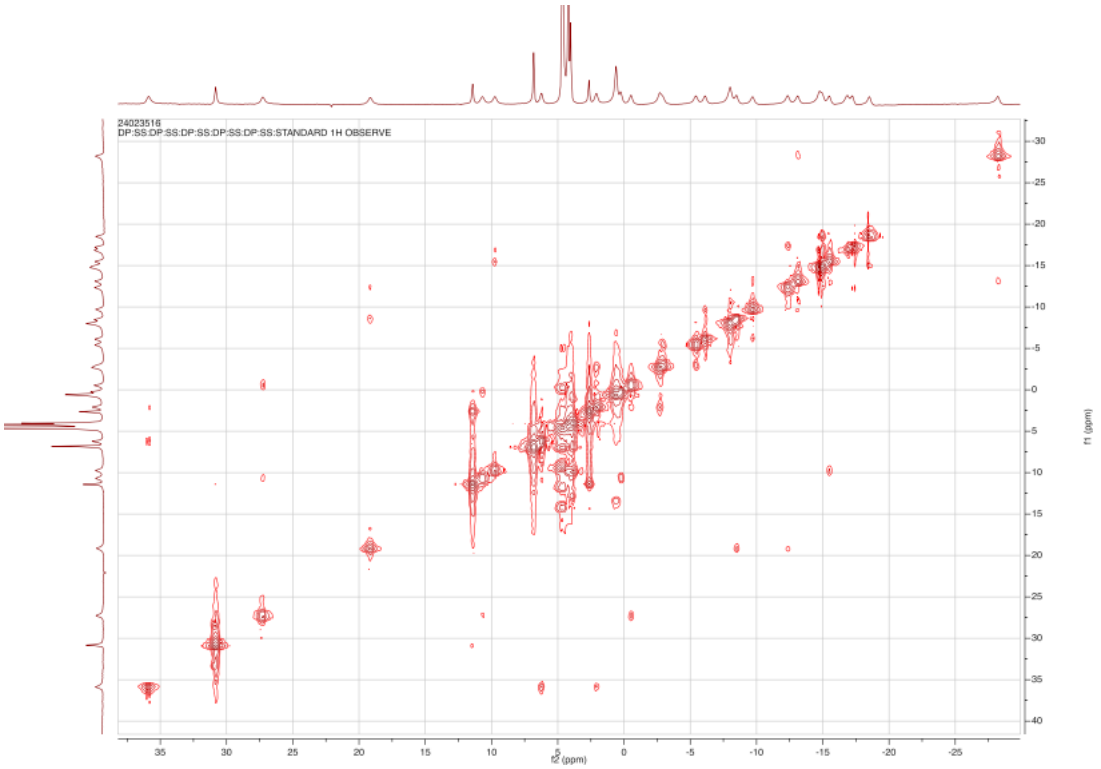

**Appendix 3**

**Job plot for [EuL$^8$] following the addition of $Zn^{2+}$ ([EuL$^8$] 2.5 µM, 0.1 M HEPES, pH = 7.40, 298 K, $\lambda_{ex}$ = 335 nm).**